THE UNIVERSITY
of EDINBURGH

Exploring the Solvent Extraction of Rhodium and Gold

Rebecca Michelle Nicolson

Doctor of Philosophy

The University of Edinburgh

2019

For Da
and Nanny

Declaration

The author has been engaged in a programme of full-time research under the supervision of Professor Carole A. Morrison and Professor Jason B. Love at The University of Edinburgh since September 2015.

The work presented in this document is the original work of the author, except where references are made to other sources. No part of the work referred to in this thesis has been submitted previously in whole or in part for another degree or qualification from this or any other university or institute of learning. In accordance with university regulations this thesis does not exceed 100,000 words in length.

Rebecca Michelle Nicolson

November 2019

All that is gold does not glitter,
Not all those who wander are lost;

– J. R. R. Tolkien
The Fellowship of the Ring

Lay summary

Precious metals, such as rhodium and gold, are important for much of today's technology: in electronics, medicine, and catalysis for chemical synthesis and in convertors in vehicle exhausts. Pyrometallurgical (using heat) and hydrometallurgical (using solution chemistry) techniques are used for their recovery and separation from ores or recyclable material, such as waste electronics. Owing to the decreasing concentration of these metals in primary sources, the increasing demand for metals for use in our expanding technologies, and the high cost and energy associated with their recovery, it is crucial to continue research into the methods by which they can be recovered. Though the techniques are well established, it is possible to make improvements in efficiency which can lead to more sustainable, cost-effective approaches.

Hydrometallurgy involves the dissolution of the mixed-metal source in an, usually acidic, aqueous solution, followed by a technique which allows for the separation of the target metal. One such separation technique is solvent extraction. It exploits solubility differences, using reagents which will associate with the metal species and render it more soluble in an immiscible organic solvent, as opposed to the aqueous solution. The reagent binds to the metal species reversibly, so the metal can be removed from the organic solution into a fresh aqueous solution, from which it can be reduced to its zero-oxidation state, e.g. by electrolysis, giving the pure metallic metal.

The reagent used in solvent extraction can be tailored to selectively associate with the desired metal over others in solution, based on differences in the size and/or charge of the metal species present in the aqueous solution and the nature of the assemblies they can form with the reagent. In order to design more selective, more efficient reagents, it is necessary to have a clear understanding of the chemistry occurring at the molecular level in the extraction process. To be able to make improvements to an existing system or to develop a new reagent, it is helpful to know the assembly that forms on extraction and the interactions which hold it together. This is often not fully characterised for industrial reagents which have been in use for a long time or for systems with particularly complex speciation.

This work focuses on the solvent extraction of gold, one of the easiest precious metals to recover from chloride solution, and rhodium, the most difficult metal to recover, owing to its

aqueous chloride solution speciation. As solvent extraction is solution based, the direct characterisation of the complexes present is difficult. To combat this, a wide variety of experimental analysis techniques in combination with computational modelling is employed. The modes of action occurring for rhodium extraction with amidoamine reagents is determined and this information is used to explore theoretically how structural changes of the reagents affect their extraction ability. In addition, new reagents, based on known rhodium precipitants, are tested in an effort to find more effective extractants for rhodium, which is currently not recovered commercially by solvent extraction. The extraction mechanism of a reagent used industrially in the recovery of gold is examined and the role of water is elucidated.

Abstract

This work explores the solvent extraction of precious metals, specifically rhodium and gold, from chloride solution, with the aims of understanding how existing extractants work and designing new extractants. A wide variety of analytical techniques are employed, demonstrating how they can be used together to assess extraction ability and provide insight into the identity of the extracted species. Computational techniques are also used; their implementation, often in conjunction with experiment, can identify the interactions which allow extraction to occur and explain differences in extraction behaviour.

Chapter 3 focuses on understanding how amidoamine extractants interact with the Rh(III) complexes present in chloride solution and thus enable their extraction. Experimental analysis shows that at low concentrations of Rh(III), the extracted species is $RhCl_5(H_2O)\cdot(LH)_2$, but at high concentrations a di-nuclear species, $Rh_2Cl_9\cdot(LH)_3$, is present in the organic phase and on aging an inner-sphere complex, $RhCl_3L$, can form. The mode of extraction is found to differ from that of a simple amine-based extractant. Computational modelling explores the extraction behaviour of a series of amidoamine extractants, finding they have different anion binding modes depending on the number of intra-extractant hydrogen bonds they can form. This results in bis- and tris-amidoamines having a more suitable binding mode for the Rh(III) *aquo*-chloridometalate compared to a mono-amidoamine, which has a more suitable binding mode for chloride. Calculated formation energies are broadly in agreement with experimental results and suggest selectivity for $[RhCl_5(H_2O)]^{2-}$ over chloride is the source of the success of this class of extractants. This work presents a full mode of action analysis of the bis-amidoamine and rationalises why the amidoamine reagents were the first effective Rh(III) extractants from chloride solution: they are proton-chelating reagents, which can adopt a binding mode that is selective for larger, more charge-diffuse anions.

Building on the work of Chapter 3, a theoretical screening study of other mono- and bis-amidoamines (or amido-quaternary ammonium compounds) is presented in Chapter 4. Different potential binding modes of the molecules are explored computationally, and it is found that, where possible, N-H to anion binding is generally more favourable than intra-molecule proton chelation and C-H to anion binding, with only one exception to this rule. Interestingly, this exception proves to have the most favourable energy of exchanging chloride for $[RhCl_5(H_2O)]^{2-}$, suggesting that it would be the most effective at extracting the

Rh(III) metalate. All other molecules are theoretically poorer extractants of Rh(III) and, based on a comparison of the energies of formation, it appears that the reason for this is less favourable association with $[RhCl_5(H_2O)]^{2-}$, more favourable association with chloride, or a combination of the two. This work highlights the importance of a favourable C-H to anion, or "soft", binding mode in the selective extraction of Rh(III) metalate over chloride, and how small structural changes to the extractant can drastically alter the favourability of this type of binding mode.

Chapter 5 explores the possibility of using polyamine-based Rh precipitants or reagents based on them for Rh extraction. It is found that "precipitant" molecules with long chain R-groups added are capable of extracting Rh(III) metalate very well, even from solutions of high HCl concentration. At high HCl concentrations, the most likely Rh(III) species extracted from the aqueous phase is $[RhCl_6]^{3-}$, with which the extractant is expected to associate in the outer-sphere. In contrast, it is found that an inner-sphere complex forms upon extraction from solutions of very low chloride concentrations. Extraction from mixed Rh(III)/Pt(IV) aqueous solutions is also investigated, but no selectivity for Rh(III) over Pt(IV) is found. Rh(III) stripping from the loaded organic is investigated using a number of reagents, with ammonium hydroxide solution found to be the most effective. The reagent designed and tested has the potential to be used for the solvent extraction of Rh industrially, offering extraction at the higher HCl concentrations typically used in existing metal recovery flow-sheets.

Industrially, Au(III) solvent extraction from chloride solution is well established, however, some of the reagents used are still not well understood. Chapter 6 aims to explain the extraction mechanism, and particularly the role of water, in Au(III) recovery with an industrial reagent via classical molecular dynamics simulations, which allow the assembly of the extracted species to be viewed and analysed. Experimental conditions can be modelled, but, in addition, so can other, non-experimental conditions to permit a better understanding of the extraction behaviour. Analysis of the output structures suggests that water's primary role in extraction is as the positive charge carrier. In some systems, where chloride is considered as the anion, the water partially hydrates the extracted anion, acting as a mediating agent between the electronegative functional groups on the extractant and the anion. This new insight into the nature of the extraction assemblies provides a greater understanding of the role of water in the extraction mechanism, and the means by which the extractant transports

$[AuCl_4]^-$ into the organic phase, information which can be used for informed modification of existing extraction processes and development of new reagents.

Acknowledgments

Firstly, thank you so much to my supervisor, Professor Carole Morrison. You put up with me for four years prior to my PhD, so thank you for taking me on for another four, even though you knew what I am like. I am very grateful for the opportunity to work with you, and I thank you for all of your help, time, patience and support.

I also thank Professor Jason Love for all the help and advice provided, particularly on synthesis and experimental analysis.

To Professor Peter Tasker, thank you for being such an inspiration, for your constant enthusiasm, and for all the help you have given me, especially with the publication. Working with you has been a true pleasure.

Thank you very much to my industrial supervisor, Dr Ross Gordon, for your help and advice, and for always laughing (at me) when I was despairing. And thank you to Dr Emma Schofield for taking over when Ross ~~abandoned solvent extraction~~ changed departments. Thank you to Johnson Matthey for funding my PhD and for all the dinners. I also extend my gratitude to Richard Grant; thank you for sharing your vast knowledge with me.

Thank you to all the collaborators on this work, but especially to Dr Mark Antonio for your time and patience in teaching me about EXAFS analysis.

A huge thank you to the Taskers/Metal Recovery Group. It has been an absolute privilege to work alongside you all. I have to start with Mary, because if I hadn't met you at Cytec I might never have joined the group (although maybe that means I shouldn't thank you, since you got me into this?!). Thank you for teaching me about solvent extraction and computational modelling, for looking after me, and for being so great. I miss you now you're across the pond.

Thank you so much to Kirsty, for being a fellow JM supervisee and coaching me on all the admin that came with that, for your help with LAMMPS simulations, for your support and advice, for your reactions to the cat photos I send you, and for all the dinners and fun we have had.

A massive thank you to Euan. You were essentially a post doc to me and I don't know how I would have coped without you. Thank you for everything you have done for me: for the chemistry and teaching help, PhD and life advice, for constantly being there for me, and for

being such a fantastic friend. I hope you know just how much it means (and you mean) to me. Though I will never forgive you for the puns.

I thank Innis for help with LAMMPS simulations too, but also for being my computational office buddy, for your sound, reasoned opinions and advice, for always being up for board games (well, except The Resistance), and for standing in disapproval with me against Euan's puns.

Thank you, Jamie. I think you had to put up with a lot from me after Euan left. I thank you for our continued agreement that lab is lab, for all your advice on synthesis, your patience helping me with NMR spectra, answering any and all of the random questions I had over the course of finishing up and writing this thesis, and for being your amazing self.

To Luke, I'd like to apologise for the miserable state I've been in for pretty much all of your PhD so far. Thank you for laughing or rolling your eyes at my complaints, for humouring all my suggestions of tests and analyses you should try, and for renewing my enthusiasm for this field with your interest and hard work in it.

I must thank the older Taskers too, for all the work that came before and for your theses (which were very helpful and vital to my sanity over the course of writing up). Special thanks to James, for the advice you gave when I was applying for the PhD.

Thank you also to all the project students over the years for your hard work and for keeping things fun. With special thanks to my students: Michael, Álvaro, Henry and Jennifer.

As much as moving labs was a pain, I will always be grateful for Office 209. My time in the Love(Morrison)Garden was amazing. Thank you to Eszter, Jay, Weronika, Annie and Yali for all the crosswords, rants, and extremely random chat (all of which make me hope IT never check our search history – they'd really question our apparent obsession with sea birds!). I have loved sharing an office with you and have immensely enjoyed all our outings. I will miss you loads. And I must thank you, Jenni, for picking such wonderful members for your group and for being so wonderful yourself.

Thank you also to everyone in the Computational Office, and to all the attendees of Cake Friday. I'm definitely missing people (I probably should just look up the script log…), so including but not limited to: Lisa, Jonny, Jordi, Salome, Darren, Toni, Sofia, Julian, Lisette, Elaine, Elanor, and Claire.

I thank the Cowleys (and previous Cowleys): Amy, Steph, Martin, Clément, Dan, Abi and Rosie, who could always be counted on to help out if there was an excess of cake. Thank you for including me and for all the fun events. Also thanks, for similar reasons, to Bec and Cora.

And, of course, Helen (pretend the yellow moon emoji is here). Thank you for our conversations, for listening to all my complaining, for the many coffee/tea breaks and dinners, the copious amounts of ice cream/bubble tea, and for being an amazing friend. I hope we can continue this way (though maybe with less complaining) and I look forward to employing you at Hel's Bells in the future.

I cannot overstate it when I say, all of you are the reason this PhD has been worthwhile. I will forever be grateful for that.

I would like to extend immense gratitude to everyone in the building who has helped me out, but particularly to Lorna for everything ICP-OES. Sorry for my numerous questions, all broken parts and extra times you've had to clean the detector window because of our organic solvent, and for all the fuss about the new instrument.

I also thank David for teaching me computational chemistry, Stores, NMR (particular thanks to Juraj for ^{15}N NMR help), mass spec (especially to Logan for training me), the teaching labs (particularly to Scott for use of the KF titrators) and all the other services I have made use of. And thank you to Davy for always having a good morning/hello to brighten my day.

Special thanks to Jen and Craig. I loved being a demonstrator in the 3th Year Inorganic Lab. Teaching the students was great (stressful, but great), but working with you was the real joy. Thank you also to Murray for employing me and for allowing me to help design a new experiment for the lab.

Thank you, Iain, for supporting me for as long as you did.

And to my family. Thank you for your constant belief in me and your endless support. Especially thank you to my grandparents, Dad, Carol, Gunther, Yasmin, and, last but most definitely not least, Mum. I wouldn't have made it this far without you.

Contributions to work presented in this thesis

Chapter 3 – Understanding the extraction of rhodium chloridometalates by amidoamines

- Hirokazu Narita and colleagues at Environmental Management Research Institute, National Institute of Advanced Industrial Science and Technology (AIST): all experimental work with BisAA in octanol and on TOA, including KF titrations and FT-IR analysis.
- Kazuko Morisaku at the Environmental Management Research Institute, National Institute of Advanced Industrial Science and Technology (AIST): synthesis of extractants/ligands and crystal complexes.
- Hideaki Shiwaku and Tsuyoshi Yaita at the Materials Sciences Research Center, Japan Atomic Energy Agency (JAEA): EXAFS (set 1) data collection and data analysis.
- Giannantonio Cibin at the Diamond Light Source on Beam Line 18: EXAFS (set 2) data collection.
- Mark Antonio at the Neutron Scattering Division, Oak Ridge National Laboratory: EXAFS (set 2) data analysis.
- Midori Goto at Environmental Management Research Institute, National Institute of Advanced Industrial Science and Technology (AIST): X-ray crystallography.
- Juraj Bella at the University of Edinburgh: 2D NMR data collection.
- Ryuhei Motokawa at the Materials Sciences Research Center, Japan Atomic Energy Agency (JAEA): SANS analysis.
- William Heller at the Neutron Scattering Division, Oak Ridge National Laboratory: SANS analysis.
- Fumiyuki Ito at Environmental Management Research Institute, National Institute of Advanced Industrial Science and Technology (AIST): DFT calculations for SANS fitting.

Chapter 6 – Modes of action in gold chloridometalate extraction

- Álvaro Gallego Jurado (University of Edinburgh MChem project student under the supervision of the author): KF titrations, protonation site calculations, MIBK parameter selection and test modelling by, and data analysis script development.
- Michael Kennealy (University of Edinburgh BSc project student under the supervision of the author): data analysis script development.

- Kirstian MacRuary (previous University of Edinburgh PhD student): data analysis script development.
- Innis Carson (previous University of Edinburgh PhD student): data analysis script development.

Publications and conference presentations

Publications

Published:

> "Proton Chelating Ligands Drive Improved Chemical Separations for Rhodium"
>
> H. Narita, R. M. Nicolson, R. Motokawa, F. Ito, K. Morisaku, M. Goto, M. Tanaka, W. T. Heller, H. Shiwaku, T. Yaita, R. J. Gordon, J. B. Love, P. A. Tasker, E. R. Schofield, M. R. Antonio, and C. A. Morrison, *Inorg. Chem.* **2019,** *58*, 8720-8734.

In preparation:

> "The effect of structural changes to amido-amine reagents on Rh(III) *aquo*-chlorido metalate extraction"
>
> R. M. Nicolson, J. P. Hunter, J. B. Love, E. R. Schofield, and C. A. Morrison
>
> "Mode of action in Au(III) chloridometalate recovery by industrial reagents: a molecular dynamics modelling study"
>
> R. M. Nicolson, Á. Galego Jurado, M. Kennealy, J. B. Love, E. R. Schofield, and C. A. Morrison

To be assessed for potential publication or patent filing by Johnson Matthey:

> "Modified polyamine precipitants as Rh(III) chloridometalate extractants"
>
> R. M. Nicolson, J. B. Love, E. R. Schofield, and C. A. Morrison

Conference presentations

Johnson Matthey Academic Conference 2019, Warwick, UK – 9th-10th April 2019: Oral Presentation (Characterising rhodium recovery by amido-amine reagents)

4th Annual Joseph Black Chemistry Conference, University of Edinburgh, UK – May 2018: Oral presentation (Understanding rhodium solvent extraction: a mode of action study) – Prize awarded

Johnson Matthey Academic Conference 2018, Loughborough, UK – 10th-11th April 2018: Poster presentation (Rhodium Recovery: using modified precipitants as extractants)

21st International Solvent Extraction Conference (ISEC), Miyazaki, Japan – 5th-9th November 2017: Oral Presentation (Understanding rhodium solvent extraction: a mode of action study)

ScotCHEM Computational Chemistry Symposium 2017, University of Edinburgh, UK – 16th June 2017: Oral presentation (Understanding rhodium solvent extraction: a mode of action study)

3nd Annual Joseph Black Chemistry Conference, University of Edinburgh, UK – 1st June 2017: Poster presentation (Understanding Rhodium Solvent Extraction: a mode of action study)

Johnson Matthey Academic Conference 2017, Loughborough, UK – 11th-12th April 2017: Flash and poster presentations (Understanding Rhodium Solvent Extraction: a mode of action study) – Prize awarded

ScotCHEM Computational Chemistry Symposium 2016, University of Edinburgh, UK – 14th June 2016: Poster presentation (Computational and Experimental Tools for Understanding Gold and Rhodium Solvent Extraction)

Johnson Matthey Academic Conference 2016, Loughborough, UK – 12th-13th April 2016: Poster presentation (Computational and Experimental Tools for Understanding Gold and Rhodium Solvent Extraction)

Contents

List of supporting information

The following is a list of the supporting information (sorted by chapter), which is included on the USB drives along with an electronic copy of the thesis itself.

Chapter 3 – Understanding the extraction of rhodium chloridometalates by amidoamines

i. Additional EXAFS fitting details
ii. HMBC NMR spectra
iii. Outputs from Gaussian calculations
iv. Record of structures, their energies, and calculations of the formation energies
v. Publication from Chapter 3 work

Chapter 4 – Theoretical effect of structural modification of amidoamines on rhodium extraction

i. Outputs from Gaussian calculations
ii. Record of structures, their energies, and calculations of the formation energies

Chapter 6 – Modes of action in gold chloridometalate extraction

i. Protonation site modelling outputs
ii. Simulation list
iii. Example input and data files
iv. Parameter list
v. Record of log file data
vi. Example analysis scripts
vii. Analysis plots for all simulations
viii. Coordination shell data
ix. Porosity data
x. Project student reports

Abbreviations

δ	chemical shift
°C	degree centigrade
°	degrees
<	less than
≤	less than or equal to
>	greater than
≥	greater than or equal to
%	percent
~	approximately
[x]	Concentration of x
Å	angstrom
AIST	National Institute of Advanced Industrial Science and Technology
APT	atomic polar tensor
ATR	attenuated total reflectance
aq.	aqueous
anal.	analysis
br	broad (spectroscopy)
calc.	calculated
$CDCl_3$	deuterated chloroform
D	distribution coefficient
d	doublet (NMR)
DBC	dibutyl carbitol
DCM	dichloromethane
DFT	Density Functional Theory
DZ	double zeta
e.g.	for example
ESI	electrospray ionisation (MS)
ESP	electrostatic potential
et al.	et alli (and others)
etc.	et cetera
EXAFS	Extended X-Ray Absorption Fine Structure
fac	facial (isomer)
FID	free induction decay
FT	Fourier Transform
g	gram
g L^{-1}	grams per litre
HCl	hydrochloric acid
HF	Hartree Fock
HPLC	high performance liquid chromatography
ICP-OES	inductively coupled plasma optical emission spectroscopy
ICR	ion cyclotron resonance (MS)
i.e.	that is
in situ	in the natural place
in vacuo	under vacuum
IR	infrared
K	Kelvin
kcal mol^{-1}	kilocalories per mole
KF	Karl Fischer (titration)
kJ mol^{-1}	kilojoules per mole
L	ligand/extractant, litre
m	multiplet (NMR), milli, metre
M	molar (moles per litre), metal
MD	molecular dynamics
Me	methyl
mer	meridional (isomer)
MHz	mega hertz)
mg	milligram
Min	minute
mL	millilitre
mmol	millimole
mol	mole
mol L^{-1}	mole per litre
MIBK	methyl iosbutyl ketone
MS	mass spectrometry
m/z	mass to charge ratio
NMR	nuclear magnetic resonance
org.	organic
PES	potential energy surface
PGMs	platinum group metals
pH	$-\log_{10}[H^+]$
PLS	pregnant leach solution
PM	precious metal
ppm	parts per million
q	quartet (NMR)
QM	quantum mechanical, quantum mechanics
RF	radio frequency
s	singlet (NMR)
SANS	small angle neutron scattering
SAXS	small angle X-ray scattering
SCF	self-consistent field
SI	supporting information
SX	solvent extraction
t	triplet (NMR)
t	tertiary
T	temperature
tert	tertiary
TBP	Tributyl phosphate
TOA	trioctylamine
TZ	triple zeta
UoE	University of Edinbrugh
UV-vis	ultraviolet-visible
via	by way of
vol.	volume
vs.	versus
wt	weight
XAS	X-ray absorption spectroscopy
XANES	X-ray absorption near edge structure
Z	charge

Chapter 1

Introduction

1 Introduction

1.1 Overview

Metals are integrated into almost all aspects of our lives: from trading and currency to technology, transport, infrastructure, jewellery, chemical production and medicine. Demand is only set to rise, especially with the increased use of alternative energy technologies, such as solar power and batteries.[1, 2] Some metals, including the platinum group metals and the rare earths, are found on the European Commission's list of Critical Raw Materials.[3] Metals can be recovered from their ores or recycled from, for example, waste electronics. Owing to high demand and decreasing natural resources,[4, 5] the latter is of particular interest,[6] with current recycling rates estimated to be above 50% for the platinum group metals.[7]

For recovery to be possible, processes are required for metal extraction from the source material and separation from other metals. Continued research in this area is key. Although there are efficient methods currently in use, the source material is changing, with ores of decreasing metal content[4] and increasingly complex recyclables.[8] In addition, there is the ever more important need for "greener" processes. Improving existing or developing new methods is made easier when there is a fundamental understanding of how the current methods work, information which is often lacking in large-scale chemical separations processes. This work investigates rhodium and gold recovery via hydrometallurgical solvent extraction, both to understand existing methods and to explore improved or new reagents, using experimental and computational techniques.

Rh is currently not recovered via solvent extraction industrially as its complex speciation in aqueous chloride solution, together with its high ionic charge, render it a difficult process. Thus Rh is recovered last in precious metal separation, via precipitation, and has the highest global warming potential and pollution metrics of all elements mined from virgin ores.[9] However, promising new reagents have been reported in the literature. This work aims to fully characterise their extraction mechanism using a combination of experimental analysis and computational modelling. In addition, possible reagent modifications and potential new extractants are explored. In contrast, because of its simplistic speciation in chloride solution, and low ionic charge, Au is one of the easiest precious metals to recover using solvent extraction, and this is well established in industry. However, as recovery is straightforward

and the reagents have been in use for a long time, building a complete understanding of the reagent mode of extraction has been neglected. This means that any improvements to the extraction process or any development of new reagents must be based on trial-and-error rather than design. This work aims to use computational modelling to elucidate the mode(s) of action of an industrial Au extractant. This introductory chapter presents a summary of the extraction processes used, the metals this work focuses on, and the specific aims of the thesis.

1.2 Extractive metallurgy

Extractive metallurgy is the process of removing metals from a source mixture, such as ores or waste electronics. There are two main branches: pyrometallurgy and hydrometallurgy, with the work in this thesis concerning the latter. Pyrometallurgy, which utilises heat as the means of extracting metals, was used traditionally[10] and is still in use to this day. It is a very effective technique but it is energy intensive, polluting, and requires the use of ores or secondary metal sources containing relatively high concentrations of the desired metal.[11] Hydrometallurgy uses solution chemistry to extract metals, usually at ambient temperatures. It can be used with sources containing a lower concentration of metal[11] and is efficient, provided that appropriate technology is available and reagent recycling is maximised. Both techniques find their place in current metal recovery processes, sometimes in conjunction with one another; in precious metal recovery, it is typical for the metal source to be first treated by pyrometallurgy, to remove non-metallic material and certain metals, before the "concentrate" generated is processed further using hydrometallurgy.[12]

1.3 Hydrometallurgy

Hydrometallurgy processes, which involve treating the metal source with solutions, follow the general scheme shown in Figure 1.1. In the first step, leaching, an acidic or basic aqueous solution is used to dissolve the metals from their source. As the leaching process dissolves many metals and other species, a technique must be used to separate out the desired metal. In addition, the concentration of metal in solution must be increased. There are several options for the separation and concentration step: for example, solvent extraction (SX), ion

exchange or precipitation.[13, 14] Once separation and concentration has occurred, the metal must be reduced to its zero-oxidation state. This is usually achieved via electrowinning but can also be done by reductive precipitation.

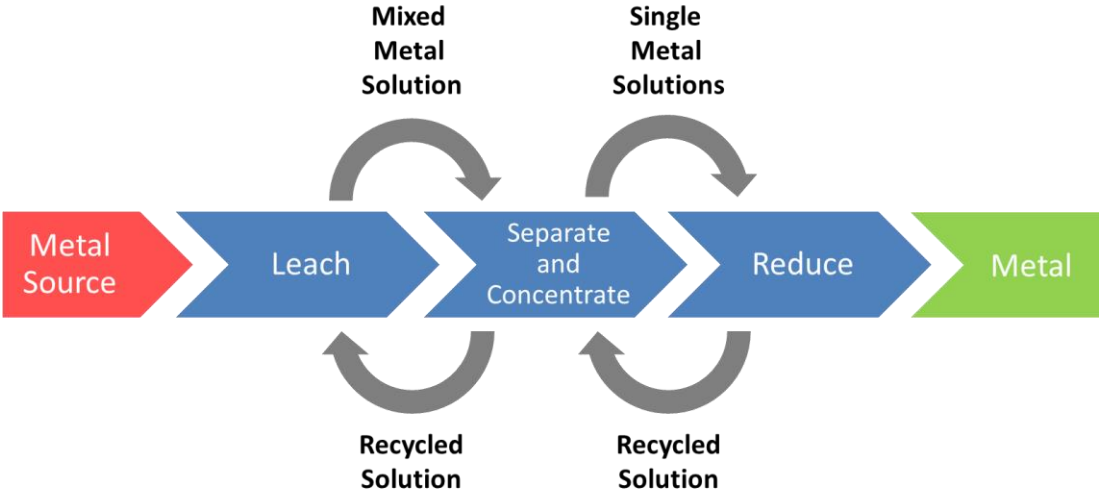

Figure 1.1. A general hydrometallurgical flow sheet.[15]

1.4 Solvent extraction

The focus of this thesis is the SX method of metal separation. It was developed during the Second World War, as part of the Manhattan Project, for the recovery of uranium,[16] and this was then extended to the separation of uranium and plutonium from nuclear waste.[16] However, since then, with the development of suitable extractants, the use of SX in hydrometallurgy has greatly expanded. It can now be used in the recovery of a wide range of metals, including the rare earth elements, platinum group metals and a variety of base metals, in particular copper, for which more than 20% of global recovery utilises SX.[17, 18]

SX works by exploiting the difference in solubility of species in different solvents. The metal-containing leach solution is treated with a water-immiscible organic solution containing extractant molecules, which have particular affinity for the desired metal. Extractants have hydrophobic groups and upon selectively binding to the desired metal transport it into the organic phase, leaving other species remaining in the aqueous phase. The so-called loaded organic phase is contacted with an aqueous solution to strip, or back-extract, the metal from the extractant molecules. The aqueous strip solution containing only the desired metal is

taken forward for reduction and the organic phase containing the extractant is recycled for use in further extraction. The various steps for the SX process are outlined in Figure 1.2.

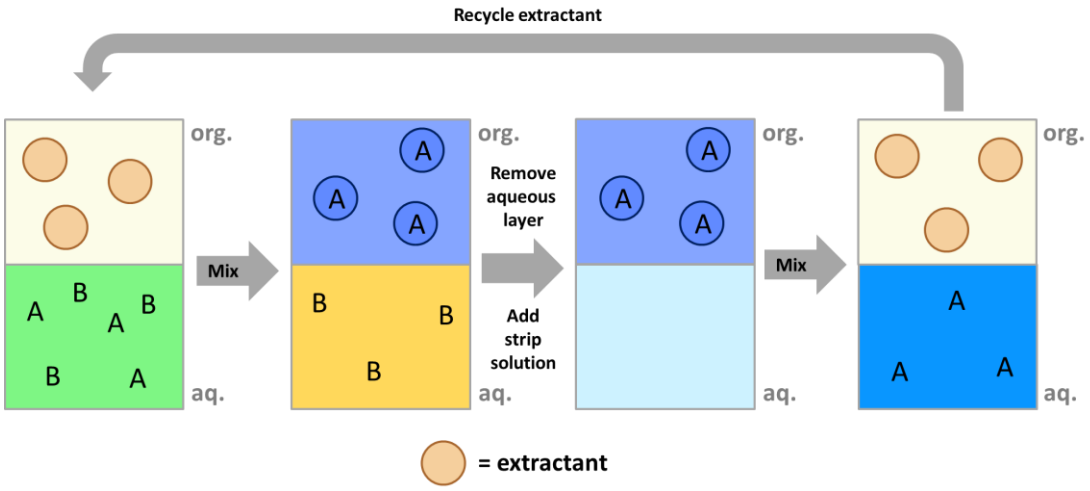

Figure 1.2. A schematic diagram of a SX process.

There are three classes of SX, based on the metal species extracted. These are cation extraction, anion or metalate extraction, and metal-salt extraction.[18] As a result of this and the variety in extractants available, there is more than one mechanism by which extraction (i.e. reagent association with the metal species) can occur. The mode by which the extractant works depends on a mixture of factors, including the nature of the extractant used, the metal species which is targeted, the source aqueous solution, and the choice of organic solvent.

1.4.1 Cation extraction

Cation extraction typically uses acidic extractants which can deprotonate to form negatively charged ligands that are capable of extracting metal cations. They form an overall neutral complex with the metal cation which is soluble in the organic phase (Equation 1.1).

$$M^{n+}_{(aq)} + nHL_{(org)} \rightleftharpoons ML_{n\,(org)} + nH^{+}_{(aq)} \qquad \textbf{1.1}$$

Cation extraction is a "pH-swing" process, meaning that the loading (extraction into the organic phase) and stripping (back-extraction into an aqueous phase) of the metal cation can be controlled by altering the pH, and so shifting the equilibrium (see Equation 1.1).[18]

Typically inner-sphere coordination (see Figure 1.3) occurs between the ligand and the metal cation, though secondary outer-sphere bonding can sometimes occur between ligands and may strengthen extraction.[15, 18] Figure 1.4 presents an example of copper cation extraction with phenolic oxime inner-sphere coordinating extractants. Here outer-sphere intra-ligand hydrogen bonding sets up a "pseudo-macrocyclic" extractant structure. The stability of the complex, and hence the extractant strength, can be further reinforced through hydrogen bond "buttressing", enacted through changing substituents on the phenolic ring.[19]

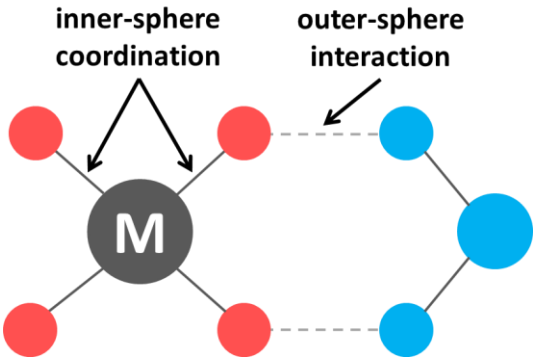

Figure 1.3. Illustration of inner-sphere vs outer-sphere coordination to a metal centre.

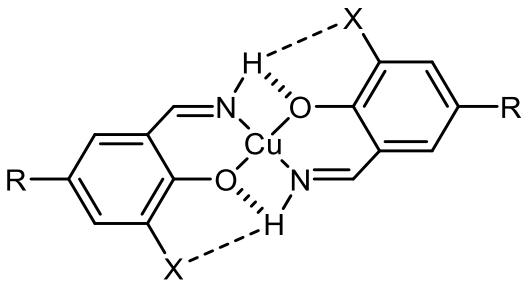

Figure 1.4. Illustration of the pseudo-macrocyclic nature of phenolic oxime extractants in the extraction of copper cations, and the additional "buttressing" interactions possible, depending on the nature of group X. Inner-sphere binding occurs to the cation and outer-sphere interactions occur between the extractants.[19]

1.4.2 Anion extraction

In anion extraction the reagents are usually basic and protonate to form positively charged extractant molecules, which are then capable of extracting metalate anions. As with cation extraction, an overall neutral species is formed and is soluble in the organic phase (Equation 1.2).

$$[MX_m]^{n-}{}_{(aq)} + nL_{(org)} + nH^+{}_{(aq)} \rightleftharpoons MX_m{\cdot}(LH)_{n\ (org)} \quad \textbf{1.2}$$

Metalate extraction is a pH- or anion-swing process. If the extractant is protonatable, the pH is altered to push the equilibrium to loading or stripping, i.e. pH-swing (see Equation 1.2). If the extractant carries a permanent positive charge and, upon extraction, exchanges its counter-anion for the metalate, then changing the concentration of the counter-anion in the aqueous phase will alter the position of the equilibrium, i.e. anion-swing, and therefore influence metal transport (see Equation 1.3.).[15, 18]

$$[MX_m]^{n-}{}_{(aq)} + nL^+Y^-{}_{(org)} \rightleftharpoons MX_m{\cdot}L_{n\ (org)} + nY^-{}_{(aq)} \quad \textbf{1.3}$$

Extraction can also be considered an anion-swing process from the point of view of the anions required to generate the metalate anion (see Equation 1.4.), but in this instance increasing the concentration of the anion in the aqueous phase will have the opposite effect on the position of the equilibrium. In theory, increasing the anion concentration should increase extraction, as the increased concentration promotes metalate formation. However, in practice, often the anion competes with the metalate anion for extraction, and so there is an ideal anion concentration, where formation of the metalate anion is maximised without the anion out-competing the metalate anion for extraction.

$$M^{m+}{}_{(aq)} + nX^-{}_{(aq)} \rightleftharpoons [MX_n]^{(n-m)-}{}_{(aq)} \quad \textbf{1.4}$$

The metalate anion has ligands bound in the inner coordination sphere, therefore the extractant must usually bind in the outer-sphere (see Figure 1.3). This results in a so-called ion-pair, or ion associate, mode of extraction,[15, 18] such as reported by Warr et al. for platinum chloridometalates (see Figure 1.5).[20]

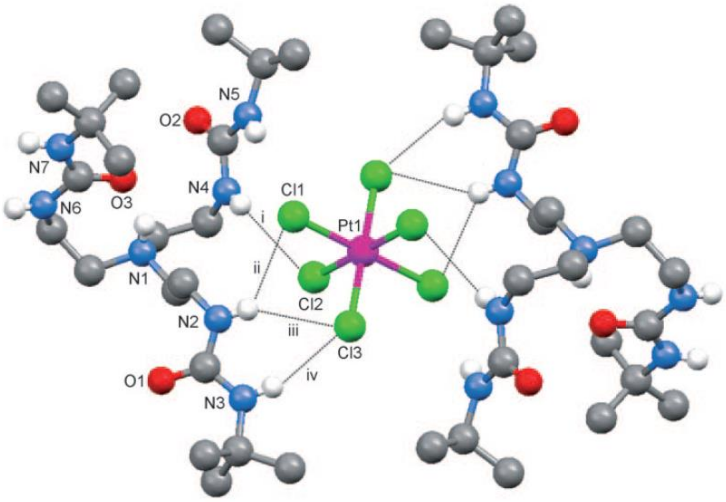

Figure 1.5. Ion-"pair", or ion-associate, of form $[(LH)_2PtCl_6]$ for hexachloroplatinate with tripodal amidoamines. Reproduced from Warr et al.[20]

1.4.3 Metal-salt extraction

Metal-salt extraction involves using neutral extractants to extract neutral metal salts. The extractant "solvates" the metal salt, rendering it soluble in the organic phase (see Equation 1.5).

$$M^{n+}_{(aq)} + nX^{-}_{(aq)} + yL_{(org)} \rightleftharpoons MX_nL_{y\,(org)} \qquad \textbf{1.5}$$

Metal salt extraction is an anion-swing process, in that increasing the concentration of the anion in the aqueous phase will favour formation of the metal salt and its loading into the organic phase, while decreasing the concentration of the anion will favour stripping.[18]

Coordination may occur in the inner and/or outer-sphere in metal salt extraction. For example, Burns et al. report a crystal structure of $[UO_2(NO_3)_2(\text{iso-TBP})_2]$, analogous to the use of tri-*n*-butyl phosphate (TBP) to extract uranyl cations from nitrate solutions, where both the extractant and the charge-balancing nitrate anions are bound in the inner-sphere (see Figure 1.6).[21]

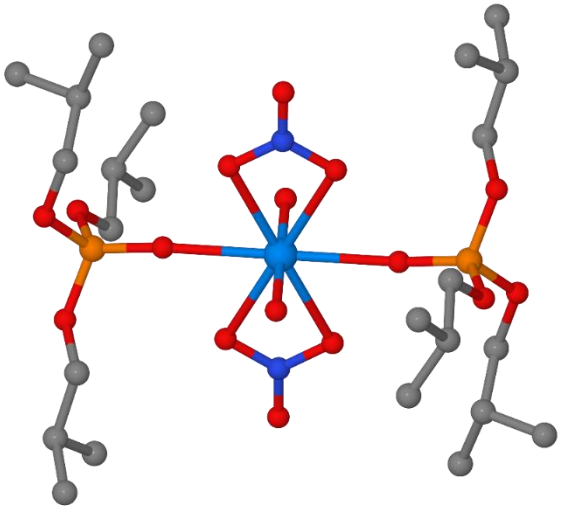

Figure 1.6. Assembly of $[UO_2(NO_3)_2(iso\text{-}TBP)_2]$ (structure from single crystal X-ray diffraction, hydrogens not shown) reported by Burns et al.[21]

1.4.4 Synergistic extraction

Synergistic extraction applies to SX where more than one extractant is used, and the combination of these reagents improves the extraction beyond that which would be seen when used individually.[18] A common synergistic combination in cation extraction is to use a charged cation extractant along with an additional solvating extractant. One or both of the extractants will bind in the inner-sphere.[18, 22, 23] Figure 1.7 illustrates an example from the work of Barnard et al. where both reagents bind in the inner-sphere to the metal centre, and the overall complex is stabilised by outer-sphere hydrogen bonds between the synergistic ligands.[22] If only one binds in the inner-sphere, the other will associate via outer-sphere interactions, as in the example from the work of Roebuck et al. shown in Figure 1.8. Note both examples show the coordination complexes formed using analogous (shorter R-groups/less "greasy") reagents to those used in the SX experiments, in order to facilitate growth of single-crystals suitable for analysis by X-ray diffraction.[23]

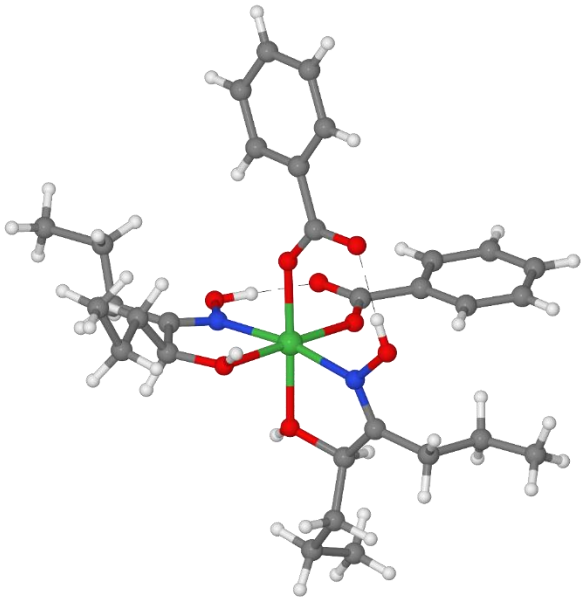

Figure 1.7. Nickel(II) complex (X-ray crystal structure) with 5-(hydroxyimino)octan-4-ol and benzoate obtained by Barnard et al.[22] Ligands here are analogous to those used in extraction (which have different R-groups).

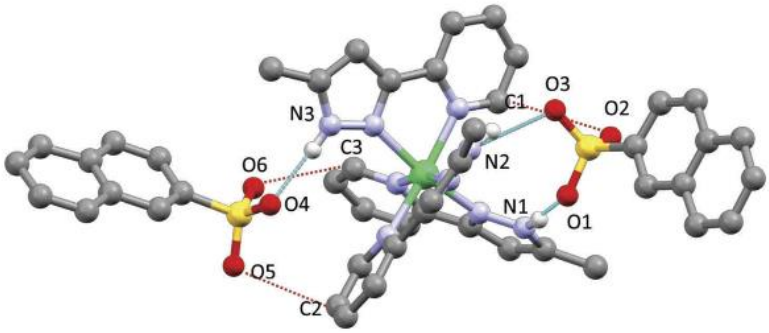

Figure 1.8. Nickel(II) complex (X-ray crystal structure, hydrogen atoms not shown unless involved in a H-bond) with inner-sphere bidentate pyridine-pyrazole ligands and outer-sphere 2-naphthalene sulfonate anions (blue lines showing the three pyrazole NH···O sulfonate H-bonds and red lines showing the three pyridine CH···O contacts). Ligands here are analogous to those used in extraction (which have different R-groups). Reproduced from Roebuck et al.[23]

1.4.5 Reverse-micelle formation

In some cases, the metal species is not fully desolvated on extraction. Instead, the extractants form a reverse micelle with the partially or fully hydrated metal species.

A micelle is formed when molecules with both hydrophilic head-groups and hydrophobic tails (i.e. surfactant-type molecules) arrange to form an assembly with the hydrophobic tails oriented inwards and the hydrophilic head groups pointed outwards to maximise favourable interactions in polar solvents. In the case of reverse-micelles, the opposite orientation is adopted (as shown in Figure 1.9) due to the use of non-polar solvent, and hydrophilic material (such as the hydrated metal species) can be encapsulated.[18] An example of this type of mode of action was reported in the extraction of lanthanides with malonamides by Ellis et al.[24]

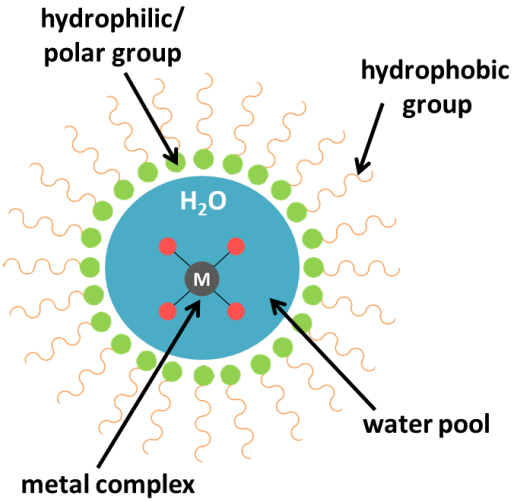

Figure 1.9. Structure of a reverse micelle containing a hydrated metal complex.

1.5 Precious metal solvent extraction

For the precious metals (PMs) SX can be an efficient, effective recovery method. Compared to traditional precipitation methods it requires fewer steps to yield metals of the desired purity; thus the process takes less time and requires less reagent.[16] Concentrated HCl solution and Cl_2 gas are often used as the leaching agents, meaning the metals are present as the chloridometalate, $[MCl_y]^{x-}$; *aquo*-chloridometalate, $[MCl_y(H_2O)_z]^{x-}$; oxo-chloridometalate, $[MOCl_y]^{x-}$; or *aquo*-oxo-chloridometalate, $[MOCl_y(H_2O)_z]^{x-}$, species. Many PMs can exist as more than one metalate species. This can prove very advantageous to achieving separation

if the species present can be easily altered by changing the oxidation potential, but can render extraction difficult if one oxidation state of the metal can exist as multiple species. Table 1.1 gives the common metalate species of the PMs, along with the oxidation state of the metal in that species. The PM metalates are mostly extracted via outer-sphere association of the extractant molecules as the ligand substitution rates are low for most oxidation states.[25]

Table 1.1. Common metalate species of the PMs in chloride solution.[16, 25]

Metal	Oxidation State	Common Metalate Species
Ag	I	$AgCl$, $[AgCl_2]^-$
Au	I	$[AuCl_2]^-$
	III	$[AuCl_4]^-$
Ir	III	$[IrCl_4(H_2O)_2]^-$, $[IrCl_5(H_2O)]^{2-}$, $[IrCl_6]^{3-}$
	IV	$[IrCl_6]^{2-}$
Os	III	$[OsCl_4(H_2O)_2]^-$, $[OsCl_5(H_2O)]^{2-}$, $[OsCl_6]^{3-}$
	IV	$[OsCl_6]^{2-}$
Rh	III	$RhCl_3(H_2O)_3$, $[RhCl_4(H_2O)_2]^-$, $[RhCl_5(H_2O)]^{2-}$, $[RhCl_6]^{3-}$
Ru	III	$RuCl_3(H_2O)_3$, $[RuCl_4(H_2O)_2]^-$, $[RuCl_5(H_2O)]^{2-}$, $[RuCl_6]^{3-}$
	IV	$[RuCl_6]^{2-}$, $[Ru_2OCl_8(H_2O)_2]^{2-}$, $[Ru_2OCl_{10}]^{4-}$
Pd	II	$[PdCl_4]^{2-}$
	IV	$[PdCl_6]^{2-}$
Pt	II	$[PtCl_4]^{2-}$
	IV	$[PtCl_6]^{2-}$

The solution speciation affects the order in which the PMs can be recovered in separation processes, due to the different solvation energies of the PM metalates. The Hofmeister bias stipulates it is more difficult to extract small, highly charged ions,[18] as it takes more energy to displace the solvating water molecules. Similarly, it is more difficult to extract species containing *aquo* ligands, which can hydrogen bond with the solvation shell. The general relative ease of extraction for many of the different anion species that form is as follows:

$$[MCl_4]^- >> [MCl_6]^{2-} >> [MCl_6]^{3-} \approx [M_2OCl_{10}]^{4-}$$

$$[MCl_6]^{2-} > [MCl_4]^{2-}$$

$$[MCl_6]^{2-} >> [MCl_5(H_2O)]^{2-}$$

As a result of the Hofmeister bias and the speciation of Au and Rh in chloride solution, these metals are recovered at very different stages of an industrial flowsheet, an example of which is shown in Figure 1.10. Au, which is present as $[AuCl_4]^-$ under the conditions typically used in PM SX, is one of the easiest to recover and is separated early on. On the other hand, Rh,

which is present as a mixture of $[RhCl_4(H_2O)_2]^-$, $[RhCl_5(H_2O)]^{2-}$ and $[RhCl_6]^{3-}$ under typical conditions, is the hardest to recover because it exists as a mixture of species, all of which are either highly charged, aquated or a mixture of both. It is therefore recovered last in most industrial flowsheets, and by precipitation instead of solvent extraction. Understanding how the industrial extractants for Au operate, along with potential new SX extractants for Rh, form the central two research themes in this thesis.

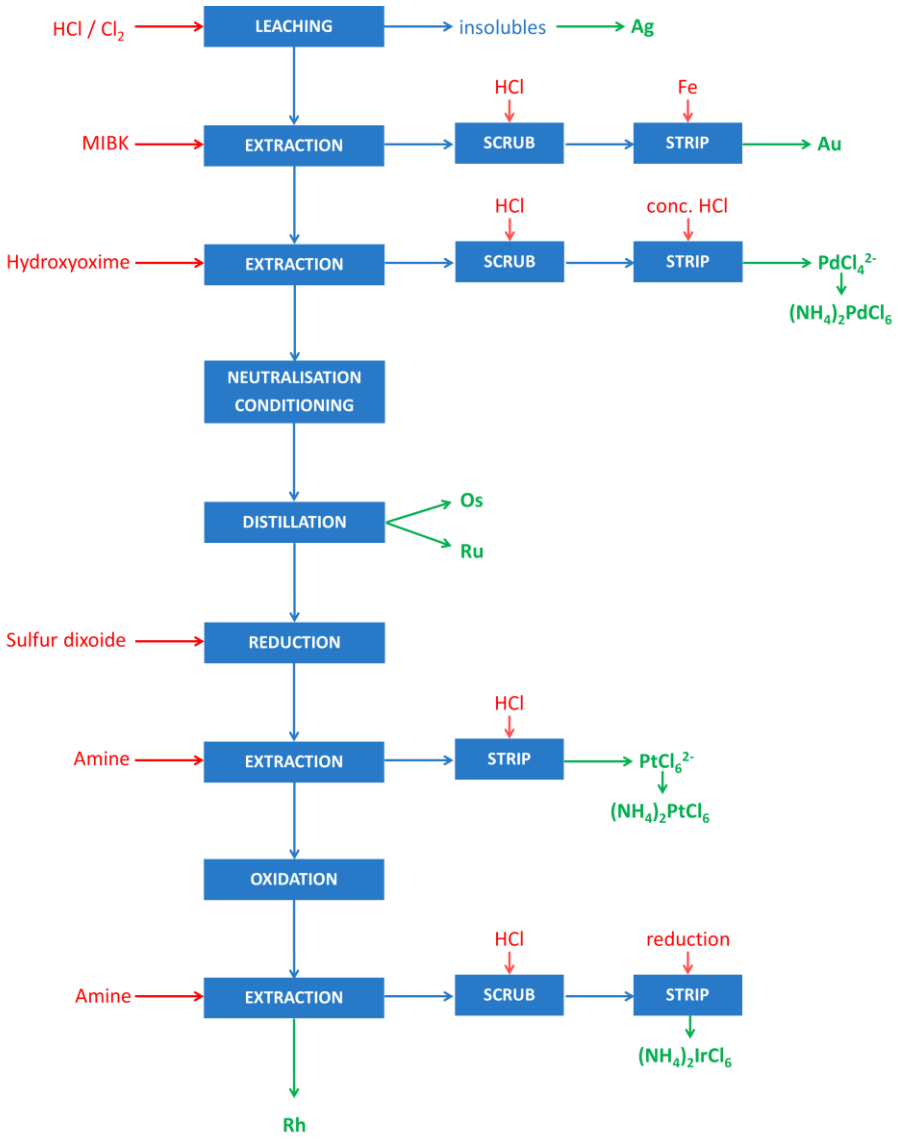

Figure 1.10. Matthey Rustenberg Refiners flowsheet for extraction and separation of PMs.[16]

1.5.1 Gold

Gold is a relatively rare metal with key properties, such as excellent electrical conductivity, chemical inertness, unusual colour and medicinal properties, which have led to its use in electronics, investment, jewellery and medicine.

Gold is most commonly recovered via cyanide leaching, but this is hazardous to human and animal health due to the toxicity of cyanide.[26] It can also be halide leached, with chloride leaching utilised in recovery from ore-material pre-treated by pyrometallurgy or from secondary sources.[12, 27] As discussed above, from chloride leach solutions, it is normally recovered as $[AuCl_4]^-$ by SX.

Commercial reagents for recovery via SX from chloride solution include dibutylcarbitol (DBC), used by INCO, and methyl isobutyl ketone (MIBK), used by JM.[16] In addition, long chain alcohols such as iso-decanol[16] and 2-ethylhexanol[28, 29] have also been proposed (see Figure 1.11).

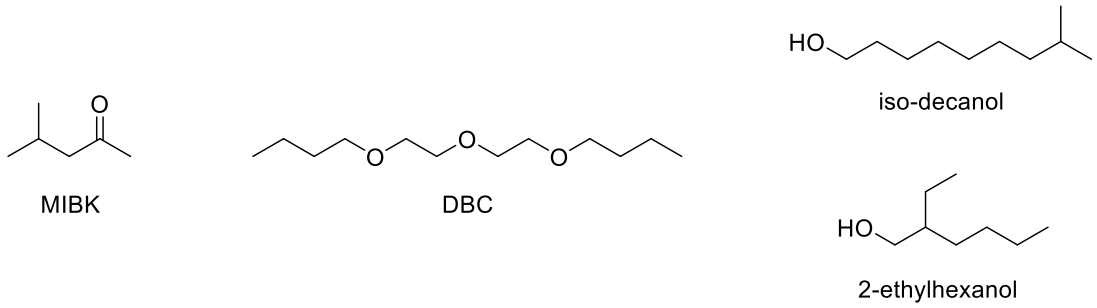

Figure 1.11. Structures of MIBK, DBC, iso-decanol and 2-ethylhexanol.

DBC displays high selectivity for gold and any co-extracted metals can be selectively stripped with dilute HCl, but the extraction kinetics are slow.[16] MIBK offers the advantage to the overall SX flowsheet of removing some base metals along with Au.[16] However, this is because it is less selective for Au than DBC is, meaning impurities are harder to remove. For both DBC and MIBK processes, Au is subsequently recovered by direct reductive precipitation to the zero-oxidation state metal as the metalate anion is very difficult to back-extract.[16] 2-ethylhexanol is a weaker extractant for Au, though stronger than iso-decanol, but provides the benefit that stripping can be carried out with water.[28]

Although the SX of Au is performed commercially with MIBK and DBC, the current understanding of the extraction mode of action is incomplete. Kyriakakis reports that "solvents based on oxygenated organic groups such as polyethers, ketones and alcohols", i.e. DBC, MIBK and the alcohols, extract via the mechanism shown in Equations 1.6 and 1.7 (where waters of hydration (n=1-4) are omitted).[29] They also propose a structure of the ion-pair formed between $[AuCl_4]^-$ and protonated DBC (as shown in Figure 1.12), though they state that the proton would likely be hydrated. However, the placement and number of the "waters of hydration" is not discussed in detail.

$$R_2O_{(org)} + HCl_{(aq)} \rightleftharpoons [R_2O(H_3O)]^+ \cdot Cl^-_{(org)} \quad \textbf{1.6.}$$

$$[AuCl_4]^-_{(aq)} + [R_2O(H_3O)]^+ \cdot Cl^-_{(org)} \rightleftharpoons [R_2O(H_3O)]^+ \cdot [AuCl_4]^-_{(org)} + Cl^-_{(aq)} \quad \textbf{1.7.}$$

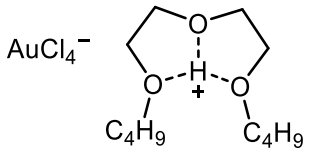

Figure 1.12. Model for the ion-pair formed from $[AuCl_4]^-$ and protonated DBC.[29]

For DBC, Mironov finds that six water molecules are extracted for every molecule of $HAuCl_4$ and state that in the organic phase there exists "a set of species", based on H^+, $[AuCl_4]^-$, $HAuCl_4$, $(HAuCl_4)_2$, $[H(AuCl_4)_2]^-$, and $[H_2(AuCl_4)]^+$ with molecules of DBC and water.[30] With alcohols, Petrova et al. propose a $[(ROH)_n(H_2O)_m(H_3O)]^+ \cdot [AuCl_4]^-$ assembly in the organic phase, with slope analysis (based on the distribution ratio of metal in the organic and aqueous phase with respect to the concentration of extractant used, see Chapter 2 Section 2.2.1 for a full explanation) suggesting that n=1; m is undefined.[31]

Kargari et al. propose $[(MIBK)_4H]^+ \cdot [AuCl_4]^-$ as the assembly on extraction with MIBK,[32] while Nguyen et al. simply report $H^+[AuCl4]^-(MIBK)_m$.[33] Considering methylethyl ketone (MEK), Jordanov et al. proposed a $H^+(H_2O)_{3\text{-}14}(MEK)_7[AuCl_4]^-$ assembly.[34]

Thus, there is a lack of agreement on the number of extractant molecules and water molecules present in the organic phase assemblies and on if the charge balancing proton resides on an extractant molecule or on a water molecule.

Research has shown that Au(III) can be extracted from HCl solution by an extremely large variety of other reagents. The following is an extensive, but by no means exhaustive, list of reported reagents: other ketones[34, 35] and ethers,[36-39] alcohols,[31, 37] phosphinic[40, 41] and thiophosphinic[41-43] acids, phosphine sulfides[43-45] and oxides,[33, 41, 43, 46-51] phosphates,[33, 41, 50, 52-56] phospholene derivatives,[47, 57] a phosphonic acid ester,[41] a phosphoric acid,[41] phenolic-[58] and hydroxy-oximes,[41] amides[59-62] and thio-[63] and thiodiglycol-[64]amides, tertiary amines,[41, 65-68] ammonium salts[41, 67-73] and other ionic liquids,[71, 74-77] an ester alcohol,[78] thioureas,[79] aminophosphonates,[80] an aminoquinoline,[81] an aniline,[82] pyridine-[83] and thiopyridine-[84]based extractants, piperidine-based extractants,[85] N-(thiocarbamoyl)benzamidines,[86] 2-mercaptobenzimidazole,[87] ω-thiocaprolactam,[88] a quaternary ammonium type of calix[4]arene,[89] an amic acid,[90] a dithiocarbamate,[91] an amide oxide,[92] a cetyltrimethylammonium bromide/n-heptane/iso-amylalcohol/Na_2SO_3 micro-emulsion,[93] and even vacuum pump oil.[94]

For some of these literature reagents, characterisation of the mode of extraction and/or the extracted species has been carried out, though the extent of this varies depending on the reagent.

For extraction with TBP, the literature has reached more of a consensus than it has for MIBK and DBC, with Tocher et al., Sadeghi et al. and Tuck reporting that three TBP molecules are involved per gold metelate anion.[50, 53, 55] Sadeghi et al. and Tuck do not discuss the co-extraction of water, but Tocher et al. suggest that the organic phase assembly may be either of those shown in Figure 1.14.

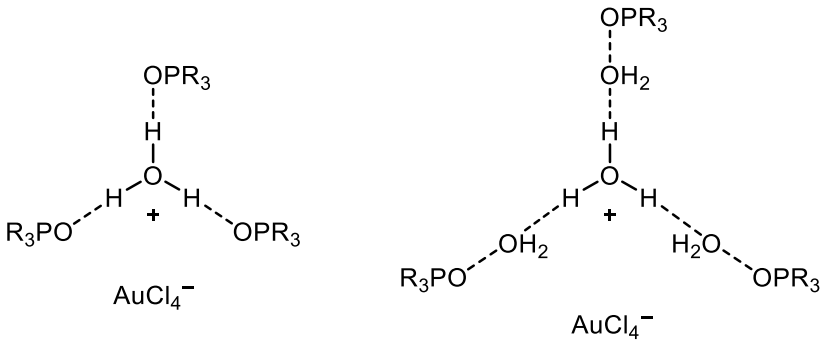

Figure 1.14. Models for the possible assemblies formed on extraction of $[AuCl_4]^-$ by TBP. Assembly of form $([H_3O]^+(3L)(y(H_2O)))\cdot[AuCl_4]^-$, where L=TBP and with $0 < y < 3$.[50]

Tocher et al. also propose the same extraction mechanism for trioctyl phosphine oxide.[50] However, both Aguacil et al.[49] and Barroso et al.[46] find a ratio of phosphine oxide (Cyanex reagents 923 and 925, respectively) to gold of 2:1, rather than 3:1, and Martinez et al. find a mix of 2:1 and 1:1 for both phosphine oxide (Cyanex 921)[48] and phosphine sulphide (Cyanex 471X)[45] extractants.

For extraction with amides, there is good agreement in the literature that the mode of extraction is based on the association of $[AuCl_4]^-$ with a protonated dimer of the amide extractant.[59, 60, 62] Narita et al. found evidence that the ratio of amide to gold was not always 2:1, however, with slope analysis suggesting 2:1 but the maximum loading of gold suggesting 5:4.[59] Doidge et al. found ratios of 2.5-3:1 from slope analysis, and ESI-MS (electrospray ionisation-mass spectrometry) analysis and MD simulations suggested that extraction was via formation of "clusters" based on $[AuCl_4]^-$ with a protonated dimer of amide but with additional amide molecules and $[AuCl_4]^-$ and H^+ ions.[60]

For phosphinic acids,[40, 41] amic acid,[90] hydroxy oxime,[41] polyoxyethylene nonyl phenyl ethers,[36] 2-mercaptobenzimidazole,[87] and vacuum pump oil[94] various ratios of extractant to $[AuCl_4]^-$ are found.

However, Nunez et al. and Domiguez et al. propose the presence of $AuCl_3$-based species in the organic phase, on extraction with ω-thiocaprolactam[88] and N-benzoyl-N',N'-diethylthiourea,[79] respectively, based on numerical analysis of the extraction data. The former did attempt fitting with $HAuCl_4$-based species and found only that that they did not "significantly improve" the fit of their model,[88] so it could be possible that a $HAuCl_4$-based species is present.

Ionic liquids, including salts of protonated amines, are found to extract almost exclusively via the anion exchange mechanism (given in Equation 1.3).[29, 65, 66, 68-70, 73-77, 93] When carried out, slope analysis of the extraction data often shows a 1:1 ratio of extractant to $[AuCl_4]^-$ in the organic phase. Zheng et al. also report UV-vis spectra which show the Au(III) speciation is the same in the organic phase as in the aqueous phase, consistent with an anion exchange process.[75]

An exception to this is the work on protic ionic liquids reported by Watanabe et al. They propose that the $AuCl_3$ species is present in the ionic liquid (organic) phase and that dimerization to Au_2Cl_6 occurs, based on equilibrium analysis.[71]

There is clearly a wide variety of modes of extraction expressed for Au(III), as well as a large selection of Au(III) extractants. In many cases, similar extraction mechanisms are found for extractants of a similar type. However, there is sometimes disagreement on the nature of the extracted species even within one class of extractants. This is particularly the case when the mode of action understanding is incomplete. For the industrial reagents, the extraction mechanism details are lacking, with the nature of the extracted assembly unclear. In order to be able to improve upon these extraction processes it would be helpful to have a complete picture of how these well-established but poorly understood reagents work.

1.5.2 Rhodium

Rhodium is a member of the platinum group metals (PGMs). It is an important, valuable metal, with its primary use in catalytic convertors in vehicle exhausts. It is also plated on jewellery and used for catalysis in the chemical industry.

Like other PGMs, Rh is typically recovered from ores or secondary sources by pyrometallurgy followed by hydrometallurgical processing. In the latter, the first step is dissolution of the PGM source, most commonly using hydrochloric acid under oxidising conditions. The particular challenges in selective Rh-recovery are associated with its speciation in HCl solution as it exists as chlorido- and *aquo*-chlorido Rh(III) complexes, $[RhCl_n(H_2O)_{6-n}]^{3-n}$, with the relative concentration depending on both the Rh(III) and chloride concentrations in solution. Whilst there are discrepancies in the speciation plots reported in the literature, there is general agreement that the degree of anation increases as the chloride concentration increases, such that at HCl concentrations around 1 M the majority of the Rh(III) exists as the $[RhCl_5(H_2O)]^{2-}$ complex, whilst at 6M HCl $[RhCl_6]^{3-}$ is the dominant species.[95] Geswindt et al.[96] worked towards producing a reliable speciation plot using NMR (nuclear magnetic resonance) spectroscopy and High Performance Liquid Chromatography (HPLC) analysis,[96] given in Figure 1.15, but it should be noted that this was done using higher concentrations of Rh(III) than much of the previous work using UV-vis spectroscopy,[95] and so the results may not be comparable.

Rh is not currently recovered by SX commercially. The high charge or presence of *aquo* ligands on the chloridometalate anions render the SX of Rh(III) from chloride solutions difficult (Hofmeister bias), hence it is recovered via ion exchange and precipitation methods.[12, 16] A selective SX solution for Rh, which would permit it to be recovered earlier in the flow sheet, is therefore highly desirable.

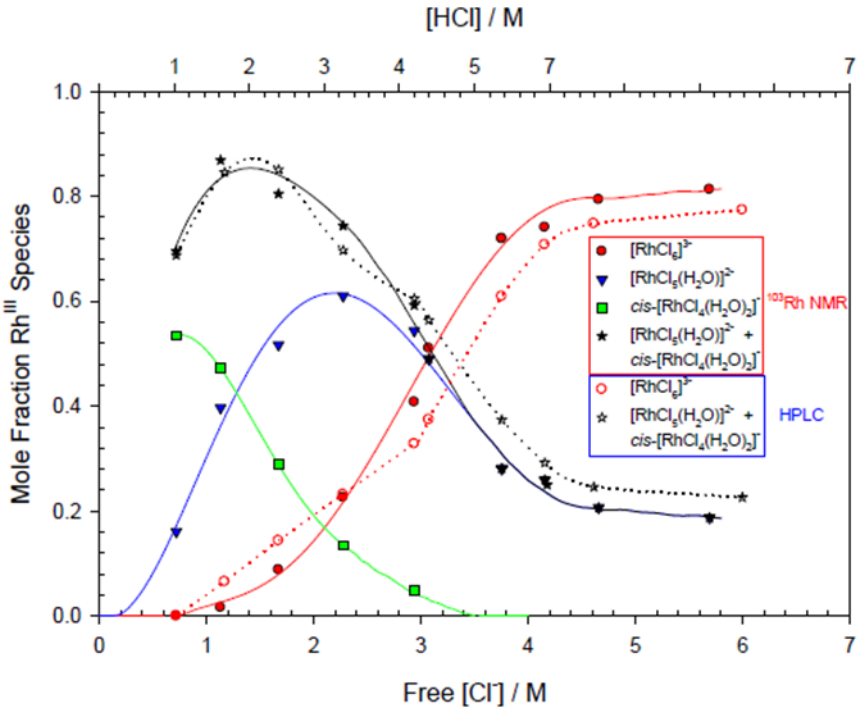

Figure 1.15. Speciation plot of Rh(III) in HCl (obtained using ^{103}Rh NMR and HPLC).[96]

SX of Rh from chloride media has been explored reasonably widely, but reports in the literature show limited success.[95] The most effective methods require the use of stannous chloride and can achieve 100% extraction.[97-106] $SnCl_2$ is added to the aqueous solution and substitution of the chloride or *aquo* ligands for $[SnCl_3]^-$ ligands occurs, with reduction of Rh(III) to Rh(I) and oxidation of Sn(II) to Sn(IV).[97] The Rh(I)-Sn(IV) metalate species is more easily extracted than the Rh(III) metalate species. The need to use stannous chloride, however, is undesirable due to its hazardous nature and the high ratio of Sn:Rh required (at least 2:1 but often much higher).[97-100]

Other alternative SX methods have included extracting from nitrate or mixed nitrate and chloride solutions,[95, 107] converting to and extracting more highly aquated species,[95, 108, 109] or

substituting the chloride ligands for others (such as SCN^-) and extracting the resulting species.[95, 110, 111]

Some more recent work on the SX of Rh(III) chlorido- and *aquo*-chloridometalate species from HCl solutions has proved very promising. Narita et al. have shown that *N*,*N*-disubstituted amide-containing tertiary amine (amidoamine) compounds can be used to achieve successful SX of Rh(III) (up to ~90%).[112, 113] Figure 1.16 gives the structure of the three extractants they tested and their extraction performance depending on the HCl concentration, alongside tri-*n*-octylamine (TOA) for comparison.

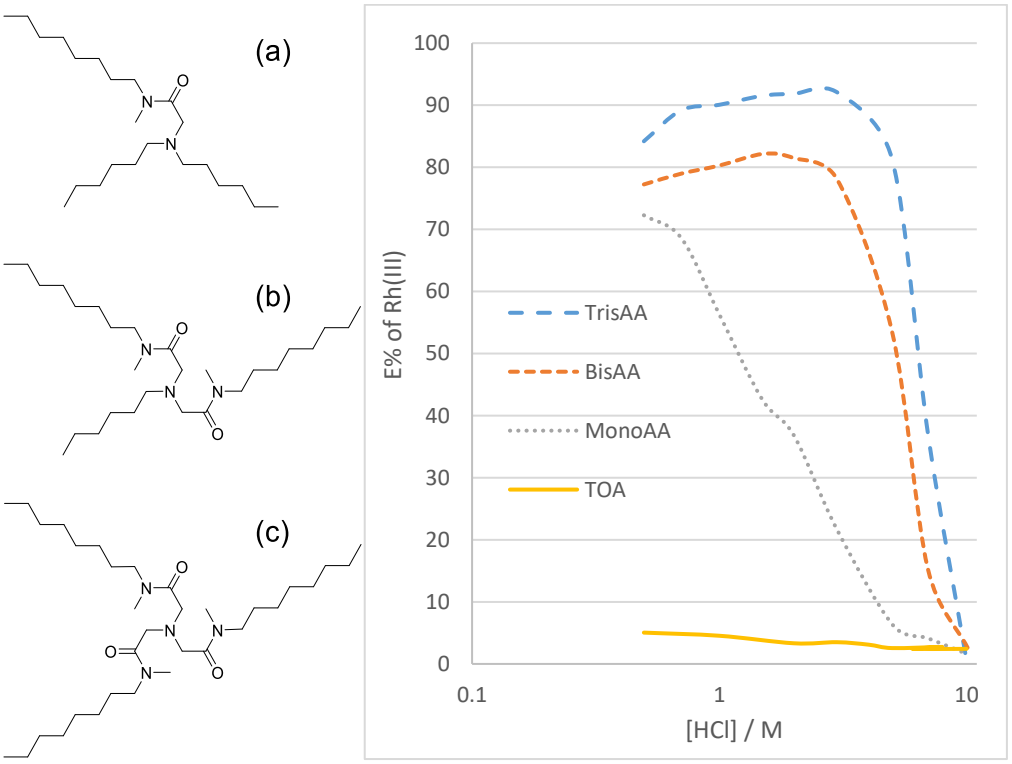

Figure 1.16. Amidoamine extractants used by Narita et al. for the SX of Rh, (A) – MonoAA, (B) – BisAA, and (C) – TrisAA, and their extraction performance.[113]

Rh is reported to be extracted as $[RhCl_5(H_2O)]^{2-}$ by two protonated amidoamine molecules, which are believed to associate in the outer-sphere. BisAA and TrisAA have different extraction profiles than MonoAA, and it is thought that some "additional effect which enhances the Rh(III) extraction efficiency is weak in the MonoAA system".[113] Although these extractants are not selective for Rh(III) over Pt(IV) and Pd(II), the Rh(III) metalate can be

selectively stripped (90%) with 10 M HCl. Unfortunately, Pd(II) and Pt(IV) are not easily stripped, with 10 M nitric acid required and recovery of only 80% and 40% achieved (for the BisAA system), respectively.[113]

Afzaletdinova et al. have also had success with amidoamine extractants. They showed that bisacylated triethylenetetramine (see Figure 1.17), in the dihydrochloride form, is capable of extracting Rh(III) from HCl solutions, and Rh(III) can be stripped (90%) with 9 M HCl.[114] Through a variety of different analyses, including elemental analysis, specific electrical conductivity measurement, NMR, and UV-vis and IR spectroscopy, they concluded that the $[RhCl_5(H_2O)]^{2-}$ species is extracted as a 1:1 ion-pair with protonated bisacylated triethylenetetramine.[114] The extractant's selectivity for Rh(III) over other PMs is not reported but it is likely, given the extractant is similar to that used by Narita et al.,[112] that it would not prove selective for Rh over others such as Pt and Pd.

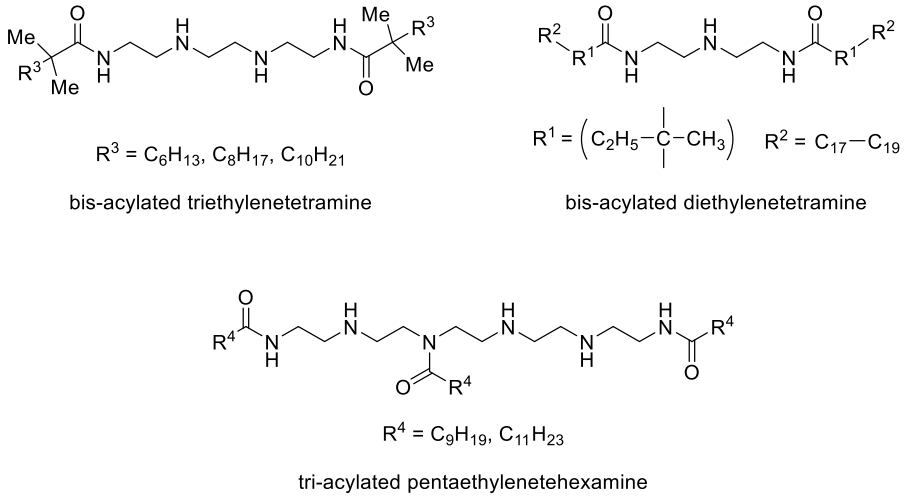

Figure 1.17. Amido-amine extractants used by Afzaletdinova and colleagues for the extraction of Rh from HCl solution.[114-116]

Afzaletdinova et al. also found that the trihydrochloride form of triacylated pentaethylenehexamine (see Figure 1.17) could extract Rh from aged HCl solutions as a dinuclear Rh(III) species. $[Rh_2Cl_9]^{3-}$ could be extracted as an ion associate (with $[LH_3]^{3+}$) if the extraction time was short, however, with longer contact times displacement of terminal chloride ligands could occur and the extracted species were $[LH_2]^{2+}\cdot[Rh_2Cl_8]^{2-}$ and $[LH]^{+}\cdot[Rh_2Cl_7]^{-}$.[115] Similarly, the extracted species changed with contact time when protonated bisacylated diethylenetriamine (see Figure 1.17) was used as the extractant from

non-aged HCl solutions.[116] With short contact times $[RhCl_5(H_2O)]^{2-}$ was found to be extracted as an ion associate with two protonated extractant ions, but with longer contact times chloride substitution for an amine N atom of an unprotonated extractant occurred and the extracted species was $[LH]^{+}\cdot[RhCl_4(H_2O)L]^{-}$.

Narita et al. have also demonstrated successful Rh(III) extraction with synergistic mixtures of TOA and sulphide-type extractants, achieving ~90% extraction with TOA and N,N'-dimethyl-N,N'-di-n-octyl-thiodiglycolamide.[117] Figure 1.18 gives the structure of the extractants they tested and their extraction performance alone and as synergistic mixtures depending on the HCl concentration.

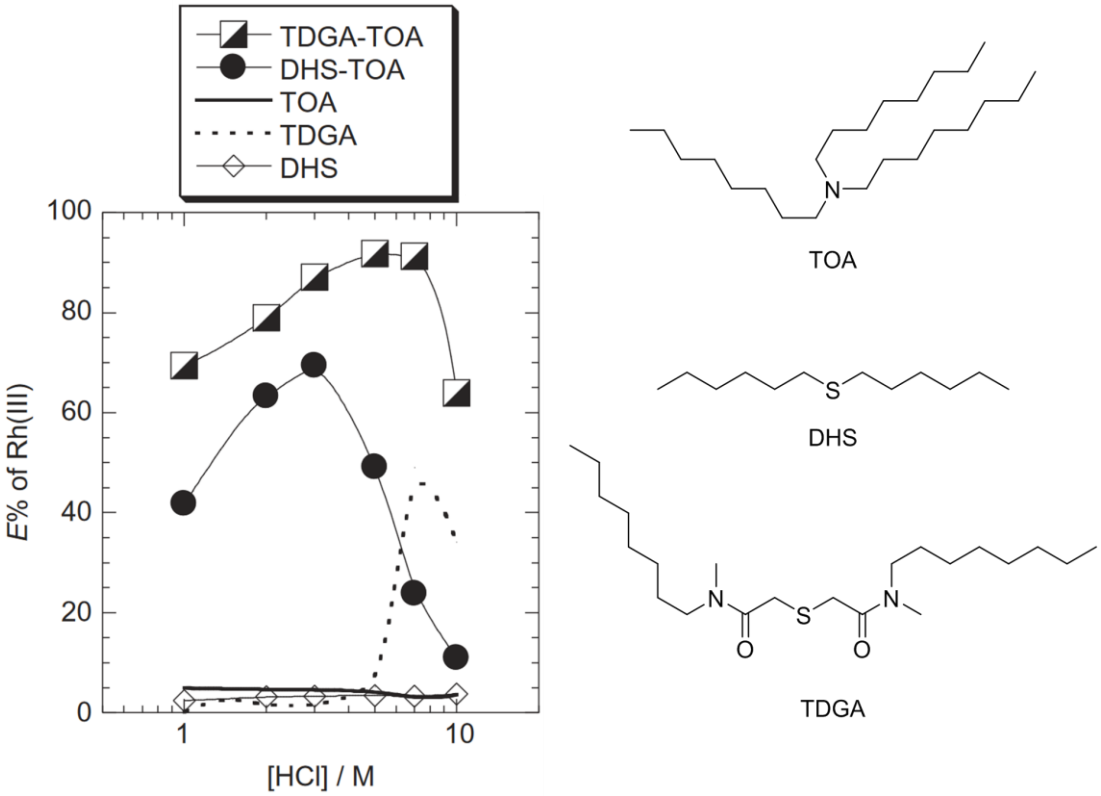

Figure 1.18. Extractants used by Narita et al. for the synergistic SX of Rh, TOA – tri-n-octylamine, DHS – di-n-hexyl sulfide, and TDGA – N,N'-dimethyl-N,N'-di-n-octyl-thiodiglycolamide, and their extraction performance synergistically and alone. Reproduced from Narita et al.[117]

Rh(III) is believed to be extracted through inner-sphere coordination of TDGA or DHS to the $[RhCl_5(H_2O)]^{2-}$ species, resulting in replacement of the *aquo* ligand, with two protonated TOA molecules associating in the outer-sphere and providing the charge balance.[117] At higher HCl concentrations, where TDGA is likely to be protonated, it is thought that extraction can occur

via a different mechanism and that $[RhCl_6]^{3-}$ may be extracted. Unfortunately, Rh(III) stripping is very difficult with these synergistic mixtures, with 10 M nitric acid only achieving 60% back-extraction for the DHS-TOA system and less than 5% for TDGA-TOA.[117] The increased binding strength due to the inner-sphere interactions likely contributes to the poor stripping performance.

Other systems have exploited inner-sphere binding to the Rh(III) centre. Bottorff et al. utilised a tridentate N and S donor ligand to extract Rh from chloride solutions, in the form of a *mer*-$[RhCl_3L]$ complex.[118] However, the kinetics of substitution on the Rh(III) were found to be slow, with low extraction obtained at room temperature, even over a period of seven days, and higher temperatures being required to achieve reasonable extraction,[118] suggesting that extraction systems which rely on large inner-sphere changes in coordination are non-ideal for Rh(III) SX.

More recently, successful Rh extraction from chloride solutions has been achieved with ionic liquid based extractants.[119, 120] Firmansyah et al. achieved Rh(III) extraction using neat phosphonium chloride based ionic liquids (see Figure 1.19).[119] Although stronger and faster extraction was achieved for Pt(IV) and Pd(II), good Rh(III) extraction of approximately 90% could be achieved within three hours at room temperature at a HCl concentration of ~0.5 M. On increasing the HCl concentration to 5 M HCl Rh(III) extraction decreased significantly and, thus, it was found that Rh(III) can be stripped reasonably well (~70%) from the loaded extractant solution by 5 M HCl solution. They report that, at low HCl concentrations, Rh(III) extraction proceeds via an anion exchange mechanism, with the $[RhCl_5]^{2-}$ dianion transported into the organic phase in exchange for two chloride anions (note that they report exchange of a $[RhCl_5]^{2-}$ species as opposed to $[RhCl_5(H_2O)]^{2-}$), and forming an ion-pair type structure with two phosphonium cations in the organic phase.[119]

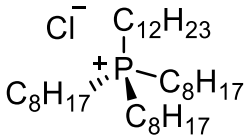

Trioctyl(dodecyl)phosphonium chloride

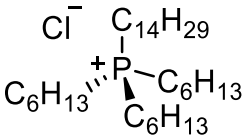

Trihexyl(tetradecyl)phosphonium chloride

Figure 1.19. Phosphonium chloride based ionic liquid extractants used by Firmansyah et al. for the extraction of Pt(IV), Pd(II) and Rh(III).[119]

Ma et al. used ionic liquids with amino moieties and the bis(trifluoromethylsulfonyl)imide counter anion for PGM extraction, obtaining up to ~70% extraction of Rh(III) at 3 M HCl, though the extraction of Pt(IV) and Pd(II) was superior.[120] The Rh(III) was able to be back-extracted well (~80%) by 8 M nitric acid or 1 wt% ammonia solution, with the ammonia solution being the preferred option as the extractant decomposed on contact with the nitric acid. As extraction of Rh(III) was lower at lower HCl concentrations, they concluded that the $[RhCl_6]^{3-}$ complex is extracted, and they determined from NMR and infrared (IR) spectra that an ion-pair, with no inner-sphere binding to the metal centre, is formed on extraction.[120]

The extraction modes occurring in these different systems varies widely, with different Rh species being extracted and different coordination modes occurring. In some cases, a full understanding of the mechanism of extraction occurring and/or the key interactions involved has not yet been fully developed. It is highly desirable to have this full understanding as it is crucial to the ability to design new extractants for Rh which do not have the drawbacks (e.g. no selectivity for Rh(III) over Pt(IV) and Pd(II), or difficult stripping of Rh(III), or Pt(IV) and Pd(II)) of these current most successful extractants, and would contribute towards the possibility of ultimately making commercial Rh SX feasible.

1.6 Determining mode of action

Determining the mode of action in SX proves challenging: SX is a solution phase process and, as a result, determination of the structure of the assemblies present in the organic phase is difficult.

Experimental techniques such as mass spectrometry, NMR spectroscopy, IR spectroscopy, small-angle neutron scattering (SANS) analysis, extended X-ray absorption fine structure (EXAFS) analysis and X-ray crystallography can all help to provide parts of the story. However, it is rare that any one technique can provide a definitive answer on what the extraction mechanism is alone. Instead, a suite of different analytical techniques must be employed and the results considered together and their limitations noted, e.g. MS may cause smaller assemblies to be observed due to fragmentation, solid state crystal structures may not be the same as the assemblies present in solution and IR spectroscopy may only provide information on the major species in solution. Computational modelling can be used to aid

mode of action understanding because it allows for the assemblies formed to be visualised at the molecular level and for the interactions occurring between components of the assembly to be explored.

There are varied examples in the literature of differing suites of analytical methods, the use of computational modelling, and the combination of both experiment and simulation.

Dourdain and colleagues have used multiple experimental analysis techniques in their work, such as IR spectroscopy (see Figure 1.20 for the spectra obtained, showing clear differences in the C=O region depending on if Nd(III) is present or not) and small angle X-ray scattering (SAXS) analysis in the extraction of palladium and neodymium from nitrate solution by alkyl- and perfluoroalkyl-substituted malonamides,[121] and dynamic and static light scattering and SAXS in the extraction of acids by an oxy-malonamide.[122] In addition, in the synergistic extraction of uranium[123, 124] and iron[123] from phosphoric acid by the combination of an organo-phosphoric acid and trioctylphosphine oxide, SAXS and SANS analysis,[123, 124] and static and dynamic light scattering and tensiometry were performed;[123] and in the synergistic extraction of europium and nitric acid by the combination of an oxy-malonamide and an organo-phosphoric acid, ESI-mass spectrometry and tensiometry were employed.[125]

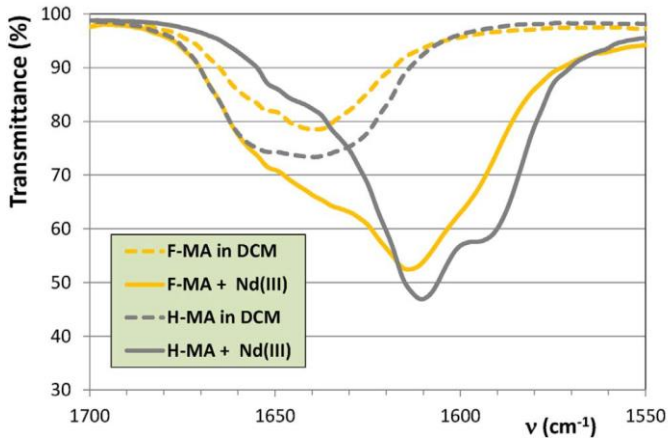

Figure 1.20. IR spectra of the organic phases containing extractant (perfluoroalkyl-substituted malonamide, F-MA, or alkyl-substituted malonamides, H-MA) with and without Nd(III). Reproduced from Dul et al.[121]

Antonio et al. have also used a range of experimental analysis techniques. In their initial work on understanding the assemblies formed in both the organic phase and the third phase (an additional phase which formed upon extraction) in the extraction of cerium from nitric acid

by TBP, extraction testing and phase composition determination (including Karl Fischer titrations for water content) and IR spectroscopy were carried out.[126] In their further investigations of this curious system a combination of voltammetry, X-ray absorption near edge structure (XANES), EXAFS and SAXS were used, allowing models for the assemblies (found to be reverse-micelles and aggregates of them) in the organic and third phases to be determined.[127] Ellis et al. also used SAXS and EXAFS to explore the structure of reverse-micelle aggregates formed in the extraction of europium from nitric acid solutions by a mixture of an organo-phosphoric acid and a diglycolamide, elucidating a switch in which reagent dominated at binding the Eu(III) cation depending on the acid concentration.[128]

Calculations, both quantum mechanical (QM) and classical, have been used in SX mode of action determination previously. Yoshizuka covered the advances in computational simulation applied to SX in 2004,[129] and Qi et al. discussed the use of density functional theory (DFT) calculations of metal complex structures, though not specifically for SX, in 2016.[130] Wipff and colleagues have used computational analysis extensively, for studies on the extraction of alkali metals,[131] lanthanides,[132] the uranyl cation, $[UO_2]^{2+}$,[133-135] and acids[136] and ammonium.[137] These have included molecular dynamics (MD) simulations of both the aqueous and organic phases together,[131-137] to incorporate the interface (see Figure 1.21 for an example from their work on ammonium complexation by 18-crown-6)[137], potential mean force simulations,[131-134, 137] and DFT calculations.[135] The computational work is accompanied by experimental analysis,[136] or the results are compared to existing experimental data.[131-135, 137] Chen et al. explored the stability of reverse micelles in lanthanide extraction by a malonamide extractant using classical MD and potentials of mean force simulations and compared the results to existing experimental data.[138] Some earlier computational studies, particularly of the extraction of alkali metal cations, lanthanides and the $[UO_2]^{2+}$ cation, are outlined in the 2007 article by Uezu and Yoshizuka.[139]

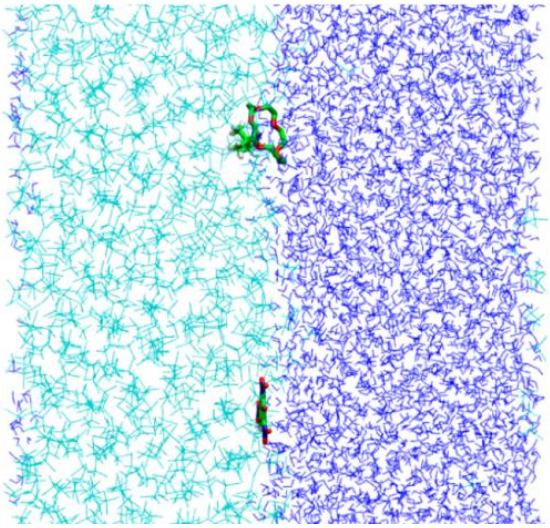

Figure 1.21. Classical MD simulation snapshot showing complexation of *t*BuNH$^+$ by 18-crown-6 at the chloroform/water interface. Reproduced from Benay and Wipff.[137]

In addition to using various combinations of different experimental techniques, Dourdain and colleagues have also combined experimental analysis with computational modelling.[140-142] DFT calculations were used alongside Karl Fischer titration, IR spectroscopy and SANS analysis to explore the extraction of acids and water by a malonamide.[140] DFT simulations and IR spectroscopy were able to identify two different acid extraction modes and SANS analysis demonstrated that there was a change in the aggregation behaviour of the extractant depending on the acid extracted. In the extraction of uranium from a phosphoric acid aqueous phase by a bifunctional amido-phosphonic acid, ESI-MS indicated that several stoichiometries of ligand to uranyl cation were possible and that phosphoric acid is weakly bound compared to the ligand.[141] In addition, SANS and SAXS analysis were able to shed light on the aggregation behaviour, and IR spectroscopy, EXAFS analysis and DFT simulations identified the favourable binding site of the extractant on U(VI). EXAFS analysis and classical MD simulations were used to probe the microstructure present in the extraction phases in the SX of uranyl from sulfuric media when using tertiary amines as the extractant.[142] The structure of the assemblies in the MD simulations were in good agreement with the EXAFS data (see Figure 1.22), with both indicating the presence of uranyl tri-sulfate structures in the organic phase.

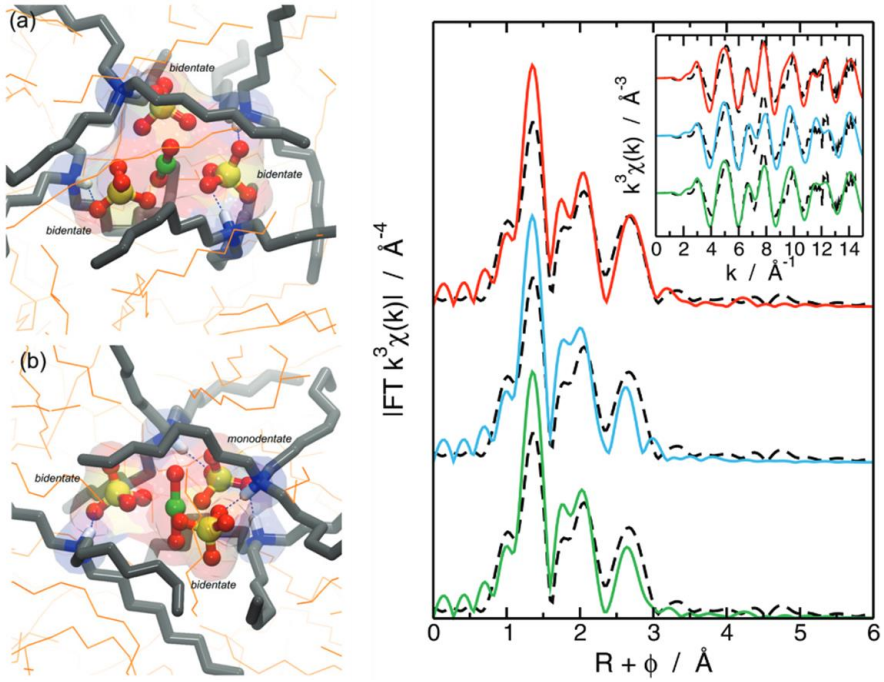

Figure 1.22. Left: snapshots from MD simulations showing the complex $UO_2(SO_4)_3(TOA)_4$ with (a) three SO_4^{2-} in the bidendate coordination, and (b) two bidentate and one monodentate SO_4^{2-}; and right: Fourier transform (FT) EXAFS spectra determined experimentally (black dashed lines) and calculated from MD simulations for the whole MD simulation (green solid line), for the (b) configurations (blue solid line) and for the (a) configurations (red solid line). Reproduced from Sukhbaatar et al.[142]

In their work on lanthanide extraction, Baldwin et al. employed both DFT calculations and classical MD simulations alongside experimental characterisation of the organic phase composition (including Karl Fischer analysis for the water content) to understand the role of water in the selectivity of extraction by diglycolamides.[143] DFT calculations and classical MD simulations were also used by Brigham et al., in combination with EXAFS analysis to determine the structure and assembly behaviour of "outer-sphere ion clusters" in the extraction of lanthanide ions by diglycolamides.[144] Ellis et al. utilised DFT calculations and EXAFS analysis in their work uncovering the effect of steric strain on the extractant in the separation of the lanthanides by diglycolamides.[145] Muller et al. also used DFT calculations alongside EXAFS, but used ESI-MS, UV-vis, Time-Resolved Laser-Induced Fluorescence and NMR in addition, in their exploration of the synergistic extraction of the lanthanides by a malonamide and an organo-phosphoric acid.[146] Hunter et al. investigated the extraction of rare earth elements by an ionic liquid using experimental analysis to characterise extraction

behaviour and the composition of the organic phase, and classical MD simulations to understand the nature of the assemblies formed on extraction.[147]

Also combining experimental and computational techniques, Healy et al. explored the extraction of copper cations by phenolic oximes[148] and phenolic pyrazoles[149] using DFT calculations in conjunction with EPR/ENDOR analysis and/or X-ray crystallography to understand the role of outer-sphere interactions. Carson et al. used DFT calculations combined with mass spectrometry and ^{31}P NMR spectroscopy to determine the mechanism of cobalt extraction by a commercial reagent and how this changed with increasing metal concentration.[150]

Specifically concerning PM metalate extraction, Doidge et al. used EXAFS and ESI-MS analysis alongside DFT calculations and MD modelling to understand the structure of the protonated extractant and the assemblies formed (see Figure 1.23) on the extraction of $[AuCl_4]^-$ with a primary amide.[60] Modelling found that the primary amide forms a protonated dimer on the extraction of the metalate and the assemblies formed are aggregates held together by outer-sphere interactions, with varying numbers of metalate anions, extractant dimers and extractant monomers present. The modelling was in good agreement with the ESI-MS spectra, in which aggregate assemblies were observed, and with the EXAFS analysis, which showed that purely outer-sphere association around the gold metallate anion occurs.[60]

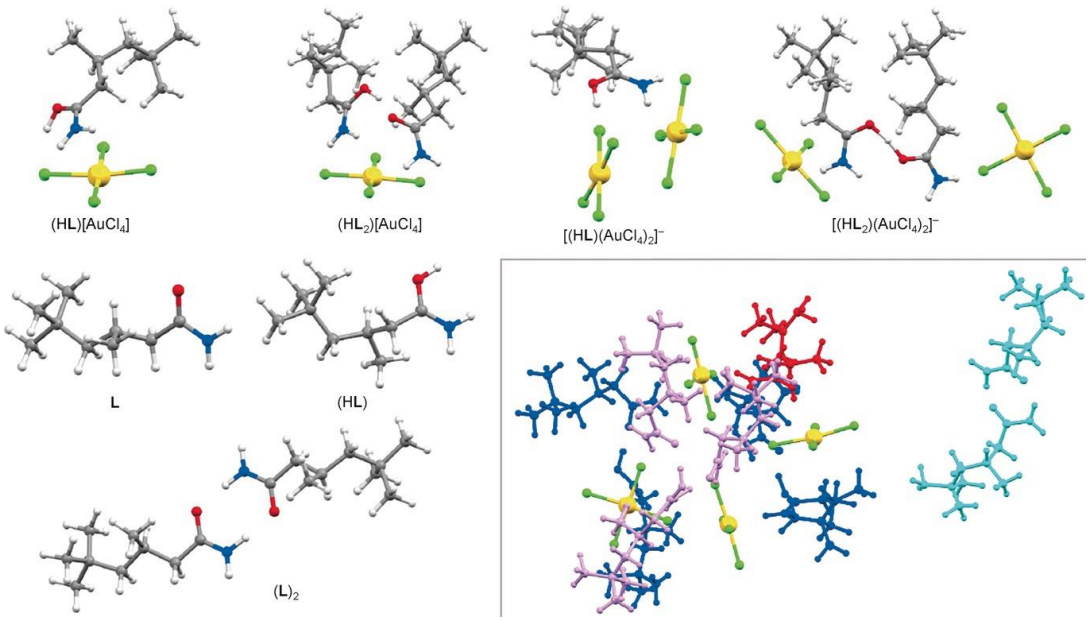

Figure 1.23. Structures of amide extractant and $[AuCl_4]^-$ metalate aggregates obtained by Doidge et al. from DFT calculations and classical MD simulations. Reproduced from Doidge et al.[60]

MacRuary et al. investigated the extraction of chloride and $[PtCl_6]^{2-}$ by TBP using analytical measurements and classical MD simulations.[151] They showed that reverse micelles formed in the organic phase, with chloride or $[PtCl_6]^{2-}$ encapsulated by water molecules, which acted as a mediating layer between the anion and the surrounding TBP molecules, assembled with their electronegative O atoms facing inwards (see Figure 1.24). By simulating systems with varying quantities of water present, assemblies with the experimentally derived ratio of TBP to anion could be formed, allowing an understanding of the amount of water required to be extracted in conjunction with the anion.[151]

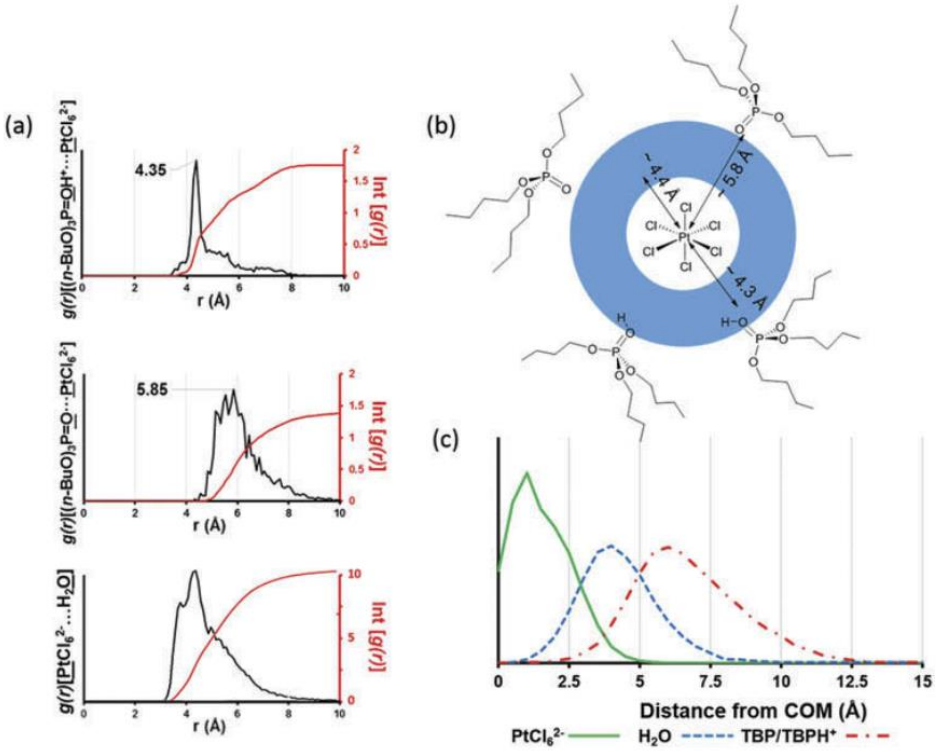

Figure 1.24. Classical MD simulation data analysis outputs of (a) plots of g(r) for the aggregate formed by four TBP molecules around a core of $(H_2O)_{10}([PtCl_6]^{2-})$ and (c) an atom probability plot, allowing (b) a representative structure (water molecules are contained within blue shell) to be elucidated. Reproduced from MacRuary et al.[151]

Carson et al. probed the role of outer-sphere coordination in the selective extraction of $[PtCl_6]^{2-}$ over chloride with amino- and ether-amide extractants.[152] DFT calculations were used to determine formation energies for the ion-associates forming during extraction and illustrated that the reason for the lower extraction ability of the etheramide compared to the aminoamide is due to the enhanced favourability of protonating the latter, to form the active

extractant, as opposed to the former having weaker binding to $[PtCl_6]^{2-}$. In addition, the structures obtained in modelling and in a X-ray crystal structure showed how the protonated extractant molecule forms a proton-chelate (see Figure 1.25), such that an array of C-H to anion interactions forms the ion-pair, resulting in selectivity over chloride.[152]

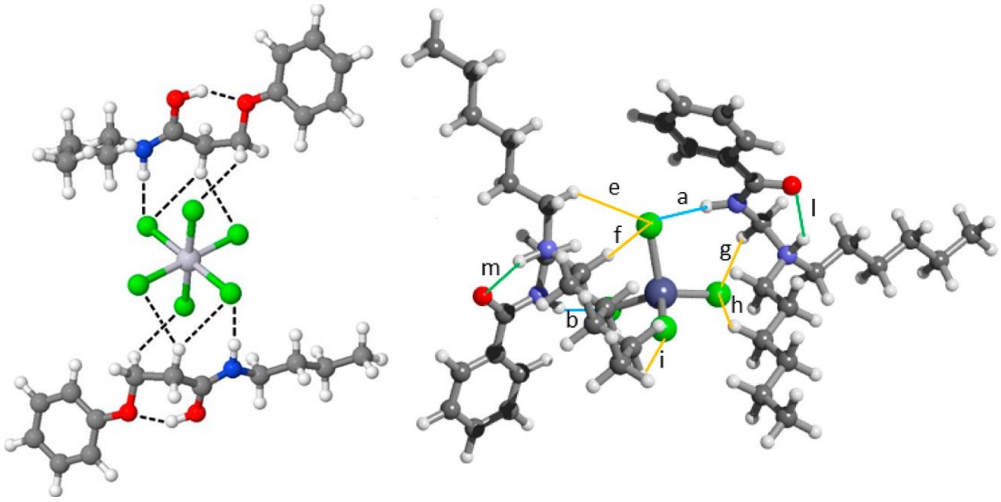

Figure 1.25. Energy minimised structures of left: $[(LH)_2PtCl_6]$ with NH…Cl, CH…Cl and intra-extractant hydrogen bonds (forming proton chelates) of Natural Bond Order (NBO) energies (donor-acceptor interactions derived from second order perturbation analysis) ≥5 kJ mol^{-1} illustrated by dashed black lines; and right: $[(LH)_2ZnCl_4]$, with the strongest NH…Cl and CH…Cl interactions displayed in blue and orange, respectively, and the proton chelate hydrogen bonds illustrated in green. Reproduced from Carson et al.[152] and Turkington et al.,[153] respectively.

Turkington et al. also demonstrated the importance of proton-chelation in their study into the extraction of $[ZnCl_4]^{2-}$ by a series of amido-ammonium extractants,[153] as did Ellis et al. in their work on the extraction of zinc and cobalt chloridometalates by amidopyridyl extractants.[154] In the former, extraction testing, X-ray crystallography and DFT calculations showed a mono-amidoammonium (L^4, see Figure 1.20) to be the strongest extractant because it adopts a proton-chelated geometry on protonation without breaking any existing amide-amide intramolecule hydrogen bonds – thus having the most favourable protonation energy – and it presents fewer highly polar N-H to anion interactions compared to the other extractants explored, making it more selective for $[ZnCl_4]^{2-}$ over the smaller, more charge dense chloride anions present in the extraction system.[153] In the latter, the same analysis techniques were used, plus NMR titration to determine association constants. It is found that the extractants are selective for zinc over cobalt, which is attributed mainly to a higher formation constant for $[ZnCl_4]^{2-}$ over $[CoCl_4]^{2-}$, but, in addition, DFT simulations suggest that

the strongest extractant binds more effectively to the zinc metalate than the cobalt metalate. The DFT simulations find the proton-chelated structures to be the minimum-energy forms (where proton-chelation is possible), and proton-chelation is also observed in the X-ray crystal structures.[154]

These studies highlight the importance of using a mixture of analytical techniques in order to fully understand the solution behaviour underpinning extraction and the valuable insight that computational modelling can provide. Thus, this work utilises a wide range of experimental techniques, coupled with both QM and classical modelling where appropriate.

1.7 Aims

The SX of gold (as a chloridometalate) is carried out commercially, but the extraction mode of action is not fully understood. Rhodium is not currently recovered by SX commercially though this is very desirable. There are some promising extractants reported in the literature,[112-115, 117] but, as with Au SX, the mechanisms occurring and the key interactions involved appear to vary and are not always well understood. A greater understanding of the modes of action of extraction for both Au and Rh is required to allow improved reagents and extraction processes to be developed. This work explores the mode of action occurring with a commercial Au extractant and promising Rh extractants on extraction of the metalates from HCl solution, with the aim of understanding these mechanisms and identifying the key components which provide strong extraction. Both computational and experimental techniques are used to achieve this. In addition, potential new Rh extractants are investigated theoretically or by extraction testing and analysis.

The aims of this work are therefore to:

1. Determine the mode of action in the extraction of rhodium by amidoamine extractants
2. Explore theoretically how structural modification affects the rhodium extraction ability of amidoamines
3. Investigate the use of known rhodium precipitants as extractants, either through modification or use in combination with another reagent
4. Characterise the extraction of gold by a commercial reagent through simulation

1.8 References

1. Kleijn, R.; van der Voet, E.; Kramer, G. J.; van Oers, L.; van der Giesen, C., *Energy* **2011,** *36*, 5640-5648.
2. Månberger, A.; Stenqvist, B., *Energy Policy* **2018,** *119*, 226-241.
3. European Commision, 2017 list of Critical Raw Materials for the EU. In Brussels, 2017; pp 1-8.
4. Prior, T.; Giurco, D.; M Mudd, G.; Mason, L.; Behrisch, J., *Resource depletion, peak minerals and the implications for sustainable resource management*. 2011; Vol. 22, p 577–587.
5. Sverdrup, H.; Koca, D.; Ragnarsdottir, K., *Peak metals, minerals, energy, wealth, food and population; Urgent policy considerations for a sustainable society*. 2013; Vol. 1, p 499-534.
6. European Commison, Report on critical raw materials and the circular economy. In Brussels, 2018; pp 1-80.
7. Graedel, T. E.; Allwood, J.; Birat, J. P.; Buchert, M.; Hageluken, C.; Reck, B. K.; Sibley, S. F.; Sonnemann, G., *J. Ind. Ecol.* **2011,** *15*, 355-366.
8. Greenfield, A.; Graedel, T. E., *The omnivorous diet of modern technology*. 2013; Vol. 74, p 1-7.
9. Nuss, P.; Eckelman, M. J., *PLOS ONE* **2014,** *9*, e101298.
10. Radetzki, M., *Resources Policy* **2009,** *34*, 176-184.
11. Schlesinger, M. E.; King, M. J.; Sole, K. C.; Davenport, W. G. I., *Extractive Metallurgy of Copper*. Elsevier: 2011; p 455.
12. Crundwell, F. K.; Moats, M. S.; Ramachandran, V.; Robinson, T. G.; Davenport, W. G., Chapter 37 - Refining of the Platinum-Group Metals. In *Extractive Metallurgy of Nickel, Cobalt and Platinum Group Metals*, Crundwell, F. K.; Moats, M. S.; Ramachandran, V.; Robinson, T. G.; Davenport, W. G., Eds. Elsevier: Oxford, 2011; pp 489-534.
13. Cheng, C. Y.; Barnard, K. R.; Zhang, W.; Robinson, D. J., *Solvent Extr. Ion Exch.* **2011,** *29*, 719-754.
14. Flett, D. S., *J. Chem. Technol. Biotechnol.* **1999,** *74*, 99-105.
15. Turkington, J. R.; Bailey, P. J.; Love, J. B.; Wilson, A. M.; Tasker, P. A., *Chem. Commun.* **2013,** *49*, 1891-1899.
16. Cox, M., Solvent Extraction in Hydrometallurgy. In *Solvent Extraction Principles and Practice*, 1st ed.; Rydberg, J.; Claude, M.; Choppin, G. R., Eds. Taylor & Francis: New York, USA, 1992; pp 357-412.
17. Ochromowicz, K.; Chmielewski, T., *Growing role of solvent extraction in copper ores processing*. 2008; Vol. 42, p 29-36.
18. Wilson, A. M.; Bailey, P. J.; Tasker, P. A.; Turkington, J. R.; Grant, R. A.; Love, J. B., *Chem. Soc. Rev.* **2014,** *43*, 123-134.
19. Forgan, R. S.; Wood, P. A.; Campbell, J.; Henderson, D. K.; McAllister, F. E.; Parsons, S.; Pidcock, E.; Swart, R. M.; Tasker, P. A., *Chem. Commun.* **2007**, 4940-4942.
20. Warr, R. J.; Westra, A. N.; Bell, K. J.; Chartres, J.; Ellis, R.; Tong, C.; Simmance, T. G.; Gadzhieva, A.; Blake, A. J.; Tasker, P. A.; Schröder, M., *Chem.: Eur. J.* **2009,** *15*, 4836-4850.
21. Burns, J. H.; Brown, G. M.; Ryan, R. R., *Acta Crystallogr. C* **1985,** *41*, 1446-1448.
22. Barnard, K. R.; Nealon, G. L.; Ogden, M. I.; Skelton, B. W., *Solvent Extr. Ion Exch.* **2010,** *28*, 778-792.

23. Roebuck, J. W.; Bailey, P. J.; Doidge, E. D.; Fischmann, A. J.; Healy, M. R.; Nichol, G. S.; O'Toole, N.; Pelser, M.; Sassi, T.; Sole, K. C.; Tasker, P. A., *Solvent Extr. Ion Exch.* **2018,** *36*, 437-458.
24. Ellis, R. J.; Meridiano, Y.; Chiarizia, R.; Berthon, L.; Muller, J.; Couston, L.; Antonio, M. R., *Chem.: Eur. J.* **2013,** *19*, 2663-2675.
25. Aspects of the platinum group metals (PGM). http://www.rsc.org/learn-chemistry/resource/res00002206/aspects-of-the-platinum-group-metals (May 1st 2016),
26. Free, M. L.; Free, M., *Hydrometallurgy fundamentals and applications*. Hoboken, New Jersey : Wiley : TMS: Hoboken, New Jersey, 2013.
27. Crundwell, F. K.; Moats, M. S.; Ramachandran, V.; Robinson, T. G.; Davenport, W. G., Chapter 38 - Recycling of Nickel, Cobalt and Platinum-Group Metals. In *Extractive Metallurgy of Nickel, Cobalt and Platinum Group Metals*, Crundwell, F. K.; Moats, M. S.; Ramachandran, V.; Robinson, T. G.; Davenport, W. G., Eds. Elsevier: Oxford, 2011; pp 537-549.
28. Grant, R. A.; Drake, V. A. In *The application of solvent extraction to the refining of gold*, 2002; South African Institute of Mining and Metallurgy: 2002; pp 940-945.
29. Kyriakakis, G., Extraction of gold from platinum group metal (PGM) ores. In *Developments in Mineral Processing*, Adams, M. D.; Wills, B. A., Eds. Elsevier: 2005; Vol. 15, pp 897-917.
30. Mironov, I. V., *Hydrometallurgy* **2013,** *133*, 15-22.
31. Petrova, A. M.; Nikolaev, A. E.; Kasikov, A. G., *Russ. J. Appl. Chem.* **2014,** *87*, 234-240.
32. Kargari, A.; Kaghazchi, T.; Soleimani, M., *Chem. Eng. Technol.* **2004,** *27*, 1014-1018.
33. Nguyen, T. H.; Wang, L.; Lee, M. S., *Korean J. Met. Mater.* **2017,** *55*, 247-255.
34. Jordanov, N.; Havesov, I., *Fresenius Z. Anal. Chem.* **1969,** *244*, 176-181.
35. Branch, C. H.; Hutchison, D., *Analyst* **1986,** *111*, 231-233.
36. Akita, S.; Yang, L.; Takeuchi, H., *Hydrometallurgy* **1996,** *43*, 37-46.
37. Oshima, T.; Ohkubo, N.; Fujiwara, I.; Horiuchi, T.; Koyama, T.; Ohe, K.; Baba, Y., *Solvent Extr. Res. Dev.* **2017,** *24*, 89-96.
38. Horiuchi, T.; Oshima, T.; Baba, Y., *Hydrometallurgy* **2018,** *178*, 176-180.
39. Oshima, T.; Horiuchi, T.; Matsuzaki, K.; Ohe, K., *Hydrometallurgy* **2019,** *183*, 207-212.
40. Xing, W. D.; Lee, M. S.; Senanayake, G., *Hydrometallurgy* **2018,** *180*, 58-64.
41. Xing, W. D.; Lee, M. S.; Kim, Y. H., *J. Ind. Eng. Chem. (Amsterdam, Neth.)* **2018,** *59*, 328-334.
42. Sarkar, S. G.; Dhadke, P. M., *J. Chin. Chem. Soc.* **2000,** *47*, 869-873.
43. Haddad, R.; Kumar, A.; Alguacil, F. J.; Sastre, A. M. In *Comparative studies of solvent extraction and liquid membrane permeation of gold(III) from chloride media*, 2001; Society of Chemical Industry: 2001; pp 1155-1160.
44. Soldenhoff, K.; Wilkins, D. In *Solvent extraction of gold from chloride copper anode slime liquors*, 2001; Society of Chemical Industry: 2001; pp 777-782.
45. Martínez, S.; Navarro, P.; Sastre, A. M.; Alguacil, F. J., *Hydrometallurgy* **1996,** *43*, 1-12.
46. Barroso, M. A.; López, F. A.; Sastre, A.; Alguacil, F. J., *Hydrometallurgy* **1997,** *45*, 199-209.
47. Sastre, A. M.; Alguacil, F. J. In *Advances in gold(III)-chloride solvent extraction using neutral organophosphorous derivatives. Estimation of $AuCl_4^-$--H^+ interaction coefficients*, 2001; Society of Chemical Industry: 2001; pp 381-385.
48. Martínez, S.; Sastre, A.; Alguacil, F. J., *Hydrometallurgy* **1997,** *46*, 205-214.

49. Alguacil, F. J.; Caravaca, C.; Martínez, S., *J. Chem. Technol. Biotechnol.* **1998,** *72*, 339-346.
50. Tocher, M. I.; Whitney, D. C.; Diamond, R. M., *J. Phys. Chem.* **1964,** *68*, 368-374.
51. Mojski, M., *J. Radioanal. Chem.* **1978,** *46*, 239-245.
52. Baba, A. A.; Adekola, F. A.; Ojutemieden, D. O.; Dada, F. K., *Chem. Bull. "POLITEHNICA" Univ. (Timisoara)* **2011,** *56(70)*, 29-37.
53. Sadeghi, N.; Alamdari, E. K., *Trans. Nonferrous Met. Soc. China* **2016,** *26*, 3258-3265.
54. Kim, J. H.; Lee, W. H., *Han'guk Chawon Konghak Hoechi* **1995,** *32*, 363-70.
55. Tuck, D. G., *J. Inorg. Nucl. Chem.* **1959,** *11*, 164-166.
56. Singh, H.; Shinde, V. M., *Fresenius J. Anal. Chem.* **1993,** *345*, 471-471.
57. Madi, A.; Miralles, N.; Cortina, J. L.; Arnaldos, J.; Sastre, A. In *Comparative studies of gold(III) extraction using phospholene derivatives from hydrochloric acid solutions*, 1996; University of Melbourne, Dep. of Chemical Engineering: 1996; pp 463-468.
58. Shen, Y. F.; Xue, W. Y., *Sep. Purif. Technol.* **2007,** *56*, 278-283.
59. Narita, H.; Tanaka, M.; Morisaku, K.; Abe, T., *Hydrometallurgy* **2006,** *81*, 153-158.
60. Doidge, E. D.; Carson, I.; Tasker, P. A.; Ellis, R. J.; Morrison, C. A.; Love, J. B., *Angew. Chem. Int. Ed.* **2016,** *55*, 12436-12439.
61. Narita, H.; Tanaka, M.; Morisaku, K.; Yaita, T.; Suzuki, S.; Isomae, Y.; Abe, T., *Solvent Extr. Res. Dev., Jpn.* **2005,** *12*, 123-130.
62. Mowafy, E. A.; Mohamed, D., *Sep. Purif. Technol.* **2016,** *167*, 146-153.
63. Huang, Y.; Li, N.; Li, Y. H.; Wu, J.; Li, S. H.; Chen, S.; Zhu, L., *Adv. Mater. Res.* **2014,** *878*, 399-405.
64. Narita, H.; Tanaka, M.; Morisaku, K. In *Solvent extraction of precious metals using thiodiglycolamide*, 2005; Minerals, Metals & Materials Society: 2005; pp 865-872.
65. Alguacil, F. J.; Caravaca, C., *Hydrometallurgy* **1993,** *34*, 91-98.
66. Alguacil, F. J., *Solvent Extr. Ion Exch.* **2003,** *21*, 841-852.
67. Diaz-Arocas, P.; Alguacil, F. J.; Caravaca, C., *Cah. Inf. Tech./Rev. Metall.* **1993,** *90*, 717-23.
68. Martínez, S.; Sastre, A. M.; Alguacil, F. J., *Hydrometallurgy* **1999,** *52*, 63-70.
69. Wei, W.; Cho, C.-W.; Kim, S.; Song, M.-H.; Bediako, J. K.; Yun, Y.-S., *J. Mol. Liq.* **2016,** *216*, 18-24.
70. Guo, J.-x.; Sun, X.; Yin, Z.-l.; Li, X.-m.; Yu, H.-y.; Yang, Y.-z.; Sun, S.-x., *J. Radioanal. Nucl. Chem.* **2003,** *256*, 595-598.
71. Watanabe, Y.; Araki, Y.; Katsuta, S., *Bunseki Kagaku* **2014,** *63*, 563-567.
72. Lopez-Delgado, A.; Lopez, F. A.; Alguacil, F. J., *Rev. Metal. (Madrid)* **2000,** *36*, 165-169.
73. Alguacil, F. J.; Martínez, S.; Sastre, A. M., *J. Chem. Res.* **2001,** *2001*, 384-386.
74. Tong, Y.; Yang, H.; Li, J.; Yang, Y., *Sep. Purif. Technol.* **2013,** *120*, 367-372.
75. Zheng, Y.; Tong, Y.; Wang, S.; Zhang, H.; Yang, Y., *Sep. Purif. Technol.* **2015,** *154*, 123-127.
76. Nguyen, V. T.; Lee, J.-c.; Jeong, J.; Kim, B.-S.; Cote, G.; Chagnes, A., *Ind. Eng. Chem. Res.* **2015,** *54*, 1350-1358.
77. Campos, K.; Vincent, T.; Bunio, P.; Trochimczuk, A.; Guibal, E., *Solvent Extr. Ion Exch.* **2008,** *26*, 570-601.
78. Davidson, N.; Eade, B.; Grant, R. A., Novel Solvent Extraction Process for the Recovery of Gold from Chloride Media. In *International Solvent Extraction Conference*, Würzburg, Germany, 2014.

79. Domínguez, M.; Anticó, E.; Beyer, L.; Aguirre, A.; García-Granda, S.; Salvadó, V., *Polyhedron* **2002,** *21*, 1429-1437.
80. Cherkasov, R. A.; Garifzyanov, A. R.; Zakharov, S. V.; Vinokurov, A. V.; Galkin, V. I., *Russ. J. Gen. Chem.* **2006,** *76*, 417-420.
81. Baba, Y.; Arima, A.; Kanemaru, S.; Iwakuma, M.; Oshima, T., *J. Chem. Eng. Jpn.* **2011,** *44*, 686-691.
82. Lokhande, T. N.; Gaikwad, S. H.; Anuse, M. A.; Chavan, M. B., *Ann. Chim. (Rome, Italy)* **2002,** *92*, 615-622.
83. Iqbal, M.; Ejaz, M.; Chaudhri, S. A.; Ahmad, R., *Sep. Sci.* **1976,** *11*, 255-278.
84. Iwakuma, M.; Baba, Y., *Anal. Sci.* **2005,** *21*, 269-272.
85. Cieszynska, A.; Wieczorek, D., *Hydrometallurgy* **2018,** *175*, 359-366.
86. Petrich, M.; Cortina, J. L.; Hartung, J.; Aguilar, M.; Sastre, A.; Beyer, L.; Gloe, K., *Solvent Extr. Ion Exch.* **1993,** *11*, 51-66.
87. Kaushal, M. A.; Turel, Z. R., *J. Radioanal. Nucl. Chem.* **1999,** *241*, 663-665.
88. Núñez, M. E.; Miguel, E. R. d. S.; Mercader-Trejo, F.; Aguilar, J. C.; de Gyves, J., *Sep. Purif. Technol.* **2006,** *51*, 57-63.
89. Ohto, K.; Ishii, H.; Kawakita, H.; Harada, H.; Inoue, K., *J. Ion Exch.* **2007,** *18*, 390-395.
90. Kubota, F.; Kono, R.; Yoshida, W.; Sharaf, M.; Kolev, S. D.; Goto, M., *Sep. Purif. Technol.* **2019,** *214*, 156-161.
91. Lee, J.-S.; Choi, J.-M.; Choi, H.-S.; Kim, Y.-S., *Anal. Sci. Technol.* **1996,** *9*, 221-234.
92. Maksimovic, Z. B.; Ruvarac, A. L.; Halasi, R. In *Solvent extraction of metal chloride complex by tri-n-laurylamine oxide*, 1974; Soc. Chem. Ind.: 1974; pp 1937-47.
93. Lu, W.; Lu, Y.; Liu, F.; Shang, K.; Wang, W.; Yang, Y., *J. Hazard. Mater.* **2011,** *186*, 2166-2170.
94. Xiong, Y.; Kawakita, H.; Inoue, J.-i.; Abe, M.; Ohto, K.; Inoue, K.; Harada, H., *Solvent Extr. Res. Dev.* **2010,** *17*, 151-162.
95. Benguerel, E.; Demopoulos, G. P.; Harris, G. B., *Hydrometallurgy* **1996,** *40*, 135-52.
96. Geswindt, T. E. Chemical speciation of RhIII complexes in acidic, halide-rich media by means of 103Rh NMR spectroscopy : the importance of speciation in the selective separation and recovery of rhodium. Stellenbosch University, 2013.
97. Benguerel, E.; Demopoulos, G. P., *J. Chem. Technol. Biotechnol.* **1998,** *72*, 183-189.
98. Narita, H.; Tanaka, M.; Yaita, T.; Okamoto, Y., *Solvent Extr. Ion Exch.* **2004,** *22*, 853-863.
99. Malik, P.; Paula Paiva, A., *Solvent Extr. Ion Exch.* **2007,** *26*, 25-40.
100. Zou, L.; Chen, J.; Pan, X., *Hydrometallurgy* **1998,** *50*, 193-203.
101. Sun, P. P.; Lee, M. S., *Hydrometallurgy* **2011,** *105*, 334-340.
102. Mhaske, A. A.; Dhadke, P. M., *Hydrometallurgy* **2001,** *61*, 143-150.
103. Malik, P.; Paiva, A. P., *Solvent Extr. Ion Exch.* **2010,** *28*, 49-72.
104. Niinae, M.; Yamamoto, M.; Sano, M.; Nakahiro, Y.; Wakamatsu, T., *Shigen-to-Sozai* **1995,** *111*, 875-879.
105. Shafiqul Alam, M.; Inoue, K., *Hydrometallurgy* **1997,** *46*, 373-382.
106. Yan, G. L.; Alstad, J. In *Solvent extraction of rhodium with cyclohexanol from HCl/SnCl2 media*, 1996; University of Melbourne, Dep. of Chemical Engineering: 1996; pp 547-552.
107. Zubareva, A. P.; Ivanova, S. N.; Plotnikova, G. I.; Torgov, V. G., *Izv. Sib. Otd. Akad. Nauk SSSR, Ser. Khim. Nauk* **1986**, 86-91.
108. Knothe, M., *J. Radioanal. Chem.* **1979,** *52*, 335-41.
109. Ali Khan, M.; Morris, D. F. C., *J. Less Common Met.* **1967,** *13*, 53-61.

110. Yan, G. L.; Alstad, J., *J. Radioanal. Nucl. Chem.* **1995,** *201*, 191-8.
111. Berg, E. W.; Lau, E. Y., *Anal. Chim. Acta* **1962,** *27*, 248-252.
112. Narita, H.; Morisaku, K.; Tanaka, M., *Chem. Commun.* **2008,** *45*, 5921-5923.
113. Narita, H.; Morisaku, K.; Tanaka, M., *Solvent Extr. Ion Exch.* **2015,** *33*, 407-417.
114. Afzaletdinova, N. G.; Khisamutdinov, R. A.; Bondareva, S. O.; Murinov, Y. I., *Russ. J. Gen. Chem.* **2015,** *85*, 1934-1938.
115. Afzaletdinova, N. G.; Khisamutdinov, R. A.; Bondareva, S. O.; Murinov, Y. I., *Russ. J. Inorg. Chem.* **2015,** *60*, 1583-1587.
116. Afzaletdinova, N. G.; Murinov, Y. I.; Khazhiev, S. Y.; Bondareva, S. O.; Muslukhov, R. R., *Russ. J. Inorg. Chem.* **2010,** *55*, 460-467.
117. Narita, H.; Morisaku, K.; Tanaka, M., *Solvent Extr. Ion Exch.* **2015,** *33*, 462-471.
118. Bottorff, S. C.; Powell, A. S.; Barnes, C. L.; Wherland, S.; Benny, P. D., *Dalton Trans.* **2016,** *45*, 3264-3267.
119. Firmansyah, M. L.; Kubota, F.; Goto, M., *J. Chem. Technol. Biotechnol.* **2017,** *93*, 1714-1721.
120. Ma, S.; Funaki, K.; Miyazaki, A.; Muramatsu, A.; Kanie, K., *Chem. Lett.* **2017,** *46*, 1422-1425.
121. Dul, M.-C.; Braibant, B.; Dourdain, S.; Pellet-Rostaing, S.; Bourgeois, D.; Meyer, D., *J. Fluorine Chem.* **2017,** *200*, 59-65.
122. Déjugnat, C.; Dourdain, S.; Dubois, V.; Berthon, L.; Pellet-Rostaing, S.; Dufrêche, J.-F.; Zemb, T., *PCCP* **2014,** *16*, 7339-7349.
123. Dourdain, S.; Hofmeister, I.; Pecheur, O.; Dufrêche, J. F.; Turgis, R.; Leydier, A.; Jestin, J.; Testard, F.; Pellet-Rostaing, S.; Zemb, T., *Langmuir* **2012,** *28*, 11319-11328.
124. Sukhbaatar, T.; Dourdain, S.; Turgis, R.; Rey, J.; Arrachart, G.; Pellet-Rostaing, S., *Chem. Commun.* **2015,** *51*, 15960-15963.
125. Rey, J.; Dourdain, S.; Dufrêche, J. F.; Berthon, L.; Muller, J. M.; Pellet-Rostaing, S.; Zemb, T., *Langmuir* **2016,** *32*, 13095-13105.
126. Antonio, M. R.; Demars, T. J.; Audras, M.; Ellis, R. J., *Sep. Sci. Technol.* **2017,** *53*, 1834-1847.
127. Antonio, M. R.; Ellis, R. J.; Estes, S. L.; Bera, M. K., *PCCP* **2017,** *19*, 21304-21316.
128. Ellis, R. J., *Inorg. Chim. Acta* **2017,** *460*, 159-164.
129. Yoshizuka, K., *Anal. Sci.* **2004,** *20*, 761-765.
130. Qi, S.-C.; Hayashi, J.-i.; Zhang, L., *RSC Advances* **2016,** *6*, 77375-77395.
131. Benay, G.; Wipff, G., *New J. Chem.* **2016,** *40*, 2102-2114.
132. Benay, G.; Wipff, G., *J. Phys. Chem. B* **2013,** *117*, 1110-1122.
133. Benay, G.; Wipff, G., *J. Phys. Chem. B* **2013,** *117*, 7399-7415.
134. Benay, G.; Wipff, G., *J. Phys. Chem. B* **2014,** *118*, 3133-3149.
135. Sieffert, N.; Wipff, G., *Dalton Trans.* **2015,** *44*, 2623-2638.
136. Gaillard, C.; Mazan, V.; Georg, S.; Klimchuk, O.; Sypula, M.; Billard, I.; Schurhammer, R.; Wipff, G., *Phys. Chem. Chem. Phys.* **2012,** *14*, 5187-5199.
137. Benay, G.; Wipff, G., *J. Phys. Chem. B* **2014,** *118*, 13913-13929.
138. Chen, Y.; Duvail, M.; Guilbaud, P.; Dufrêche, J.-F., *PCCP* **2017,** *19*, 7094-7100.
139. Uezu, K.; Yoshizuka, K., *Computational Chemistry in Solvent Extraction*. 2007; Vol. 38.
140. Déjugnat, C.; Berthon, L.; Dubois, V.; Meridiano, Y.; Dourdain, S.; Guillaumont, D.; Pellet-Rostaing, S.; Zemb, T., *Solvent Extr. Ion Exch.* **2014,** *32*, 601-619.
141. Pecheur, O.; Guillaumont, D.; Dourdain, S.; Berthon, L.; Turgis, R.; Fillaux, C.; Arrachart, G.; Testard, F., *Solvent Extr. Ion Exch.* **2016,** *34*, 260-273.

142. Sukhbaatar, T.; Duvail, M.; Dumas, T.; Dourdain, S.; Arrachart, G.; Solari, P. L.; Guilbaud, P.; Pellet-Rostaing, S., *Chem. Commun.* **2019,** *55*, 7583-7586.
143. Baldwin, A. G.; Ivanov, A. S.; Williams, N. J.; Ellis, R. J.; Moyer, B. A.; Bryantsev, V. S.; Shafer, J. C., *ACS Cent. Sci.* **2018,** *4*, 739-747.
144. Brigham, D. M.; Ivanov, A. S.; Moyer, B. A.; Delmau, L. H.; Bryantsev, V. S.; Ellis, R. J., *J. Am. Chem. Soc.* **2017,** *139*, 17350-17358.
145. Ellis, R. J.; Brigham, D. M.; Delmau, L.; Ivanov, A. S.; Williams, N. J.; Vo, M. N.; Reinhart, B.; Moyer, B. A.; Bryantsev, V. S., *Inorg. Chem.* **2017,** *56*, 1152-1160.
146. Muller, J. M.; Berthon, C.; Couston, L.; Guillaumont, D.; Ellis, R. J.; Zorz, N.; Simonin, J.-P.; Berthon, L., *Hydrometallurgy* **2017,** *169*, 542-551.
147. Hunter, J.; Dolezalova, S.; Ngwenya, B.; Morrison, C.; Love, J., *Metals* **2018,** *8*.
148. Healy, M. R.; Carter, E.; Fallis, I. A.; Forgan, R. S.; Gordon, R. J.; Kamenetzky, E.; Love, J. B.; Morrison, C. A.; Murphy, D. M.; Tasker, P. A., *Inorg. Chem.* **2015,** *54*, 8465-8473.
149. Healy, M. R.; Roebuck, J. W.; Doidge, E. D.; Emeleus, L. C.; Bailey, P. J.; Campbell, J.; Fischmann, A. J.; Love, J. B.; Morrison, C. A.; Sassi, T.; White, D. J.; Tasker, P. A., *Dalton Trans.* **2016,** *45*, 3055-3062.
150. Carson, I.; Tasker, P. A.; Love, J. B.; Moser, M.; Fischmann, A. J.; Jakovljevic, B.; Soderstrom, M. D.; Morrison, C. A., *Eur. J. Inorg. Chem.* **2018,** *2018*, 1511-1521.
151. MacRuary, K. J.; Gordon, R. J.; Grant, R. A.; Woollam, S.; Ellis, R. J.; Tasker, P. A.; Love, J. B.; Morrison, C. A., *Solvent Extr. Ion Exch.* **2017,** *35*, 531-548.
152. Carson, I.; MacRuary, K. J.; Doidge, E. D.; Ellis, R. J.; Grant, R. A.; Gordon, R. J.; Love, J. B.; Morrison, C. A.; Nichol, G. S.; Tasker, P. A.; Wilson, A. M., *Inorg. Chem.* **2015,** *54*, 8685-8692.
153. Turkington, J. R.; Cocalia, V.; Kendall, K.; Morrison, C. A.; Richardson, P.; Sassi, T.; Tasker, P. A.; Bailey, P. J.; Sole, K. C., *Inorg. Chem.* **2012,** *51*, 12805-12819.
154. Ellis, R. J.; Chartres, J.; Henderson, D. K.; Cabot, R.; Richardson, P. R.; White, F. J.; Schröder, M.; Turkington, J. R.; Tasker, P. A.; Sole, K. C., *Chem.: Eur. J.* **2012,** *18*, 7715-7728.

Chapter 2

Methods

2 Methods

2.1 Computational modelling

Computational chemistry is a growing field, finding application in the rationalisation of experimental phenomena and in the exploration and prediction of unknown behaviour.

Computational calculations or simulations can be broadly divided into two categories, based on the underlying mathematics involved: classical and quantum mechanical (QM). As the names suggest, classical calculations make use of classical mechanics and experimentally or QM derived parameters to describe atoms and molecules, while QM calculations use quantum mechanics and attempt to solve the multi-electron Schrödinger Equation.

Both methods have their individual merits and drawbacks: classical calculations are far less computationally demanding and hence can be used to describe larger systems; however, QM calculations are more accurate and are able to obtain information about a system which classical calculations cannot.

In SX mode of action research, it is can be very important to explore the interactions that lead to metal extraction and determine their relative strengths. For this, QM structure calculations are required. However, as discussed previously, in PM SX larger assemblies than simple ion-associates have been observed, such as aggregates or reverse micelles. The structures of these larger assemblies are very difficult to predict, therefore molecular dynamics (MD) simulations are useful to allow their self-assembly to be simulated. This can be done quantum mechanically or classically, but if the assemblies are expected to be particularly large, or the aggregation times are long, or if there is a desire to include explicit solvent molecules in the simulation classical methods offer the most practical solution.

Both QM and classical calculations have been employed in the elucidation of solvent extraction mode of action previously, and both are utilised in this work. This section presents the techniques used along with their background theory.

2.1.1 Quantum Mechanical Theory

The basis of QM computational chemistry lies in the time-independent Schrödinger equation (Equation 2.1). This is an eigenvalue problem: the Hamiltonian operator, $\hat{H}$, acts on the wavefunction, Ψ (the eigenfunction), to give the permitted energy levels, E (the eigenvalues), of the atom or molecule.

$$\hat{\mathrm{H}}\Psi = E\Psi \qquad 2.1$$

The Hamiltonian operator describes the total energy of the system, which comprises potential and kinetic energy terms, as shown in Equation 2.2, where T_e, T_n, V_{nn}, V_{ee} and V_{ne} represent the kinetic energy of electrons, the kinetic energy of nuclei, the potential energy of the nucleus-nucleus repulsions, the potential energy of the electron-electron repulsions and potential energy of nucleus-electron attraction, respectively.[1, 2]

$$\hat{\mathrm{H}} = T_e + T_n + V_{nn} + V_{ee} + V_{ne} \qquad 2.2$$

By solving the Schrödinger equation and determining the eigenvalues many different chemical properties can be calculated for the system. However, the Schrödinger equation can only be solved for a one-electron system. The electron-electron potential energy term is impossible to solve for a multi-electron system. This is because electron motion is correlated; the electrostatic field of one electron will influence others and be influenced by the others. Therefore, in order to "solve" the Schrödinger equation of systems with more than one electron approximations must be made. The accuracy of the calculations for multi-electron systems therefore depend on the validity of the approximations made.

2.1.1.1 The Born-Oppenheimer approximation

The primary approximation employed is the Born-Oppenheimer approximation. It states that, because light electrons move so much faster than the heavy nuclei, electron and nuclear motion can be treated independently and, from the point of view of an electron, the nucleus can be considered stationary. Therefore, in the Hamiltonian operator, the kinetic energy term for the nuclei is set to zero and the nucleus-nucleus repulsion term is a constant (which is calculated classically and so not included in the QM equations). This gives the electronic Hamiltonian, $\hat{H}_{elec}$, in Equation 2.3.[3]

$$\hat{\mathrm{H}}^{elec} = T_e + V_{ee} + V_{ne} \qquad 2.3$$

This equation could be solved for one electron at a time. However, the Born-Oppenheimer approximation has not removed the issues with multi-electron systems: all the electron related terms still remain in the electronic Hamiltonian. There is still the problem of electron correlation and also of electron exchange (each orbital will accommodate a pair electrons, but the electrons must be of opposite spin), which affects each of the remaining three terms in Equation 2.3. The combination of two theories, Hartree and Fock, allow a first approximation to treating these issues.

2.1.1.2 Hartree Fock theory

Hartree Fock (HF) theory employs both Hartree theory and Fock theory. Hartree theory approximates the multi-electron correlation problem (each electrons movement influencing and being influenced by the others' movement) to a single electron moving in a uniform field generated by the other electrons, setting the correlation energy to zero.[4] Fock theory allows electron exchange to be accounted for via the use of an anti-symmetric wavefunction: the wavefunction must be antisymmetric "with respect to the interchange of the coordinate *x* (both space and spin) of any two electrons".[4] For example, in the two electron system given in Equation 2.4, where both electrons are of spin up, if x_1 (the position of the electron) is set equal to x_2 the wavefunction is zero. As the square of the wavefunction defines the electron probability function, in effect this renders impossible the positioning of two electrons with the same spin in the same place. This antisymmetry principle equates to the Pauli Exclusion Principle.[4]

$$\Psi_a \uparrow (x_1)\Psi_b \uparrow (x_2) - \Psi_a \uparrow (x_2)\Psi_b \uparrow (x_1) \qquad 2.4$$

While the approximations introduced through HF theory may work well for many systems, for some they do not, particularly in systems with areas of high electron density. However, there are higher levels of theory which improve upon HF theory, by using additional terms to better account for the missing energy attributed to electron correlation. Improved representation of the wavefunction and Hamiltonian operator is easy to verify because of the variation principle, which states that the energy obtained through approximations will always be higher than the true energy,[1] thus a decrease in energy on changing the level of theory or wavefunction description indicates that the model chemistry is improved. HF

theory and the higher levels of theory are termed *ab initio* methods. Although *ab initio* methods can prove very successful and accurate (especially the higher level of theory methods), the computational demand associated with them quickly becomes extremely high as system size increases. However, there is an alternative theory which is somewhat less computationally demanding: density functional theory.

2.1.1.3 Density Functional Theory

Density functional theory (DFT) uses electron density to calculate the energy and ultimately the properties of a ground state system. Hohenberg and Kohn[5] showed that there is a one-to-one correspondence of electron density and the ground state energy of a system,[3] which indicates there is a functional connecting these two properties. This functional (a function of a function: in this case a function of the electron density) is used to calculate the energy and, in theory, this should yield an exact answer, which fully considers electron correlation and exchange. In practice, however, this is not the case, because the identity of the correct functional is unknown. Thus, a wide variety of approximate functionals are employed instead, with each better suited to different systems.

Using these functionals, the *N* one-electron Schrödinger equations, introduced in the previous section, are replaced with *N* equations of the form given in Equation 2.5, which are based on the electron density. The electron-electron repulsion term is split into a Coulomb part, $J[\rho]$, and an Exchange part (incorporated into the exchange-correlation term).[3] An exchange-correlation term, $E_{XC}[\rho]$, is formed to encompass the electron correlation and exchange effects, which are impossible to solve exactly for almost all systems. This term is customarily separated into pure exchange, $E_X[\rho]$, and correlation, $E_C[\rho]$.[3]

$$E[\rho] = T_e[\rho] + E_{ne}[\rho] + J[\rho] + E_X[\rho] + E_C[\rho] \qquad 2.5$$

DFT methods differ in how they treat the exchange-correlation energy, i.e. in how they approximate the functional for $E_{XC}[\rho]$. For example, this can be done by making use of the Local Density Approximation, which assumes that the density varies slowly and so the local density can be treated as a uniform electron gas.[3] This method therefore fails when the electron density has sharp variations, such as for a molecular system. For these, the Generalised Gradient Approximation can be utilised, where the gradient of the electron density is incorporated into the functionals.[3]

All pure DFT methods use an approximate functional for $E_{XC}[\rho]$ and are thus approximating both the electron exchange and correlation. However, the exact treatment of electron exchange from HF can be incorporated into DFT, providing a combination method known as hybrid DFT.[1, 3] Hybrid functionals incorporate varying amounts of HF treatment of the exchange energy, as demonstrated in Equation 2.6, where E_{XC} is the exchange and correlation energy, E_{XC}^{DFT} is the DFT treatment of exchange and correlation energy, E_X^{HF} is the HF treatment of the exchange energy, and a is the weighting factor.

$$E_{XC} = (1 - a)E_{XC}^{DFT} + aE_X^{HF} \quad 2.6$$

Some functionals and hybrid functionals are lacking in their treatment of dispersion interactions between atoms.[6-8] As the work in this thesis focuses on binding modes in which dispersion interactions may contribute significantly, it is important that these are accounted for in this work. Therefore, the hybrid functional M06[9] is used. This functional includes 27% HF exchange and is highly parameterised (incorporating 35 empirically optimised parameters into the exchange-correlation functional) to better account for dispersion interactions.

2.1.1.4 Basis sets

The wavefunction, the mathematical description of a molecular orbital, is constructed from basis sets, which are linear combinations of functions to describe atomic orbitals, which in turn are used to construct molecular orbitals. Two common ways of describing the orbitals are Slater-Type orbitals[10] or Gaussian-Type orbitals.[11] The former mirror the orbitals for the hydrogen atom and are more accurate but more demanding to solve. The latter are less demanding to calculate and can mimic the atomic radial functions if a linear combination of them is employed. This means the wavefunction is expressed as a sum of i weighted (by coefficients, c_i, in order to best mimic the size and shape of the orbital), "primitive" Gaussian functions, φ_i as expressed in Equation 2.7, where φ_i captures both the radial (i.e. size) and angular momentum (i.e. shape) components for describing the orbital.

$$\Psi = \sum_i c_i \phi_i \quad 2.7$$

For example, consider the 6-311+G** basis set,[12, 13] which is one of those used in this work. It consists of a function built from six primitive Gaussian functions, which are used to describe

the core orbitals, and three functions built from three, one, and one primitive Gaussian functions, respectively, which describe the valence orbitals. More flexibility is introduced to describe the valence orbitals as they are the orbitals involved in chemical bonding. This basis set is of the split-valence, Triple Zeta (TZ) type, as it treats the core orbitals separately from the valence and it uses three times as many functions as the minimum basis set (which is e.g. two *s* functions, one each for the 1*s* and 2*s* orbitals, and one set of *p* functions, for the 2*p* orbitals) to describe the (valence) orbitals.[3] Using more functions increases the accuracy of the basis set, so a TZ basis set will be better than, e.g. a Double Zeta basis set (one which uses two times the number of functions as the minimum basis set), such as 6-31+G**, which is also used in this work.

The 6-311+G** basis set also contains additional functions which increase its accuracy: polarisation and diffuse functions, denoted by the * and + symbols, respectively. Polarisation functions add a function with a higher angular momentum than that required for the ground state description for each atom, allowing the orbitals to change shape. For example, a hydrogen atom only requires an *s*-type orbital to be described, but a *p*-type can be added. This allows for a more accurate description of the molecular orbitals formed in atomic orbital overlap. A single * means that polarisation is only applied to heavy atoms (i.e. only *d*-type functions have been added); the double ** means that polarisation is applied to heavy atoms and hydrogen (i.e. *d*-type functions are added to heavy atoms and *p*-type functions are added to hydrogen atoms). Polarisation functions on hydrogen atoms are important to include in this work as the interactions present in many of the explored structures arise from the interaction of hydrogen atoms with other atoms.

Diffuse functions allow orbitals to take up more space and extend further from the nuclei. They are larger versions of the functions and are important when loosely bound electrons are present.[3] As with the notation for polarisation functions, the single + denotes that a diffuse function has been added to heavy atoms and a ++ that they have been added to heavy atoms and hydrogen atoms. In this work, diffuse functions are included on heavy atoms because some of the structures modelled are anions (e.g. the metalate anions).

Although increasing the size of the basis set (the number of functions used) will improve the accuracy of the calculation, in practice this is only possible to a certain extent, depending on how much compute time is available. Therefore, there will always be some error in the

calculations, and this error can be quite large.[3] However, provided the same basis set(s) are used between systems, the relative energies can be calculated and used as a means of comparison and understanding as the errors will usually be similar.

2.1.1.5 Pseudopotentials

Effective core potential basis sets can be used for elements from the third row or higher, which have a large number of core electrons that have little influence on the chemical properties but which cannot be ignored without resulting in an inaccurate description of the valence orbitals.[3] These basis sets use an effective core potential, or pseudopotentials, to represent the core electrons.[14] The valence electron wavefunction is unaltered by this process.[15] This method also provides an opportunity to correct for the effects of relativity, which the core electrons of heavy elements experience, in a less computationally demanding manner than using a basis set for all electrons which is able to model relativistic behaviour.[16]

In this work the LANL2TZ[17] basis set/pseudopotential is used for Rh. The core elections of Rh are replaced by the pseudopotential and TZ-level functions treat the valence electrons. Similarly, the LANL2DZ basis set is employed for Au.

2.1.1.6 Basis set superposition error

As discussed, for energy comparisons to be made the basis set(s) used must be consistent between the systems. However, a problem arises with basis sets that are localised on atoms.[3] An error is introduced due to the "overlap" of basis sets: that is, the basis set from one atom on one molecule may also treat another atom in a neighbouring molecule, meaning there are more basis functions per atom for e.g. two molecules interacting as a dimer than for isolated molecules. The overall effect is an artificial lowering in energy (i.e. stabilisation) of the dimer. This is known as the Basis Set Superposition Error (BSSE), and must be corrected for if, for example, formation energies are sought for complexes formed from multiple components.

BSSE can be corrected for in two ways. The first is to use basis sets which are so large that the overlap produces no lowering in energy. However, this is computationally very demanding and therefore not practical for many systems. The second is to use the Counterpoise correction:[18] a means of approximately calculating the size of the error in energy and removing it. The Counterpoise correction calculates the energy of a system (e.g. the monomers) using both the "enhanced" basis set of the system where basis set overlap

occurs (e.g. the dimer) and the regular basis set and considers the difference to be the BSSE. So, for the calculation of the dimer formation energy (Equation 2.8, where * denotes the geometry of A, B or AB in the dimer and $_{ab}$ and $_{a}$ or $_{b}$ denote the larger basis set due to overlap in the dimer and the regular basis set used for the monomers, respectively), the Counterpoise energy correction (Equation 2.9) would be subtracted from the value obtained ($\Delta E_{f\,corrected} = \Delta E_f - \Delta E_{CP}$). This is the way in which BSSE has been addressed in this work.

$$\Delta E_f = E(AB)^*_{ab} - E(A)_a - E(B)_b \qquad 2.8$$

$$\Delta E_{CP} = E(A)^*_{ab} + E(B)^*_{ab} - E(A)^*_{a} - E(B)^*_{b} \qquad 2.9$$

2.1.1.7 Implicit solvent modelling

Explicit solvation (including individual solvent molecules) is not done in this work, due to the increased computational demand this would involve. Instead implicit solvent modelling is used, where the solvent is treated as a continuous medium. The Self-Consistent Reaction Field (SCRF) model is employed. In this model the solvent is considered to be a uniform polarisable medium with a specific dielectric constant and the solute is in a suitably shaped hole within the solvent medium.[3, 19] The energy of solvation is determined from the (destabilisation) energy of creating the hole for the solute, the (stabilisation) energy for the dispersion interactions of the solute with the solvent, and the (stabilisation) energy of the electrostatic interaction of the solute with the solvent due to the charge distribution on the solute. Different reaction field methods treat the aspects of the model (e.g. how the size and shape of the solute hole is defined, how the dispersion contributions are calculated, etc.) in different ways. In this work the Polarizable Continuum Model (PCM)[20] is used. It uses "a van der Waals surface type cavity, a detailed description of the electrostatic potential, and parameterizes the cavity/dispersion contributions based on the surface area" of the cavity.[3]

2.1.2 Quantum Mechanical Calculations

2.1.2.1 Geometry optimisation

Geometry optimisation calculations allow the minimum energy structure of a molecule or assembly to be found. From this, other calculations can be conducted (e.g. vibrational

frequency calculations) to gain extremely valuable information, such as the Gibbs free formation energies and simulated spectra.

Set up as a series of iterative calculations (as illustrated in Figure 2.1), geometry optimisation begins with the specification of a starting geometry. This can be taken from many sources, e.g. from a crystal structure or drawn in a model builder, however, geometry optimisation will only target the local minimum close to the starting structure, so it is important to choose a starting structure close to the target minimum or to use multiple different starting structures. The first step in the actual geometry optimisation cycle is the determination (or estimation) of the wavefunction for the starting configuration of atoms. This is a self-consistent field (SCF) cycle where the weighting coefficients of the basis set are varied until the wavefunction converges to one that most accurately approximates the electronic ground state of the system. The energy of the input structure is calculated from this wavefunction, along with the forces acting on the atoms and estimates of the force constants. From this a set of new atomic coordinates is predicted, and the atoms are moved to this position. The SCF cycle is repeated for this new geometry and the energy obtained is compared to the energy of the previous geometry. This iterative process continues until the convergence criteria are met: usually that the forces on the atoms are close to zero, determined by the gradient of the potential energy surface (PES) being close to zero, and the atomic displacements have become very small. At this point, the geometry is considered optimised (within the convergence criteria specified).

However, this process does not guarantee that the optimised geometry is a minimum. For example, the gradient of the PES is also zero at a transition state. To confirm the nature of the stationary point obtained, a vibrational frequency calculation should be employed, wherein the force constants are calculated (and consequently the vibrational frequencies of the optimised geometry are determined). If negative force constants are found, giving rise to imaginary frequencies, then a transition state structure has been obtained instead of a minimum. If a minimum is desired, the geometry optimisation process can be repeated with a slightly modified structure or with tighter convergence criteria.

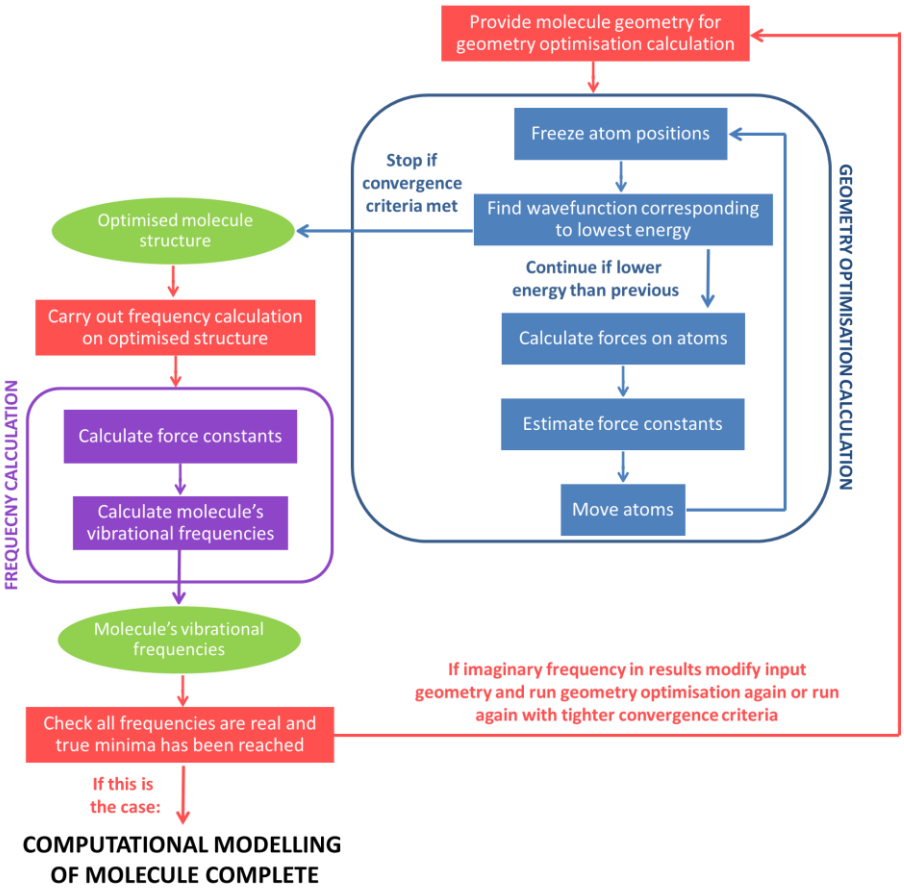

Figure 2.1. Procedure of a QM geometry optimisation and frequency calculation to determine the minimum energy structure, including most likely user steps (in red). Convergence criteria are based on how close the forces and atomic displacements are to zero.

The energies reported in geometry optimisation calculations are SCF energies but corrections, such as the zero-point energy correction and those for enthalpy and entropy to convert SCF energies to Gibbs free energies, can be determined from the vibrational data given by the frequency calculations. The energies discussed in this work are all Gibbs free energies, unless otherwise specified.

2.1.2.2 Formation energies

Formation energies, such as extractant protonation energies, assembly formation energies and anion exchange energies, can be calculated from the energies obtained for the geometry optimised structures. Formation energies are calculated according to Equation 2.10, as simply the difference between the sum of the Gibbs free energies of the products minus the

sum of the Gibbs free energies of the reactants, provided the effects of BSSE are accounted for.

$$\Delta G_f = \sum G_{products} - \sum G_{reactants} \qquad 2.10$$

2.1.2.3 General QM calculation details

All calculations in this work were carried out on the Edinburgh Compute and Data Facility's Eddie Mark 2 and 3 clusters. Geometry optimization and frequency calculations were carried out using the Gaussian 09 program.[21] The functionals and basis sets used are given in the corresponding results chapters. Structures were considered optimized when the forces and atomic displacements fell to within the program default or the tight convergence criteria, if required, in order to reach a minimum point on the potential energy surface, verified by a subsequent vibrational frequency calculation. Where minima were not obtained (and could not be obtained) this has been flagged in the results and structures corresponding to the lowest SCF energies calculated were taken forward. BSSE corrections were applied where appropriate by carrying out counterpoise calculations,[22, 23] and the energy corrections obtained are applied in the calculation of formation energies.

2.1.3 Classical molecular mechanics theory

Rather than considering the electrons and nuclei as in QM modelling, classical mechanics treats atoms as hard spheres, with fixed radius, mass and charge. Molecules are treated using a "ball and stick" model, with atom-atom interaction terms determining the potential energy (V) of a system (as given in Equation 2.11)[1]. This expression represents an energy penalty function if a molecule is stretched, bent, or twisted away from some pre-determined minimum energy structure. The first term considers bond stretching, as a simple derivation of a harmonic potential as defined by Hooke's Law, (where k_l is the force constant of the bond stretch, l_0 is the reference bond length defining the minimum energy structure, and l is the length the bond may stretch or compress to in the simulation).[1] The second term considers angle bending (where k_θ is the force constant of the angle bend, θ is the size of the angle in the particular geometry being considered, and θ_0 is the reference angle size). The

third term treats the dihedral (or torsional) twists using a cosine series expansion (where τ is the torsion angle, *K* is, qualitatively, the energy 'barrier' height and φ is the phase factor which determines where the torsion angle is at a minimum). The non-bonding interactions (considering only atoms that are more than three bonds apart) are covered in the fourth term, which models through space interactions as a function of the inverse power of the distance between pairs of atoms (*i,j*), combining the Coulomb potential (for electrostatic interactions) and the Lennard Jones Potential (for van der Waals interactions). In Equation 2.11 *q* is the partial atomic charge, ε_{ij} is the well depth, σ_{ij} is the collision diameter (separation between atoms for which the energy is zero), and r_{ij} is the distance between the two atoms.[1]

$$V(r^N) = \sum_{bonds} \frac{k_l}{2}(l - l_0)^2 + \sum_{angles} \frac{k_\theta}{2}(\theta - \theta_0)^2 + \sum_{dihedrals} \frac{K}{2}[1 + cos(n\tau - \varphi)] + \sum_{i=1}^{N} \sum_{\substack{j=i+1 \\ non-bonded}}^{N} \left(4\varepsilon_{ij}\left[\left(\frac{\sigma_{ij}}{r_{ij}}\right)^{12} - \left(\frac{\sigma_{ij}}{r_{ij}}\right)^{6}\right] + \frac{q_i q_j}{4\pi\varepsilon_0 r_{ij}}\right) fij \quad 2.11$$

The reference values that are required to define the potential energy equation are obtained from experiment or from high-level QM calculations. The force fields formed from the reference values and the potential energy equation provide generic structural chemistry information, distilling a complex molecule down to reference atom types. Through this approximation significant errors can be incurred if the molecule of interest is very different from those from which the force field was built. To a certain extent, this can be mitigated against by choosing an appropriate force field for the problem in hand, with specialised force fields existing for, for example, protein simulations (e.g. AMBER[24] and CHARMM[25]) and condensed phase simulations (such as the Drieding force field[26] or OPLS-AA force field,[27] as used in this work). However, classical calculations are significantly less computationally demanding than QM simulations, allowing for much larger systems to be explored. This is beneficial in this work where the formation of large aggregates from neat solvent is explored.

2.1.4 Classical molecular dynamics simulations

MD simulations allow the particles in an assembly to move and interact by introducing kinetic energy (temperature) into the simulation. MD is thus a very useful technique for modelling SX as it allows the theoretical self-assembly of extracted complexes to be observed. MD simulations are based on Newton's equations of motion, in particular Newton's Second Law, which states that force is equal to mass times acceleration. In classical MD, the forces are derived from the gradient of the potential energy surface, as defined by Equation 2.11, for the given molecular configurations. MD simulations predict where the particles will be a certain time step into the future, based on the forces acting on the particles under user set conditions, and then move them. This process is repeated for a desired number of time steps to build up what is essentially a "molecular movie" where the particle positions at each time step make up the frames of the movie. Figure 2.2 gives the general scheme of the process of an MD simulation.

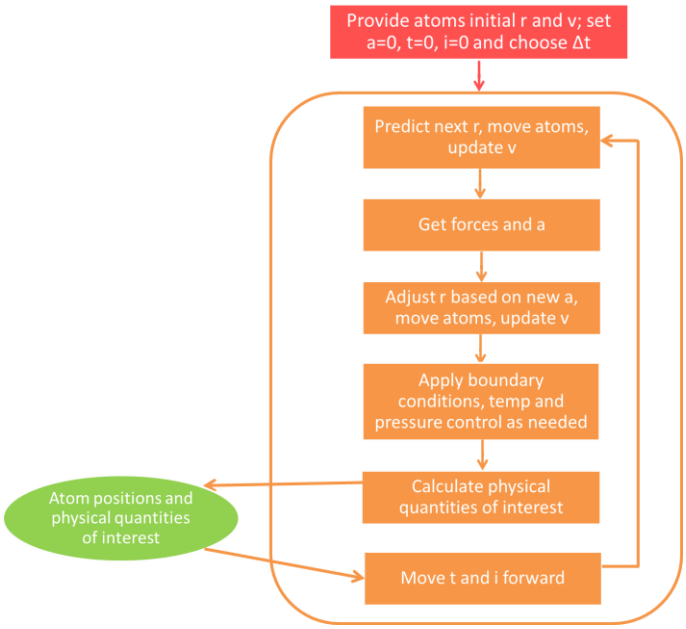

Figure 2.2. Procedure of a molecular dynamics simulation; a = acceleration, i = iteration, r = position/coordinates, t = time, v = velocity.

The simulation timestep, the time between each frame of the simulation, must be chosen carefully. If too large a timestep is employed instabilities may occur in the integration algorithm due to atom overlaps, while too small a timestep means the trajectory will only cover a very small portion of phase space.[1] When simulating flexible molecules it is suggested

that a timestep of approximately one-tenth of the shortest vibration be used.[1] The groups with the highest frequency vibrations in the systems of study are O-H groups, with a frequency of ~10 fs, meaning the maximum suggested timestep to avoid instabilities is 1 fs. In this work, a timestep of 0.5 fs has been employed.

2.1.4.1 OPLS-AA force field and parameters

The force field applied in the classical MD simulations in this work is the Optimised Potentials for Liquid Simulations – All Atom (OPLS-AA),[28, 29] with exceptions in the parameters used as discussed in Chapter 6 Section 6.4.3.1. The form of the force field is similar to that given in Equation 2.11, excepting the addition of a scaling factor (f_{ij}) to the non-bonded term, which is 0.5 for 1,4 interactions and 1.0 otherwise (non-bonded interactions only counted for atoms three or more bonds apart);[28] and the description of the dihedral energy as a Fourier series for the torsional movement of the dihedrals (as given in Equation 2.12, where K_n are the coefficients in the Fourier series and ϕ is the dihedral angle size).[28, 30]

$$E_{dihedrals} = \sum_{dihedrals} \frac{1}{2}K_1[1 + cos(\phi)] + \frac{1}{2}K_2[1 + cos(2\phi)] + \frac{1}{2}K_3[1 + cos(3\phi)] + \frac{1}{2}K_4[1 + cos(4\phi)] \quad 2.12$$

2.1.4.2 MD calculation details

All simulations were carried out on the Edinburgh Compute and Data Facility's Eddie Mark 2 and 3 clusters, running the LAMMPS (Large-scale Atomic/Molecular Massively Parallel simulator)[31, 32] code. For each system (i.e. different molecular constituents), two simulations were carried out. Input "boxes" were prepared using Packmol,[33] which randomly packed the anion, cation, extractant molecules and the desired number of water molecules into a box of specified size. The structures of the input molecules packed into the box were those obtained from geometry optimisation calculations with Gaussian 09[21] (see Chapter 6 Section 6.4.2 for details). Visual Molecular Dynamics (VMD)'s[34] Topo tools were then used to specify the partial charges (see Chapter 6 Section 6.4.3.1 for parameter discussion) on the atoms and generate a LAMMPS data file from the xyz output file from Packmol. Additional parameters (masses, pair coefficients, bond, angle and dihedral parameters) were manually added to the data file.

A LAMMPS input script (an example is included in the SI) was used to define the calculation specifications. All simulations were carried out in a cubic simulation cell (of length 55 Å, unless otherwise specified) with periodic boundary conditions applied in all directions. Initial simulation runs were as follows: a minimisation cycle (maximum of 1000 iterations) was carried out, then 0.25 ns (time step of 0.5 fs) of canonical (constant number of atoms, volume of box, and temperature, NVT) ensemble conditions, followed by a minimum of 12 ns (time step 0.5 fs) of isothermal-isobaric (constant number of atoms, pressure, and temperature, NPT) conditions. The simulations were thermostated at 293 K using the Nosé-Hoover thermostat and the NPT simulations were barostated using the Nosé-Hoover barostat.

2.2 Experimental

As discussed in Chapter 1, structural analysis of the assemblies formed in the organic phase during extraction is made difficult by the fact that they are present in solution. There is no one technique that can provide all the information desired. Thus, a range of experimental analysis techniques are used in this work.

2.2.1 Solvent Extraction Experiments

All contacts were carried out in sample vials or Schott bottles and mixed with stirrer bars on a stirrer plate. An equal volume of aqueous phase and organic phase were added to the vial/bottle and stirring was conducted for the time specified. After stirring, the phases were allowed to disengage or were centrifuged (see specific details in the results chapters). The two phases were then physically separated. Figure 2.3 gives an illustration of the general processes for extraction and stripping (back extraction).

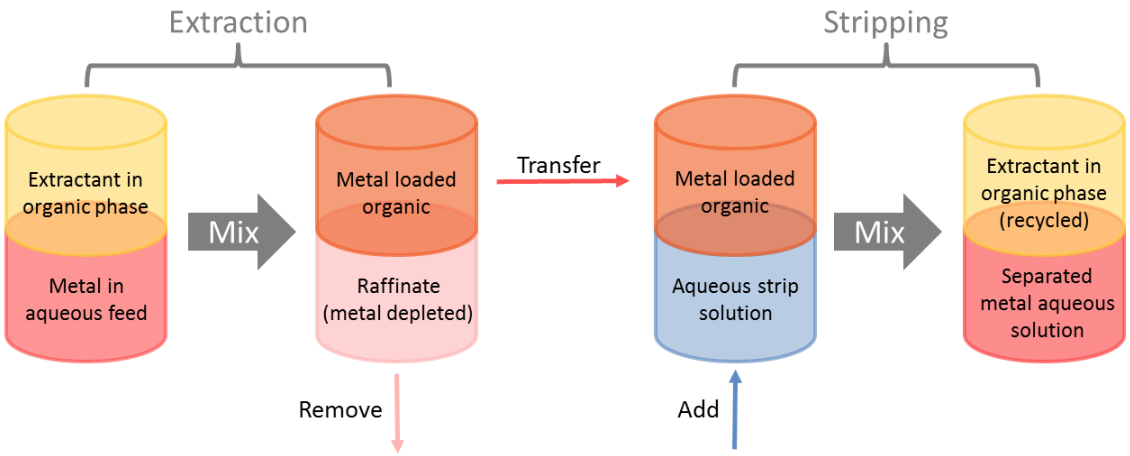

Figure 2.3. General method of an extraction and stripping experiment.

The basic equations used to calculate percentage extraction and stripping are given in Equations 2.13 and 2.14 (where $metal_{(x)}$ is the absolute amount of metal in solution x). If the volume of the aqueous phase and the organic phase used in the experiment are equal (as is the case with all experiments conducted in this work) and no significant volume change of either phase occurs upon extraction (as is assumed for all experiments conducted in this

work), then the concentration of metal in the phases can be used in place of the absolute amount of metal in the phases.

$$\%extraction = \frac{M_{(loaded\ org.)}}{M_{(aq.\ feed)}} \times 100 \quad 2.13$$

$$\%stripping = \frac{M_{(aq.\ strip)}}{M_{(loaded\ org.)}} \times 100 \quad 2.14$$

The concentration of metal in the loaded organic can be directly measured, or it can be inferred from the metal removed from the aqueous phase (provided metal can only be in either the aqueous or organic phases, i.e. third phase or precipitate has not formed). Similarly, if a value for the concentration of metal in the feed is not available/is less reliable due to the dilution required for analysis, the sum of metal in the aqueous and organic phases post-extraction can be used in its place.

Distribution (*D*) values (the ratio of metal in the organic phase compared to the aqueous phase) are calculated using Equation 2.15.

$$D_M = \frac{[M]_{(org)}}{[M]_{(aq)}} \quad 2.15$$

Separation factors, which provide information on how preferentially a metal is extracted over another, are given by the ratio of the D values for the two metals in question, as in Equation 2.16.

$$S_{AB} = \frac{D_A}{D_B} \quad 2.16$$

It is also possible to use the *D* value to provide information on the ratios of metal to other components in the organic phase complexes. This numerical analysis, called “slope analysis”, is possible due to the relationship (based on the equilibrium in Equation 2.17) found between the *D* value and the concentration of the species involved in the extraction, as given in Equation 2.18. Plotting log *D* against log [X^-], log [L] or log [H^+] will give a straight line with a gradient that corresponds to the ratio of anion, extractant or proton to metal. This depends, however, on a single metal assembly forming in the organic phase.[35]

$$M + aX^- + bL + bH^+ \rightleftharpoons [MX_a(LH)_b] \quad (2.17)$$

$$K = \frac{[MX_a(LH)_b]}{[M][X^-]^a[L]^b[H^+]^b}$$

$$D_M = \frac{[M]_{(org)}}{[M]_{(aq)}} = \frac{[MX_a(LH)_b]}{[M]}$$

$$K = \frac{D}{[X^-]^a[L]^b[H^+]^b}$$

$$D_M = K[X^-]^a[L]^b[H^+]^b$$

$$\log D_M = \log K + \log[X^-]^a + \log[L]^b + \log[H^+]^b$$

$$\log D_M = \log K + a\log[X^-] + b\log[L] + b\log[H^+] \quad (2.18)$$

For the majority of the work contained in this thesis, only percentage extraction or *D* values are discussed. However, numerical analysis techniques such as slope analysis are very common within SX literature and are thus detailed here to allow for better understanding of any relevant literature discussion.

2.2.2 ICP-OES Analysis

Inductively Coupled Plasma Optical Emission Spectroscopy (ICP-OES) is an emission spectroscopy technique used for elemental analysis. Liquid sample solutions are aspirated into a plasma where the sample is ionised and excited. The emission from the excited ions, which is of a wavelength characteristic to the ion and its excitation, is measured and, by comparison to standards of known concentration, the concentration of particular elements in a sample can be determined. A schematic representation of an ICP-OES spectrometer is given in Figure 2.4. This technique can be used to measure the metal concentration of the different phases in extraction.

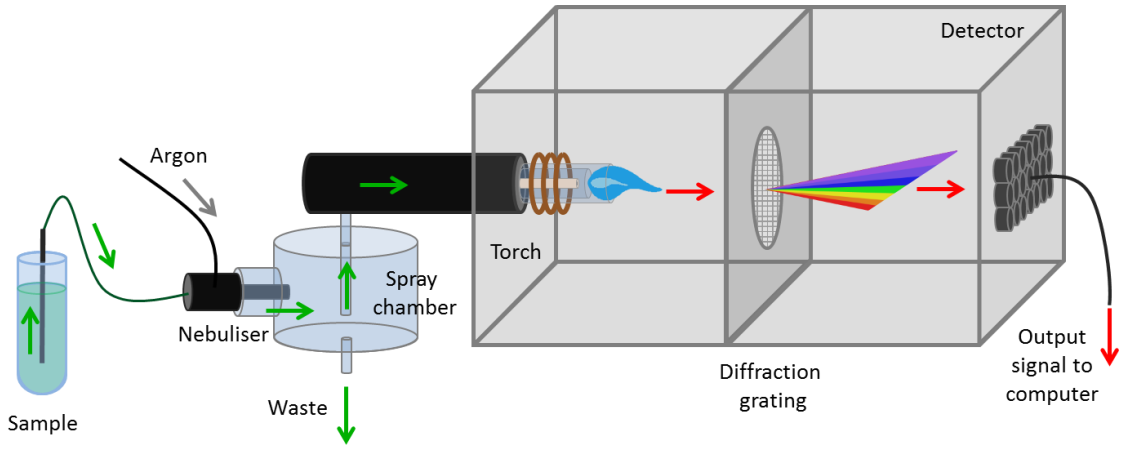

Figure 2.4. Illustration of an ICP-OES spectrometer.

In this work, samples (of both organic and aqueous phases) were prepared for ICP-OES analysis by dilution of at least ten times in 1-methoxy-2-propanol.

ICP-OES analysis was carried out on a Perkin Elmer Optima 5300DC Inductively Coupled Plasma Optical Emission spectrometer or a Perkin Elmer Optima 8300 Inductively Coupled Plasma Optical Emission spectrometer. Table 2.1 gives the details of the set-up and instrument conditions in each case. ICP-OES calibration standards were obtained from VWR International or Sigma-Aldrich and standards of the appropriate concentrations prepared by dilution in 1-methoxy-2-propanol.

Table 2.1. ICP-OES analysis conditions

Spectrometer	PerkinElmer Optima 5300DC	PerkinElmer Optima 8300
Nebuliser	Gem Tip cross-flow	Gem Tip cross-flow
Spray chamber	Glass Cyclonic	Glass Cyclonic
Radio frequency power	1500 W	1500 W
Plasma gas flow (argon)	20.0 L min^{-1}	15 L min^{-1}
Auxiliary gas flow (argon)	1.4 L min^{-1}	1.0 L min^{-1}
Nebuliser gas flow (argon)	0.45 L min^{-1}	0.5 L min^{-1}
Peristaltic pump rate	2.0 mL min^{-1}	1.0 mL min^{-1}

2.2.3 Karl Fischer Titrations

Karl Fischer (KF) titrations were used to quantify the amount of water that was soluble or extracted into the organic phase. They work on the basis of the electrochemical reaction of water with iodine and sulfur dioxide (Equation 2.19).[36, 37]

$$I_2 + SO_2 + 2\ H_2O \rightleftharpoons 2\ HI + H_2SO_4 \qquad 2.19$$

Fischer showed that, in the presence of an excess of sulfur dioxide, this reaction could be used to determine the concentration of water in non-aqueous solvent.[38] In alcohol solvent and in the presence of a base (B), which neutralises the acids formed in the reaction, the titration proceeds via the reactions given in Equations 2.20 and 2.21.[37, 39] Methanol is the most common alcohol used as the solvent, however, it can be replaced with others,[40] as is done when the sample may react with methanol.[37] In modern KF titrations, imidazole is used as the base, providing the benefits over traditionally used pyridine of being less toxic and buffering in a pH range more suitable for KF titrations (ideal pH range of 5.5 to 8).[37, 41, 42]

$$ROH + SO_2 + B \rightleftharpoons (BH)\cdot SO_3R \qquad 2.20$$

$$(BH)\cdot SO_3R + 2\ B + I_2 + H_2O \rightleftharpoons (BH)\cdot SO_4R + 2\ (BH)I \qquad 2.21$$

Two different approaches to KF titrations are in use: volumetric and coulometric (see Figure 2.5). In volumetric KF titration, the iodine (as part of the titrant, which also contains sulfur dioxide and imidazole dissolved in alcohol) is added via a burette to the sample dissolved in the alcohol solvent. In coulometric KF titration, the iodine is generated electrochemically during the titration from a reagent which is present in the titration cell.

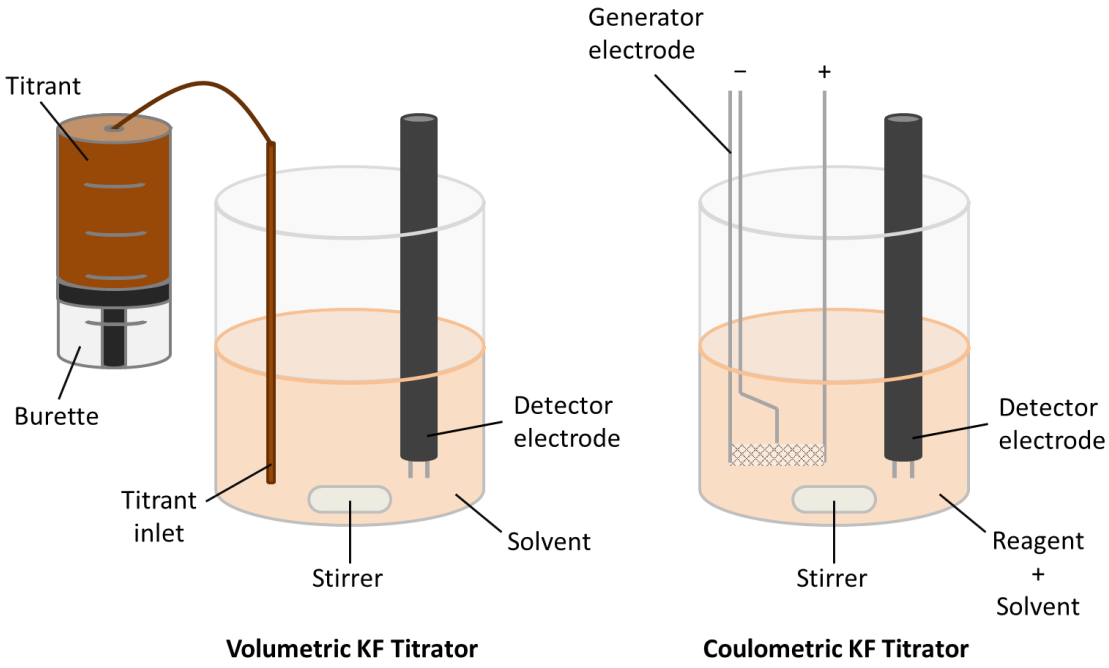

Figure 2.5. Illustration of the setups for volumetric (left) and (diaphramless) coulometric (right) KF titration.

In both cases, a detector electrode is present: a double pin platinum electrode that monitors the potential of the solution by voltammetry,[37] allowing for the titration endpoint to be determined. In coulometric KF titration a generator electrode is also present, where iodine is formed from iodide at the anode. The electrons liberated react with H^+ at the cathode to form hydrogen gas.[37]

In volumetric KF titration, the volume of titrant added to reach the endpoint of the titration gives the amount of iodine which reacted, and so the amount of water present in the sample. In coulometric titration, the amount of electrical current used to generate iodine is measured, giving the amount of iodine (and so the amount of water) based on the fact that 96485 C is required per mole of electrons and two moles of electrons are involved in the oxidation of two moles of iodide to one mole of iodine.[37]

Volumetric KF titrations were carried out using a Mettler Toledo V30 or K5 titrator, using a DGi115-SC electrode. HYDRANAL Methanol dry was used as the solvent and HYDRANAL Composite 5 was used as the titrant for non-ketone samples. For titrations of MIBK-containing samples HYDRANAL Medium K was used as the solvent and HYDRANAL Composite 5 K was used as the titrant. All titrations were carried out in duplicate unless otherwise

specified. HYDRANAL Water Standard 10.0 was used for titre determination and HYDRANAL Standard 5.0 was used for spot checks. Coulometric KF titrations were carried out using a Mettler Toledo C30 or C30S diaphragmless titrator, using a DM 143-SC electrode. HYDRANAL Coulomat AD was used as the titration reagent. These titrations were used only as a check on the performance of the KF titrations and were typically carried out singly. Known masses of sample were injected into the titration vessel(s) and the titrators gave the absolute mass of water contained within the sample.

2.2.4 Acid-base titrations

Acid-base titrations are used to measure the concentration of protons in the organic phase. In this work, sodium hydroxide is used as the titrant base. The end point of the titration, when just enough base has been added to neutralise all the acidic protons, can be determined either with an indicator or potentiometrically.

In this work, manual titrations were conducted using the indicator method. Phenolphthalein, which is colourless in acidic and pink in basic conditions, was used. As acidic samples were titrated with a basic titrant, this resulted in the colour change of colourless to pink indicating that the endpoint had been reached.

A known volume of organic sample (typically 1 mL) was dissolved in 4 mL of propan-2-ol and a few drops of phenolphthalein indicator were added. This solution was then titrated with 0.005 M NaOH with mixing until the colour change from colourless to pink indicated that the end-point had been reached. Titrations were carried out in duplicate.

2.2.5 ESI-MS

Mass spectrometry measures the mass-to-charge ratio of ions, generating a mass spectrum: a plot of intensity versus the mass-to-charge ratio. From this, the mass of the ion can be determined and its likely identity can be confirmed by fitting of chemical formula to the mass and isotope pattern in the spectrum.

Many different techniques can be used to generate ions from a sample and to sort and detect the ions. In this work an Electrospray-Ionisation (ESI) Fourier Transform-Ion Cyclotron Resonance (FTICR) mass spectrometer was used.

ESI is considered a "soft" ionisation technique, i.e. it causes less fragmentation of the molecules in the sample, thereby permitting a greater chance that ionic fragments most representative of the species formed in the SX experiments will be captured in the spectrometer. In ESI, a liquid sample is passed through a needle through which a high voltage is supplied, generating an aerosol of charged droplets which are sprayed into the detection apparatus.[43] The solvent is evaporated and/or the charged droplets "burst" or eject ions, resulting in the production of charged and uncharged particles in the gas phase. The mass-to-charge ratio of the charged particles can be determined by the mass analyser.

The FTICR mass analyser determines the mass-to-charge ratio of the ions based on their cyclotron frequency in a fixed magnetic field.[43] The ions are trapped in a magnetic field with electric trapping plates where they rotate at a frequency (their cyclotron frequency) which is dependent on their mass-to-charge ratio. In the trap they are excited to a higher orbit by an oscillating electric field (at the same frequency as the ion cyclotron frequency) orthogonal to the magnetic field.[44] A charge is induced on a pair of electrodes when the ions pass close to them, producing a free induction decay (FID) signal. Ions of different mass-to-charge ratio can be extracted by using a different radio-frequency (RF) of electric field; when a different RF is employed the excited ions will relax and different ions of the corresponding frequency will be excited. In practice, a swept RF pulse is employed to give essentially simultaneous analysis of all the different ions present in the trap. The complicated FID produced can be treated by Fourier transformation to give a mass spectrum.[43]

ESI FTICR MS measurements were recorded in positive or negative-ion mode using the standard Bruker ESI sprayer operated in "infusion" mode coupled to a SolariX FTICR mass spectrometer. Direct infusion spectra were typically a sum of 10 acquisitions. All mass spectra were analysed using DataAnalysis software version 4.4 (Bruker Daltonics). Ions were assigned manually. Samples were prepared for analysis by dilution in acetonitrile.

2.2.6 EXAFS

Extended X-Ray Absorption Fine Structure (EXAFS) is a subset of X-ray Absorption Spectroscopy (XAS). Some of the energy of the incident X-rays is absorbed by the atoms of the sample, leading to excitation or ejection of core electrons. The amount of absorption can be determined from the difference in the intensity of the incident beam and the transmitted beam, by quantifying the fluorescence produced by the excited atoms as an electron fills the vacant core hole, or by measuring the electrons ejected when the vacant core orbital is filled. This is done for many energies of incident X-rays, allowing a spectrum to be created.[45]

XAS spectroscopy generates a spectrum with distinct regions (see Figure 2.6). A notable feature is the edge: the sharp rise in energy that occurs once the incident X-rays have enough energy to excite electrons from an orbital. The X-ray absorption near-edge structure (XANES) originates from this part of the spectrum. Following the rising edge comes the section of data that is captured in EXAFS. This data permits structural information at a local level, i.e. around the atom that has absorbed the X-ray, to be obtained.

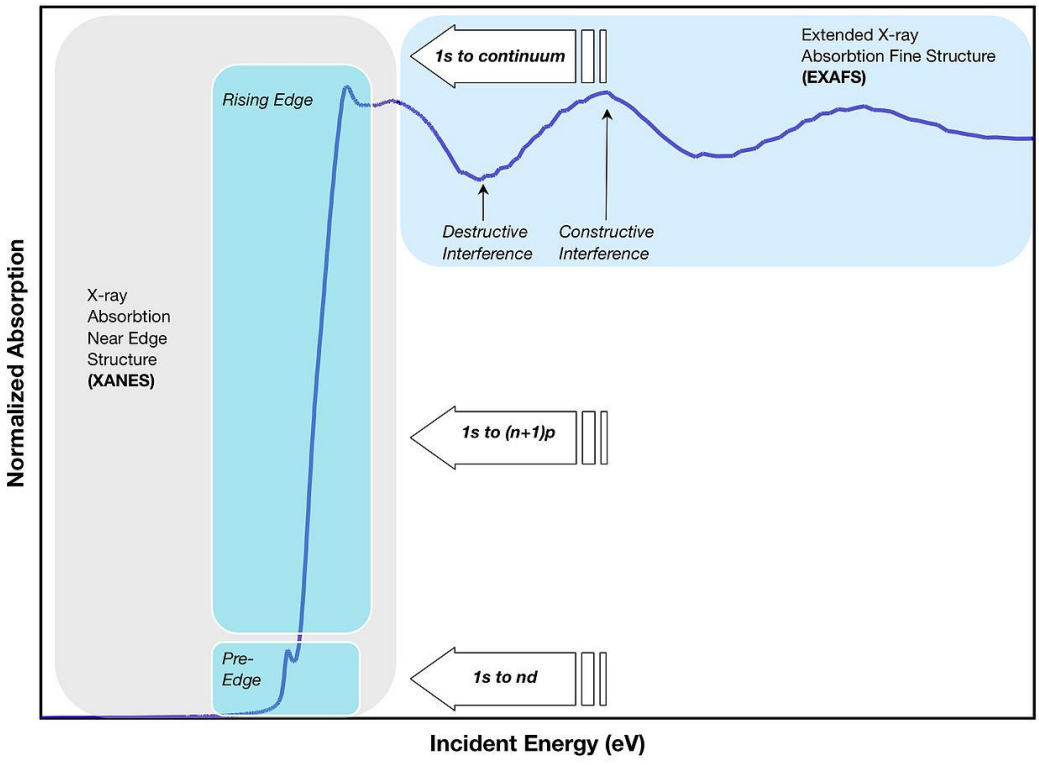

Figure 2.6. Illustration of spectra obtained from XAS, showing the different features observed and the areas of XANES and EXAFS.[46]

The EXAFS signal is produced by the interference of a photoelectron, an electron ejected from an atom in the sample by the X-ray bombardment, with itself. The photoelectron can be considered an electromagnetic wave that can scatter off nearby atoms. The scattered wave can interfere constructively or destructively with the original wave on returning to the absorbing atom.[45] The wavelength of the photoelectron, the distance between the absorbing atom and the scattering atom, and the identity of the scattering atom dictate the nature of the interference. The wavelength of the photoelectron is related to its kinetic energy, which is equal to the energy of the incident photon minus the energy required to eject the photoelectron from the absorbing atom.[45] If the energy of the incident X-ray is changed this changes the kinetic energy, and so the wavelength, of the photoelectron produced. In this way, a scan of photoelectron wavelength can be done, the interference pattern recorded, and this analysed (via Fourier transform) to give information on the coordination sphere around the source atom: the nature of and the distance to the scattering atom(s) can be elucidated.

In this work, Rh K-edge X-ray absorption spectra were collected by Giannantonio Cibin in fluorescence mode at beamline B18, the Core-XAS beamline at the Diamond Light Source, using a Canberra 36-element Germanium detector with XSPRESS2 readout electronics. Data were acquired using a double crystal monochromator with Si(311) crystals, and Pt coated mirrors for beam collimation and focusing. The beam size on the sample was adjusted to have a footprint of approximately 1×1 mm^2. The incident X-ray energy was calibrated against the first inflection point of the K-edge of Rh foil. All solutions were contained in glass capillary tubes, 3 mm diameter for measurements in a gas exchange liquid nitrogen cryostat at 90 K. 10 to 40 three-minute scans in QEXAFS mode to k_{max} = 15 Å^{-1} were averaged for each of the solutions.

Details of data fitting (done by Mark Antonio at the Neutron Scattering Division, Oak Ridge National Laboratory) are given in Chapter 3 Section 3.3.4.

2.2.7 NMR

In Nuclear Magnetic Resonance (NMR) spectroscopy an oscillating magnetic field (RF pulse) is applied to molecules in a static magnetic field. The spin-active nuclei present produce an electromagnetic signal at a characteristic frequency in response to the effect of the oscillating

magnetic field, with the signal characteristic of the electronic environment of the nucleus.[47] Thus, NMR allows for identical nuclei in different chemical environments to be distinguished and it is therefore used widely for structural determination.

Upon excitation by the RF pulse, a nuclear magnetic resonance response or FID signal is obtained. By Fourier transformation, the FID can be transformed into the NMR spectrum.[48] Multiple acquisitions are typically required to achieve good resolution.

In this work, both 1D and 2D NMR are utilised. In 1D NMR the acquisition of the FID is performed immediately after the application of the RF pulse. In 2D NMR acquisition occurs after intermediate stages (evolution and mixing). The evolution stage is a period of time where the nuclear spins are allowed to precess freely following the initial RF pulse(s) which produce magnetisation coherence. The mixing stage is when other RF pulses are used to manipulate the magnetization coherence in order to produce the desired signal for the detection period. To record a 2D data set the pulse sequence is repeated for increasing lengths of evolution time, with the free induction decay measured as a function of the detection time for each evolution time.[48]

In a 2D NMR spectrum there are two frequency axes (representing chemical shift). Each axis is associated with one of the two time variables: the length of the evolution stage or the time elapsed during detection. Each is converted from a time series to a frequency series through a two-dimensional Fourier transform.[48] The final spectrum is a plot of frequency (chemical shift) versus frequency, with a third dimension giving the intensity of each pair of frequency variables.

Various NMR techniques were carried out as part of this work, for synthesis product identification and for characterisation of extraction assemblies.

^{1}H NMR spectra were recorded at 300 K on a Bruker AVA500 or AVA600 spectrometer at 500.12 MHz or 600.75 MHz, respectively. Spectra are referenced internally to residual protio solvent, and chemical shifts are reported in δ (ppm).

^{13}C NMR spectra were recorded at 300 K on a Bruker AVA500 or AVA600 spectrometer at 125.77 MHz or 151.06 MHz, respectively. Chemical shifts are reported in δ (ppm).

^{1}H-^{13}C HMBC and ^{1}H-^{15}N HMBC spectra were recorded at 300 K on a Bruker AVA800 at 799.72 MHz by Juraj Bella. Chemical shifts are reported in δ (ppm).

2.2.8 Other methods and instrumentation

IR spectroscopy for extractant characterisation was carried out on a PerkinElmer Spectrum 65 FT-IR spectrometer with a PIKE MIRacle Attenuated Total Reflectance (ATR) sampling accessory.

CHN elemental analysis was carried out by Dr Stephen Boyer of the London Metropolitan University's Elemental Analysis Service.

In Chapter 2, FT-IR, SANS and X-ray crystallography results are also discussed. These techniques were conducted by collaborators (see Chapter 3 Section 3.2.1 for details) and the experimental details are given in the publication by Narita et al.[49] (which is included in the SI).

2.2.9 Chemicals

All solvents and reagents were used as received from Sigma-Aldrich, Fisher Scientific UK, Alfa Aesar, Acros Organics, VWR International or Merck Millipore. All precious metal salts were used as received from Johnson Matthey PLC. Reverse osmosis and ultrapure waters were obtained from a Milli-Q purification system.

2.2.10 Sources of Error

There are a large number of sources of error associated with SX experiments. In addition to errors associated with instruments, measurements and systematic handling of samples and data (see Table 2.2), there are some more ambiguous sources giving uncertainties that are difficult to quantify. The evaporation of solvents during the solvent extraction experiment, whilst preparing samples for and during ICP-OES analysis, leads to an artificial increase the metal concentration, and there is the possibility of precipitation of metal species on dissolution of samples from the solvent extractions into 1-methoxy-2-propanol, which leads to an artificial decrease in the metal concentration detected by ICP-OES. The concentration detected can also be affected with the changes in volume of the phases on mixing due to entrainment, water extraction, or extractant solubility. In an effort to combat these sources of error, each sample is prepared and analysed in a small timeframe and the same total

volumes are used in dilutions where possible, so some of these effects are at least consistent across all the samples.

Table 2.2. Errors associated with instruments used for SXs

Instrument	**Associated Error**
Mass Balance	± 0.05 mg
1 mL automatic pipette	± 8 µL
5 mL automatic pipette	± 60 µL
1 mL manual pipette	± 8 µL
5 mL manual pipette	± 30 µL
0.5 mL glass pipette	± 5 µL
2 mL glass pipette	± 12 µL *
3 mL glass pipette	± 20 µL *
4 mL glass pipette	± 20 µL *
5 mL glass pipette	± 20 µL *
Positive-displacement pipette	± 3.5% †, ± 7.0% ‡
10 mL volumetric flask	± 0.025 mL
25 mL volumetric flask	± 0.040 mL
100 mL volumetric flask	± 0.080 mL
ICP–OES calibration data	$R^2 > 0.995$
ICP–OES, acid/base titration, or KF titration sample data #	$\sigma = \sqrt{\frac{\sum(x-\mu)^2}{n}}$ σ = standard deviation x = value of sample µ = mean of samples n = number of samples

* Exact error for specific pipettes used unknown – errors given are maximum allowed for Class B volumetric pipettes.
† Maximum systematic error with pipette tips used (actual error at volumes used up to ±0.9%).
‡ Maximum random error with pipette tips used (actual error at volumes used up to ±0.55%).
# Acid/base titrations and KF titrations of samples are usually carried out in duplicate; ICP-OES analysis of the prepared sample (diluted for ICP-OES analysis) is carried out in triplicate but samples are usually only prepared singly for ICP-OES analysis – see further discussion below for the errors used for ICP-OES analysis.

For acid-base titrations and KF titrations, samples are typically analysed in duplicate. In ICP-OES analysis each sample prepared for ICP-OES by dilution is measured in triplicate as part of the analysis process. Typically, the error (relative standard deviation) is less than 2.5%, though for lower concentration samples (approaching the quantification limit of the

instrument) the errors usually are higher (often around 20%). Although the intensity produced by the prepared samples is measured in triplicate, in this work samples are usually only prepared for analysis singly. Also, owing to the potential for error due to drift in the instrument over the course of the ICP-OES analysis process, it is necessary to decide upon a larger, more generic error value than that given by the instrument for a specific sample analysed three times immediately one after the other.

Some error determination work has been done here, including a determination of the error found in reanalysing the same sample later in an ICP-OES analysis run (Table 2.3). It is found that the maximum error for concentrations above 1 ppm is around ±5%; however, below 1 ppm the error is much higher, at around 30% on average.

Table 2.3. Percentage error in Rh standards reanalysed as samples in ICP-OES analysis. Errors given for the two different Rh wavelengths used. *Errors given are the average (between three sets) difference in Rh concentration measured between the "sample" and the stated concentration of the standard as a percentage of the stated concentration of the standard.

Approximate concentration / ppm	Average relative error magnitude / % *		
	343.489 nm	233.477 nm	Average of wavelengths
0.1	30.7	29.7	30.2
1	6.1	3.8	5.0
2.5	5.7	1.4	3.5
5	3.5	0.9	2.2
10	2.0	1.1	1.6
15	3.0	1.8	2.4

In addition, the error in preparing the sample for ICP-OES analysis was estimated by preparing some samples in duplicate and determining the standard deviation in their measured concentrations. It was found that the average relative standard deviation is around ±2.5%, with most below ±5% error though some did reach as high as 10%.

Doidge considered the overall error in a solvent extraction experiment with respect to the metal concentration measurements by carrying out the same set of extractions in quadruplicate (see Figure 2.7).[50] The four sets were run independently but under comparable conditions and from this the absolute error in the percentage metal extraction was estimated to be within ±5%.

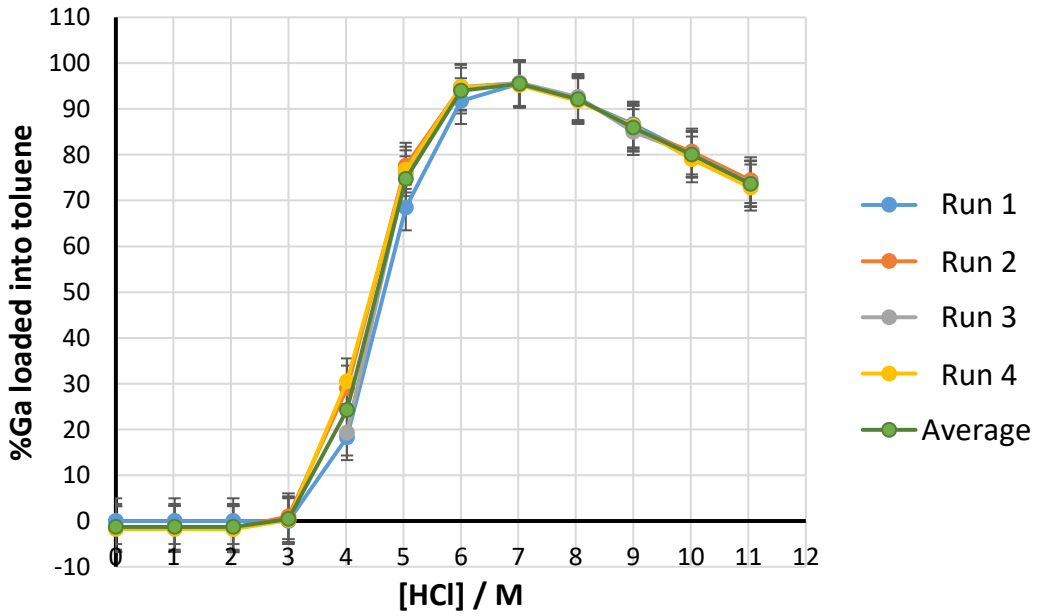

Figure 2.7. Extraction of gallium by a 0.1 M solution of a primary amide in toluene from an aqueous solutions of 0.01 M Ga in varying [HCl]. 1 hour contact time. Results from four independently run experiments (run 1 and run 4 were undertaken around 2 years apart), with an error bar of ± 5% shown for each data point. Reproduced from Doidge.[50]

Considering this work and Doidge's findings,[50] a blanket ±5% relative error is assumed for all metal concentrations determined from ICP-OES analysis in this work and a ±5% absolute error is assumed for all percentage extraction values. This should encompass the concentration error in most samples fully (and perhaps will be an over-estimation for some), though it is likely to be low for some of the very low concentration samples analysed. However, as very low metal concentrations are typically only found for samples where the metal has been almost fully extracted/removed and these values are usually presented as percentages of the original amount of metal present, the assumed error of ±5% on that percentage value will essentially cover the error in the small value used as part of the calculation.

The data presented in this thesis are accompanied by error values wherever possible and the nature of these errors (e.g. assumed error, standard deviation or sigma confidence level value) are stated alongside the data.

2.3 References

1. Leach, A. R., *Molecular Modelling Principles and Applications*. Second Edition ed.; Pearson Education Limited: Harlow, England, 2001.
2. Atkins, P.; Friedman, R., *Molecular Quantum Mechanics*. Fourth Edition ed.; Oxford University Press: Oxford, UK, 2005.
3. Jensen, F., *Introduction to Computational Chemistry*. John Wiley & Sones Ltd.: Chichester, England, 1999.
4. Szabo, A.; Ostlund, N. S., *Modern Quantum Chemistry: Introduction to Advanced Electronic Structure Theory*. First Edition, Revised ed.; McGraw-Hill, Inc: New York, 1989.
5. Hohenberg, P.; Kohn, W., *Phys. Rev.* **1964,** *136*, B864-B871.
6. Kristyán, S.; Pulay, P., *Chem. Phys. Lett.* **1994,** *229*, 175-180.
7. Goerigk, L.; Grimme, S., *PCCP* **2011,** *13*, 6670-6688.
8. Grimme, S.; Antony, J.; Ehrlich, S.; Krieg, H., *J. Chem. Phys.* **2010,** *132*, 154104.
9. Zhao, Y.; Truhlar, D. G., *Theor. Chem. Account.* **2008,** *120*, 215-241.
10. Slater, J. C., *Phys. Rev.* **1930,** *36*, 57-64.
11. Boys, S. F., *Proc. Royal Soc. Lond. A* **1950,** *200*, 542-554.
12. Krishnan, R.; Binkley, J. S.; Seeger, R.; Pople, J. A., *J. Chem. Phys.* **1980,** *72*, 650-654.
13. Raghavachari, K.; Trucks, G. W., *J. Chem. Phys.* **1989,** *91*, 1062-1065.
14. Frenking, G.; Antes, I.; Boehme, M.; Dapprich, S.; Ehlers, A. W.; Jonas, V.; Neuhaus, A.; Otto, M.; Stegmann, R.; et, a., *Rev. Comput. Chem.* **1996,** *8*, 63-144.
15. Yin, M. T.; Cohen, M. L., *Phys. Rev. B* **1982,** *25*, 7403-7412.
16. Dolg, M.; Cao, X., *Chem. Rev.* **2012,** *112*, 403-480.
17. Roy, L. E.; Hay, P. J.; Martin, R. L., *J. Chem. Theory Comput.* **2008,** *4*, 1029-1031.
18. van Duijneveldt, F. B.; van Duijneveldt-van de Rijdt, J. G. C. M.; van Lenthe, J. H., *Chem. Rev.* **1994,** *94*, 1873-85.
19. Tomasi, J.; Persico, M., *Chem. Rev.* **1994,** *94*, 2027-2094.
20. Cossi, M.; Barone, V.; Cammi, R.; Tomasi, J., *Chem. Phys. Lett.* **1996,** *255*, 327-335.
21. Frisch, M. J.; Trucks, G. W.; Schlegel, H. B.; Scuseria, G. E.; Robb, M. A.; Cheeseman, J. R.; Scalmani, G.; Barone, V.; Mennucci, B.; Petersson, G. A.; Nakatsuji, H.; Caricato, M.; Li, X.; Hratchian, H. P.; Izmaylov, A. F.; Bloino, J.; Zheng, G.; Sonnenberg, J. L.; Hada, M.; Ehara, M.; Toyota, K.; Fukuda, R.; Hasegawa, J.; Ishida, M.; Nakajima, T.; Honda, Y.; Kitao, O.; Nakai, H.; Vreven, T.; Montgomery Jr., J. A.; Peralta, J. E.; Ogliaro, F.; Bearpark, M. J.; Heyd, J.; Brothers, E. N.; Kudin, K. N.; Staroverov, V. N.; Kobayashi, R.; Normand, J.; Raghavachari, K.; Rendell, A. P.; Burant, J. C.; Iyengar, S. S.; Tomasi, J.; Cossi, M.; Rega, N.; Millam, N. J.; Klene, M.; Knox, J. E.; Cross, J. B.; Bakken, V.; Adamo, C.; Jaramillo, J.; Gomperts, R.; Stratmann, R. E.; Yazyev, O.; Austin, A. J.; Cammi, R.; Pomelli, C.; Ochterski, J. W.; Martin, R. L.; Morokuma, K.; Zakrzewski, V. G.; Voth, G. A.; Salvador, P.; Dannenberg, J. J.; Dapprich, S.; Daniels, A. D.; Farkas, Ö.; Foresman, J. B.; Ortiz, J. V.; Cioslowski, J.; Fox, D. J. *Gaussian 09*, Gaussian, Inc.: Wallingford, CT, USA, 2009.
22. Boys, S. F.; Bernardi, F., *Mol. Phys.* **1970,** *19*, 553-566.
23. Simon, S.; Duran, M.; Dannenberg, J. J., *J. Chem. Phys.* **1996,** *105*, 11024-11031.
24. The Amber Project website. http://ambermd.org/AmberModels.php
25. CHARMM Chemistry at HARvards Macromolecular Mechanics website. https://www.charmm.org/charmm/?CFID=6f55f5f0-a79e-4ef4-b768-7188a9417e4f&CFTOKEN=0

26. Mayo, S. L.; Olafson, B. D.; Goddard, W. A., *J. Phys. Chem.* **1990,** *94*, 8897-8909.
27. Jorgensen, W. L.; Tirado-Rives, J., *J. Am. Chem. Soc.* **1988,** *110*, 1657-1666.
28. Jorgensen, W. L.; Maxwell, D. S.; Tirado-Rives, J., *J. Am. Chem. Soc.* **1996,** *118*, 11225-11236.
29. Rizzo, R. C.; Jorgensen, W. L., *J. Am. Chem. Soc.* **1999,** *121*, 4827-4836.
30. LAMMPS website: OPLS dihedral style. https://lammps.sandia.gov/doc/dihedral_opls.html
31. Plimpton, S., *J. Comput. Phys.* **1995,** *117*, 1-19.
32. LAMMPS website. https://lammps.sandia.gov/index.html
33. Martinez, L.; Andrade, R.; Birgin, E. G.; Martinez, J. M., *J. Comput. Chem.* **2009,** *30*, 2157-2164.
34. Humphrey, W.; Dalke, A.; Schulten, K., *J. Mol. Graph.* **1996,** *14*, 33-38.
35. Rydberg, J.; Sekine, T., Solvent Extraction Equilibria. In *Solvent Extraction Principles and Practice*, 1st ed.; Rydberg, J.; Claude, M.; Choppin, G. R., Eds. Taylor & Francis: New York, USA, 1992; pp 101-156.
36. Bunsen, R. W., *Leibigs Ann. Chem.* **1853,** *86*, 265.
37. *Good Titration Practice in Karl Fischer Titration*. Mettler Toledo: Switzerland, 2009.
38. Fischer, K., *Angew. Chem.* **1935,** *48*, 394-396.
39. Scholz, E., *Fresenius J. Anal. Chem.* **1983,** *314*, 567-571.
40. Grünke, S.; Wünsch, G., *Fresenius J. Anal. Chem.* **2000,** *368*, 139-147.
41. Verhoef, J. C.; Barendrecht, E., *J. Electroanal. Chem. Interf. Electrochem.* **1976,** *71*, 305-315.
42. Verhoef, J. C.; Barendrecht, E., *Anal. Chim. Acta* **1977,** *94*, 395-403.
43. de Hoffmann, E.; Stroobant, V., *Mass Spectrometry Principles and Applications*. Third ed.; John Wiley & Sons Ltd: Chichester, England, 2007.
44. Marshall, A. G.; Hendrickson, C. L.; Jackson, G. S., *Mass Spectrom. Rev.* **1998,** *17*, 1-35.
45. Calvin, S., *XAFS for Everone*. CRC Press: Boca Raton, FL, 2013.
46. Wikipedia. Extended X-ray absorption fine structure. https://en.wikipedia.org/wiki/Extended_X-ray_absorption_fine_structure
47. Hore, P. J., *Nuclear Magnetic Resonance*. Oxford University Press: 1995.
48. Keeler, J., *Understanding NMR Spectroscopy*. Second ed.; Wiley: Cambridge, 2010.
49. Narita, H.; Nicolson, R. M.; Motokawa, R.; Ito, F.; Morisaku, K.; Goto, M.; Tanaka, M.; Heller, W. T.; Shiwaku, H.; Yaita, T.; Gordon, R. J.; Love, J. B.; Tasker, P. A.; Schofield, E. R.; Antonio, M. R.; Morrison, C. A., *Inorg. Chem.* **2019,** *58*, 8720-8734.
50. Doidge, E. D. Designing reagents for the solvent extraction of critical metal resources. University of Edinburgh, 2018.

Chapter 3

Understanding the extraction of rhodium chloridometalates by amidoamines

3 Understanding the extraction of rhodium chlorido-metalates by amidoamines

3.1 Introduction

3.1.1 Background

In 2008, Narita et al. reported "the first effective extractant for trivalent rhodium in hydrochloric acid solutions".[1] As discussed in Chapter 1, before this seminal paper, reports of other potential extraction reagents showed only moderate effectiveness, usually from low HCl concentration solutions only,[2] unless additional reagents, such as stannous chloride, were employed.[2-12]

The reagent reported to be an effective Rh extractant is *N*-*n*-hexyl-bis-(*N*-methyl-*N*-*n*-octylethylamide)amine (BisAA) (see Figure 3.1). This bisamidoamine molecule is shown to be able to extract over 80% of Rh(III) from a 2 M HCl solution, whereas trioctlyamine (TOA) extracts less than 5% of Rh(III) at this HCl concentration. BisAA also has reasonable extraction resilience to HCl: it is able to maintain extraction of greater than 70% over the range of 0.5 to 4 M HCl, and only reaches negligible extraction at 10 M HCl (see Figure 3.2).[1]

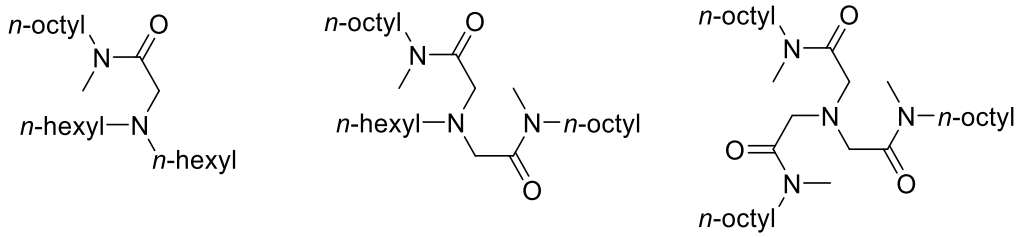

Figure 3.1. Structures of *N*,*N*-di-*n*-hexyl(*N*-methyl-*N*-*n*-octyl-ethylamide)amine (MonoAA), *N*-*n*-hexyl-bis-(*N*-methyl-*N*-*n*-octylethylamide)amine (BisAA), and tris(*N*-methyl-*N*-*n*-octyl-ethylamide)amine (TrisAA).[13]

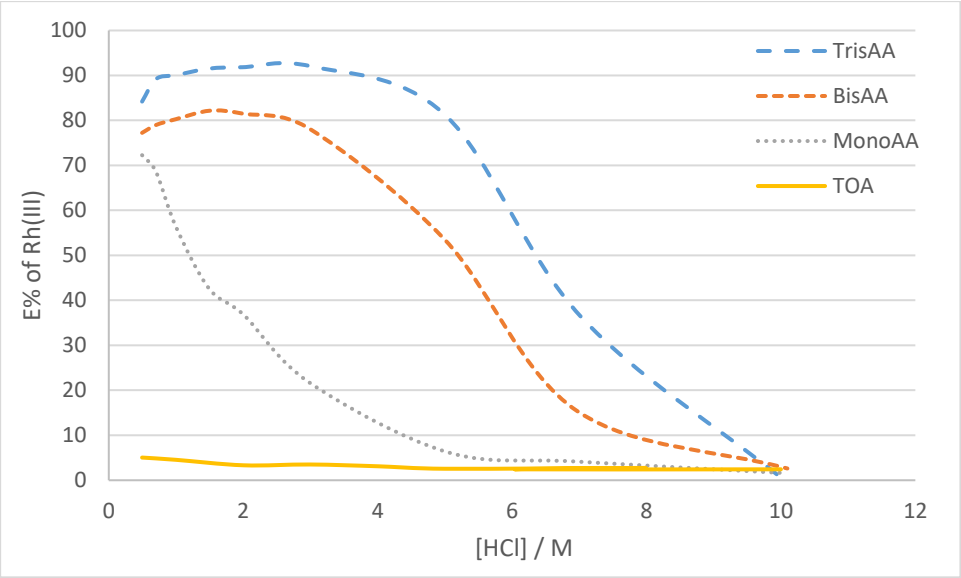

Figure 3.2. Percentage extraction of Rh by TOA, MonoAA, BisAA and TrisAA with varying [HCl] as reported by Narita et al.[13]

In addition, Narita et al. found that the related amidoamines *N*,*N*-di-*n*-hexyl(*N*-methyl-*N*-*n*-octyl-ethylamide)amine (MonoAA) and tris(*N*-methyl-*N*-*n*-octyl-ethylamide)amine (TrisAA) (see Figure 3.1 for their structures) were also superior extractants to TOA (see Figure 3.2).[13] However, MonoAA displays significantly poorer extraction performance (maximum extraction in the range tested of ~70% at 0.5 M HCl) compared to BisAA and TrisAA. TrisAA has a very similar extraction profile to BisAA but gives slightly higher extraction (~90% at 2 M HCl).[13]

All three amidoamines are very good extractants for Pd(II) and Pt(IV), in fact, they are superior Pd(II) and Pt(IV) extractants than Rh(III) extractants as they extract Pd(II) and Pt(IV) "almost quantitatively" over the range of HCl concentrations shown in Figure 3.2.[13] This is a drawback as selectivity for Rh(III) is compromised, however they are still useable for Rh separation from Pt and Pd as they display selective stripping of Rh(III).[13]

It is reported that 10 M HCl can be used to back extract around 90% of Rh(III), while not stripping any Pd(II) or Pt(IV).[13] This is a very promising result, as it illustrates a system where Rh(III) could be recovered first in a SX flowsheet involving Pd(II) and Pt(IV). However, stripping of Pd(II) and Pt(IV) proves more difficult, with 10 M nitric acid only achieving recovery of ~80% and ~60% from MonoAA, ~80% and ~40% from BisAA, and ~50% and ~30% from TrisAA from Pd(II) and Pt(IV), respectively.[13] This is problematic because recovery, especially of

Pt(IV), is low and even if adequate stripping could be achieved with multiple passes or an alternative reagent, the system is being changed from chloride aqueous media to nitric media, or something else. This means that in order for these reagents to be used early in a flowsheet, where Pd(II) and Pt(IV) are still present, major changes would need to be made to accommodate the presence of mixed Pd(II) and Pt(IV) in non-chloride aqueous media.

3.1.2 Understanding the mode of action

As discussed above and in Chapter 1, the amidoamine extractants are the first to show real promise as Rh(III) extractants, being the first to achieve high Rh(III) extraction at relatively high HCl concentrations without the use of additional reagents. However, they do have drawbacks, such as the co-extraction of Pd(II) and Pt(IV) metalates and the difficulty of back-extracting these metals. In order to optimise the performance of amidoamine extractants and potentially design new but related extractants which overcome these limitations, it is important to understand their mode of action. It is hypothesised that they work via an ion-pair mechanism and the Rh complex extracted is $[RhCl_5(H_2O)]^{2-}$ (slope analysis provides a ratio of 2:1 for extractant molecules to Rh(III) and extraction drops at higher HCl concentrations where the speciation of Rh(III) would be changing from predominantly $[RhCl_5(H_2O)]^{2-}$ to $[RhCl_6]^{3-}$).[1] It is also hypothesised that BisAA and TrisAA have features that favour binding to anionic Rh(III) complexes that MonoAA lacks.[13] In addition, the extractants may hydrogen bond to the *aquo* ligand on the Rh metalate anion.[1, 13]

So far, the hypotheses discussed above are theories as to how the amidoamines work and why they provide better extraction than amines. Further work is required to understand what is occurring during extraction at the molecular level and to elucidate the differences in performance between MonoAA and BisAA and TrisAA.

A feature of great interest in using the amidoamines as extractants of $[RhCl_5(H_2O)]^{2-}$ is whether protonation preorganises the receptor to provide a “soft” binding site for the coordinated chloride ions, whilst also allowing the coordinated water molecule to act as an hydrogen bond donor to a carbonyl O-atom of the extractant. The resulting ditopic receptor is shown schematically as (a) in Figure 3.3. Other possibilities include binding of the Rh(III) dianion using just the polarised CH groups of the “proton chelated” cation as in (b) or using a more conventional hydrogen bonding arrangement with the ammonium NH group

functioning as a donor to coordinated chloride atoms as in (c) or (d). In the case of (c), like (a), binding via a hydrogen bond between the carbonyl O atom and an *aquo* H atom is also possible, resulting in the extractant functioning as a ditopic receptor. Further mechanisms, involving inner-sphere complexes in which the *aquo* ligand is displaced by an amide carbonyl group or substitution of the chloride ligands takes place, must also be considered, especially when longer contact times are involved in the SX process.

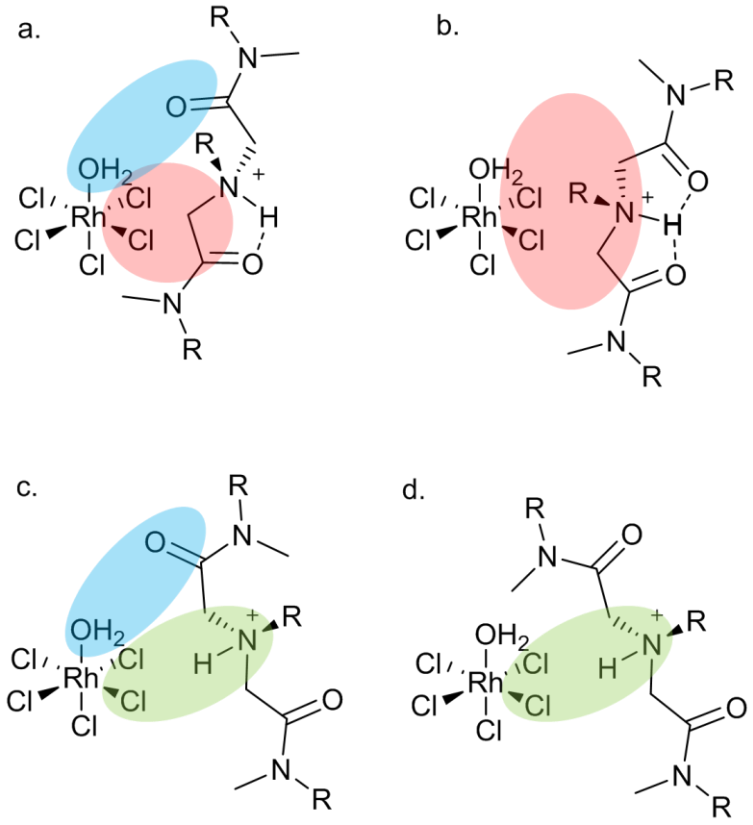

Figure 3.3. Potential outer-sphere ion-pair extractant mode of action, illustrated for one protonated BisAA molecule. Red: proton chelate ring formed, maximising the number of C-H interactions with the Rh(III) *aquo*-chloridometalate anion; green: direct N-H interaction with the anion, negating formation of proton chelate ring; and blue: hydrogen bond between the extractant and the *aquo* ligand.

3.1.3 Scope of this work

This work aims to use a mixture of experimental analytical methods, including titrations, EXAFS and NMR spectroscopies, mass spectrometry, and computational modelling, specifically quantum mechanical structure calculations, to probe the structures of assemblies formed in the organic phase upon Rh(III) extraction.

The study focuses on BisAA, but some comparative experimental work is done with the trialkylamine TOA and the computational modelling includes MonoAA and TrisAA. Experimental work also encapsulates a range of Rh(III) concentrations, from 0.001 M (as reported in the original study) to 0.1 M, which match extraction conditions more routinely encountered in industrial SX processes and allowed for analyses where high Rh(III) concentrations were required to be performed. Structural analyses under short (48 hours) and long (7 months) timescales have also been investigated to shed light on the variable speciation of Rh(III) metalate anions that form in the aqueous and organic phases. While the experimental measurements seek to obtain further evidence to support the postulated ion-pair mechanism and to explore the nature of the Rh(III) coordination shell, the computational modelling aims to provide a full picture of the assemblies which form during extraction, and provide an understanding of how the amidoamines work and why they achieve higher extraction at higher HCl concentrations than amines.

3.1.4 Aims

The aims of this work are to:

i. Use a variety of experimental analysis techniques to determine the nature of the extracted assembly in the SX of Rh(III) from HCl solution with an amidoamine extractant
ii. Compare this to the extraction behaviour with a trialkylamine
iii. Model extraction assemblies with the Rh(III) metalate and chloride using QM calculations to illuminate interactions which contribute to strong SX
iv. Establish the mode of action and why the amidoamine reagents are superior extractants to simple amines

3.2 Results and discussion

3.2.1 Contributions to this work

The work presented in this chapter is the result of a collaboration and has been published.[14]

The contributions to the work are detailed here.

Work carried out by the author of this thesis:

- Synthesis of BisAA for University of Edinburgh (UoE) work and all extractions with BisAA in chloroform.
- KF and acid-base titrations of the extractions in chloroform.
- NMR data analysis.
- ESI-MS data collection and analysis.
- All DFT calculations (except those for fitting).

Work carried out by other contributors:

- All experimental work with BisAA in octanol and on TOA, including KF titrations and FT-IR analysis were carried out by Hirokazu Narita and colleagues at Environmental Management Research Institute, National Institute of Advanced Industrial Science and Technology (AIST).
- Synthesis of extractants/ligands and crystal complexes was carried out by Kazuko Morisaku at the Environmental Management Research Institute, National Institute of Advanced Industrial Science and Technology (AIST).
- EXAFS (set 1) data collection and data analysis were carried out by Hideaki Shiwaku and Tsuyoshi Yaita at the Materials Sciences Research Center, Japan Atomic Energy Agency (JAEA),
- EXAFS (set 2) data collection was carried out by Giannantonio Cibin at the Diamond Light Source on Beam Line 18, and data analysis was done by Mark Antonio at the Neutron Scattering Division, Oak Ridge National Laboratory.
- X-ray crystallography was carried out by Midori Goto at Environmental Management Research Institute, National Institute of Advanced Industrial Science and Technology (AIST).
- 2D NMR data collection was carried out by Juraj Bella at the University of Edinburgh.
- SANS analysis was carried out by Ryuhei Motokawa at the Materials Sciences Research Center, Japan Atomic Energy Agency (JAEA) and William Heller at the

Neutron Scattering Division, Oak Ridge National Laboratory, and the DFT calculations for fitting were carried out by Fumiyuki Ito at Environmental Management Research Institute, National Institute of Advanced Industrial Science and Technology (AIST).

3.2.2 EXAFS study

Initial work focused on verifying if an ion-pair/associate extraction mechanism was indeed the most likely to be occurring. Therefore, techniques were employed to determine if there was any evidence of inner-sphere binding of the extractant to the Rh(III) centre, through one of the amide arms by displacement of the *aquo* ligand, and/or of significant or increased water uptake with Rh(III), potentially implying a reverse micelle mechanism could be occurring.

Two sets of EXAFS experiments were conducted on a range of aqueous and organic Rh(III) containing samples in an attempt to determine which complexes were present. Set 1 relates to BisAA samples in 1-octanol (AIST work),[14] and includes a loaded organic phase from an extraction with trioctylamine (TOA) for comparison alongside two Rh(III) complexes formed with BisAA and BisAA(alt), a molecule with the same functional groups as BisAA but different R-groups (see Figure 3.4). Set 2 relates to Rh(III) BisAA samples in chloroform (UoE work), and explores varying Rh(III) and HCl concentration to determine Rh(III) speciation in the aqueous phase and the organic phase. The main findings are presented in Table 3.1.

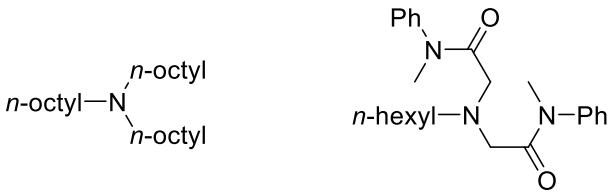

TOA BisAA(alt)

Figure 3.4. Structures of TOA and BisAA(alt) (*N*-*n*-hexyl-bis(*N*-methyl-*N*-phenyl-ethylamide)amine).

Table 3.1. Summary of curve fitting for Rh-EXAFS data, where Atom denotes the identity of the *N* (number) atoms used in the fit and *R* the corresponding bond distance. The estimated standard deviations are reported (in parentheses) at the 2σ level for set 1 and 3σ level for set 2.

Sample	[Rh(III)] / M	[HCl] / M	Atom	*N*	*R* / Å
Set 1					
(a). $RhCl_3$(aq)	0.1	2	O Cl	1.0(1)[a] 5.0(1)[a]	2.06(1) 2.328(4)
(b). 0.5 M BisAAH·Cl in octanol, after contact with solution (a).	0.06	-	O Cl	0.6(3) 5.3(6)	2.06(2) 2.342(9)
(c). 0.5 M **TOA**H·Cl in octanol, after contact with solution (a)	0.06	-	O Cl	1.5(6) 3.8(6)	2.12(3) 2.352(6)
(d). RhBisAA (oil)			O Cl	3.0(10) 3.0(10)	2.06(2) 2.34(2)
(e). [$RhCl_3$(BisAA(alt))] (solid)	-	-	N/O Cl	3[b] 3[b]	2.06(1) 2.320(6)
Set 2					
(f). Na_3RhCl_6(aq)	0.0060	2	Cl	5.5(7)	2.336(7)
(g). Na_3RhCl_6(aq)	0.007	4	Cl	5.8(5)	2.344(4)
(h). Na_3RhCl_6(aq)	0.007	10	Cl	6.1(6)	2.351(4)
(i). 0.1 M BisAAH·Cl in $CDCl_3$ after contact with 0.1 M Rh(III) in 2 M HCl (sample aged by 1 month)	0.041	-	Cl Rh	5.4(5) 1.0(2)	2.347(4) 3.11(1)
(j). 0.1 M BisAAH·Cl in $CDCl_3$ after contact with 0.1 M Rh(III) in 2 M HCl (sample aged by 6 months)	0.05	-	Cl Rh	5.3(7) 0.9(3)	2.348(6) 3.11(2)

[a] Set to equal 6.

[b] Fixed parameter.

Starting with the simplest samples, (f)-(h), which relate to the speciation of Rh(III) with respect to varying chloride concentration in the aqueous phase, Fourier transformations of the EXAFS data show dominance from one large peak at just under 2 Å (see Figure 3.5). Fitting shows this is consistent with a Rh-Cl distance of approximately 2.3 Å (phase corrected). The number of atoms close to Rh (in Table 3.1) indicate that most of the aqueous samples must comprise a mixture of Rh(III) complexes (most likely $[RhCl_6]^{3-}$, $[RhCl_5(H_2O)]^{2-}$, and possibly also $[RhCl_4(H_2O)_2]^-$ and $[RhCl_3(H_2O)_3]$). Whilst it is not possible to determine the proportion of each if there are more than two complexes present, the higher Cl number (6.1±0.6) for (h) suggests that the 10 M HCl sample consists of mostly or exclusively $[RhCl_6]^{3-}$. If the samples are assumed to contain only a mix of $[RhCl_6]^{3-}$ and $[RhCl_5(H_2O)]^{2-}$ (as may be the case at the

HCl concentrations used),[2, 15] (f) must contain 50% of each, while (g) has 80% $[RhCl_6]^{3-}$ and 20% $[RhCl_5(H_2O)]^{2-}$. By inference, sample (a) will therefore consist exclusively of $[RhCl_5(H_2O)]^{2-}$.

That the aqueous sample data appears to support high concentrations of $[RhCl_6]^{3-}$ being present is in line with ^{103}Rh NMR and HPLC-ICP-MS measurements reported in the literature[15, 16] but is contrary to that found in many of the UV-Vis studies,[2, 17] particularly that of Samuels et al. who report that $[RhCl_6]^{3-}$ is essentially not present, even at HCl concentrations as high as 12 M.[17] However, it must be noted that many of the studies have used different sources of Rh ($RhCl_3$ versus Na_3RhCl_6), a variety of Rh concentrations, and have prepared and equilibrated solutions in different ways (length of time before analysis, refluxing, etc.); these factors may have a significant effect on the nature of the Rh complex(es) present.

Turning to the organic samples, fitting the spectra from samples (b) and (c) in Figure 3.5 produces a best fit that corresponds to a 5:1 ratio of Cl : N/O atoms in the Rh(III) coordination sphere (see Table 3.1 for summary). Spectra (d) and (e) have a very different form, with more prominent peaks arising from N/O atoms at shorter distances than those of the Rh-Cl bonds. This highlights that inner-sphere binding is present in the $[RhCl_3$(BisAA(alt))] complex and in the $[RhCl_3$(BisAA)] complex formed over a long time period.

In contrast to the loaded organic samples in set 1, Fourier transforms of the EXAFS data for set 2 samples are dominated by a single large peak at just under 2 Å and an additional smaller peak at around 2.7 Å (see Figure 3.5). Fitting shows that the large peak is a good match to bound chloride, with a bond distance of 2.3 Å (phase corrected), and the smaller peak present in the organic samples match a Rh-to-Rh distance of 3.1 Å (phase corrected). This distance is consistent with that of the dinuclear species, $[Rh_2Cl_9]^{3-}$,[18] which has not been previously observed on extraction using BisAA, mostly likely because the earlier studies used lower concentrations of Rh(III) in the extractions.[1, 13] However, the presence of assemblies based on the $[Rh_2Cl_9]^{3-}$ complex in the organic phases of SX experiments have been reported by others, which can most likely be attributed to differences in extraction conditions.[19, 20]

The absence of this additional feature in the spectra from the aqueous samples (a), (f)-(h) suggests that $[Rh_2Cl_9]^{3-}$ does not exist in the aqueous phase at Rh(III) concentrations below 0.1 M. This is contrary to the UV-vis and DFT work of Samuels et al.[17] Alternatively, it may be present at a concentration too low to be detected by EXAFS analysis. If it is not present in the

aqueous feed solutions, this would suggest that the dinuclear species must form during extraction or over time in the Rh-loaded organic following extraction. This possibility is further explored in Section 3.2.7.

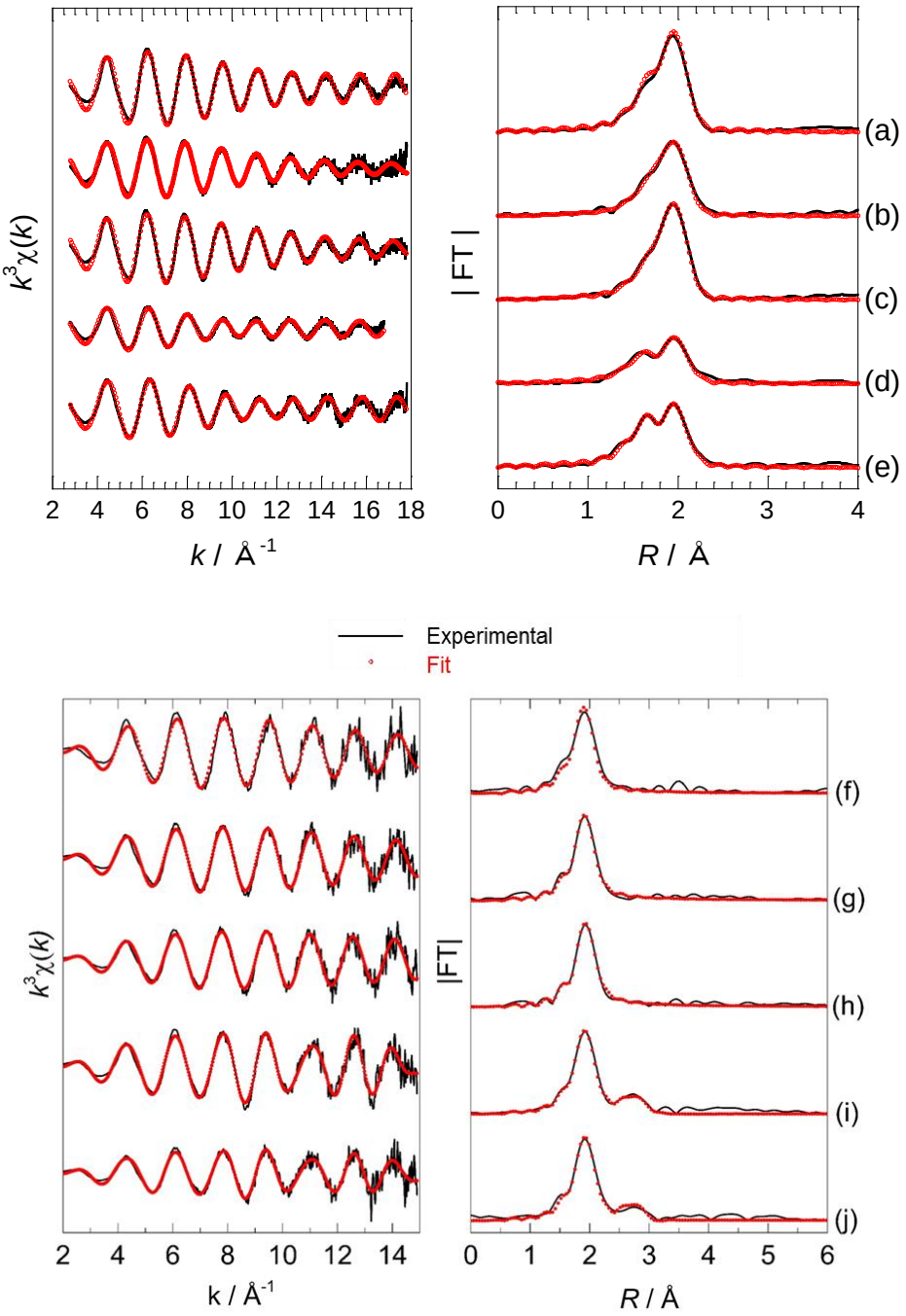

Figure 3.5. (Top, set 1) Rh K-edge k^3-weighted EXAFS (transmission mode) spectra and their Fourier transforms (phase shifts are not corrected) for samples (a)-(e); (bottom, set 2) Rh K-edge k^3-weighted EXAFS (fluorescence mode) spectra and their Fourier transforms (phase shifts are not corrected) for samples (f)-(j) as defined in Table 3.1.

In loaded organic samples (i) and (j) the count of Rh is less than one and the count of Cl is less than six. This suggests a mixture of species is present in the organic phase, some based on the dinuclear Rh(III) species, and some based on mononuclear Rh(III) complexes (some of which must have less than six chloride ligands). Where the CN of Cl is less than six, either O from H_2O or O/N from BisAA will be present and make up the "missing" coordination number. Therefore, it is likely a mix of $(Rh_2Cl_9)\cdot(BisAAH)_3$, $(RhCl_5(H_2O))\cdot(BisAAH)_2$, and $RhCl_3(BisAA)$ complexes are present in the aged loaded organic.

3.2.3 FT-IR spectroscopy and X-ray diffraction

Work done at AIST on the BisAA system (and BisAA(alt)) used FT-IR spectroscopy to probe whether there is any evidence of an amide O atom bound to the Rh(III) centre.[14] The carbonyl stretching frequency ($\nu_{C=O}$) was considered and its value used to determine whether the O atom coordinates to the Rh(III) centre within the timescales used in extraction.

The spectra given in Figure 3.6 show that when BisAA is dissolved in 1-octanol (the solvent used in the AIST work) and is contacted with water, HCl, and Rh(III) in HCl solution, only minor shifts in the frequency of the carbonyl stretch are observed compared to neat, uncontacted BisAA (1649 cm^{-1}). Although they are small, the shifts do provide useful insight. A similar, but slightly lower wavenumber than for neat, uncontacted BisAA (a), is observed for BisAA in 1-octanol (b) and this solution after contact with water (c), implying that BisAA molecules interact with each other or with 1-octanol molecules, but that no direct interaction occurs between water and the amide O atoms. Though slightly higher than for (a), the peak position and shape for the 1-octanol BisAA solution after contact with HCl (d) and after contact with a Rh(III) in HCl solution (e) is near identical, suggesting that the coordination environment around the amide O atom is the same in both systems. This supports an ion-pair extraction mechanism for both Cl and the Rh(III) complex, where no inner-sphere coordination to the Rh(III) centre occurs.

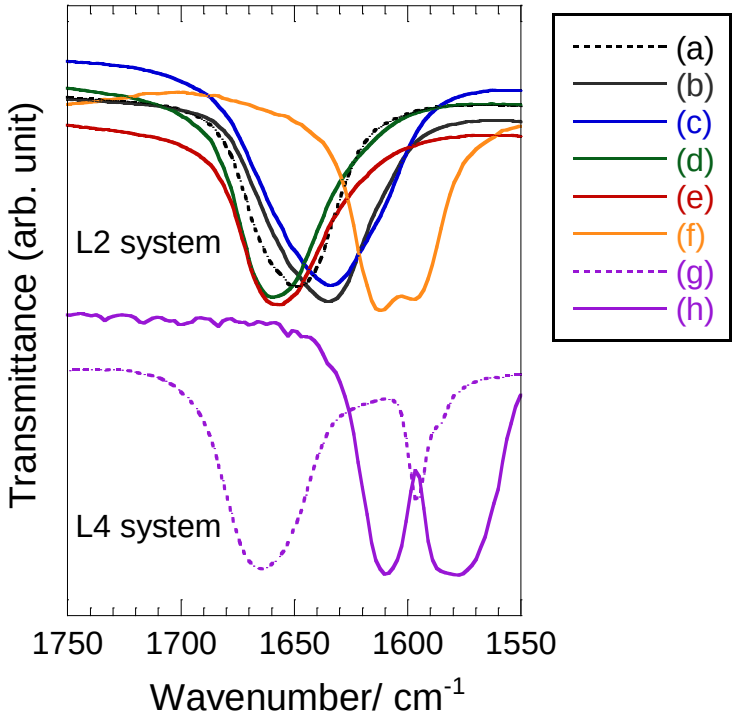

Figure 3.6. Amide carbonyl stretching frequencies for BisAA neat (a), a solution in 1-octanol (b) and solutions in 1-octanol after contacting with water (c), aqueous 2 M HCl (d) and aqueous 0.3 M $RhCl_3$ in 2 M HCl (e) compared with the Rh-L2 oily complex (no diluent) (f) and for BisAA(alt) (g) and *fac*-[$RhCl_3$(BisAA(alt))] (h), as solids.

A very different spectrum is obtained for a sample of Rh(III) complex obtained as an oil following a long reaction of $RhCl_3.3H_2O$ and BisAA in methanol (f). Here the carbonyl stretching band is split into two peaks. A similar spectrum is obtained for the Rh(III) complex with BisAA(alt) (h), which was synthesised in a similar manner. The spectrum for the neat, uncontacted BisAA(alt) is also provided for reference (g). This splitting of the carbonyl stretching frequency for these two Rh(III) complexes implies that the coordination environment around the amide O atoms is similar between the two complexes, but very different to that of the other samples. Indeed, a crystal structure obtained for the Rh(III) complex with BisAA(alt) shows that an inner-sphere complex of Rh(III) and the ligand has formed (Figure 3.7), where the amine N and the two amide O atoms are coordinating directly to the Rh(III) centre to form *fac*-[$RhCl_3$(BisAA(alt))].[14]

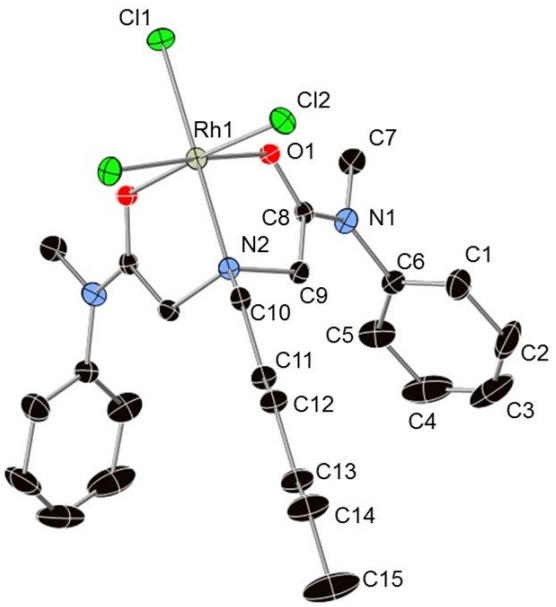

Figure 3.7. Part of the X-ray crystal structure of fac-[$RhCl_3$(BisAA(alt))]. Ellipsoids are represented at the 30% probability level. H-atoms and those of $CHCl_3$ solvate molecules are omitted for clarity.

This work indicates that, while it is unlikely to form within the confines of a "normal" extraction, it could be possible for an inner-sphere complex to form in an extraction system, if the conditions were favourable.

3.2.4 ^{1}H-^{15}N and ^{1}H-^{13}C NMR spectroscopy of the loaded organic phases

NMR spectra were also collected to further establish whether extractant interaction with the Rh(III) species proceeds via outer- or inner- sphere coordination. 2D ^{1}H-^{15}N and ^{1}H-^{13}C HMBC NMR spectra were obtained for BisAA in *d*-chloroform (organic), and for this solution contacted with HCl solution (Cl-loaded organic) and with a Rh(III) in HCl solution (Rh-loaded organic). Samples were approximately four months old at the time of analysis. The spectra allowed chemical shifts to be compared across the samples and allowed the amine and amide N shifts to be identified. The ^{1}H-^{15}N HMBC spectra, a zoomed version for the H shift region (0 ppm to 6 ppm) and the amide N shift region (100 ppm to 140 ppm), is given below in Figure 3.8, which also gives the structure and atomic labelling of BisAA for reference. The full version is provided in the SI. Table 3.2 gives the ^{15}N shifts assigned to the amine and amide N atoms for the three samples based on the HMBC spectra shown in Figure 3.8.

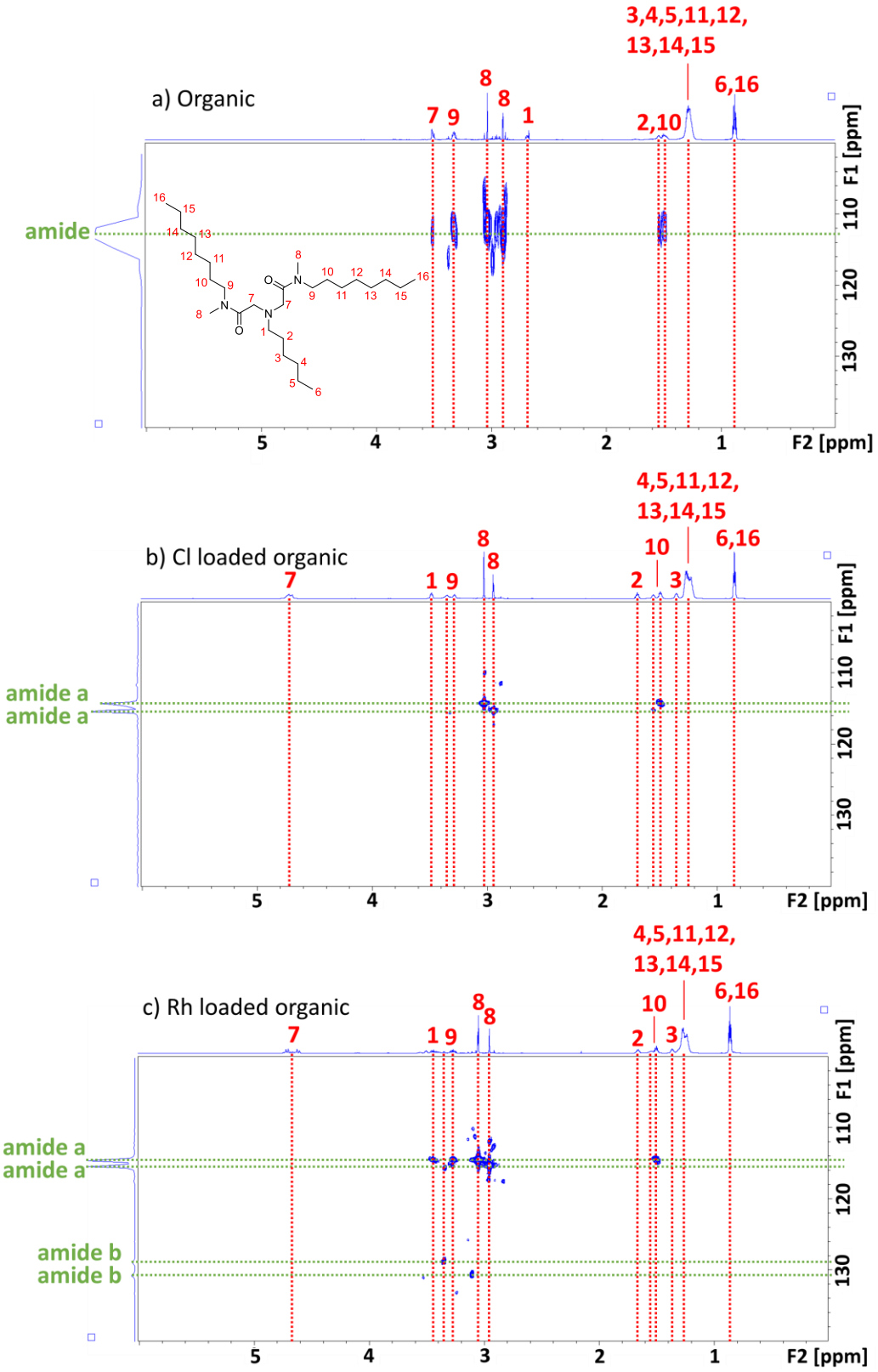

Figure 3.8. 2D ^{1}H-^{15}N HMBC spectra (in the ^{1}H 0-6 ppm region and ^{15}N 100-140 ppm region) of a $CDCl_3$ solution of **(a)** BisAA (0.1 M), **(b)** BisAA (0.1 M) after contacting with 2 M HCl and **(c)** BisAA (0.1 M) after five contacts with aqueous Na_3RhCl_6 (0.1 M) in 2 M HCl to maximise Rh loading.

Table 3.2. ^{15}N shifts (ppm) for amine and amide N atoms in the spectra shown in (**a-c)** in Figure 3.8.

Spectrum		Amine	Amide	Amide	Amide	Amide
(**a**) BisAA	^{15}N shift / ppm	35.2	112.1	-	-	-
	Cross-peak…	1	2,7,8,9,10	-	-	-
(**b**) BisAAH·Cl	^{15}N shift / ppm	51.7	114.1	115.2	-	-
	Cross-peak…	1†,2	8,10	8,9*,10	-	-
(**c**) $RhCl_5(H_2O)\cdot(BisAAH)_2$	^{15}N shift / ppm	52.2	114.5	115.4	128.9	130.7
	Cross-peak…	2,7,8*	1,8,9,10	8,9*	9#	8#

*Weak or very weak cross-peaks.

#Cross-peak with region of H-peaks, but potentially not the same H-signal

†Not visible at peak intensity level displayed in spectra

Comparing the spectra obtained for the free extractant with those obtained for the Cl- and Rh(III)-loaded samples, there are notable changes in the chemical shift: protonation of the extractant causes a major shift in the amine ^{15}N signal from 35.2 ppm to 51.7 ppm for the Cl-loaded organic and 52.2 ppm for the Rh-loaded organic. There is also a shift in the amide signal(s) but it is much less significant.

Notably, the changes in chemical shift are similar for both the Cl-loaded organic and the Rh-loaded organic samples, suggesting the extractants associate with the anions, at least with respect to the amine and amide N atoms, in a similar way. A significantly different chemical shift would be expected for the amide ^{15}N signals in the Cl-loaded organic and the Rh-loaded organic if the amide O atom was directly coordinated to the Rh(III) centre in the Rh-loaded organic. In addition, if a fully inner-sphere complex, like that observed in the crystal structure, was formed a significant difference in shift would also be expected for the amine ^{15}N signal. This therefore supports the ion-pair mechanism and is consistent with that observes in the FT-IR results.

However, in the spectra for the Rh-loaded organic sample, there exists a set of small peaks at ~128.9 and 130.7 ppm (labelled “amide b” in Figure 3.8), which appear to have weak correlations with H atoms 8 and 9. This set of peaks is absent from the Cl-loaded organic sample spectrum. It likely these new peaks, which appear to be amide peaks, on the basis of their chemical shift values, are indicative of a different amide environment present in the Rh-

loaded organic sample, but not the Cl-loaded organic sample, i.e. a potential inner-sphere bound amide O atom. There is no direct evidence of a $[RhCl_3L]$ complex, however, as there does not appear to be a second amine N peak present. That said, the shift for an amine N atom bonded directly to Rh(III) could be in the negative ppm range,[21] and so be outside the range investigated here.

A possible complication to this analysis is that the high Rh(III) concentrations required for maximum loading into the organic phase result in the formation of $(Rh_2Cl_9)^{\cdot}(L_2H)_3$ assemblies (as suggested by the EXAFS results), potentially in addition to the $(RhCl_5(H_2O))\cdot(LH)$ assembly. If this dinuclear complex is also an outer sphere complex, it is unlikely that ^{1}H, ^{13}C and ^{15}N NMR spectroscopy will be able to differentiate between the mono- and di-nuclear forms, as they will likely have very similar environments for both the amine and amide groups, leading to comparable chemical shifts.

The ^{1}H-^{13}C HMBC spectra (see SI) show very similar evidence to the ^{1}H-^{15}N HMBC spectra, of a major mode of association which is common between the Cl- and Rh-loaded samples (based on essentially the same shift in the amide C peaks) but an additional set of amide peaks for the Rh-loaded organic that indicate the presence of a second mode of association.

3.2.5 Extraction of water and acid

The work presented so far has shown that, under normal extraction conditions, two protonated BisAA molecules form an outer-sphere complex with $[RhCl_5(H_2O)]^{2-}$. This structure could take the form of a simple ion-associate, or water molecules could be incorporated such that a reverse micelle is formed. To this end, KF titrations were carried out to measure the water content of the loaded organics upon extraction of Rh(III). Figure 3.9 plots the variation in the water content of the organic phase with Rh concentration. The results appear to suggest that little or no water is extracted in association with Rh(III) metalate, as the water content decreases slightly with increasing Rh concentration, but water is extracted with chloride. The trendlines suggest that between approximately one and three water molecules are lost for every Rh(III) complex extracted (depending on if all the Rh is assumed to be extracted as $[RhCl_5(H_2O)]^{2-}$ and so one mole of water is introduced per mole of Rh(III) metalate or not). This result is similar to that found when 1-octanol is the solvent and when TOA is the extractant, though there is a more apparent decrease in the water

concentration of the organic phase (six per Rh for BisAA) with increasing Rh concentration than seen here (see Figure 3.10 for the plot).[14]

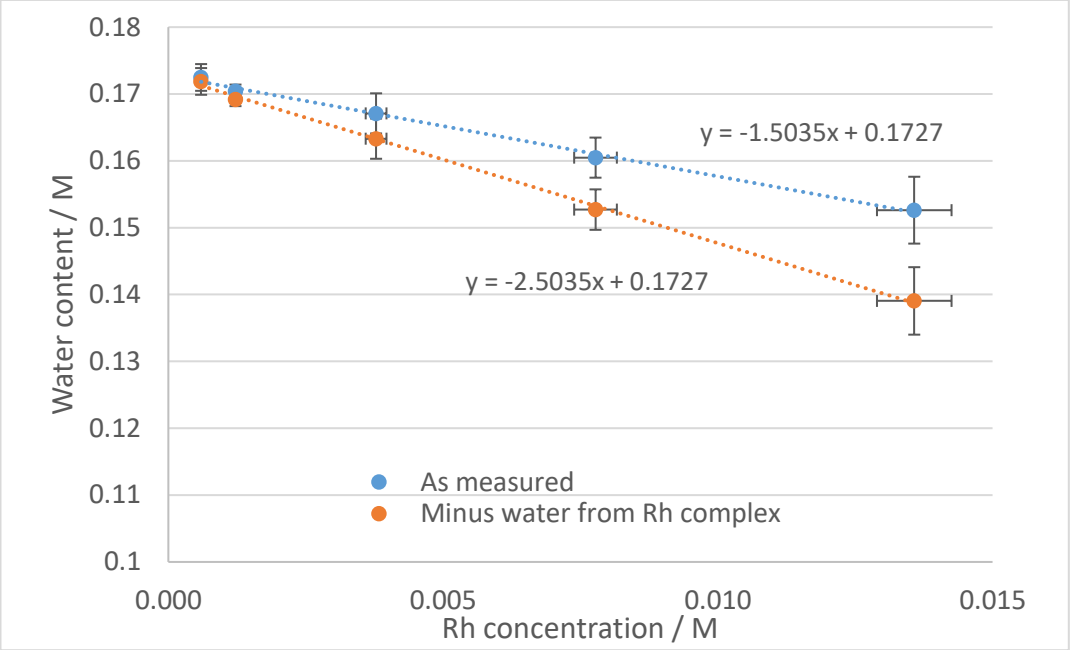

Figure 3.9. Water content of the loaded organics (from extractions of 0.1 M BisAA in chloroform with 2 M HCl solutions of varying Rh(III) concentrations) with varying Rh(III) concentration in the loaded organic. Relative error of ±5% in the Rh(III) concentration and standard deviations (from duplicate analysis) in the water concentration values are displayed on the plot.

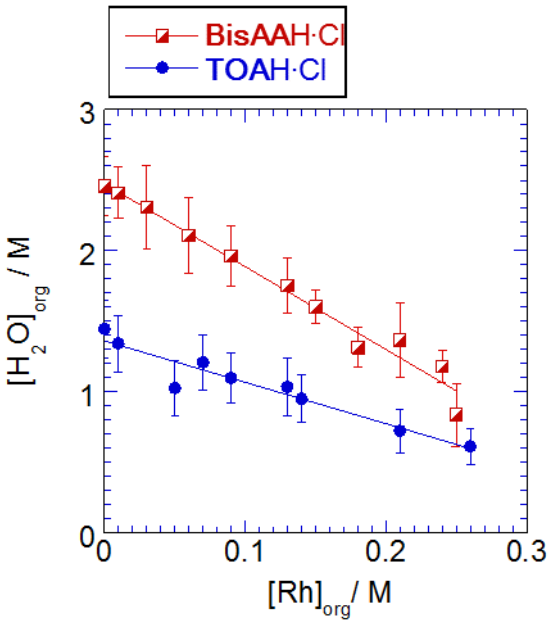

Figure 3.10. Change in water concentration in 1-octanol with uptake of $[RhCl_5(H_2O)]^{2-}$ by 0.5 M BisAAH·Cl or by 1.0 M TOAH·Cl. The error bars represent 1σ.

Contacting varying concentrations of BisAA in chloroform with 2 M HCl appears to suggest that the water content is directly proportional to the concentration of BisAA plus a constant underlying water level. Figure 3.11 gives a plot of the water concentration verses the concentration of BisAA. This plot is a straight line and from the equation of fit, it appears that the ratio of water to BisAA (or $BisAAH^+$ or Cl^-, if the BisAA is assumed to have fully protonated and be associated with chloride) may be close to 1, and an additional 0.063 M of water is extracted.

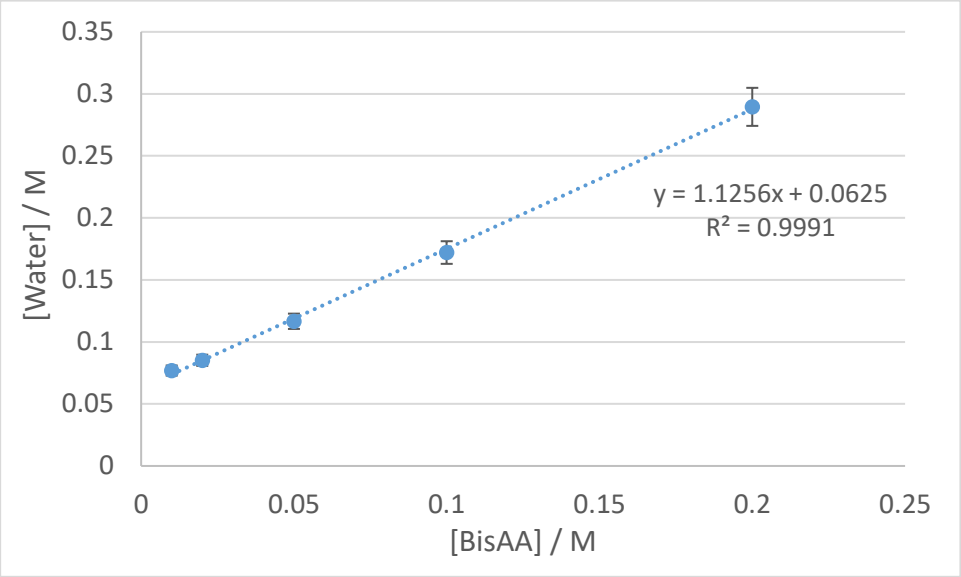

Figure 3.11. Water concentration of organic phases as a function of varying BisAA in chloroform concentrations contacted with 2 M HCl. Only single replicate data is reported as for some BisAA concentrations there was not enough sample for duplicate analysis, therefore estimated error of ±5.3% included based on standard deviation typical in KF analysis of these samples.

Further analysis was done to explore the possibility of a 1:1 ratio of water to $BisAAH^+$ and Cl^-. Varying HCl concentrations were also used to determine any effect on the amount of water extracted. Chloroform and 0.1 M BisAA in chloroform solution was contacted with HCl of varying concentration. Figure 3.12 gives a plot of the water content of the organic after contact. Even with the subtraction of water in chloroform, water is still observed to be extracted into the organic phase from HCl solution. A much smaller amount of water is brought over on contact with water alone. In general, the water extracted appears to decrease with increasing HCl concentration. However, this decrease is not apparent when the subtraction of water in chloroform is included, suggesting it is the chloroform that takes

over less water when the HCl concentration is higher and, thus, the water associated with BisAA is relatively constant.

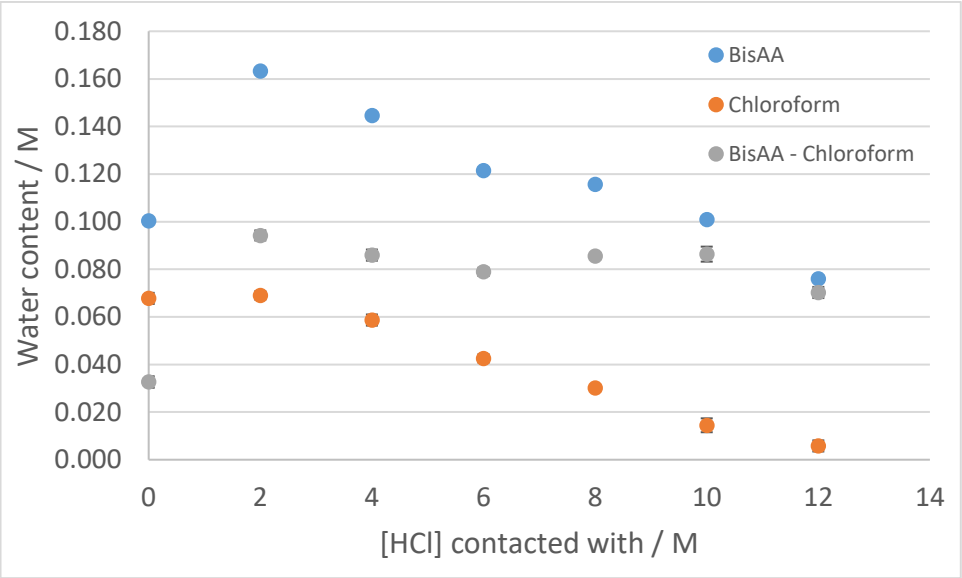

Figure 3.12. Plot of the water content (as wt% and M) of organic phases after contact with varying concentrations of HCl. BisAA refers to 0.1 M BisAA in chloroform as the organic. BisAA – Chloroform is the subtraction of the chloroform plot from the 0.1 M BisAA in chloroform. Point at 0 M HCl obtained from a contact with water. Standard deviations (from duplicate analysis) in the water concentration values are displayed on the plot (some bars may be too small to see).

On contacting with 2 M HCl, the water content of chloroform was measured to be 0.069 M. This is similar to the possible underlying water content of 0.063 M implied by the results in Figure 3.11. In addition, the water content in the 0.1 M BisAA in chloroform solution after contact with 2 M HCl is 0.163 M, which leaves 0.092 M if the contribution from the chloroform is subtracted. This appears to suggest that, at least after contact with 2 M HCl, there may be one water molecule associated with each BisAA (or $BisAAH^+$ or Cl^-).

The discussion above has assumed that all BisAA is protonated and associated with Cl^- after contact with any concentration of HCl. This is the case after contact with a 2 M HCl solution, as shown by the acid-base titration results presented in Figure 3.13. Full protonation is occurring on contact with 2 M HCl, but the proton concentration increases thereafter. As there should be no other possible counter ion present, it can be assumed that each $BisAAH^+$ is associated with Cl^-. Where the ratio of H^+:BisAA exceeds 1:1 it is likely that $[BisAAH]^+Cl^-$ H^+Cl^- has formed, in addition to BisAAH·Cl.

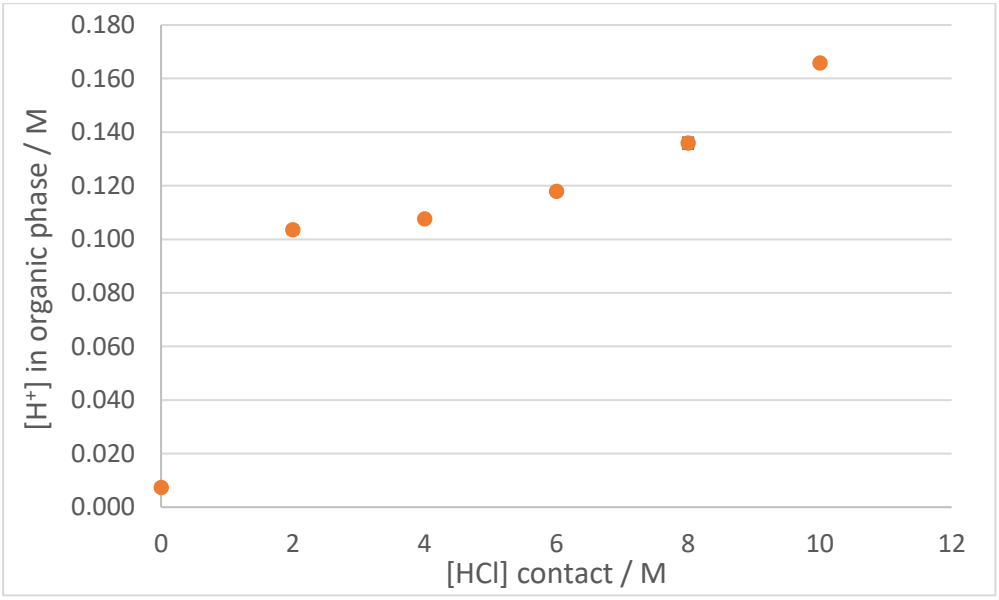

Figure 3.13. Plot of the acid (H^+) concentration in the organic phase (0.1 M BisAA in chloroform) after contact with varying concentrations of HCl. Point at 0 M HCl obtained from a contact with water. Errors are the standard deviations obtained from duplicate analysis (some bars may be too small to see).

It is thus still possible that after contact with 2 M HCl, there is one water molecule associated with each $BisAAH^+$ or Cl^-, however, the ratio of water to chloride will be lower after contacts with higher concentrations of HCl.

These results suggest that no water is extracted in association with the BisAA-Rh assembly, supporting the simple ion-associate mechanism, but that some water (around one water molecule per chloride ion) may be extracted in association with the BisAA-chloride assembly.

3.2.6 Small-angle neutron scattering (SANS) analysis

SANS analysis was performed on the BisAA and TOA extraction systems,[14] and the profiles obtained are given in Figure 3.14. The values of aggregation number, $N_{agg,}$ which were evaluated from the forward scattering intensity, $I(q = 0\ Å^{-1})$,[14] for BisAA in octanol-d_{17} is in the range of 2 to 3, suggesting dimeric and trimeric aggregates form. That BisAA forms an aggregate is consistent with the FT-IR results, where the $\nu_{C=O}$ stretching frequency shifted to a slightly lower frequency on dissolution in 1-octanol (see Figure 3.6, sample (b)). The results for BisAAD·Cl suggest that it forms a dimer (N_{agg} = 2.1) in solution, while for $(RhCl_5(H_2O))\cdot(BisAAD)_2$ the N_{agg} value of 1.1 suggests that it exists as a monomeric species.

The relative sizes and aggregation numbers recorded in Figure 3.14 are compatible with the water content of the organic phases as determined by the KF titrations. They support a Rh-loading mechanism in which two chloride ions and some water molecules (likely two to six, potentially solvent dependent) are displaced by the $[RhCl_5(H_2O)]^{2-}$ dianion for association with two protonated BisAA molecules.

In contrast, very different behavior is observed for TOA. Much higher aggregation numbers are recorded for both TOA and TOAD·Cl (N_{agg} = 22.2 and 7.5, respectively), suggesting large aggregates exist in the organic phase. However, for $(RhCl_5(H_2O))\cdot(TOAD)_2$ an N_{agg} value of 2.0 is obtained, indicating that a dimer is present and that the large aggregates are dispersed on the extraction of Rh.

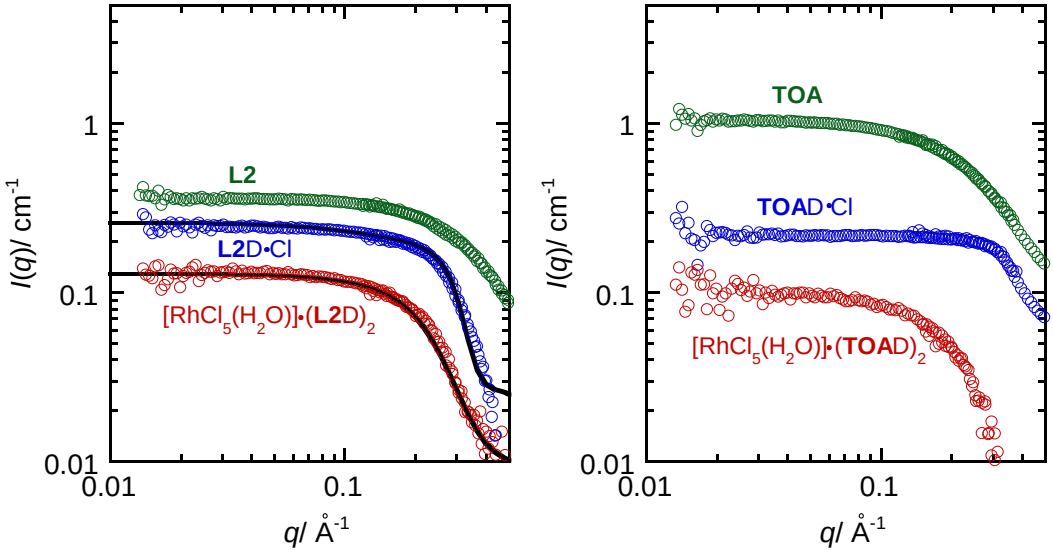

Sample	BisAA	BisAAD·Cl	$[RhCl_5(H_2O)]\cdot(BisAAD)_2$
N_{agg}	2.7	2.1	1.1
Sample	TOA	TOAD·Cl	$[RhCl_5(H_2O)]\cdot(TOAD)_2$
N_{agg}	22.2	7.5	2.0

Figure 3.14. SANS profiles for 1-octanol-d_{17} solutions of (on the left): BisAA, BisAAD·Cl and $(RhCl_5(H_2O))\cdot(BisAAD)_2$; and (on the right): TOA, TOAD·Cl and $(RhCl_5(H_2O))\cdot(TOAD)_2$. Corrections for the scattering contributions from octanol-d_{17} have been made to all the profiles and the plots for the Rh-loaded solutions have been corrected for the contributions expected from the unloaded extractants present in the forms BisAAD·Cl and TOAD·Cl. Solid black curves are the best-fits obtained from a hard-sphere model with the optimized solute structures obtained from DFT calculations.[14] Aggregation numbers for the same samples are summarized in the inset table.

3.2.7 Electrospray ionisation mass spectrometry of Rh-loaded organic phases

Positive ion spectra of loaded organic phases obtained after contacting with aqueous solutions of different Rh(III) concentrations are displayed in Figure 3.15. The dominant peak can be assigned to $[(BisAAH)_3(RhCl_5)]^+$, m/z 1683.11. This would correspond to the neutral complex (BisAAH)·($RhCl_5$BisAA), if protonated BisAA provides the positive charge in the MS. The replacement of an inner-sphere water molecule or a chloride ligand to form this species might be a consequence of the fact that the loaded organic sample (from a 30 minute contact) sat for 48 hours before analysis. However, when ESI-MS was conducted within 5 minutes on loaded organics from very short contacts (<1 min, see Figure 3.18 below) the $[(BisAAH)_3(RhCl_5)]^+$ ion is still the most intense peak, suggesting that changes to the inner coordination sphere take place during ionization in the mass spectrometer (since IR and NMR spectra suggest that no inner-sphere BisAA is likely to form in the loaded organic under the conditions used here).

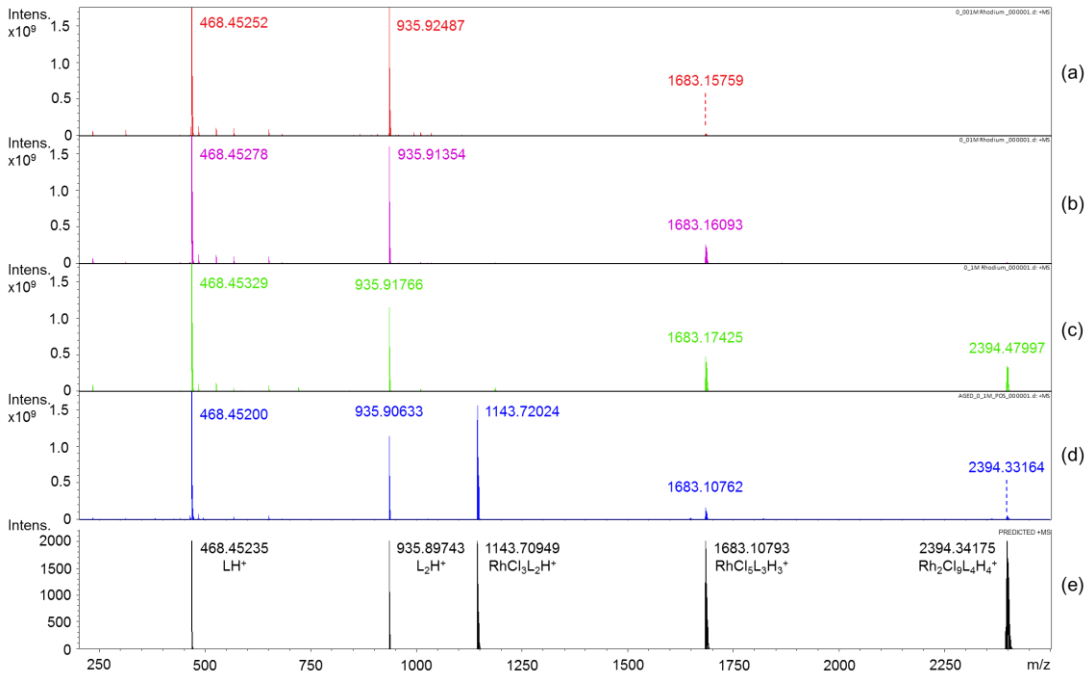

Figure 3.15. Positive ion ESI-MS of Rh(III)-loaded $CHCl_3$ solutions of BisAA (0.5 M) samples ((a)-(c)) from extractions from 0.001 M, 0.01 M, and 0.1 M Rh in 2 M HCl solutions, analysed 48 hours after extraction, compared with sample (d) which is (c) after ageing for 7 months. (e) provides the simulated spectra. Monoisotopic mass labelling given.

After setting aside the loaded organic obtained by the extraction from the 0.1 M Rh(III) solution for seven months the dominant peak becomes that at m/z 1143.72 (see Figure 3.15), corresponding to $[(BisAAH)(RhCl_3(BisAA))]^+$. This likely corresponds to the presence of a $RhCl_3$BisAA complex in the organic phase, similar to the crystal structure reported in Section 3.2.2, again indicating that an inner sphere complex can form in solution but on a timescale of greater than 48 hours. This suggests that for the short contact times typical of an SX experiment association of the extractant with the Rh(III) complex will be outer-sphere.

A further notable result from this analysis is the observation of an additional peak corresponding to $[(BisAAH)_4(Rh_2Cl_9)]^+$ (m/z 2394.34) in the loaded organics of extractions from solutions of higher Rh(III) concentration, which likely indicates the presence of a $(BisAAH)_3{\cdot}(Rh_2Cl_9)$ assembly in the loaded organic. The EXAFS analysis suggested that the dinuclear species is not present in the aqueous phase (unless at a concentration too low to be detected). If this is the case, it may form in the extraction process or over time in the loaded organic.

In order to further explore how the dinuclear species forms, ESI-MS was conducted immediately (within 5 mins) on a Rh-loaded organic from a very short contact (<1 min) of the aqueous and organic phase (spectrum in Figure 3.16). The species is observed, which suggests that the dinuclear complex either present in the aqueous phase or forms upon extraction, rather than forming over time in the organic phase.

As the amount of dinuclear species present in the organic phase appears to vary depending on the Rh(III) concertation in the aqueous phase, its presence may stem from the use of high concentration Rh(III) solutions. This could either be because the ratio of Rh(III) to BisAA is key in the formation of the dinuclear species (if it is formed upon extraction), or that it is only present in the aqueous phase (albeit at concentrations too low to be detected by EXAFS analysis) when the Rh(III) concentration is high.

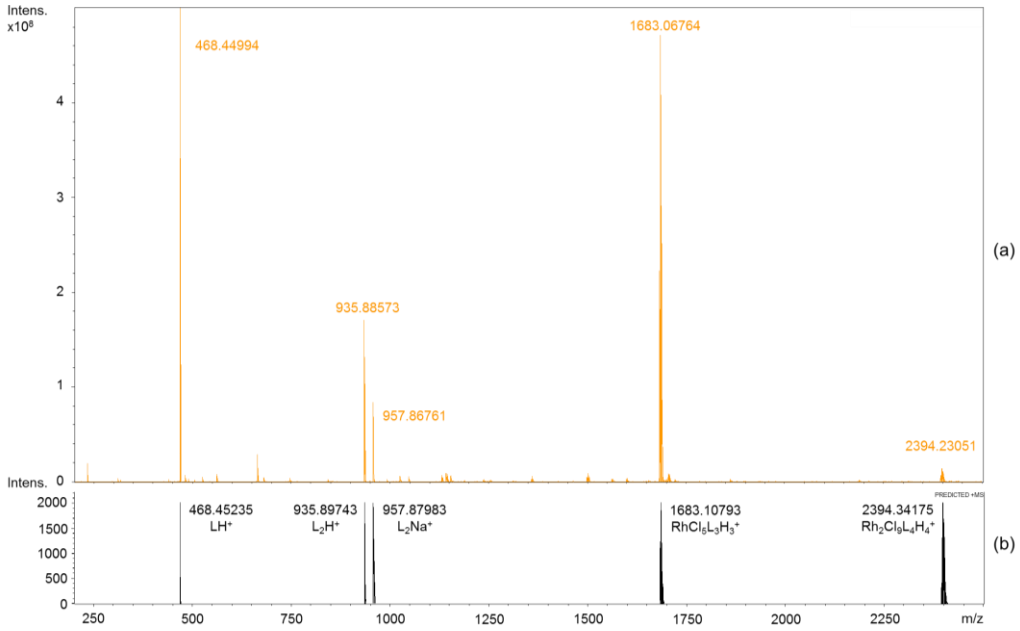

Figure 3.16. Positive ion ESI-MS spectra of (a) loaded organic after <1 minute contact of 0.1 M BisAA with 0.1 M Rh in 2 M HCl. (b) provides the simulated spectra. Monoisotopic mass labelling given.

3.2.8 Extraction profile over time

Afzaletdinova et al. have shown that plots of extraction over time can highlight a change in the mode of extraction.[20, 22] This can be the case when an outer-sphere interaction governs the association in one mechanism, while inner-sphere interactions are required for the other. In these circumstances, the purely outer-sphere based mechanism occurs on shorter timescales, while the inner-sphere based mechanism takes longer to be visible, resulting in extraction profiles with distinct shapes. If the dinuclear species is present in the aqueous phase and extracted, outer-sphere association of the extractant with the $[Rh_2Cl_9]^{3-}$ is all that will need to occur, similar to association with $[RhCl_5(H_2O)]^{2-}$. However, if it forms during extraction, though the binding of the extractant is not via an inner-sphere interaction with the Rh(III), a change in the coordination around the Rh(III) centres will have to occur. Therefore, it is possible that a difference in extraction profile over time could be seen, indicating the mononuclear species being extracted on short timescales, and the dinuclear species forming over longer timescales.

To investigate this a series of extractions was carried out, with each having a different mixing time. These were done using a solution with a high concentration of Rh(III) (0.1 M) as

extractions from this have shown the presence of significant quantities of assemblies containing $[Rh_2Cl_9]^{3-}$ in the loaded organic (EXAFS and ESI-MS results). Figure 3.17 shows a plot of the distribution of Rh(III) between the two phases with time of mixing.

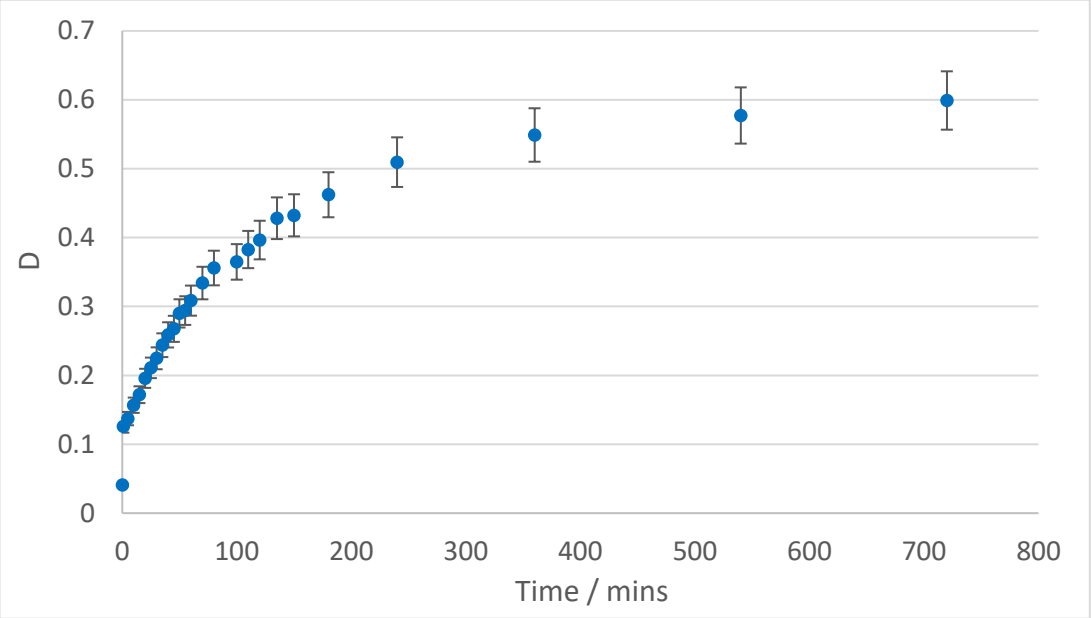

Figure 3.17. Extraction with time using 0.1 M BisAA (precontacted with HCl) and 0.1 M Rh in 2 M HCl solution, with all extractions started at the same time and no centrifuging carried out. Absolute error of ±7.1% in the D value (based on ±5% error in the Rh(III) concentrations) displayed on the full plot.

While there is a potential change in gradient at around 60 to 100 minutes, this graph does not appear to show the clear change in extraction mechanism observed by Afzaletdinova et al. In addition, as the dinuclear complex is seen in the organic phase on very short contact times (as evidenced by the ESI-MS results), it is unlikely that any change after 100 mins can be attributed to this mechanism.

3.2.9 Computational modelling of extractant and $[RhCl_5(H_2O)]^{2-}$ or Cl^- assemblies

Given that most evidence points to the major extracted complex being an ion-associate assembly of the form $RhCl_5(H_2O)\cdot(LH)_2$, quantum mechanical modelling was carried out to explore how the protonated amidoamine extractants associate with chloride or the $[RhCl_5(H_2O)]^{2-}$ metalate. The aim is to understand why BisAA and TrisAA are better extractants for Rh(III) than MonoAA, and why the amidoamine extractants perform better than trialkylamines. Note to reduce compute time, truncated forms of the extractants (with

methyl groups in place of *n*-hexyl and *n*-octyl groups) have been used throughout (see Figure 3.18).

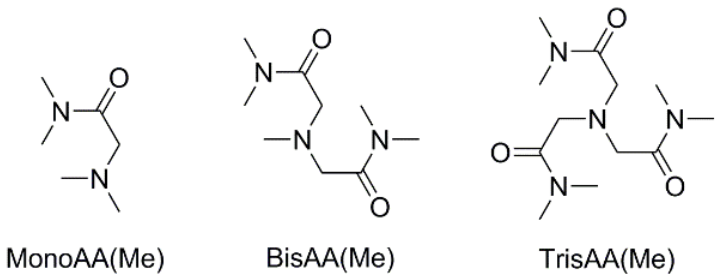

Figure 3.18. Truncated extractant structures for computational modelling.

The computational study began with establishing that the most favourable protonation site for all extractants was the central amine nitrogen atom. The calculated protonation energies for the whole extractant set, as defined by Equation 3.1 and reported in Table 3.3, show very similar values for all extractants, with slightly increased favourability of protonation for the more substituted extractants. This indicates that variation in the ease of extractant protonation is not likely to account for the overall variation in extractant behaviour. This is in contrast to the related aminoamide and ether-amide systems, where variations in extractant protonation energies were much more pronounced and matched the trend for increasing metalate extraction (for $PtCl_6^{2-}$ in this case).[23]

$$L_{(org)} + H_3O^+_{(aq)} \rightleftharpoons LH^+_{(org)} + H_2O_{(aq)} \quad \textbf{3.1.}$$

$$LH^+_{(org)} + Cl^-_{(aq)} \rightleftharpoons LH{\cdot}Cl_{(org)} \quad \textbf{3.2.}$$

$$2LH^+_{(org)} + [RhCl_5(H_2O)]^{2-}_{(aq)} \rightleftharpoons (RhCl_5(H_2O)){\cdot}(LH)_{2\,(org)} \quad \textbf{3.3.}$$

$$2LH{\cdot}Cl_{(org)} + [RhCl_5(H_2O)]^{2-}_{(aq)} \rightleftharpoons (RhCl_5(H_2O)){\cdot}(LH)_{2\,(org)} + 2Cl^-_{(aq)} \quad \textbf{3.4.}$$

$$(LH{\cdot}Cl)_{2\,(org)} + [RhCl_5(H_2O)]^{2-}_{(aq)} \rightleftharpoons (RhCl_5(H_2O)){\cdot}(LH)_{2\,(org)} + 2Cl^-_{(aq)} \quad \textbf{3.5.}$$

Table 3.3. Free energy changes for the processes outlined in Equations 3.1-3.5. Note, in order to keep the formation energies from Equation 3.4 and 3.5 consistent with those of Equations 3.2 and 3.3, BSSE corrected energies have been used for Cl·LH and $(RhCl_5(H_2O))\cdot(LH)_2$ in the exchange energy calculations. Also note, the BSSE corrected energy for the $(LH\cdot Cl)_2$ dimer used here is different from that used to calculate the dimerization energy (see Section 3.4.10 for details of the BSSE correction calculations). Energies used in the calculation of these formation energies are provided in the SI.

Process	Extractant	ΔG/ kJ mol^{-1}
Equation 3.1	MonoAA(Me)	-116.4
	BisAA(Me)	-117.5
	TrisAA(Me)	-117.3 #
Equation 3.2	MonoAA(Me)	-22.5
	BisAA(Me)	-10.6
	TrisAA(Me)	-8.5 #
Equation 3.3	MonoAA(Me)	-18.2
	BisAA(Me)	-31.4
	TrisAA(Me)	-25.1 #
Equation 3.4	MonoAA(Me)	26.8
	BisAA(Me)	-10.2
	TrisAA(Me)	-8.2 #
Equation 3.5	BisAA(Me)	-6.8

Energies were calculated using structures not fully optimised – see Methods section for more details.

A large number of possible ion-pair motifs exist (as summarised in Figure 3.3), with, for example, binding proceeding directly via protonated amine N-H…anion interactions. Alternatively, intra-extractant N-H…O proton chelate hydrogen bond(s) could form, such that the 'back-side' of the extractant is presented to the ion and association occurs via an array of C-H…anion interactions. The lowest energy ion-pairs obtained with chloride shown in Figure 3.19.

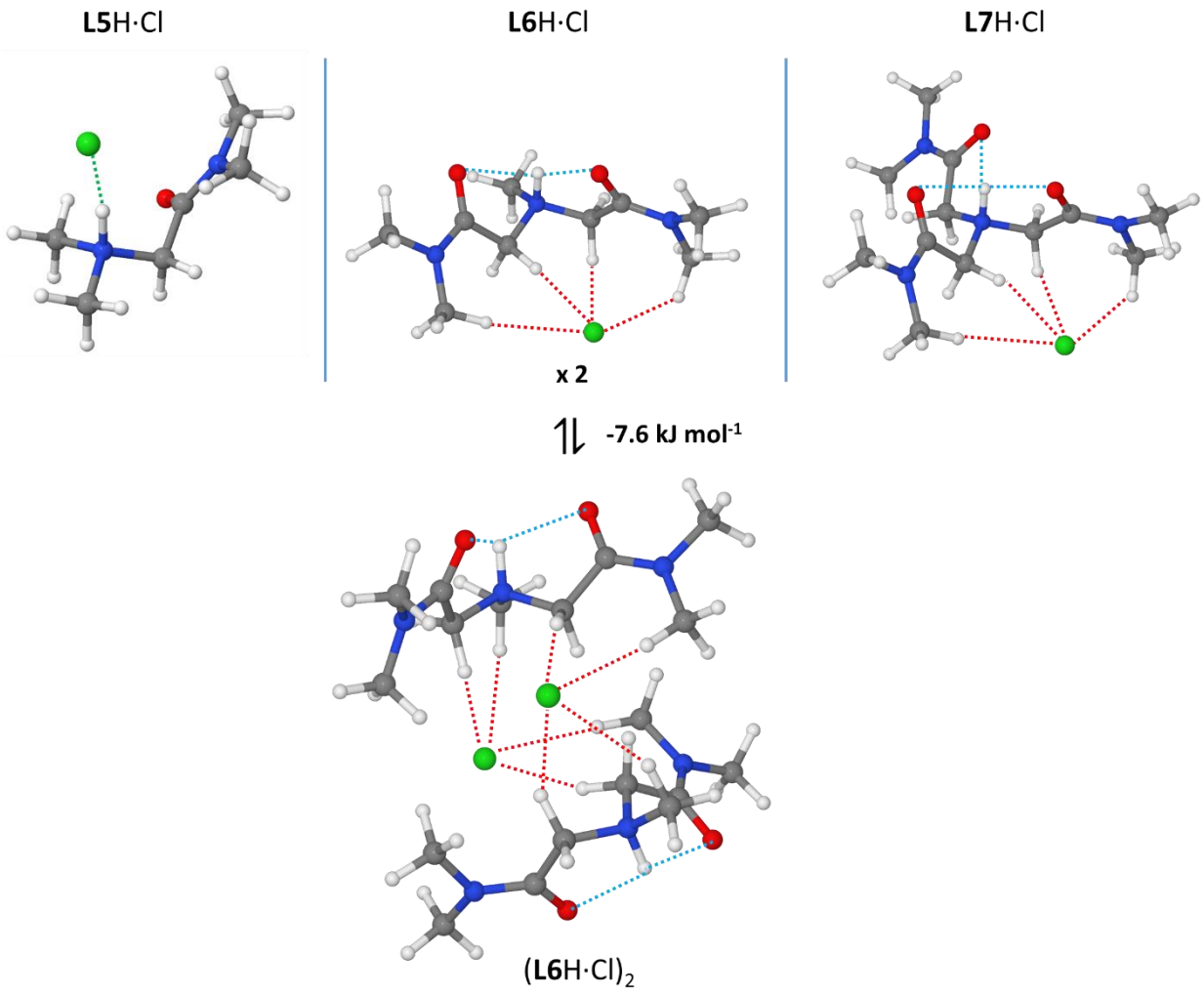

Figure 3.19. The lowest energy structures of the ion-pairs formed with Cl^- (shown in green) by $[MonoAA(Me)H]^+$, $[BisAA(Me)H]^+$ and $[TrisAA(Me)H]^+$ and the dimer $(BisAA(Me)H{\cdot}Cl)_2$. Hydrogen bonds involving the carbonyl oxygen atom are shown in blue and short contacts made by N-H and C-H hydrogen atoms to Cl^- in green and red, respectively. Output files containing structure coordinates provided in the SI. Note the dimerization energy shown here is different to that which can be determined from comparison of the formation energies in Table 3.3, on account of different BSSE corrected energies being using in the calculations (see Section 3.4.10 for details of the different BSSE correction calculations).

In addition to the binding modes possible with chloride, in the case of the Rh(III) metalate, it is also possible that hydrogen bonding may occur between the *aquo* ligand on the metalate and an amide O atom. A set of these was explored for each of the three extractants, with some possible structures excluded from consideration as analysis progressed based on the results of previous calculations. Figures 3.20, 3.21 and 3.22 give the sets of possible

structures explored and their relative Gibbs free energies for MonoAA(Me), BisAA(Me) and TrisAA(Me), respectively.

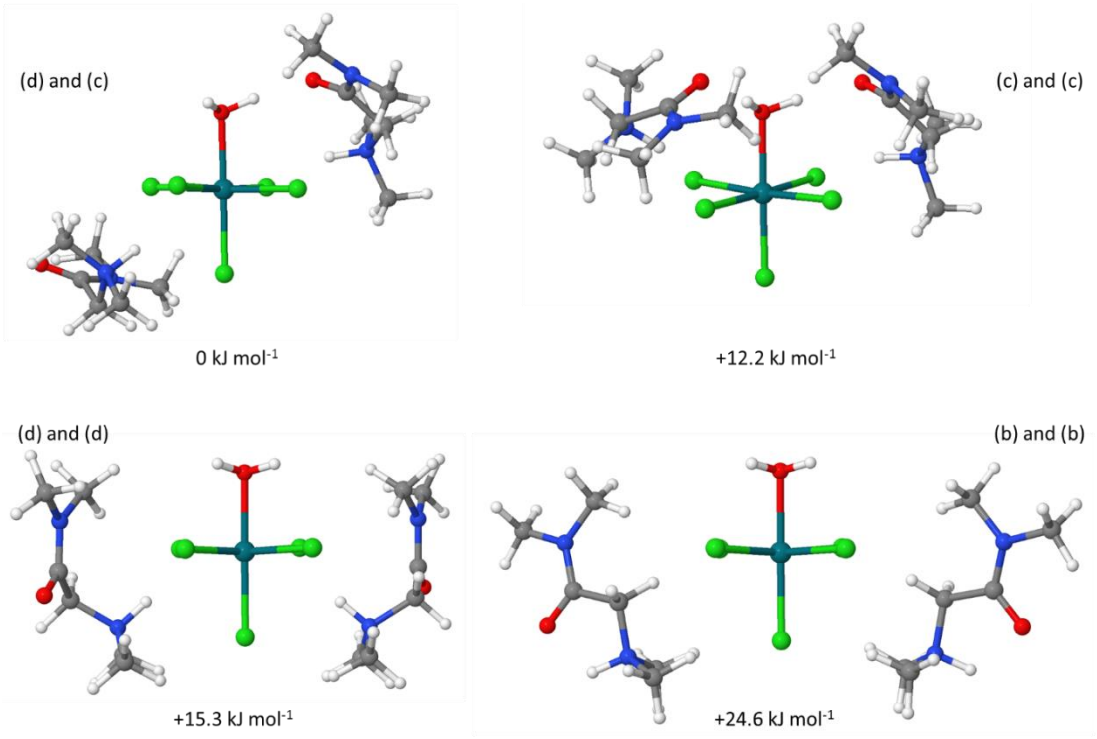

Figure 3.20. Different binding mode combinations explored for $(RhCl_5(H_2O))\cdot$(MonoAA(Me)H). Labelled according to similarity to binding motifs given for BisAA(Me) in Figure 3.3. Output files containing structure coordinates provided in the SI.

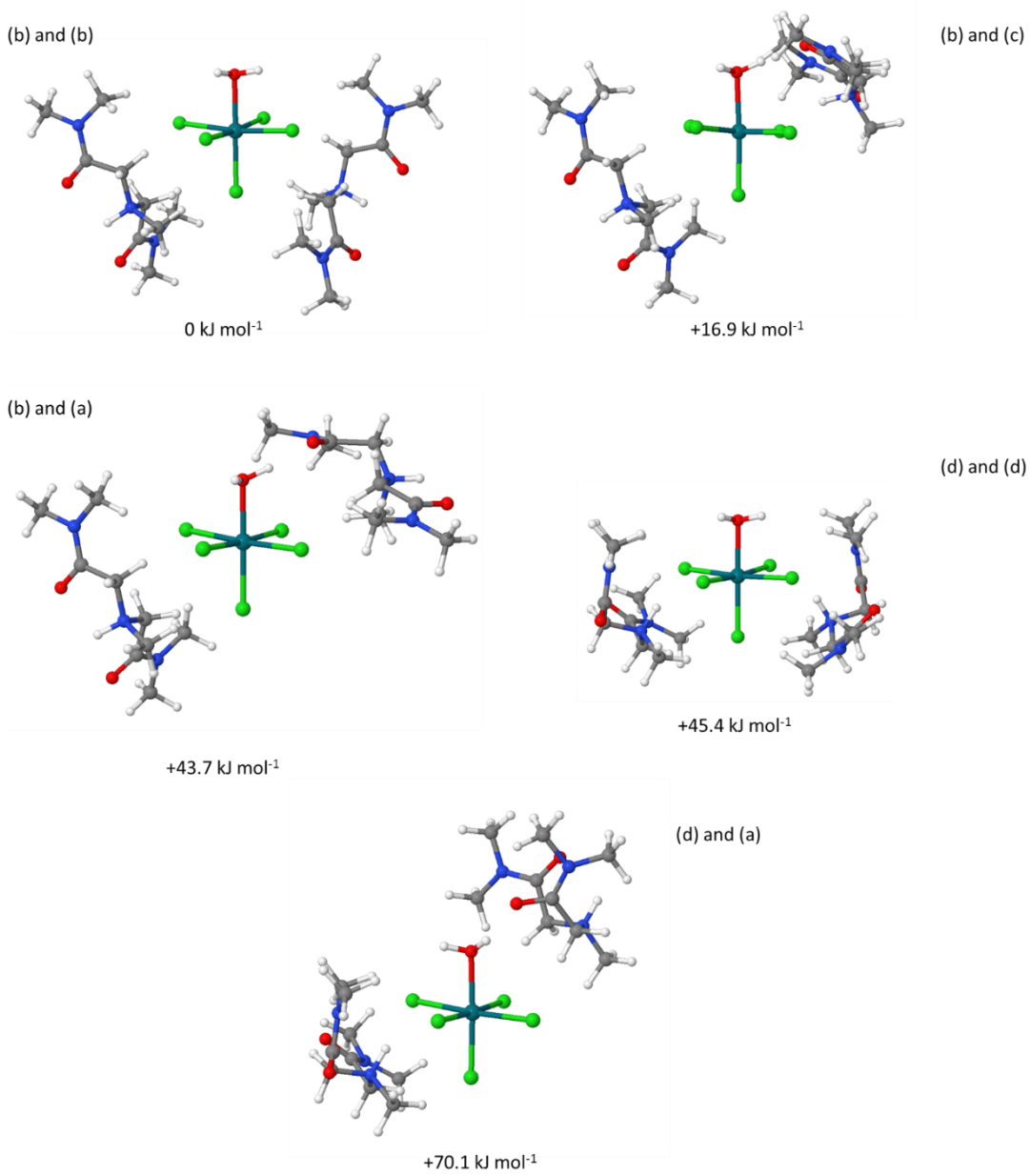

Figure 3.21. Different binding mode combinations explored for $(RhCl_5(H_2O))\cdot(BisAA(Me)H)$. Labelled according to similarity to binding motifs given in Figure 3.3. Output files containing structure coordinates provided in the SI.

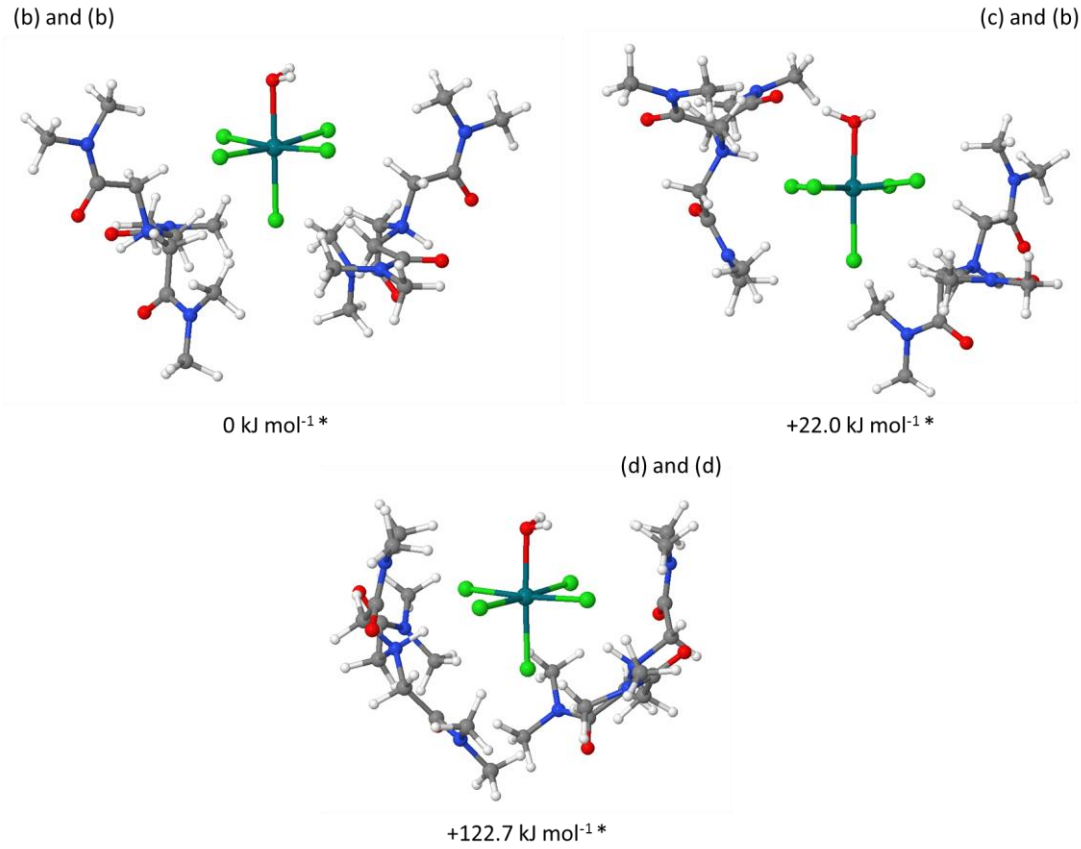

Figure 3.22. Different binding mode combinations explored for $(RhCl_5(H_2O))\cdot$(TrisAA(Me)H). Labelled according to similarity to binding motifs given for BisAA(Me) in Figure 3.3. *These structures are from calculations which did not optimise under the default program criteria or alternate criteria tried. The have the following imaginary frequencies: 19.2, 34.0 and 49.8 cm^{-1}; 30.7 and 50.2 cm^{-1}; and 18.2 cm^{-1}, respectively. Output files containing structure coordinates provided in the SI.

Figure 3.23 displays the lowest energy binding modes explored for the three extractants and illustrates the interactions/close-contacts occurring. With the exception of the hydrogen bond occurring in the MonoAA(Me) complex, which was not possible with chloride, the extractants adopt the same type of binding modes with $[RhCl_5(H_2O)]^{2-}$ as they do with Cl^-, though the C-H…anion based binding modes differ in the area of the extractant they present between the two anions. With chloride it is the C-H groups on the "side" of the extractant which interact, but with $[RhCl_5(H_2O)]^{2-}$ it appears that the larger "back" face of the extractant is presented.

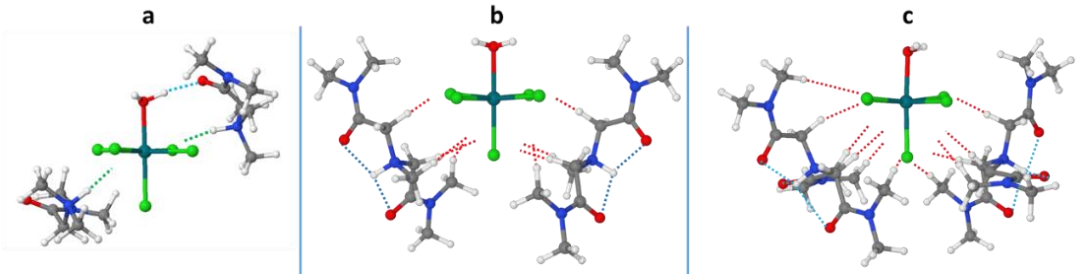

Figure 3.23. Structures of lowest energy forms of the assemblies $(RhCl_5(H_2O))\cdot(\mathbf{L}H)_2$ formed by [MonoAA(Me)H]$^+$, **[**BisAA(Me)H]$^+$ and [TrisAA(Me)H]$^+$ (**a**, **b** and **c** respectively). Hydrogen bonds involving the carbonyl oxygen atom are shown in blue and those involving N-H and C-H hydrogen atoms to chloride ions or the edges or faces of the octahedron in green and red, respectively.

The mode of binding varies significantly between MonoAA(Me) and Bis- and TrisAA(Me). For [MonoAA(Me)H]$^+$ a direct N-H…anion interaction is present between the protonated amine and the anion. In contrast, both [BisAA(Me)H]$^+$ and [TrisAA(Me)H]$^+$ adopt the N-H…O proton chelate form (motif (b) in Figure 3.3). Consequently, these cations are conformationally constrained to present multiple C-H bond interactions, which represent a large area of diffuse positive charge (as illustrated by the electrostatic potential plot for [BisAA(Me)H]$^+$ shown in Figure 3.24), to attract the anion. The formation of the proton chelate is therefore likely to favour binding to larger, more diffusely charged anions, whereas the less substituted extractant, which does not support the proton chelate form, will likely be more selective for smaller, more densely charged anions.

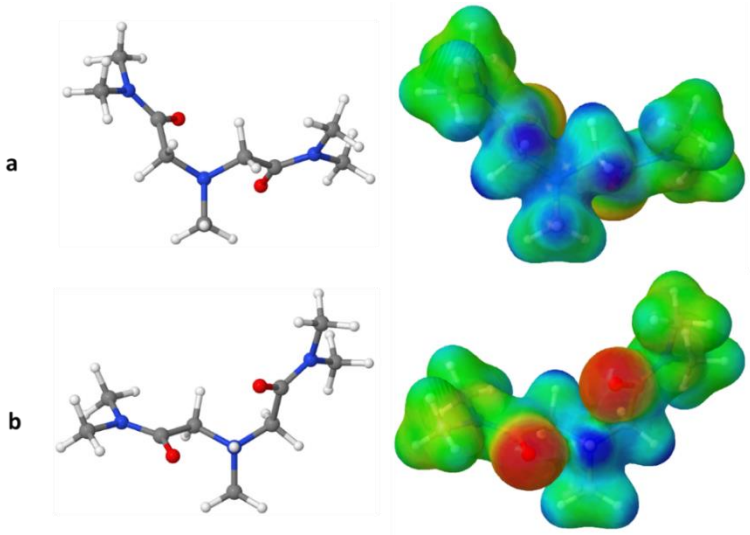

Figure 3.24. Two views of [BisAA(Me)H]$^+$ and its associated electrostatic potential plot. The cavity of polarised C-H$^{\delta+}$ groups is shown in (a) and the proton chelated units in (b) (blue and red areas indicate relative positive and negative charge, respectively).

Interestingly, $[MonoAA(Me)H]^+$ is the only extractant which displays a hydrogen bond with the $[RhCl_5(H_2O)]^{2-}$ complex (Figure 3.20). As the extractant proton interacts directly with the anion, and no intra-extractant hydrogen bond forms between the proton and the amide oxygen atom, the proton is free to form a hydrogen bond with the *aquo* ligand on the $[RhCl_5(H_2O)]^{2-}$ complex. However, it appears that for the more highly substituted extractants chelation of the proton with more than one amide oxygen atom is more favourable than forming a hydrogen bond to the *aquo* ligand. Structures with BisAA(Me) and TrisAA(Me) where the hydrogen bond to the *aquo* ligand is present along with the direct N-H…anion interaction were found to be of higher energy (see Figures 3.21 and 2.22). And in a similar vein, MonoAA(Me) structures with the hydrogen bond severed in favour of forming the proton chelate (and thus interacting through C-H…anion interactions only) is less favourable geometry (see Figure 3.20).

In order to ascertain whether the calculations can quantitatively support the difference in extractant binding mode of action behaviour towards the small densely charged Cl^- and the larger more diffusely charged $[RhCl_5(H_2O)]^{2-}$, Gibbs free energy values were computed for all extractants for the formation and anion exchange equilibria defined by Equations 3.1 – 3.5, with data presented in Table 3.3.

Modelling of the amidoamine extractants shows that the favourability of forming an assembly with $[RhCl_5(H_2O)]^{2-}$ (Equation 3.3) is greater with BisAA(Me) than with MonoAA(Me), and that the opposite is true for the formation of an assembly with chloride (Equation 3.2). Overall, in a competitive anion environment (Equation 3.4) the strength of binding to $[RhCl_5(H_2O)]^{2-}$ outstrips binding to Cl^- for BisAA and TrisAA, but not MonoAA(Me). These findings are consistent with the experimental extraction behaviour, which demonstrates that, over the [HCl] range tested, the extraction efficiency increases in the order MonoAA < BisAA < TrisAA.[13] However, the fit to the trend is not perfect as the exchange energy of TrisAA(Me) is slightly less favourable than that of BisAA(Me) (by 2 kJ mol^{-1}). This is likely because full optimisation of some of the TrisAA(Me) based structures was not achieved. Thus, there is an error in the Gibbs free energies obtained for the TrisAA(Me) formation energies, and so in the placement of TrisAA(Me) in the trend.

As the SANS results suggest that for chloride complexes with BisAA dimeric structures are formed, this possibility was explored computationally for BisAA(Me). As the dimerisation

energy in Figure 3.19 shows, the formation of the dimer is favourable. This means that the energy of exchange of chloride for $RhCl_5(H_2O)^{2-}$ is slightly higher (and so less favourable) when considering that the chloride complexes would be of the form $(BisAAH{\cdot}Cl)_2$, however, the formation is ultimately still favourable. Note: the dimerisation energy given in Figure 3.19 (of -7.6 kJ mol^{-1}) is different than difference in the exchange energies from Equation 3.4 and Equation 3.5 (which give a dimerisation energy of -3.4 kJ mol^{-1}) due to different BSSE corrections being used for the energy of the dimer in each case (see Section 3.4.10 for details of the BSSE correction calculations). Since the energy difference when considering the exchange energy from two monomeric chloride complexes vs one dimeric complex to the Rh(III) complex is small and given there is no experimental evidence for MonoAA and TrisAA available (though TrisAA at least is likely to behave similarly to BisAA) the dimer calculations were not performed for MonoAA(Me) and TrisAA(Me).

Based on these results, it could be assumed that the success of the amidoamine extractants in extracting Rh(III) metalate lies in strong binding of the protonated extractant with the $[RhCl_5(H_2O)]^{2-}$ complex. However, as it is observed that MonoAA has both a lower binding affinity for the Rh(III) metalate and a higher one for chloride, it is likely that the success of the amidoamines lies in good selectivity for the Rh(III) metalate over chloride. Indeed, this would prove consistent with the experimental findings for simple amines, such as TOA, that Rh(III) is extractable at very low chloride concentrations but not at the higher concentrations the amidoamines are capable of functioning as Rh(III) extractants at; the amidoamines are more selective for Rh(III) metalate over chloride than amines are. Modelling of TOA and the related extraction structures has not been done here as the SANS analysis shows the association of TOA and chloride is much more complicated than a simple ion-pair, and TOA and the Rh(III) complex appear to form a dimeric structure.

3.2.10 Computationally exploring the dinuclear complex

Thus far, it has been assumed that the extractant mode of action proceeds solely via ion-pairing. However, the ESI-MS and EXAFS results have shown that a dinuclear Rh(III) complex can exist in the organic phase. Experimental analysis has not been able to determine whether this species is a result of the $[Rh_2Cl_9]^{3-}$ metalate being present in and extracted from the aqueous phase or if it forms during the extraction process. To this end, QM modelling was

undertaken to determine the structure of the assembly in the organic phase and to explore the formation energies of the possible formation processes given in Equations 3.6-3.10. Figure 3.25 gives the ion-pair assembly structure of $(BisAA(Me)H)_3 \cdot (Rh_2Cl_9)$, where three protonated BisAA(Me) molecules surround the dinuclear metalate, interacting via C-H…metalate contacts. Both processes in Equations 3.6 and 3.7 present formation of the $(Rh_2Cl_9) \cdot (LH)_3$ complex in the organic phase by extraction of the $[Rh_2Cl_9]^{3-}$ complex from the aqueous phase (i.e. assuming the dinuclear complex exists in the aqueous phase). Equations 3.8 and 3.9 present formation during extraction from the $[RhCl_5(H_2O)]^{2-}$ complex (i.e. assuming the dinuclear complex does not exist in the aqueous phase and is instead formed during the extraction process/at the interface). Equation 3.10 concerns formation from the $(RhCl_5(H_2O)) \cdot (LH)_2$ complex in the organic phase (i.e. assuming the formation of the dinuclear complex occurs in the organic phase from the $(RhCl_5(H_2O)) \cdot (LH)_2$ extraction assembly).

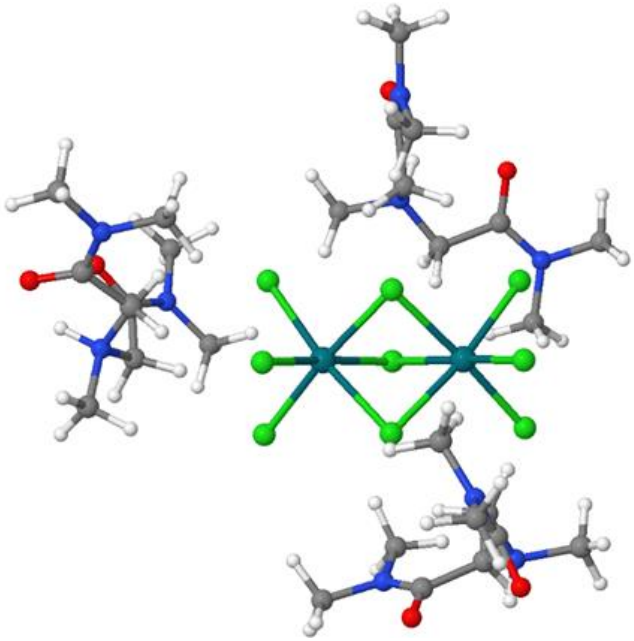

Figure 3.25. Lowest energy structure of $(BisAA(Me)H)_3 \cdot (Rh_2Cl_9)$.

$$3LH^{+}_{(org)} + [Rh_2Cl_9]^{3-}_{(aq)} \rightleftharpoons (Rh_2Cl_9)\cdot(LH)_{3\,(org)} \quad \textbf{3.6.}$$

$$3(Cl\cdot LH)_{(org)} + [Rh_2Cl_9]^{3-}_{(aq)} \rightleftharpoons (Rh_2Cl_9)\cdot(LH)_{3\,(org)} + 3Cl^{-}_{(aq)} \quad \textbf{3.7.}$$

$$3LH^{+}_{(org)} + 2[RhCl_5(H_2O)]^{2-}_{(aq)} \rightleftharpoons (Rh_2Cl_9)\cdot(LH)_{3\,(org)} + 2H_2O_{\,(aq)} + Cl^{-}_{(aq)} \quad \textbf{3.8.}$$

$$3(Cl\cdot LH)_{\,(org)} + 2[RhCl_5(H_2O)]^{2-}_{(aq)} \rightleftharpoons (Rh_2Cl_9)\cdot(LH)_{3\,(org)} + 2H_2O_{\,(aq)} + 4Cl^{-}_{(aq)} \quad \textbf{3.9.}$$

$$2(RhCl_5(H_2O))\cdot(LH)_{2\,(org)} \rightleftharpoons (Rh_2Cl_9)\cdot(LH)_{3\,(org)} + Cl\cdot LH_{\,(org)} + 2H_2O_{\,(aq)} \quad \textbf{3.10.}$$

The formation energies (given in Table 3.4) associated with the processes in Equations 3.6-3.10 are all energetically favourable. However, the most favourable process is the formation from $[RhCl_5(H_2O)]^{2-}$ and Cl·LH during extraction. This suggests (as supported by the ESI-MS analysis, which suggests the dinuclear complex is present immediately following extraction and is not formed over time in the organic phase, and the EXAFS analysis, which shows no evidence of the dinuclear complex in the aqueous phase) that the dinuclear complex is formed during the extraction process from mononuclear $[RhCl_5(H_2O)]^{2-}$.

Table 3.4. Free energy changes for the processes outlined in Equations 3.6-3.10. Energies used in the calculation of these formation energies are provided in the SI. Note: BSSE correction has been applied to the energy calculated for Equation 3.6 and, to keep the energy from Equation 3.7 consistent with those of Equations 3.2 and 3.6, BSSE corrected energies for Cl·LH, and $(Rh_2Cl_9)\cdot(LH)_3$ have been used for the Equation 3.7 energy calculation. BSSE corrections are not applied for Equations 3.8 through 3.10, owing to the change in the inner-coordination sphere of the Rh(III) centres and the fact that these energies cannot be obtained from combinations of the other equilibria considered.

Process	ΔG/ kJ mol^{-1}
Equation 3.6	-46.3
Equation 3.7	-14.5
Equation 3.8	-120.0
Equation 3.9	-75.6
Equation 3.10	-18.7

3.3 Conclusions and future work

Rh SX is a difficult, complicated process, made so due to the varied speciation of Rh(III) in HCl solution. This work has further highlighted this point, with the organic phase speciation also appearing to be complex. A wide array of analytical work has been undertaken, with most results pointing to a ion-associate form of extraction, the hypothesis posed by Narita et al. in their first work on the amidoamine systems.[1] KF titrations suggest a reverse micelle-type mechanism is unlikely, at least for Rh, though some water appears to be involved in the extraction of chloride. EXAFS, NMR, FT-IR and SANS analysis support the existence of an ion-pair mode, with the SANS analysis highlighting the difference in the extraction behaviour of BisAA and TOA, the latter of which appears to form larger aggregates.

NMR, ESI-MS and EXAFS have also highlighted the existence of complexes in the organic phase other than $(BisAAH)_2 \cdot (RhCl_5(H_2O))$. Evidence of a dinuclear Rh complex, of the form $(BisAAH)_3 \cdot (Rh_2Cl_9)$, is seen in loaded organics of extractions from aqueous solutions containing high concentrations of Rh(III) in the ESI-MS spectra and a short Rh…Rh distance is also observed in the EXAFS results. Unfortunately, it has proven very difficult to determine how this complex arises in the organic phase. ESI-MS has illustrated that this complex is present in the organic phase very soon after extraction, and so it is unlikely that the complex forms over time in the organic phase. Instead, either some Rh(III) must be present in the aqueous phase in the form $[Rh_2Cl_9]^{3-}$ (but at a concentration too low to be detected by EXAFS analysis) and be extracted as such, or the dimeric Rh(III) species must form during extraction. Computational analysis suggests that either of these options is possible with both energetically favourable, though the latter being more so.

In addition, ESI-MS has shown that the inner-sphere complex $RhCl_3BisAA$ can form in the organic phase upon aging. A similar complex was synthesised using a BisAA analogue by researchers at AIST, and the X-ray structure confirms that a single BisAA(alt) molecule bind in a tridentate fashion to the Rh(III) centre through its amine N atom and its amide O atoms. FT-IR analysis of this sample is comparable to that of an oil sample obtained from a synthesis with BisAA instead of the analogue. Given that this complex is only observed in the ESI-MS at appreciable levels after aging and that long reaction times had to be employed to synthesise the oil sample, it is unlikely that this complex is formed under normal extraction conditions.

NMR analysis also supports the presence of inner-sphere coordinated BisAA in aged Rh-loaded organic samples.

The computational study has shown that the extraction assemblies and formation energies can be determined and used to understand why amidoamine extractants are so effective for Rh extraction. It is found that the possibility of a hydrogen bond between the *aquo* ligand of $[RhCl_5(H_2O)]^{2-}$ and the extractant does not appear to be a key feature of extraction, contrary to previous suggestion.[1, 13] Indeed, this hydrogen bond is only found to occur with MonoAA(Me), which corresponds to the weakest of the three amidoamine extractants. Instead, it appears that the existence of multiple intra-extractant hydrogen bonds between the proton on the amine N and the amide O atoms assembles the extractant in such a way that it presents an array of C-H contacts to anions. This large area of diffuse positive charge, i.e. a "soft" binding site, appears to favour association with the larger, more diffusely charged, i.e. "softer", $[RhCl_5(H_2O)]^{2-}$ anion, compared to the small, charge dense, i.e. "hard", chloride anion. This "chelating" happens with BisAA(Me) and TrisAA(Me), making them more selective for the Rh(III) metalate over chloride than MonoAA(Me) is, for which chelation of the proton is less favourable than a direct protonated amine N-H to anion interaction. The computational results match reasonably well with the experimental extraction results and help explain the success of the amidoamines: their comparatively weak association with chloride. Experimentally, amines, such as TOA, are found to extract Rh(III) at very low chloride concentrations but not at the higher concentrations the amidoamines still extract at, suggesting they have poorer selectivity for Rh(III) metalate over chloride than the amidoamines.

Though the aims of this work, to characterise the mode of action of the amidoamine extractants and rationalise their excellent extraction ability, have largely been achieved there are several avenues of research remaining that would be of interest to study.

In particular, all of the experimental work reported here has focussed on the BisAA extractant. Carrying out the same analysis on MonoAA could potentially highlight the differences in its extraction mode, as suggested in the calculations, which lead to it being a poorer extractant. It would also be good to analyse the TrisAA system, to verify the extractant does indeed possess the same extraction mode as BisAA.

There is also scope for continuation of the simulations, depending on the results of any future experimental work. If analysis on the MonoAA and TrisAA systems showed that dimeric aggregates with chloride form, structures for these dimers should be modelled and the amended formation energies and exchange energies calculated.

There is likely water in the chloride aggregates, as suggested by the KF titrations, but how it is incorporated is unknown. Molecular dynamics (MD) simulations could be of use here, to allow the water molecules to move to their equilibrium position and their interactions with the extractant and/or chloride anion to be elucidated.

MD simulations, in particular classical MD simulations, could also be of interest if further exploration of the extraction mode of TOA is desired. These would allow the large numbers of molecules required to represent the system to be modelled together and for the aggregation behaviour to be observed.

3.4 Methods

For AIST BisAA synthesis, EXAFS (set 1), FT-IR, X-ray crystallography, KF titration of samples in octanol, and SANS analysis details see Narita et al.[14] (the paper and its accompanying SI are provided in the SI).

For UoE BisAA synthesis, EXAFS (set 2), NMR, ESI-MS, KF titration of samples in chloroform, acid/base titrations, time-dependant extraction analysis, and computational modelling details see sections below.

3.4.1 UoE reagent and instrumentation details

See Chapter 2 for details of all reagents and instruments used in experimental work conducted at the University of Edinburgh, and the set 2 EXAFS instrumentation used at Diamond Light Source.

3.4.2 UoE BisAA synthesis

BisAA was synthesised and purified using a slightly modified version of the method reported by Narita et al.[1] The synthesis was carried out in batches. Different masses were synthesised each time. The following synthesis is an example of one carried out (the others followed the same general procedure):

Intermediate synthesis: Chloroacetyl chloride (30.6 g, 0.271 mol) in diethyl ether (45 mL) was added dropwise to a solution of *N*-methyl-*N*-*n*-octylamine (77 g, 0.537 mol) in diethyl ether (175 mL) in an ice bath. The mixture was stirred at room temperature for around 26 hours, the white solid that formed was removed by filtration (and retained for recovery of *N*-methyl-*N*-*n*-octylamine) and the filtrate reduced *in vacuo*. The residue was purified by column chromatography (silica gel; ethyl acetate in hexane gradient: 5 v/v% to start and approximately until product started coming off, then ramping up to 25%) to yield approximately 38.2 g (0.174 mol, 64 % yield) of a very pale-yellow oil which was confirmed to be *N*-methyl-*N*-*n*-octylchloroacetamide by NMR.

Note: Some syntheses of intermediate used "fresh" N-methyl-N-n-octylamine as received, while some used that recovered from previous syntheses.

BisAA synthesis: *N*-methyl-*N*-*n*-octylchloroacetamide (38.2 g, 0.174 mol) in chloroform (90 mL) was added slowly to a solution of *n*-hexyl amine (8.5 g, 0.084 mmol) and triethylammine (19.5 g, 0.193 mmol) in chloroform (125 mL) at room temperature. The mixture was refluxed at 75 °C for 40 hours. After cooling, the mixture was washed subsequently with 0.5 M HCl, 2.5 wt% sodium carbonate solution and water, dried over sodium sulfate and reduced *in vacuo*. The residue was purified by column chromatography (silica gel; methanol in DCM gradient: 2-3 v/v% to start and approximately until product started coming off, then ramping up to 7-10%), dissolved in DCM, dried over sodium sulfate and the solvent removed *in vacuo* to yield approximately 26.3 g (0.056 mol, 67 % yield (based on mass of *n*-hexyl amine used)) of a very pale yellow oil which was confirmed to be N-*n*-hexyl-bis(*N*-methyl-*N*-*n*-octylethylamide)amine (BisAA) by NMR.

Three batches of columned BisAA were dissolved in DCM, dried over sodium sulfate and filtered. The solvent was removed *in vacuo* before the batches were combined. The combined purified BisAA was analysed and used in extractions. ^{1}H NMR (500 MHz, $CDCl_3$, ppm): δ 0.81-0.88 (m, 9H), 1.18–1.30 (m, 26H), 1.45–1.51 (m, 6H), 2.59–2.66 (m, 2H), 2.86 and 3.00 (2s, 6H), 3.26–3.32 (m, 4H), 3.40–3.47 (m, 4H). ^{13}C NMR (126 MHz, $CDCl_3$, ppm) δ: 14.00, 22.58, 26.71, 26.85, 27.00, 27.13, 27.22, 27.44. 27.59, 28.40, 28.42, 29.18, 29.21, 29.35, 31.72, 31.75, 33.19, 34.78, 34.79, 47.81, 49.33, 55.07, 55.32, 55.50, 56.36, 56.41, 169.96, 170.01, 170.31, 170.33. ESI-MS (m/z): $[(C_{24}H_{33}N_3O_2)+H]^+$ calculated: 468.452; found: 468.453. Elemental analysis: calculated for $C_{24}H_{33}N_3O_2$: C, 71.89; H, 12.28; N, 8.98; found. C, 72.00; H, 12.22; N, 8.77. IR (ATR, cm^{-1}): 1642 ($\nu_{(C=O)}$).

3.4.3 UoE solvent extractions

Aqueous metal solution preparation: The appropriate mass of Na_3RhCl_6 was dissolved in the desired concentration of HCl or water. This solution was then either used as is or diluted to achieve the desired Rh and acid concentration. All Rh-containing aqueous solutions used in the SX experiments were prepared 24 hours in advance, and used within 48 hours of preparation.

Organic solution preparation: The appropriate mass of BisAA was dissolved in chloroform. This solution was then pre-contacted with an equal volume of 2 M HCl solution (stirring for 30 mins, followed by centrifuging for 10 mins before separation) unless otherwise stated.

Solvent extraction procedure: Chapter 2 Section 2.2.1 describes the general solvent extraction procedure. For specific details of extractions carried out to produce samples for each analysis technique, see corresponding section below.

ICP-OES analysis: The metal content of the aqueous and organic phases was determined via organic ICP-OES analysis. See Chapter 2 Section 2.2.2 for details.

3.4.4 Set 2 EXAFS

Set 2 sample preparation:

(f)-(h): The appropriate mass of Na_3RhCl_6 was dissolved in water to produce a 0.4 M Rh solution stock solution. The appropriate volume of this solution, 12 M HCl and water were mixed to give a Rh concentration of approximately 0.01 M in (f) 2 M HCl, (g) 4 M HCl and (h) 10 M HCl.

(i): 0.1 M BisAA in *d*-chloroform pre–contacted with 2 HCl was contacted five times with 0.1 M Rh(III) in 2 M HCl solution (stirring of 30 mins for each contact, followed by centrifuging for 10 mins). Multiple contacts were carried out to achieve high Rh(III) loading. Sample was one month old at point of EXAFS analysis.

(j): Prepared as sample 5. Sample was 6 months old at point of EXAFS analysis.

Set 2 data collection: See Chapter 2 Section 2.2.6 for details.

Set 2 data processing: All analyses of the $k^3\chi(k)$ EXAFS were performed in identical fashion in the usual manner with EXAFSPAK modules PROC and OPT.[24] The curve-fitting with a fixed scale factor ($S_0^2 = 0.9$) entailed a series of step-wise fits of increasing complexity as employed elsewhere,[24, 25] and found to be particularly important for Rh and In chlorometalate anions.[26-28] At the most fundamental level, a one-shell (4 parameter) model of the Rh-Cl interactions

was obtained for all data sets; the results in terms of Rh-Cl interatomic distances, *r* (Å), and Debye-Waller factors, σ^2 (Å^2); Cl coordination numbers (CN); energy threshold parameter, ΔE_0 (eV), are presented in the SI. Where distant correlations beyond the Rh-Cl interactions were observed in the FT data and identified as Rh backscattering by 'best-Z' fitting,[24] two-shell (7 parameter) models of Rh-Cl and Rh-Rh provided the metrical results shown in Table 3.1. Other fitting models (beyond one shell Rh-Cl and two shell Rh-Cl and Rh-Rh, to include Rh-O) were tried but found to be problematic. For details and the results of this fitting see the SI. All modelling employed the theoretical phase and amplitude functions calculated with FEFF8.01.[29] Based upon the statistical information obtained for each fitting model, *i.e.* χ^2/ν, where χ^2 is the goodness-of-fit and ν is the number of degrees of freedom of the fit, along with the Fχ test,[30] the data were best modelled with either one- (Cl) or two-shell (Cl, Rh) fits to the $k^3\chi(k)$ EXAFS. For each model the numbers of variables (≤ 11) was less than the number of relevant independent data points available in the primary spectra, which was estimated $N_I = (2\Delta k \Delta r)/\pi = (2\times13\times1.5)/\pi = 12$. The expected resolution of the Rh K-edge EXAFS in r-space is *ca*. 0.12 Å (for k_{max} = 15 Å^{-1}), meaning that shells of backscattering atoms about Rh with this (and smaller) interatomic separations are not resolved in the Fourier transform (FT) data. In order to obtain semi-quantitative information about the possibility of chlorido*aquo*-Rh(III) solution speciation, an algebraic approach based upon the Cl CNs was used, with the constraint that total Cl + O CN = 6. For example, for a Cl CN of 6, the EXAFS response was assumed to from a monodisperse (100%) solution of $RhCl_6^{3-}$ without inner-sphere water coordination. In contrast, for Cl CNs less than 6, it was assumed that the values reflected the presence of the hexachloroanion and one of the aquated anions (with integer Cl CNs of 5, 4, 3, *etc.*).

3.4.5 NMR

For the 2D NMR studies, 0.1 M BisAA (in chloroform and pre–contacted with 2 HCl) was contacted five times with 0.1 M Na_3RhCl_6 in 2 M HCl solution (stirring of 30 mins for each contact followed by centrifuging for 10 mins). Samples of the 0.1 M BisAA solution, the chloride-loaded BisAA (from the pre-contact) and Rh-loaded organic phases were analysed by ^{1}H, ^{13}C, ^{1}H-^{13}C HMBC, and ^{1}H-^{15}N HMBC spectroscopy. For some samples, additional d-

chlorofom was added prior to analysis to dilute them. The samples were approximately four months old at the time of analysis.

3.4.6 ESI-MS

0.5 M BisAA in chloroform (pre–contacted with 2 HCl) was contacted with 0.001, 0.01 and 0.1 M Na_3RhCl_6 in 2 M HCl solutions (contacts for 30 minutes, followed by 10 mins of centrifuging). The loaded organic phases were analysed by ESI-MS within 48 hours. Analysis of the organic phase from the extraction from 0.1 M Rh in 2 M HCl solution was repeated after seven months.

The short contact loaded organic was prepared by contacting 0.1 M Na_3RhCl_6 in 2 M HCl solution with 0.1 M BisAA in chloroform solution (30 second manual shake, no centrifuging to minimise contact time, total contact time of about a minute). This loaded organic was analysed immediately.

Samples were diluted in acetonitrile prior to analysis.

3.4.7 UoE Karl Fischer Titrations

Solutions of 0.1, 0.05, 0.025, 0.01 and 0.005 M Rh(III) in 2 M HCl were contacted with 0.1 M BisAA in chloroform (pre-contacted with 2 M HCl solution) for 30 minutes of stirring followed by 10 minutes of centrifuging before separation.

Solutions of 0.01 M, 0.02 M, 0.05 M, 0.1 M and 0.2 M BisAA in chloroform were contacted with 2 M HCl solutions (30 minutes of stirring followed by 10 minutes of centrifuging before separation).

0.1 M BisAA in chloroform and HCl solutions of varying concentration were contacted (30 minutes of stirring followed by 10 minutes of centrifuging before separation). Chloroform alone was also contacted with the HCl solutions (30 minutes of stirring followed by 10 minutes of centrifuging before separation).

The organic phases were analysed in duplicate (unless otherwise specified) for their water content by KF titration.

3.4.8 Acid-base titrations

0.1 M BisAA in chloroform and HCl solutions of varying concentration were contacted (30 minutes of stirring followed by 10 minutes of centrifuging before separation). The organic phases were analysed by manual acid–base titration using phenolphthalein as the indicator.

3.4.9 Varying time extractions

0.1 M Na_3RhCl_6 in 2 M HCl solutions and pre-contacted 0.1 M BisAA in chloroform solutions were contacted for various times. The two phases were separated without centrifuging to allow for all the extractions to be started at the same time.

3.4.10 Computational modelling details:

All calculations were carried out as described in Chapter 2, Section 2.1.2.3.

The M06[31] exchange/correlation functional was used with the LANL2TZ[32] basis set/pseudopotential for Rh and the 6-311+G**[33, 34] basis set for all other atoms. Implicit solvent modelling was included in the optimisation (PCM[35] with the solvent model for chloroform or water, as appropriate).

Octyl and hexyl R-groups for MonoAA, BisAA and TrisAA were replaced with methyl groups throughout to reduce computational expense and to aid structure optimisation, as the presence of long chain side groups considerably increases the probability of many similar energy local minima.

Optimisation was carried out from a variety of starting structures, which were built based on the conformations of the extractants and on the possible binding modes that could occur to an anion (see Figure 3.3). Different conformations of LH^+ were used and placed in different orientations around chloride or $[RhCl_5(H_2O)]^{2-}$. All structures explored are given in the SI.

All optimised structures were found to be minima with the exceptions of TrisAA(Me)H^+ and $RhCl_5(H_2O)\cdot(TrisAA(Me)H)_2$ (imaginary frequencies of 93.4 cm^{-1} for TrisAA(Me)H^+ and of 19.2, 34.0 and 49.8 cm^{-1} for the lowest energy structure of $RhCl_5(H_2O)\cdot(TrisAA(Me)H)_2$). For these structures, it proved not possible to reach minima and the eigenvectors suggested the source

of the geometry optimisation problem stemmed from a competitive attraction for the amine H^+ by the three amide groups.

Counterpoise correction calculations were carried out on the lowest energy structures for the LH·Cl, $(RhCl_5(H_2O))\cdot(LH)_2$ and $(Rh_2Cl_9)\cdot(LH)_3$ assemblies and Table 3.5 gives details of the fragments defined in these calculations. Two different sets of fragment identities were used for the $(BisAA(Me)H\cdot Cl)_2$ calculations as in Equation 3.5 the energies used needed to be compatible with those of Equations 3.1-3.4 and so four fragments needed to be defined, whereas for the dimerization energy given in Figure 3.21 it was more appropriate to use two fragments to describe the coming together of the dimer from two monomers.

Table 3.5. Fragments used for counterpoise corrections. Two calculations, using different fragmentation, used for $(LH\cdot Cl)_2$ structure(s) on account of two different formation processes being considered and the need to be compatible with other formation energies.

Structure	Fragment 1	Fragment 2	Fragment 3	Fragment 4
LH·Cl	LH^+	Cl^-	-	-
$(LH)_2\cdot[RhCl_5(H_2O)]$	LH^+	LH^+	$[RhCl_5(H_2O)]^{2-}$	-
$(LH\cdot Cl)_2$	LH^+	LH^+	Cl^-	Cl^-
	LH·Cl	LH·Cl	-	-
$(LH)_3\cdot[Rh_2Cl_9]$	LH^+	LH^+	LH^+	$[Rh_2Cl_9]^{3-}$

3.5 References

1. Narita, H.; Morisaku, K.; Tanaka, M., *Chem. Commun.* **2008,** *45*, 5921-5923.
2. Benguerel, E.; Demopoulos, G. P.; Harris, G. B., *Hydrometallurgy* **1996,** *40*, 135-52.
3. Benguerel, E.; Demopoulos, G. P., *J. Chem. Technol. Biotechnol.* **1998,** *72*, 183-189.
4. Narita, H.; Tanaka, M.; Yaita, T.; Okamoto, Y., *Solvent Extr. Ion Exch.* **2004,** *22*, 853-863.
5. Malik, P.; Paula Paiva, A., *Solvent Extr. Ion Exch.* **2007,** *26*, 25-40.
6. Zou, L.; Chen, J.; Pan, X., *Hydrometallurgy* **1998,** *50*, 193-203.
7. Sun, P. P.; Lee, M. S., *Hydrometallurgy* **2011,** *105*, 334-340.
8. Mhaske, A. A.; Dhadke, P. M., *Hydrometallurgy* **2001,** *61*, 143-150.
9. Malik, P.; Paiva, A. P., *Solvent Extr. Ion Exch.* **2010,** *28*, 49-72.
10. Niinae, M.; Yamamoto, M.; Sano, M.; Nakahiro, Y.; Wakamatsu, T., *Shigen-to-Sozai* **1995,** *111*, 875-879.
11. Shafiqul Alam, M.; Inoue, K., *Hydrometallurgy* **1997,** *46*, 373-382.
12. Yan, G. L.; Alstad, J. In *Solvent extraction of rhodium with cyclohexanol from HCl/$SnCl_2$ media*, 1996; University of Melbourne, Dep. of Chemical Engineering: 1996; pp 547-552.
13. Narita, H.; Morisaku, K.; Tanaka, M., *Solvent Extr. Ion Exch.* **2015,** *33*, 407-417.
14. Narita, H.; Nicolson, R. M.; Motokawa, R.; Ito, F.; Morisaku, K.; Goto, M.; Tanaka, M.; Heller, W. T.; Shiwaku, H.; Yaita, T.; Gordon, R. J.; Love, J. B.; Tasker, P. A.; Schofield, E. R.; Antonio, M. R.; Morrison, C. A., *Inorg. Chem.* **2019,** *58*, 8720-8734.
15. Geswindt, T. E. Chemical speciation of RhIII complexes in acidic, halide-rich media by means of ^{103}Rh NMR spectroscopy : the importance of speciation in the selective separation and recovery of rhodium. Stellenbosch University, 2013.
16. Gerber, W. J.; Koch, K. R.; Rohwer, H. E.; Hosten, E. C.; Geswindt, T. E., *Talanta* **2010,** *82*, 348-358.
17. Samuels, A. C.; Boele, C. A.; Bennett, K. T.; Clark, S. B.; Wall, N. A.; Clark, A. E., *Inorg. Chem.* **2014,** *53*, 12315-12322.
18. Cotton, F. A.; Ucko, D. A., *Inorg. Chim. Acta* **1972,** *6*, 161-172.
19. Levitin, G.; Schmuckler, G., *React. Funct. Polym.* **2003,** *54*, 149-154.
20. Afzaletdinova, N. G.; Khisamutdinov, R. A.; Bondareva, S. O.; Murinov, Y. I., *Russ. J. Inorg. Chem.* **2015,** *60*, 1583-1587.
21. Pazderski, L., *Magn. Reson. Chem.* **2008,** *46*, S3-S15.
22. Afzaletdinova, N. G.; Murinov, Y. I.; Khazhiev, S. Y.; Bondareva, S. O.; Muslukhov, R. R., *Russ. J. Inorg. Chem.* **2010,** *55*, 460-467.
23. Carson, I.; MacRuary, K. J.; Doidge, E. D.; Ellis, R. J.; Grant, R. A.; Gordon, R. J.; Love, J. B.; Morrison, C. A.; Nichol, G. S.; Tasker, P. A.; Wilson, A. M., *Inorg. Chem.* **2015,** *54*, 8685-8692.
24. Ellis, R. J.; Meridiano, Y.; Chiarizia, R.; Berthon, L.; Muller, J.; Couston, L.; Antonio, M. R., *Chem.: Eur. J.* **2013,** *19*, 2663-2675.
25. Antonio, M. R.; Jing, J.; Burton-Pye, B. P.; Francesconi, L. C., *Dalton Trans.* **2010,** *39*, 7980-7992.
26. Deferm, C.; Onghena, B.; Vander Hoogerstraete, T.; Banerjee, D.; Luyten, J.; Oosterhof, H.; Fransaer, J.; Binnemans, K., *Dalton Trans.* **2017,** *46*, 4412-4421.
27. Narita, H.; Tanaka, M.; Shiwaku, H.; Okamoto, Y.; Ikeda-Ohno, A.; Yaita, T., *Bull. Chem. Soc. Jpn.* **2013,** *86*, 203-209.

28. Narita, H.; Tanaka, M.; Shiwaku, H.; Okamoto, Y.; Suzuki, S.; Ikeda-Ohno, A.; Yaita, T., *Dalton Trans.* **2014,** *43*, 1630-1635.
29. Rehr, J. J.; Albers, R. C., *Rev. Mod. Phys.* **2000,** *72*, 621-654.
30. Lukens, W. W.; Bucher, J. J.; Shuh, D. K.; Edelstein, N. M., *Environ. Sci. Technol.* **2005,** *39*, 8064-8070.
31. Zhao, Y.; Truhlar, D. G., *Theor. Chem. Acc.* **2007,** *120*, 215-241.
32. Roy, L. E.; Hay, P. J.; Martin, R. L., *J. Chem. Theory Comput.* **2008,** *4*, 1029-1031.
33. Krishnan, R.; Binkley, J. S.; Seeger, R.; Pople, J. A., *J. Chem. Phys.* **1980,** *72*, 650-654.
34. Raghavachari, K.; Trucks, G. W., *J. Chem. Phys.* **1989,** *91*, 1062-1065.
35. Cossi, M.; Barone, V.; Cammi, R.; Tomasi, J., *Chem. Phys. Lett.* **1996,** *255*, 327-335.

Chapter 4

Theoretical effect of structural modification of amidoamines on rhodium extraction

4 Theoretical effect of structural modification of amidoamines on rhodium extraction

4.1 Introduction

4.1.1 Background

Amidoamine reagents have been shown to be effective Rh(III) extractants both in the literature[1-6] and in Chapter 3 of this work. This appears to be due to their selective extraction of Rh(III) metalate over chloride, when compared to simple amines, and is likely related to the ability of amidoamine extractants to form proton chelates and display a large array of C-H contacts to the anion. Recent results have highlighted the importance of proton chelation in the selective extraction of metalate anions over chloride.[1, 2, 7, 8]

It is illustrated in the work of Narita et al.[2] and in Chapter 3 that structural modifications of amidoamines can alter their effectiveness as Rh(III) extractants. MonoAA, BisAA and TrisAA have different numbers of amide groups present and it is found that BisAA and TrisAA are significantly better Rh(III) extractants than MonoAA, but the improvement in performance of TrisAA over BisAA is marginal. This variation in performance and in the magnitude of effect on the performance makes it attractive to explore how other structural modifications may influence the Rh extraction ability of amidoamines.

4.1.2 Structure of modified amidoamines

There are clearly a multitude of different structural modifications that could be made, but several are of immediate interest owing to previous work.

- Wilson found that an amido thioether extractant predicted computationally to form a 6-membered chelate ring, through hydrogen bonding between the thioether and amide groups upon protonation, gives more efficient extraction experimentally than extractants predicted to from a 7-membered or 5-membered chelate.[9] Thus, it is interesting to determine if the same effect is observed for amidoamine extractants.
- The “orientation” of the amide group(s) with respect to the amine can be altered. Afzaletdinova et al. used extractants with reverse orientation to that which Narita et

al. used.[3-5] This changes the chelate ring size and also the shape constraints on the extractant, but the details of how this effects extraction behaviour have not been explored.

- In addition, Afzaletdinova et al. used secondary amines/amides in their work,[3-5] while Narita et al. used tertiary analogues.[1, 2] However, a comparison of which is better is difficult to make as the same conditions were not used in each case and the extractants often had other structural differences (e.g. number of amide or amine groups). This work aims to see if the effect of the amide group is changed when presented as secondary amide functional groups (as opposed to tertiary) and to quantify any changes in mode of action behaviour if the central amine is presented as a secondary amine functional group.
- Some recent work using ionic liquids has shown success in Rh(III) extraction from chloride media.[10, 11] Quaternary ammonium-based ionic liquids have been used in the solvent extraction of other metals[12] and it is desirable to determine if they could work for Rh(III) extraction too. Also, in the absence of a potential intra-extractant hydrogen bond, there is the increased possibility that a hydrogen bond to the *aquo* ligand on the Rh(III) complex will occur. Therefore, the behaviour of an amido-quarternary ammonium extractant compared to the amidoamine version is also of interest.

The molecules thus chosen for study are shown in Figure 4.1. Note, to save on computational resources and reduce the number of potential local minima, as with the modelling study presented in Chapter 3, all R-groups are methyl groups. From here, in this chapter, molecule names shall refer to those with R=CH_3 (i.e. from here in this chapter MonoAA refers to MonoAA(Me), BisAA refers to BisAA(Me), etc.).

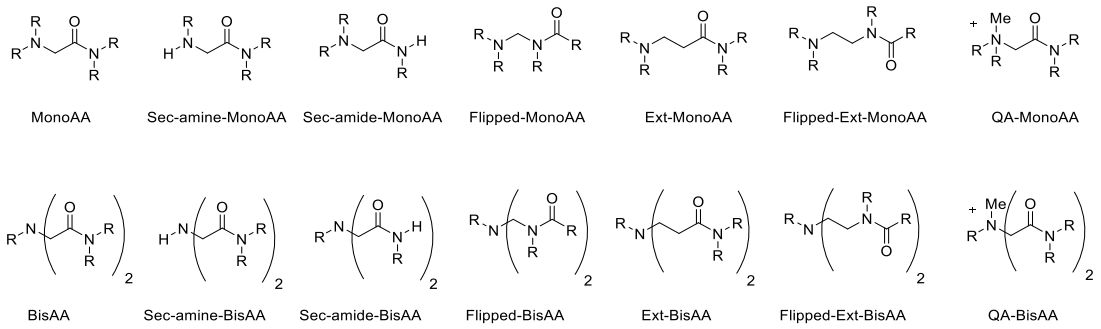

Figure 4.1. Variations on the MonoAA and BisAA structures to be explored computationally as potential Rh extractants. These comprise: secondary amine versions (Sec-amine-); secondary amide versions (Sec-amide-); versions with the orientation of the amide group relative to the amine flipped (Flipped-); versions with an addition -CH_2- group between the amine and the amide (Ext-); versions with an additional -CH_2- group and the orientation of the amide flipped (Flipped-Ext-); and versions based on a quaternary ammonium instead of an amine (QA-). Note R=CH_3 in all the modelling conducted.

4.1.3 Screening study approach

This work has been carried out as a "screening study" to determine if any of the structural modifications could potentially provide stronger Rh extraction than BisAA and TrisAA. Using computational modelling to assess this is more sustainable and time-efficient than synthesising many different (potentially useless) reagents.

In order to keep the outcomes of the computational modelling realistic and sensible to use as a guide for which extractants would be best, this work focuses on a small number of minor changes to the structure of MonoAA and BisAA. This allows the general structure of the extractants to be kept close to that of MonoAA and BisAA, for which both computational and experimental data have already been obtained and found to support each other (see Chapter 3 and the work of Narita et al.[2]). Assuming (see Section 4.4.2 for more information on the assumptions made in this work) extractants which are very similar in structure to MonoAA and BisAA will extract in a very similar manner (i.e. MonoAA and BisAA are ion-pair type extractants, therefore the potential extractants are likely ion-pair type also) then the results of this computational study can provide a reliable general ranking of the extraction ability of these possible extractants and an in-depth look at how their small structural differences impact on their anion binding behaviour.

4.1.4 Aims

This goal of this work is to begin exploring how structural changes affect the extraction ability of amidoamine extractants, by using computational modelling to predict the theoretical binding modes and the relative formation energies of the resulting complexes.

The aims are to:

i. Model the theoretical extraction behaviour of structurally modified amidoamine molecules
ii. Use the output structures to illuminate interactions and determine differences between the modes of action
iii. Compare formation and exchange energies to determine if any modified extractants are theoretically stronger Rh extractants than those reported in Chapter 3

4.2 Results and discussion

4.2.1 Extractant structures

Initial calculations obtained the geometry optimised structures of all the extractants using DFT calculations. The geometry optimised structures are given in Figures 4.2-4.8.

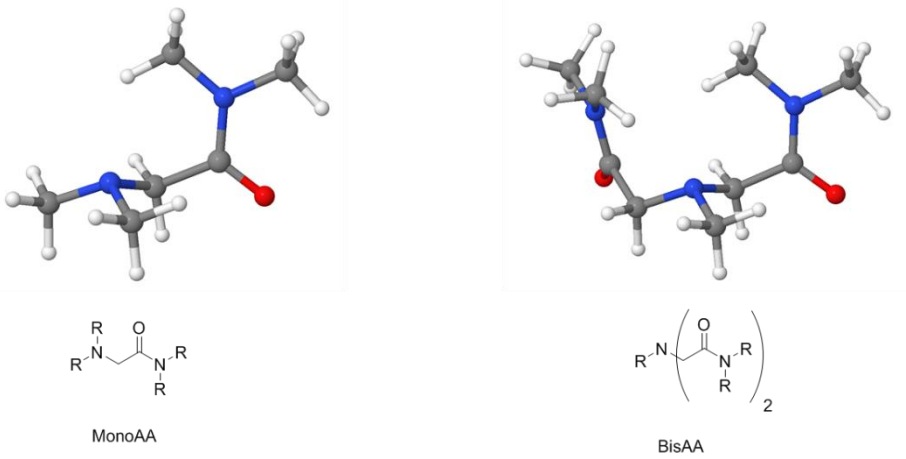

Figure 4.2. Optimised structures (lowest Gibbs Free energy forms found) of MonoAA (left) and BisAA (right).

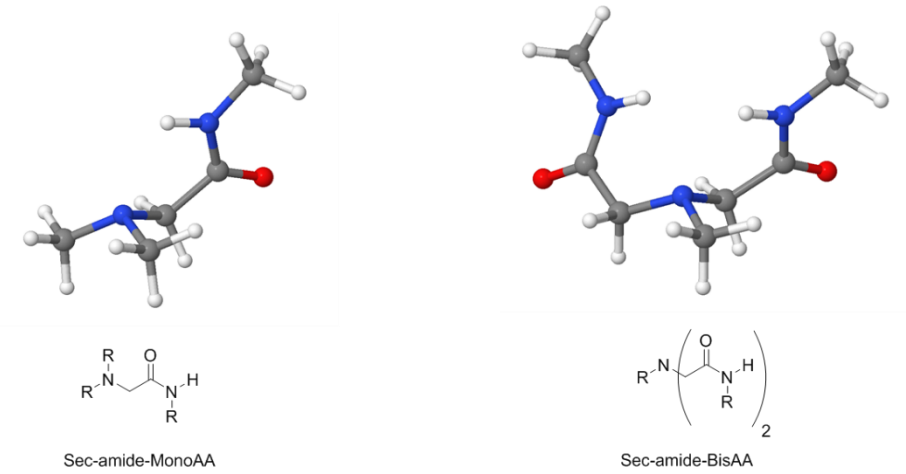

Figure 4.3. Optimised structures (lowest Gibbs Free energy forms found) of Sec-amide-MonoAA (left) and Sec-amide-BisAA (right).

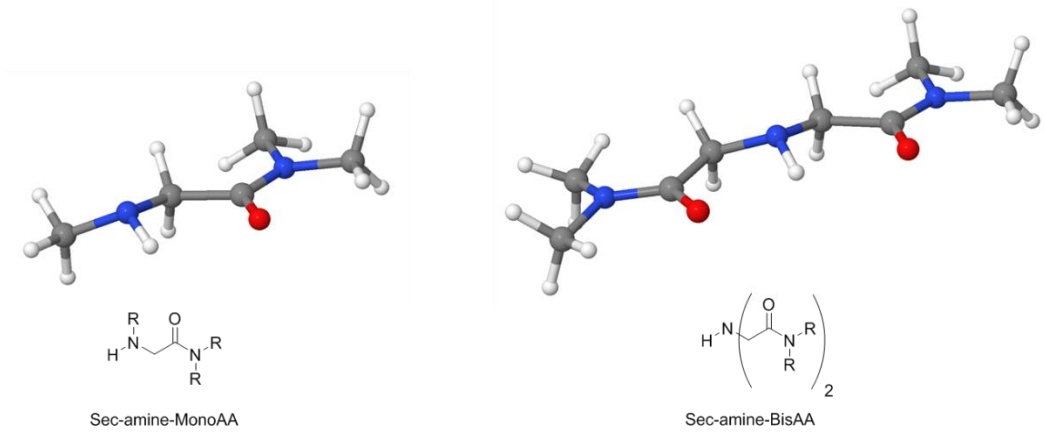

Figure 4.4. Optimised structures (lowest Gibbs Free energy forms found) of Sec-amine-MonoAA (left) and Sec-amine-BisAA (right).

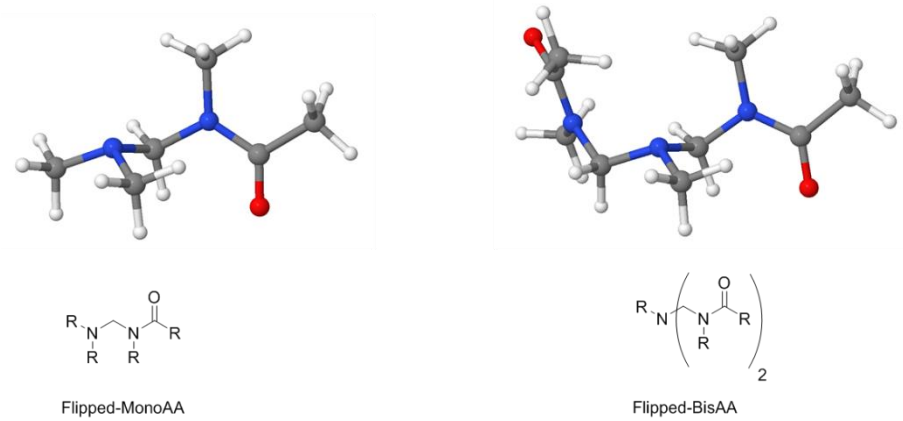

Figure 4.5. Optimised structures (lowest Gibbs Free energy forms found) of Flipped-MonoAA (left) and Flipped-BisAA (right).

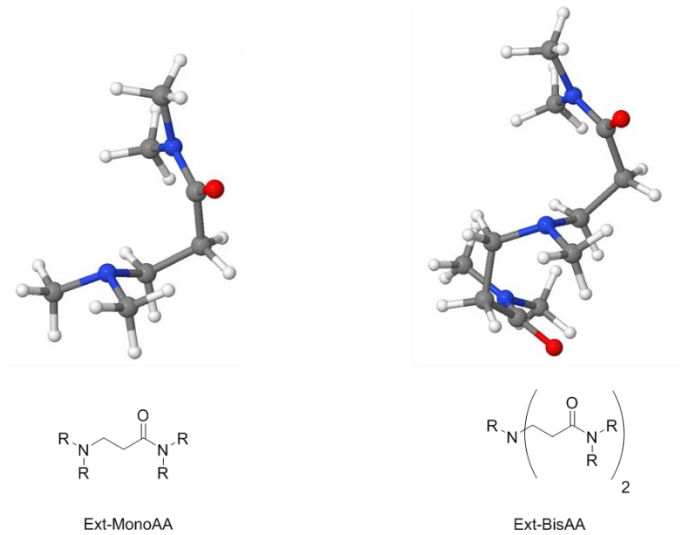

Figure 4.6. Optimised structures (lowest Gibbs Free energy forms found) of Ext-MonoAA (left) and Ext-BisAA (right).

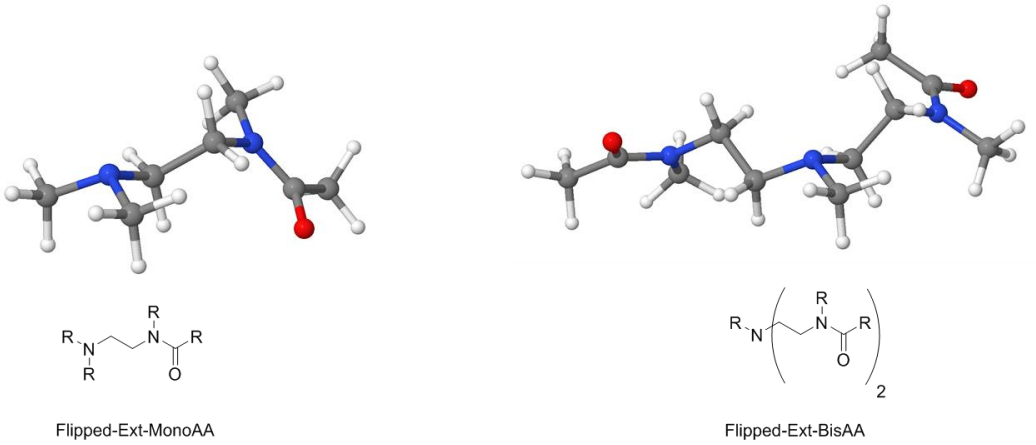

Figure 4.7. Optimised structures (lowest Gibbs Free energy forms found) of Flipped-Ext-MonoAA (left) and Flipped-Ext-BisAA (right).

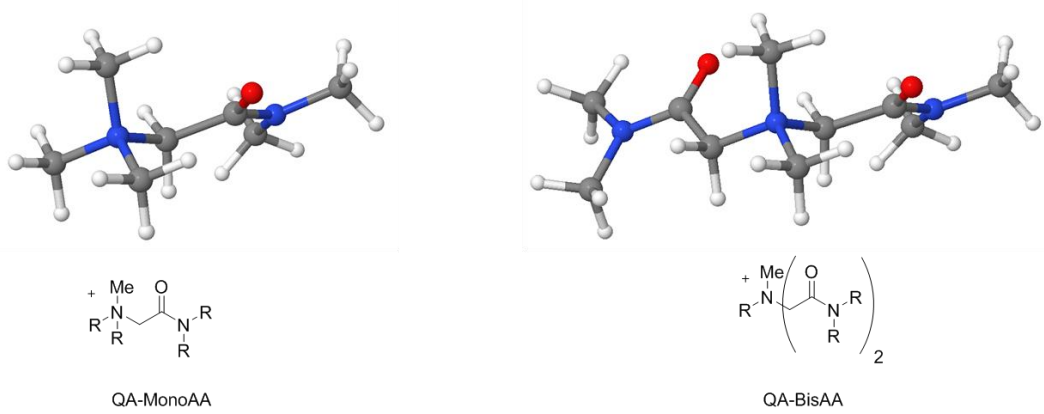

Figure 4.8. Optimised structures (lowest Gibbs Free energy forms found) of QA-MonoAA (left) and QA-BisAA (right).

For most of the extractants there is little to note bar the presence of intramolecular N-H…O/N interactions in some. In the Sec-amine-type extractants shown in Figure 4.4, a single amine N-H to amide O interaction is present for Sec-amine-MonoAA and two are present for Sec-amine-BisAA.

In the Sec-amide-type extractants it is favourable for the amide N-H group(s) to point/face in the direction of the centre of the molecule, to interact with the amine N atom. For Sec-amide-BisAA it is possible that the two amide N-H groups could face the amine N atom, or one amide N-H group could hydrogen bond to the other amide O atom. The latter would occur across the amine group, so there is the potential that some interaction could also occur between the amide N-H and the amine N at the same time. Both these structures were explored and

it was found that two amide N-H groups facing the amine N atom is the lower (Gibbs Free) energy form of the extractant, though the energy difference is very small: 2.0 kJ mol^{-1}.

The interactions are hydrogen bonds (and will be termed as such) but have longer donor-acceptor distances and more acute angles than typical: generally ~2.1-2.4 Å (hydrogen atom to acceptor atom) and ~100-115°. This classes them as weak, electrostatic/dispersion-based hydrogen bonds.[13, 14] Similarly long, acute hydrogen bonds are observed in the protonated forms of the extractants, discussed below.

4.2.2 Protonated extractant structures

Protonated forms of the extractants were modelled and the geometry optimised structures (lowest Gibbs Free energy forms found) are given in Figures 4.9-4.20. In addition, electrostatic potential plots were produced and are also presented in the figures. These are important, as they highlight the delocalisation of the positive charge (shown in blue), and thus show the likely binding site for an anion. Large, diffuse positively charged binding sites will likely favour binding to a large, diffuse anion such as a Rh(III) (*aquo*-)chloridometallate anion. The figures for the amido-quarternary ammonium (QA) based extractants are presented in this section even though they are not protonated, because the QA-extractant cation is more similar to the other protonated extractants than to the unprotonated forms, and are given in Figures 4.21 and 4.22.

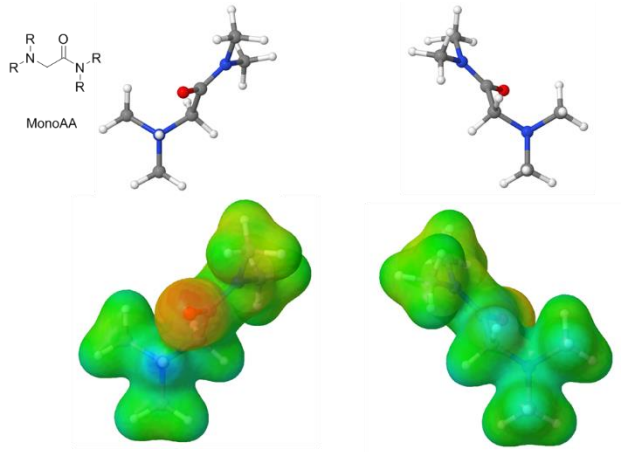

Figure 4.9. Front (left) and back (right) views of optimised structure of $MonoAAH^+$ and corresponding ESP plots (red: relative negative charge; blue: relative positive charge).

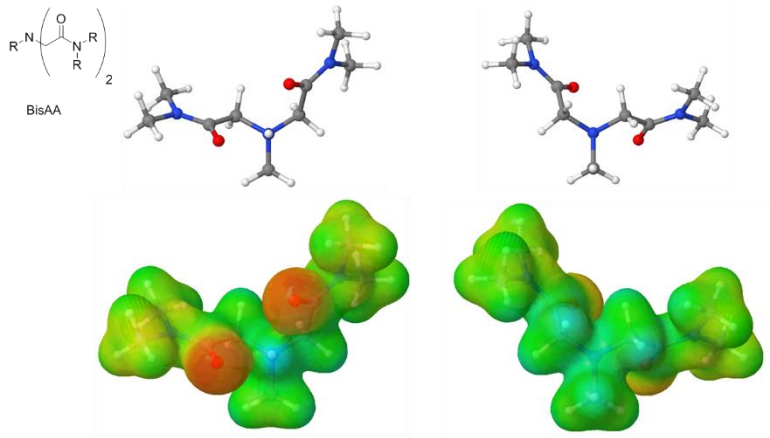

Figure 4.10. Front (left) and back (right) views of optimised structure of BisAAH$^+$ and corresponding ESP plots (red: relative negative charge; blue: relative positive charge).

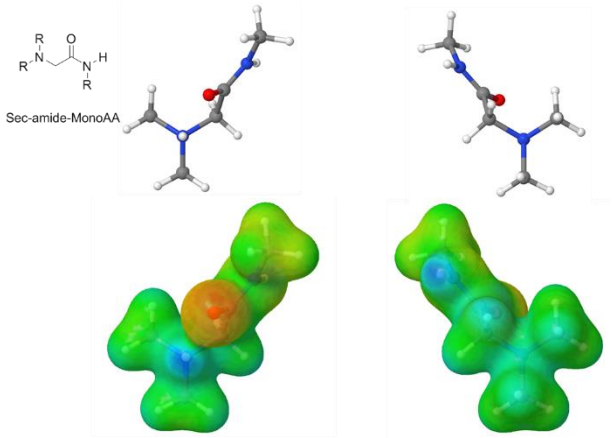

Figure 4.11. Front (left) and back (right) views of optimised structure of Sec-amide-MonoAAH$^+$ and corresponding ESP plots (red: relative negative charge; blue: relative positive charge).

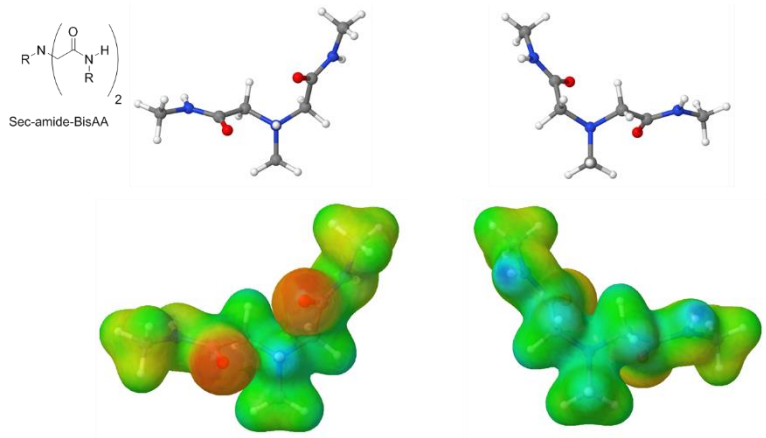

Figure 4.12. Front (left) and back (right) views of optimised structure of Sec-amide-BisAAH$^+$ and corresponding ESP plots (red: relative negative charge; blue: relative positive charge).

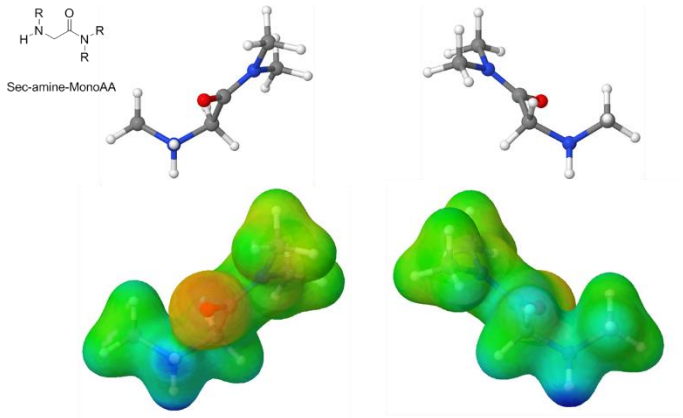

Figure 4.13. Front (left) and back (right) views of optimised structure of Sec-amine-MonoAAH+ and corresponding ESP plots (red: relative negative charge; blue: relative positive charge).

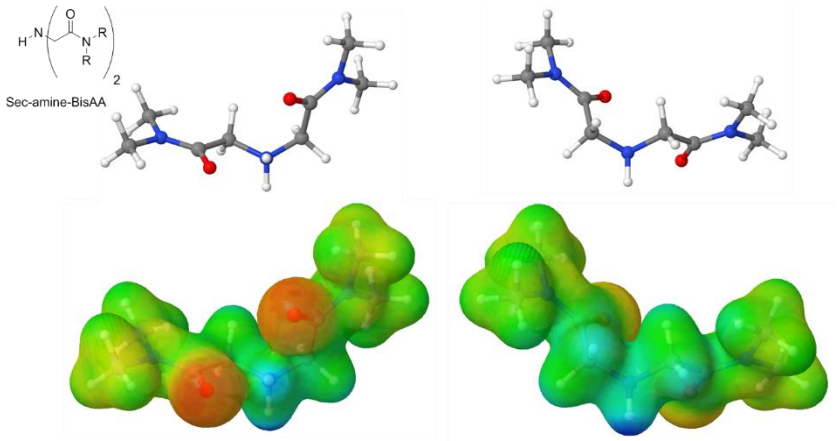

Figure 4.14. Front (left) and back (right) views of optimised structure of Sec-amine-BisAAH$^+$ and corresponding ESP plots (red: relative negative charge; blue: relative positive charge).

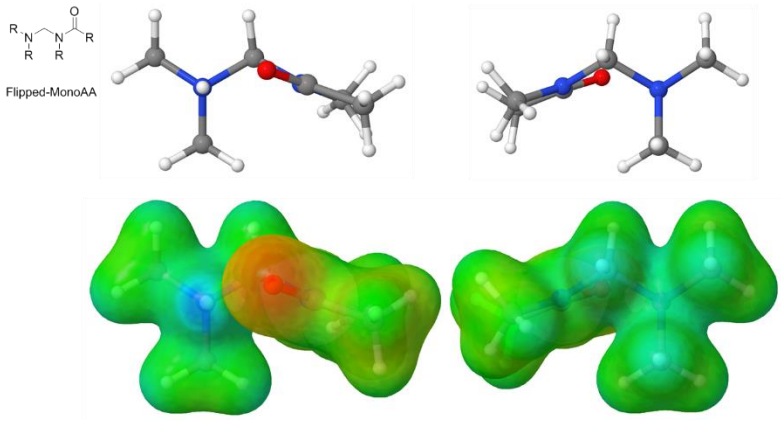

Figure 4.15. Front (left) and back (right) views of optimised structure of Flipped-MonoAAH$^+$ and corresponding ESP plots (red: relative negative charge; blue: relative positive charge).

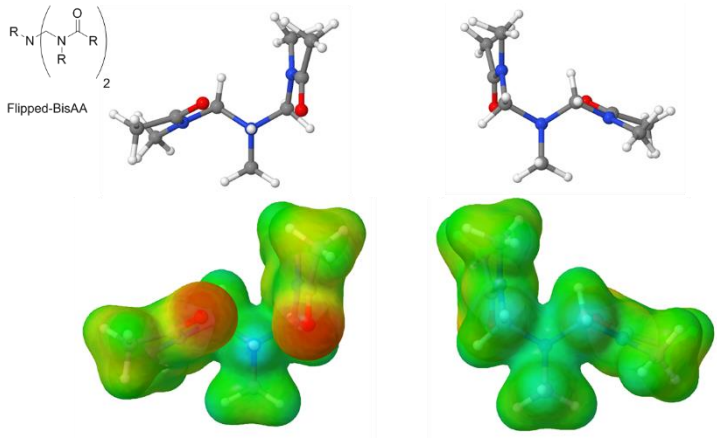

Figure 4.16. Front (left) and back (right) views of optimised structure of Flipped-BisAAH$^+$ and corresponding ESP plots (red: relative negative charge; blue: relative positive charge).

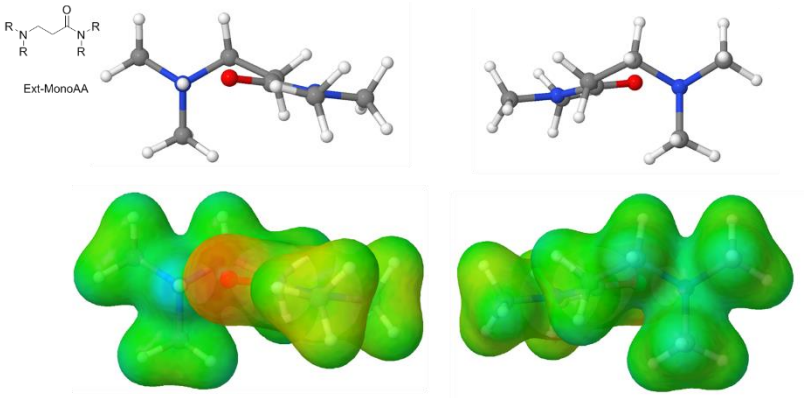

Figure 4.17. Front (left) and back (right) views of optimised structure of Ext-MonoAAH$^+$ and corresponding ESP plots (red: relative negative charge; blue: relative positive charge).

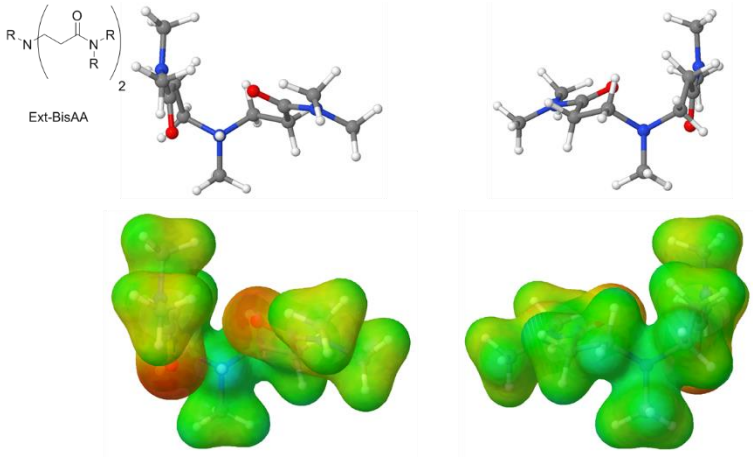

Figure 4.18. Front (left) and back (right) views of optimised structure of Ext-BisAAH$^+$ and corresponding ESP plots (red: relative negative charge; blue: relative positive charge).

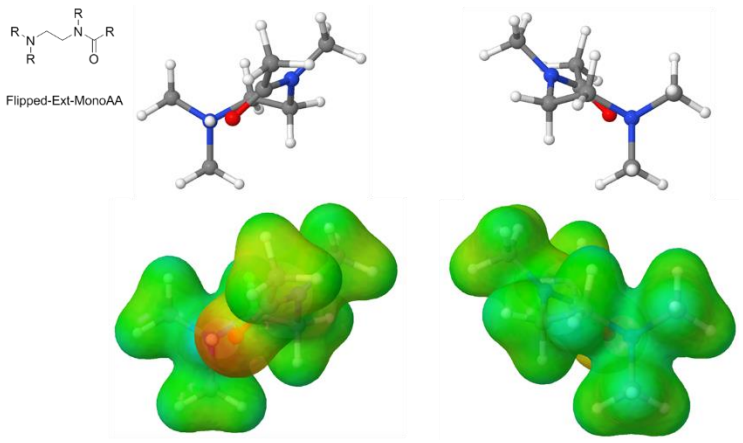

Figure 4.19. Front (left) and back (right) views of optimised structure of Flipped-Ext-MonoAAH$^+$ and corresponding ESP plots (red: relative negative charge; blue: relative positive charge).

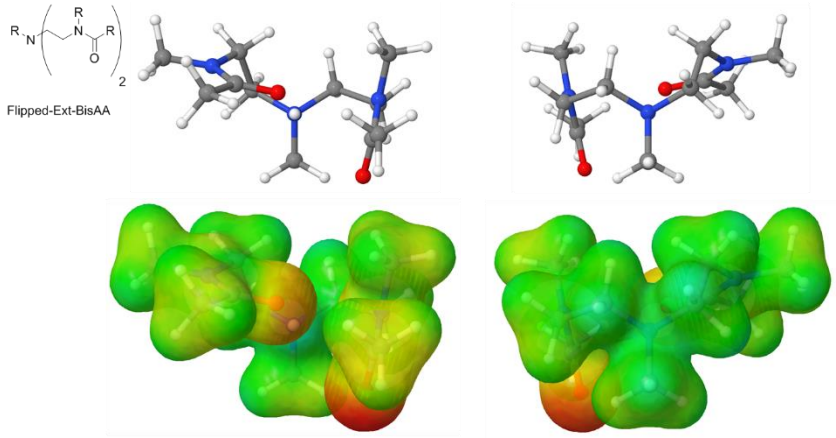

Figure 4.20. Front (left) and back (right) views of optimised structure of Flipped-Ext-BisAAH$^+$ and corresponding ESP plots (red: relative negative charge; blue: relative positive charge).

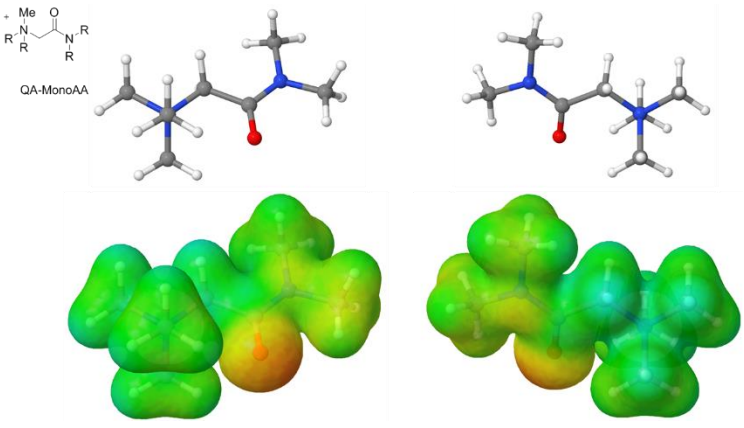

Figure 4.21. Front (left) and back (right) views of optimised structure of QA-MonoAA$^+$ and corresponding ESP plots (red: relative negative charge; blue: relative positive charge).

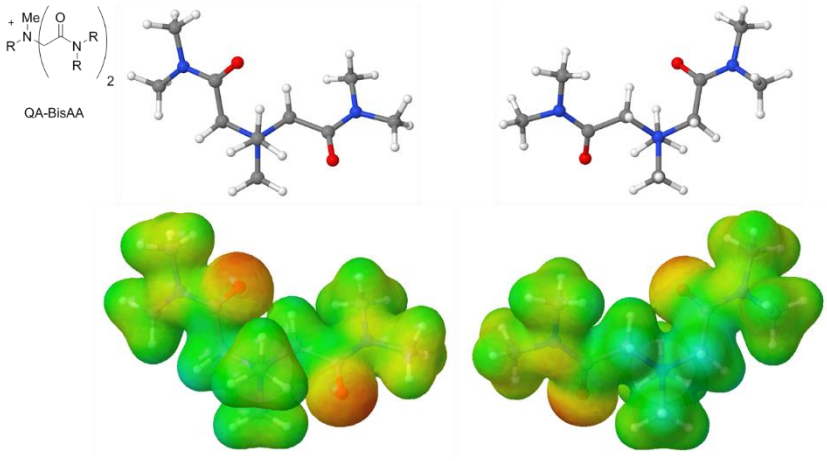

Figure 4.22. Front (left) and back (right) views of optimised structure of QA-BisAA$^+$ and corresponding ESP plots (red: relative negative charge; blue: relative positive charge).

Where possible, all protonated extractants adopt a proton-chelate structure, with hydrogen bonding between the proton on the amine N atom and the amide O atom. For the BisAA-type extractants a double chelate is present for all extractants except Flipped-Ext-BisAAH$^+$, where only a single amide O hydrogen bonds with the N-H proton (Figure 4.19). This appears to be due to the unfavourable configuration that the two amide groups would have to adopt relative to one another, in order for the double chelate to take place.

With Sec-amine-BisAAH$^+$ (Figure 4.14) there are two possible ways that two intramolecular protonated amine N-H to amide O H-bonds can form. Either each amide O atom can form a hydrogen bond with a separate proton on the amine, or both amide O atoms can hydrogen bond with the same proton on the amine. Structures for both modes were optimised and the former was found to have a lower SCF energy (by 7.2 kJ mol^{-1}) while the latter was found to have the lower Gibbs free energy (by 5.9 kJ mol^{-1}). For the purposes of later calculations, the lower energy Gibbs free structure is considered to be the minimum energy structure.

There is also an alternate intramolecular hydrogen bonding mode available for Sec-amide-BisAAH$^+$ (Figure 4.12). Either two intramolecular hydrogen bonds can be formed between the protonated amine N-H group and the two amide O atoms or a hydrogen bond can form between the one amide N-H and the other amide O atom. Both possibilities were explored, and it was found that the former is lower in energy (by 18.6 kJ mol^{-1}, Gibbs free energy) and so more favourable.

The ESP plots show the areas of relative positive and negative charge on the protonated extractants, highlighting that the main areas of positive charge are the protonated amine groups and any additional amine or amide protons. These appear to be localised areas of strongly positive charge density. However, the structures also show positive charge on the hydrogen atoms of the C-H groups on the opposite side of the extractants to the N-H group or along the "edge" of the extractants. These areas are clearly less strongly positively charged; however, they are larger and more spread out in size, creating a large, diffuse area of positive charge. Therefore, both N-H and C-H bonds are possible binding sites for anions, though there may be a different favourability depending on the nature of the anion.

The QA-extractants (Figures 4.21 and 4.22) only have C-H bonds available for anion binding and the ESP plots show the areas of the most positive C-H protons are on the other side of the molecules to where the amide O atom(s) are orientated.

4.2.3 Chloride complex structures

As the ESP plots illustrate, the protonated extractants have more than one type of potential binding site for an anion: interacting directly with the very positive N-H group(s), or with the array of more diffuse positive charge provided by the C-H groups. Both potential binding modes were explored with chloride as the anion. The geometry optimised structures for both modes for each of the extractants are given in Figures 4.23-4.28. In addition, the geometry optimised structures for the QA-extractant cations interacting with chloride are given in Figure 4.29 (with the QA-extractants only C-H interactions are possible). Included in these figures is a "strain" energy, which is calculated as the SCF energy difference between the structure of the protonated extractant when interacting with the chloride (derived from a single point energy calculation) and the minimum energy form. This gives an indication of how much strain is on the protonated extractant when it is binding to chloride, or how much less favourable the geometry it has adopted to accommodate binding to the chloride is.

Note for Figures 4.23 through 4.29: Energies given in black are the Gibbs Free energy of the binding mode relative to the lowest energy of the two binding modes. The energies given in blue/in brackets are the strain energies for the protonated extractants in the binding modes shown (relative to the lowest energy protonated form of the extractant).

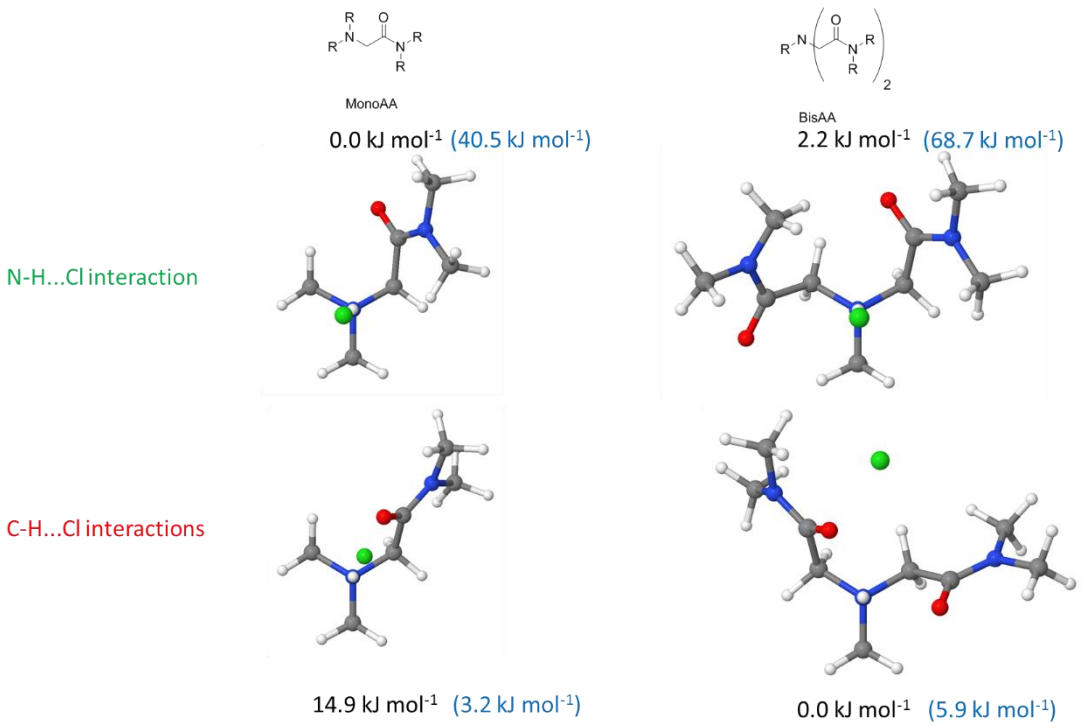

Figure 4.23. N-H and C-H binding modes for MonoAAH$^+$ (left) and BisAAH$^+$ (right) with chloride.

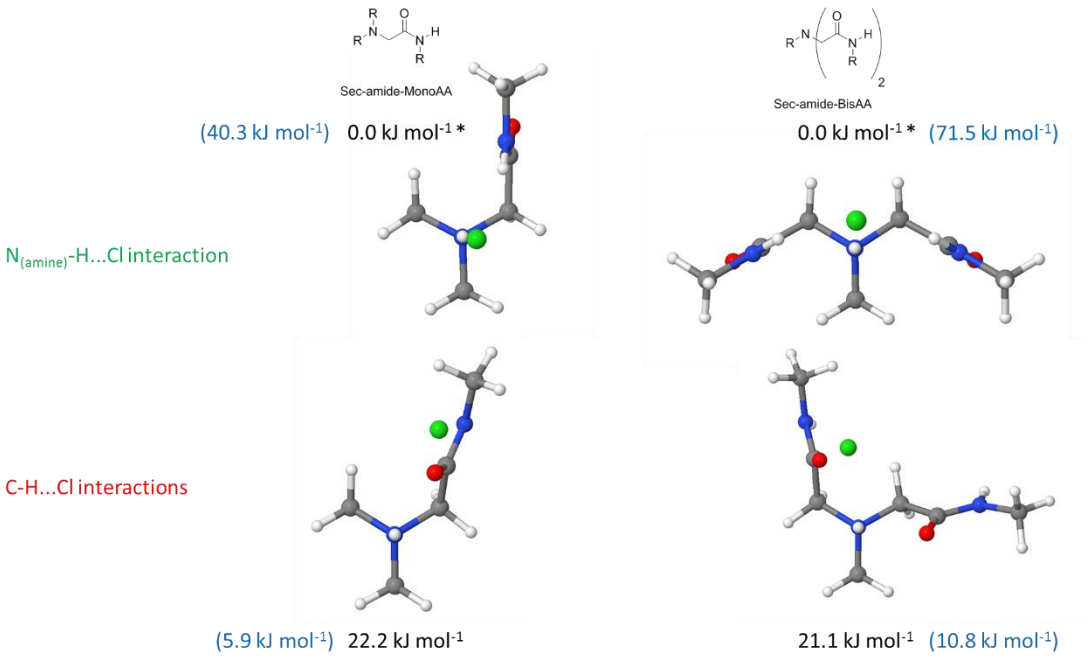

Figure 4.24. N-H and C-H binding modes for Sec-amide-MonoAAH$^+$ (left) and Sec-amide-BisAAH$^+$ (right) with chloride. * Structures are 1st order transition states (Imaginary frequencies of Sec-amide-MonoAA: 36.2 cm^{-1}; and Sec-amide-BisAA: 33.4 cm^{-1}).

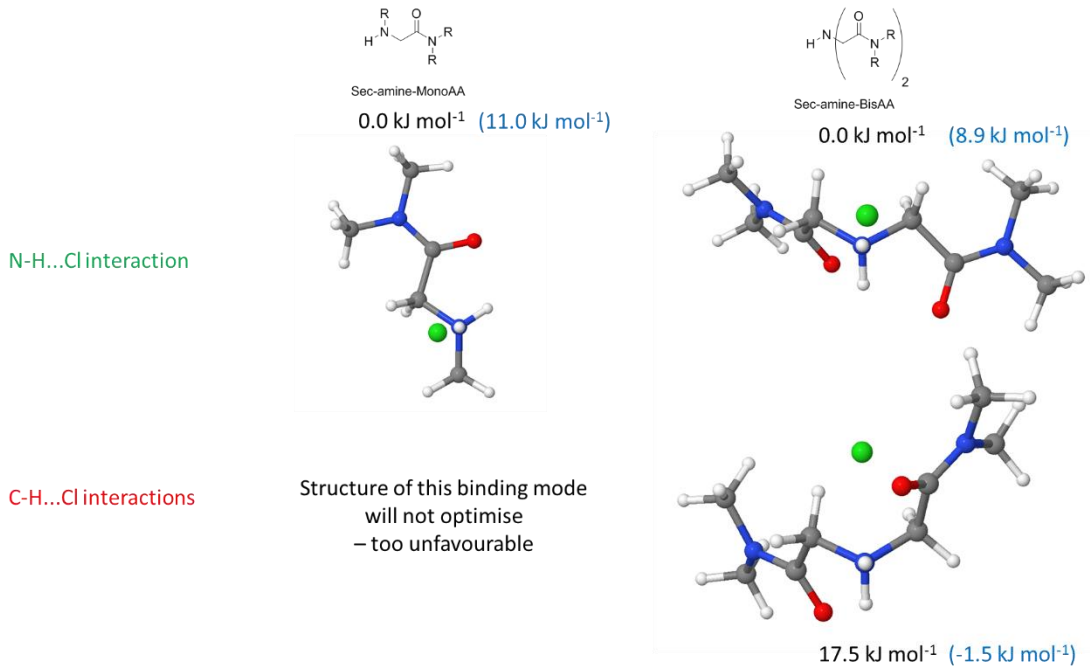

Figure 4.25. N-H and C-H binding modes for Sec-amine-MonoAAH$^+$ (left) and Sec-amine-BisAAH$^+$ (right) with chloride. Note: a starting structure of Sec-amine-MonoAA with only C-H…Cl interactions optimises to a structure with an N-H…Cl interaction. Note: the negative strain energy in the bottom right structure indicates that when considering SCF energies this structure is lower in energy (this is not the case if Gibbs Free energies are considered).

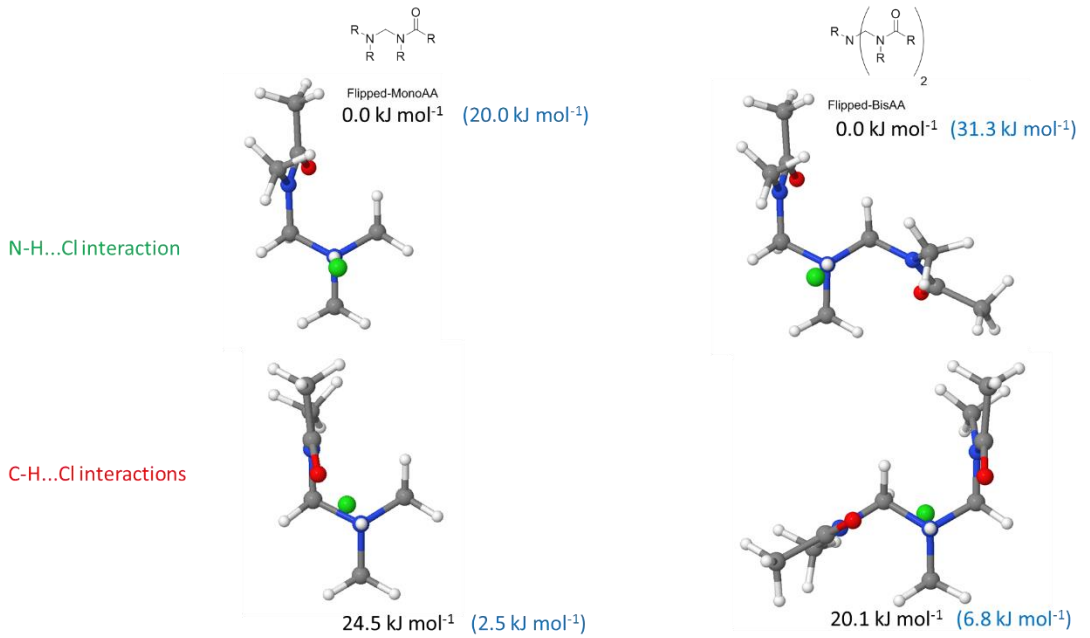

Figure 4.26. N-H and C-H binding modes for Flipped-MonoAAH$^+$ (left) and Flipped-BisAAH$^+$ (right) with chloride.

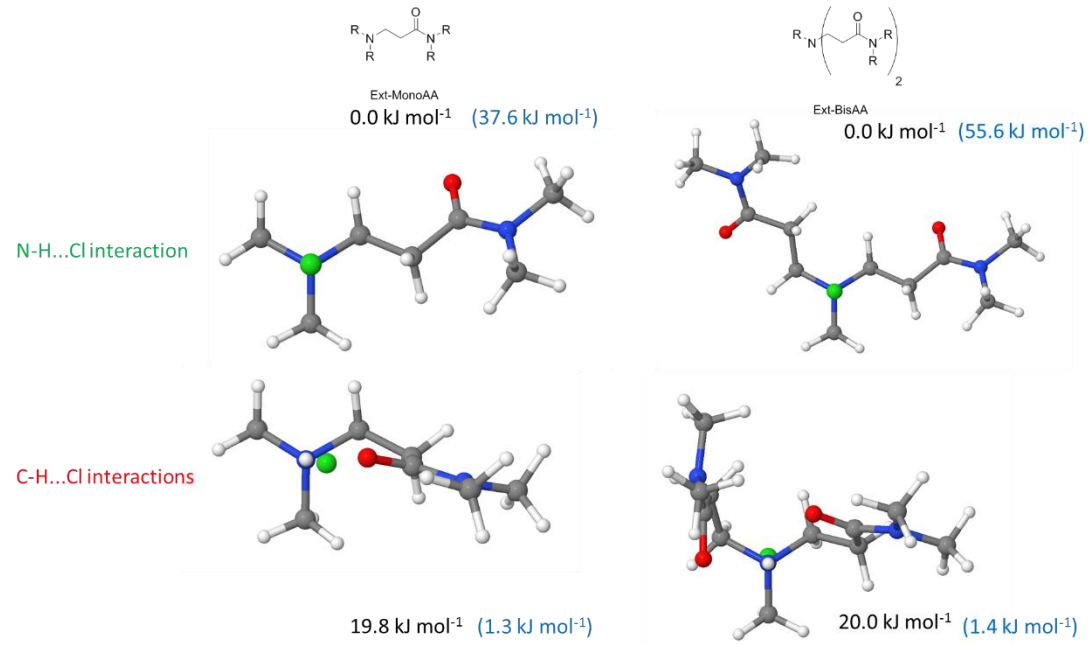

Figure 4.27. N-H and C-H binding modes for Ext-MonoAAH$^+$ (left) and Ext-BisAAH$^+$ (right) with chloride.

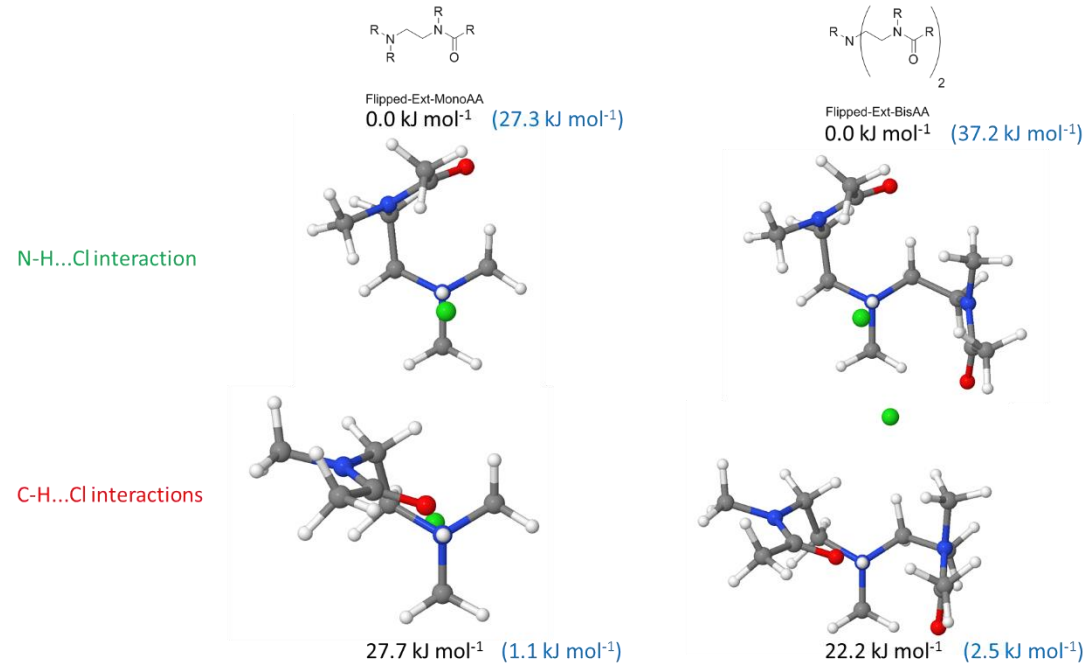

Figure 4.28. N-H and C-H binding modes for Flipped-Ext-MonoAAH$^+$ (left) and Flipped-Ext-BisAAH$^+$ (right) with chloride.

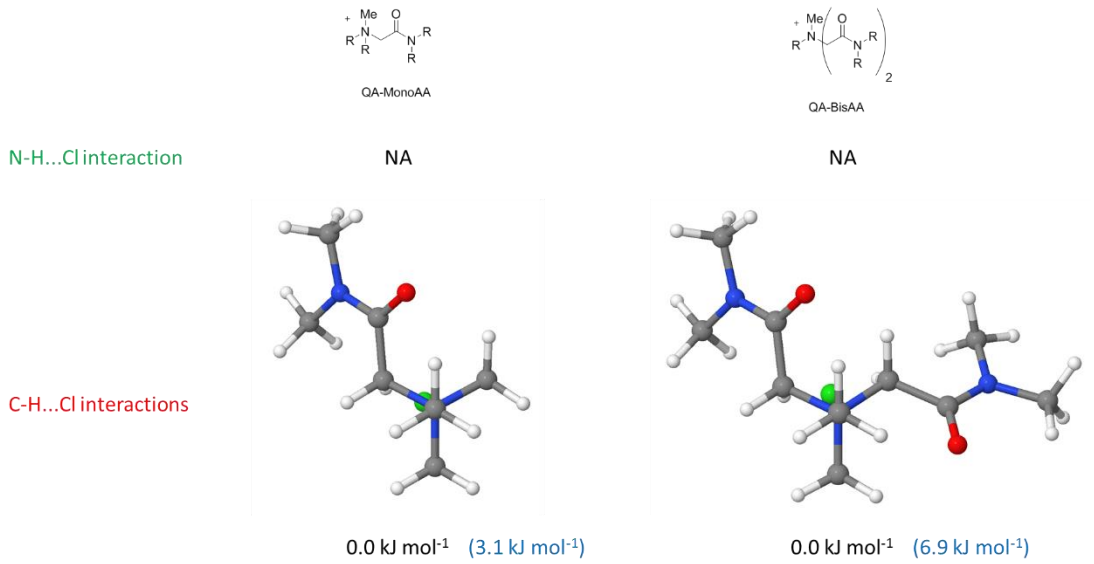

Figure 4.29. N-H and C-H binding modes for QA-MonoAA$^+$ (left) and QA-BisAA$^+$ (right) with chloride.

Interestingly, with the exception of BisAA (and the QA-extractants where an N-H binding mode does not exist) the lower energy binding modes are all N-H…Cl type. These modes have the protonated extractant in a less favourable conformation, as the strain energies are all higher than for the C-H binding modes, and therefore, the favourability of the N-H…Cl interaction must outweigh the energy penalty associated with adopting the conformation required for the N-H…Cl interaction to occur.

The strain energy associated with BisAAH$^+$ adopting the conformation required to form the N-H…Cl interaction (Figure 4.23) is higher than all the other extractants except for Sec-amide-BisAAH$^+$ (Figure 4.24) (however, when considering the difference in strain energy between the N-H…Cl and C-H…Cl structures, BisAAH$^+$ has the highest). This, and the fact that the C-H…Cl binding mode is very slightly more favourable for BisAAH$^+$, suggests that for BisAAH$^+$ the energy lowering due to having the strong N-H…Cl interaction is not enough to counterbalance the high strain on the extractant when it adopts the conformation required for the interaction to take place.

Sec-amide-BisAAH$^+$ (Figure 4.24) also has a high strain energy when in the conformation required for N-H…Cl binding, however, it has three N-H…Cl interactions (one from the protonated amine and two from the secondary amides), which likely are more able to account for the stain than BisAAH$^+$'s single N-H…Cl interaction. This is an interesting result as it was hypothesised that adopting the proton chelated form and binding to chloride via the

amide N-Hs would be more favourable as it would provide two intra-extractant hydrogen bonds and two amide N-H…Cl interactions. However, in reality it appears that the protonated extractant is not flexible enough to have a double proton-chelate and double N-H…Cl interactions, and so only one N-H…Cl interaction is present. Thus, it seems that having three N-H…Cl interactions (two amide and one amine) and a more strained extractant conformation is more favourable to having a single amide N-H…Cl interaction, a double proton chelate and a less strained extractant conformation.

Although for MonoAAH$^+$ the N-H…Cl binding mode is more favourable (Figure 4.23), the energy difference between the two binding modes is lower than for any of the other MonoAA-type extractants. This is likely due to MonoAAH$^+$ having the highest strain energy associated with the N-H…Cl conformation of the MonoAA-version extractants, though Sec-amide-MonoAAH$^+$ has essentially the same strain energy (Figure 4.24) (but again, MonoAAH$^+$ does have the highest difference in strain energy between the N-H and C-H binding modes).

The fact that the N-H…Cl binding mode is favoured for all extractants except for BisAA suggests this mode is good at accommodating a small, charge dense anion. From this it can be hypothesised that the potential extractants will be less suited to accommodating a large, more charge-diffuse anion such as $[RhCl_5(H_2O)]^{2-}$.

For the QA-extractants, only C-H…Cl binding modes are possible and, as is illustrated in Figure 4.29, the strain energies associated with binding to Cl^- are low, and comparable to the strain energy for the C-H…Cl binding modes of the other extractants, for both QA-MonoAA$^+$ and QA-BisAA$^+$.

4.2.4 Rh complex structures

In addition to either interacting via the very positive N-H or through an array of more diffusely positively charged C-H groups, the protonated extractants can also interact with $[RhCl_5(H_2O)]^{2-}$ via hydrogen bonding with its *aquo* ligand. Both N-H and C-H to anion binding modes are explored for $[RhCl_5(H_2O)]^{2-}$, and both the presence and absence of a hydrogen bond from the *aquo* ligand to the amide O atom(s) is considered. Figure 4.30 gives the general binding modes possible, illustrated with BisAA as an example.

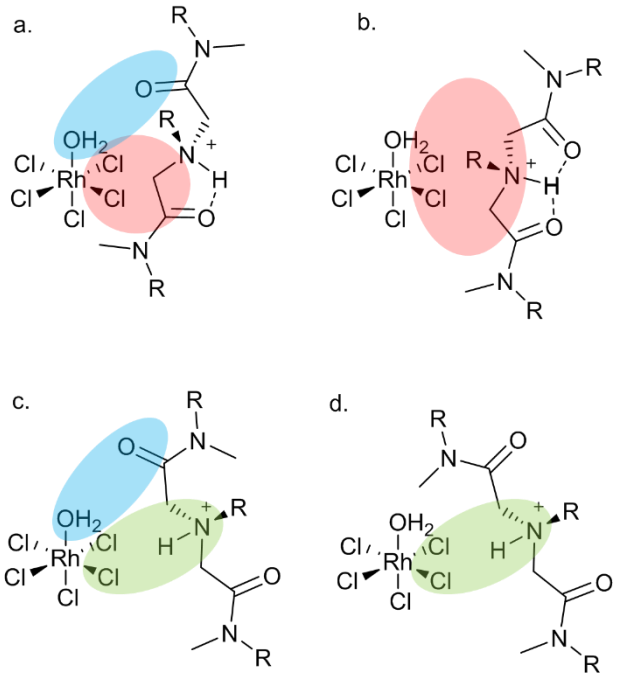

Figure 4.30. General potential binding modes of the extractants (BisAA used here as an example) to $[RhCl_5(H_2O)]^{2-}$: (a) C-H…anion interactions (red shading) and *aquo* ligand to amide O atom hydrogen bond (blue shading); (b)) C-H…anion interactions (red shading); amine N-H…anion interaction (green shading) and *aquo* ligand to amide O atom hydrogen bond (blue shading); and (d) amine N-H…anion interaction (green shading).

The current geometry optimised structures for each of the extractants are given in Figures 4.31-4.44. The letter labels in brackets for each of the structures refers to the binding mode in Figure 4.30 they correspond to, and the energies reported are their Gibbs free energies relative to that of the lowest energy structure.

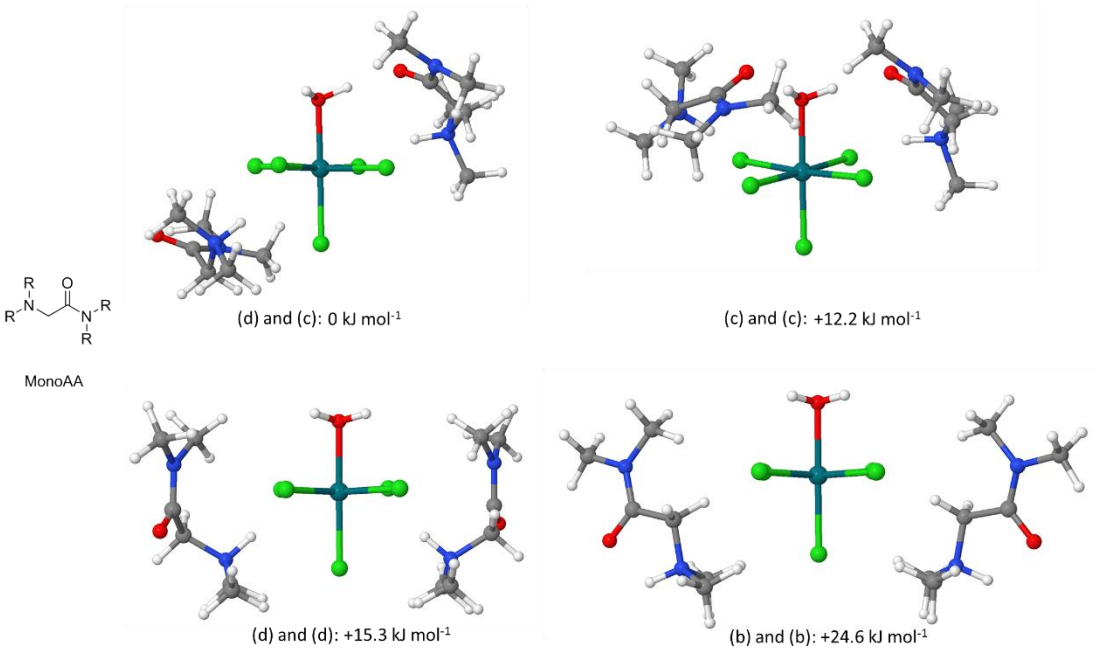

Figure 4.31. Binding modes for MonoAAH^{+} with $[RhCl_5(H_2O)]^{2-}$.

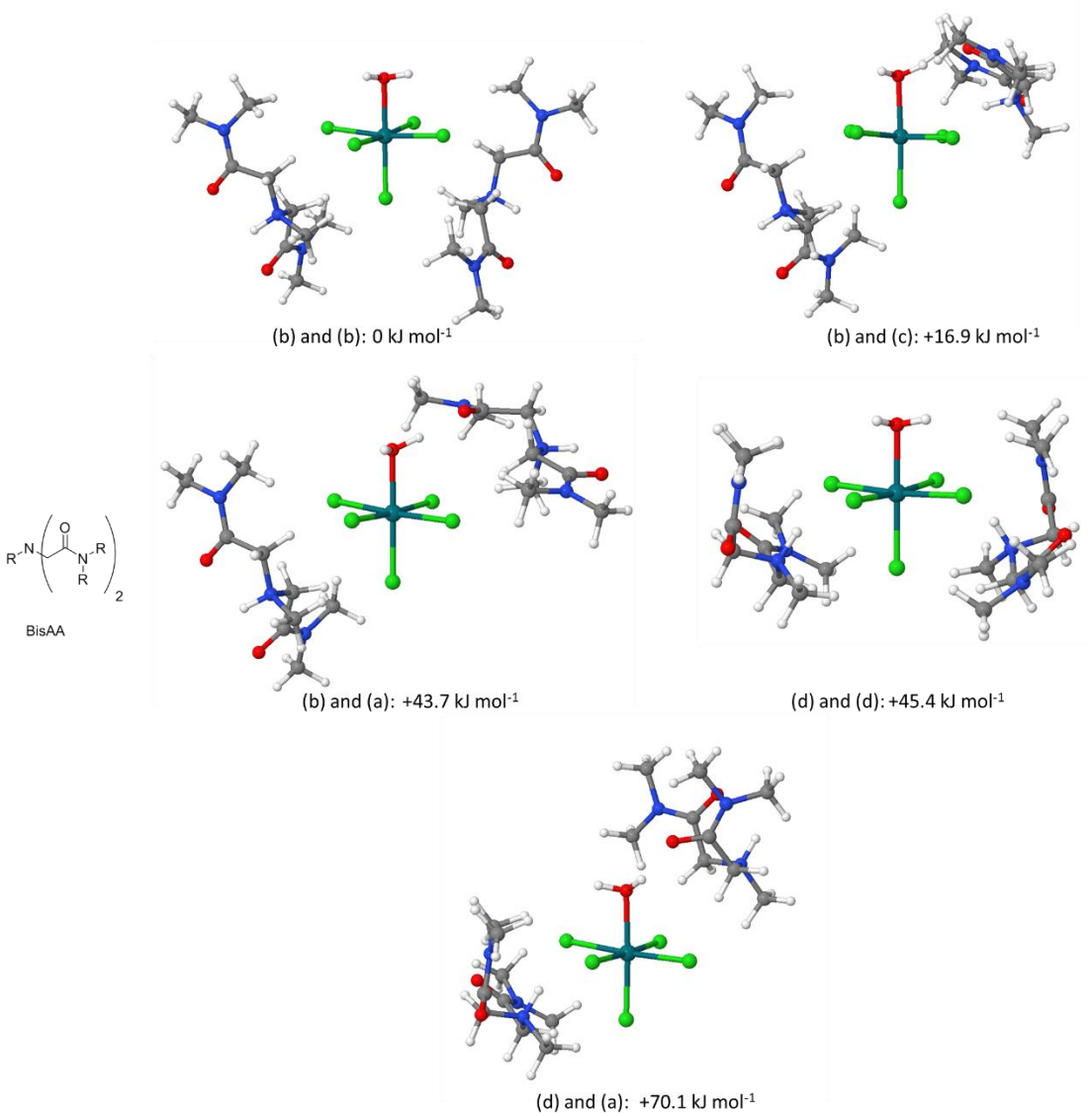

Figure 4.32. Binding modes for $BisAAH^{+}$ with $[RhCl_5(H_2O)]^{2-}$.

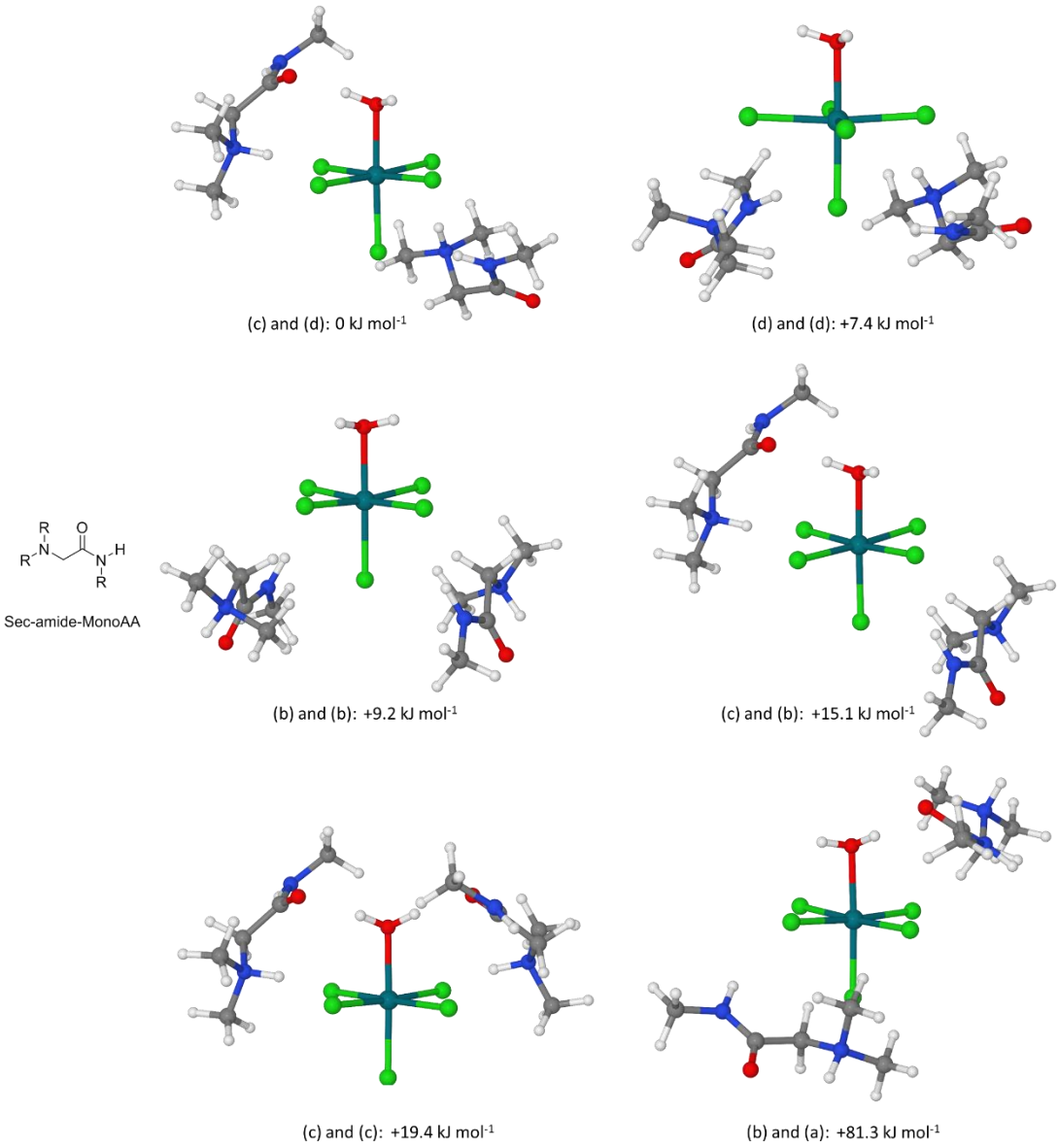

Figure 4.33. Binding modes for Sec-amide-MonoAAH^{+} with $[RhCl_5(H_2O)]^{2-}$.

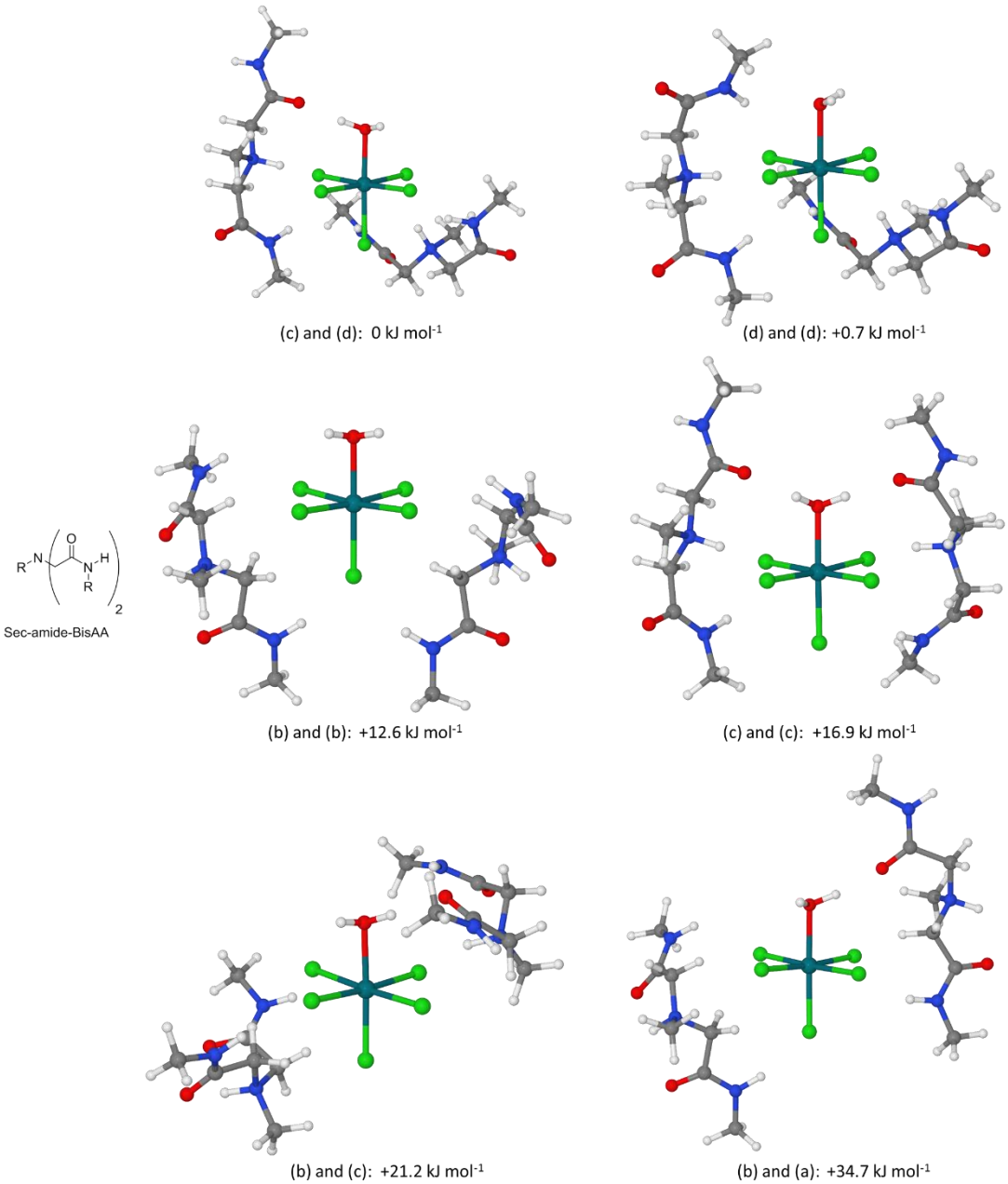

Figure 4.34. Binding modes for Sec-amide-BisAAH$^+$ with $[RhCl_5(H_2O)]^{2-}$.

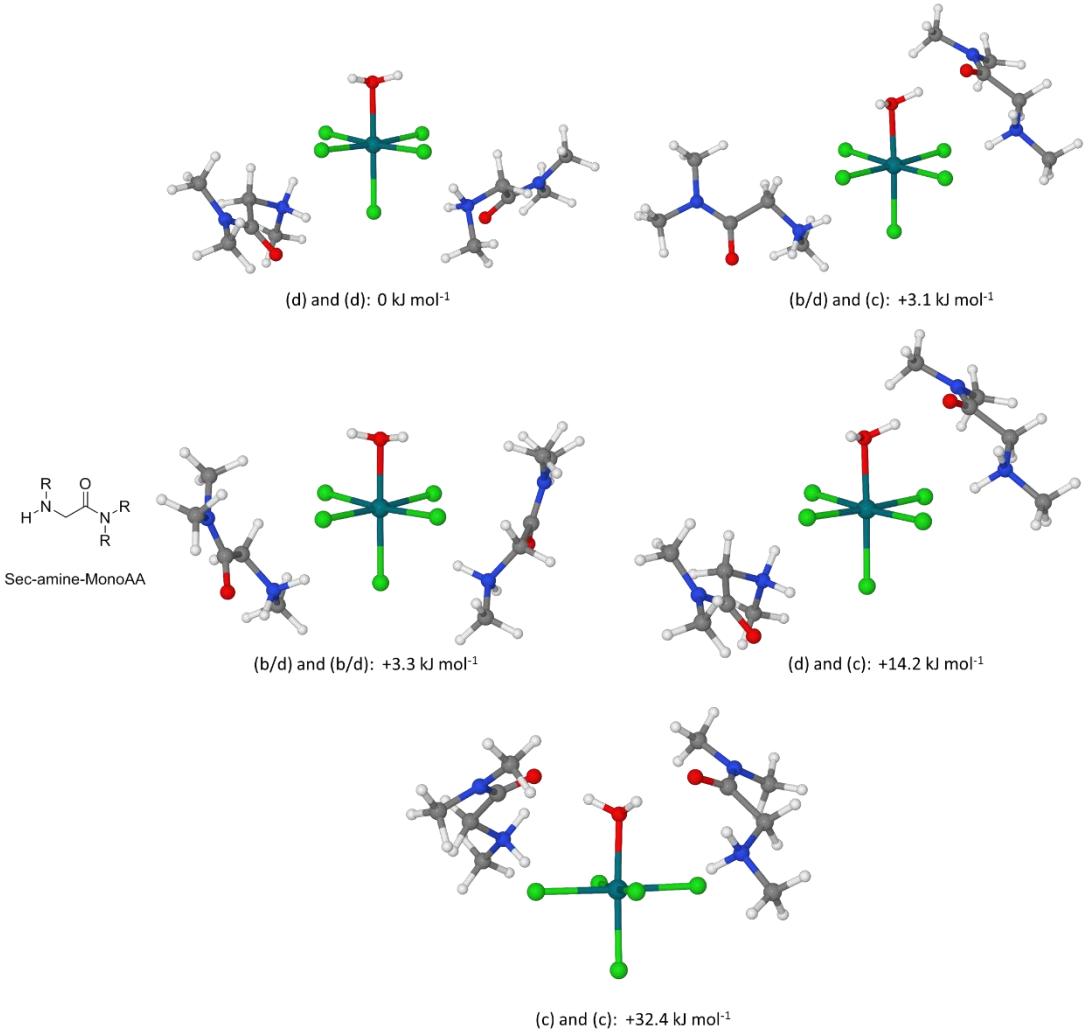

Figure 4.35. Binding modes for Sec-amine-MonoAAH^{+} with $[RhCl_5(H_2O)]^{2-}$.

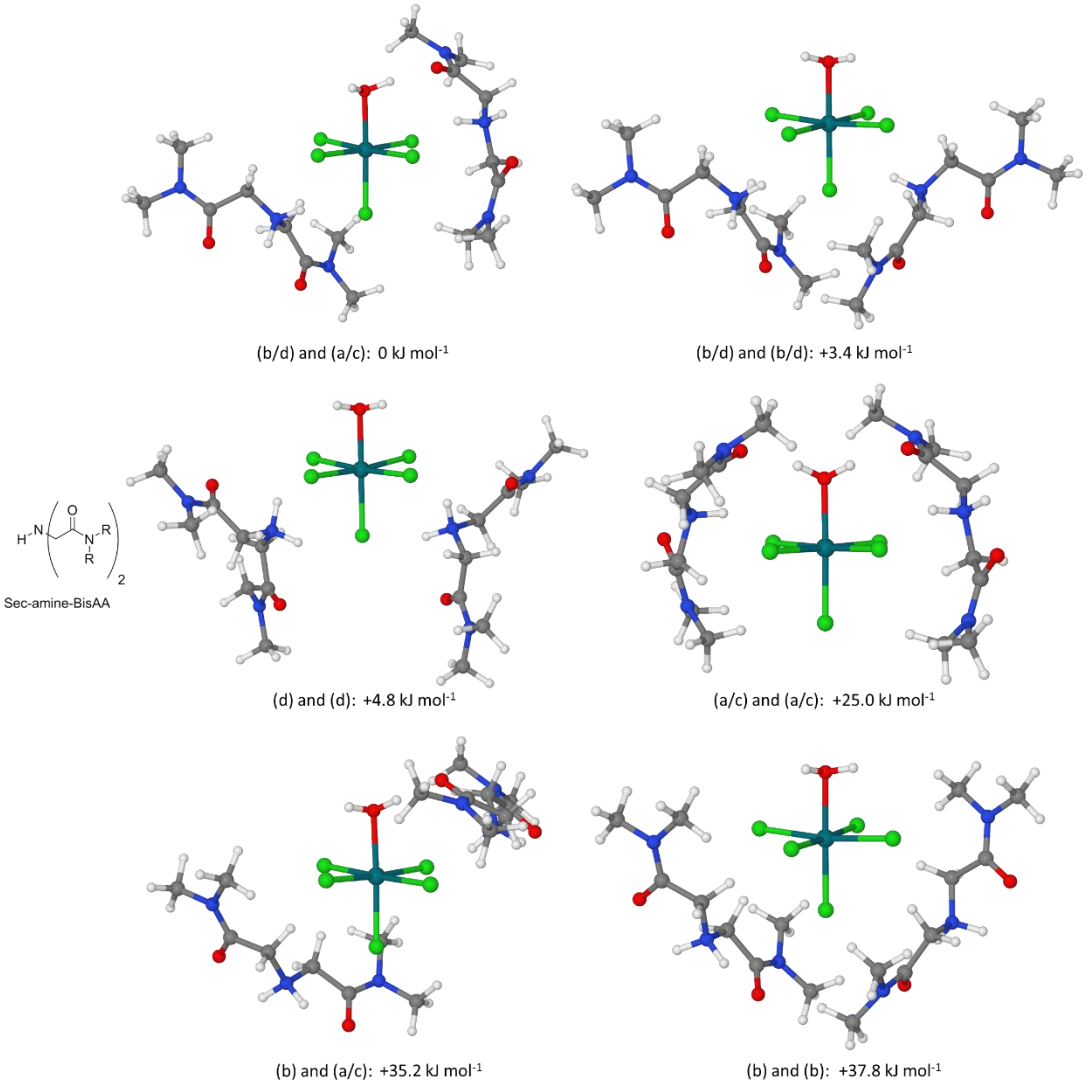

Figure 4.36. Binding modes for Sec-amine-BisAAH^{+} with $[RhCl_5(H_2O)]^{2-}$.

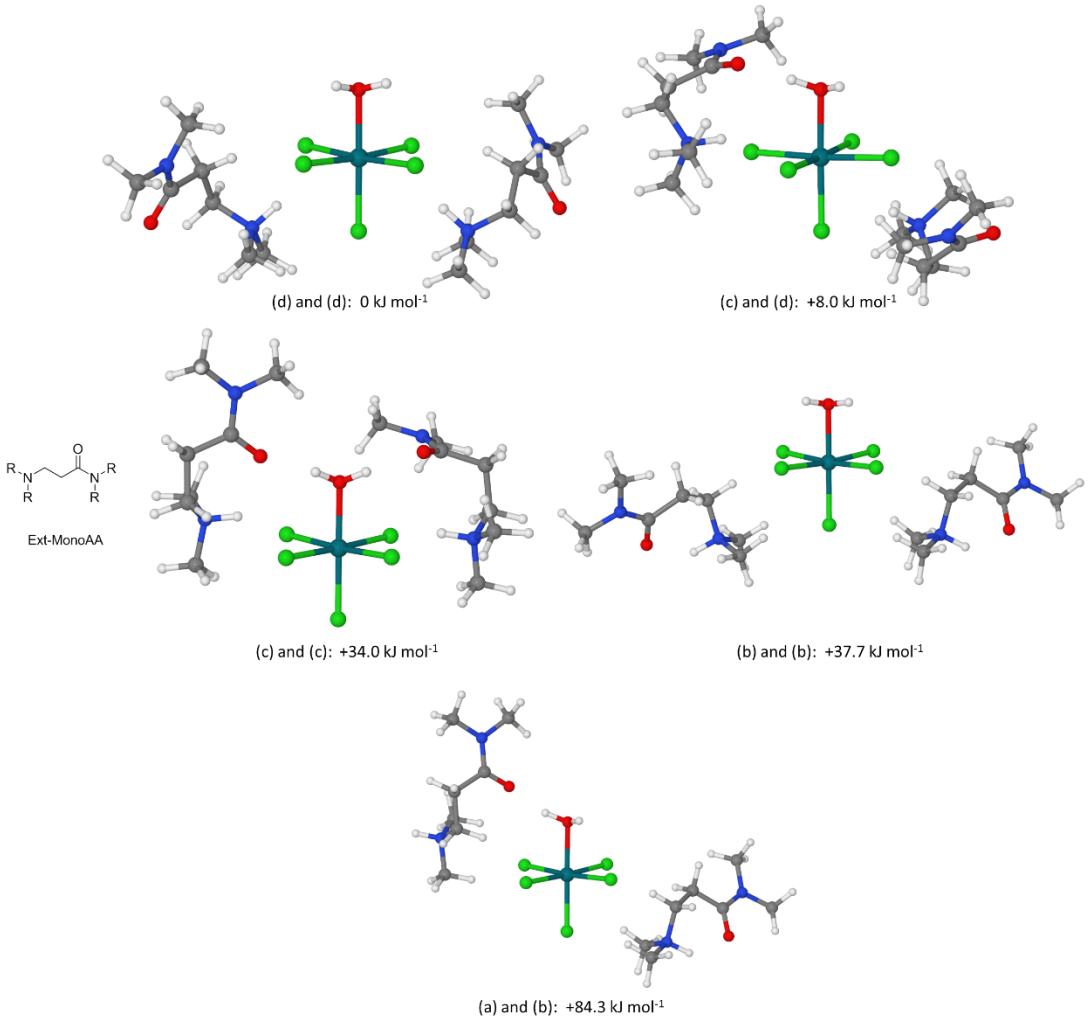

Figure 4.37. Binding modes for Ext-MonoAAH^{+} with $[RhCl_5(H_2O)]^{2-}$.

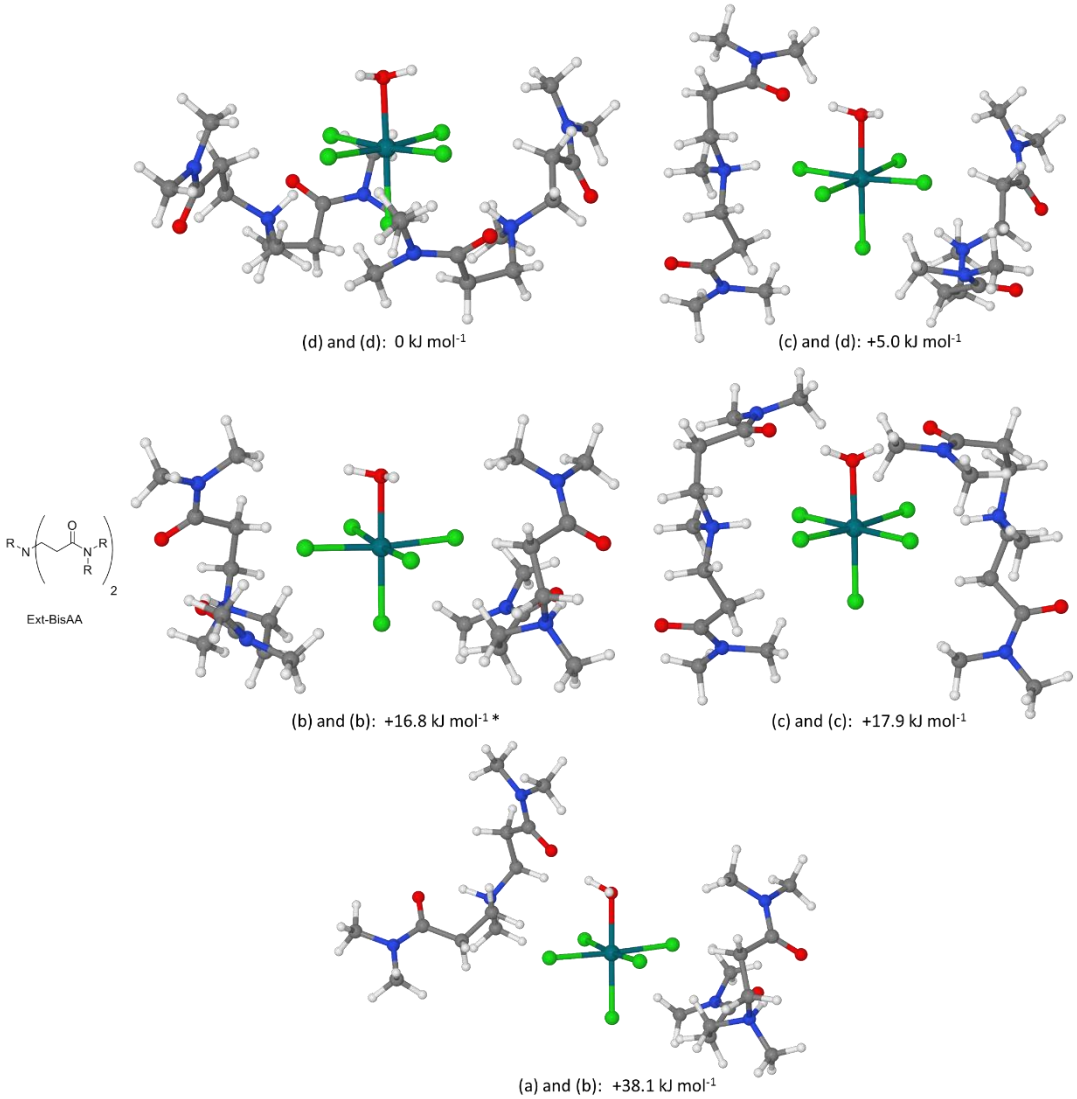

Figure 4.38. Binding modes for Ext-BisAAH^{+} with $[RhCl_5(H_2O)]^{2-}$. * Structure is a 1st order transition state (imaginary frequency: 12.8698 cm^{-1}) and the energy is from this transition state structure.

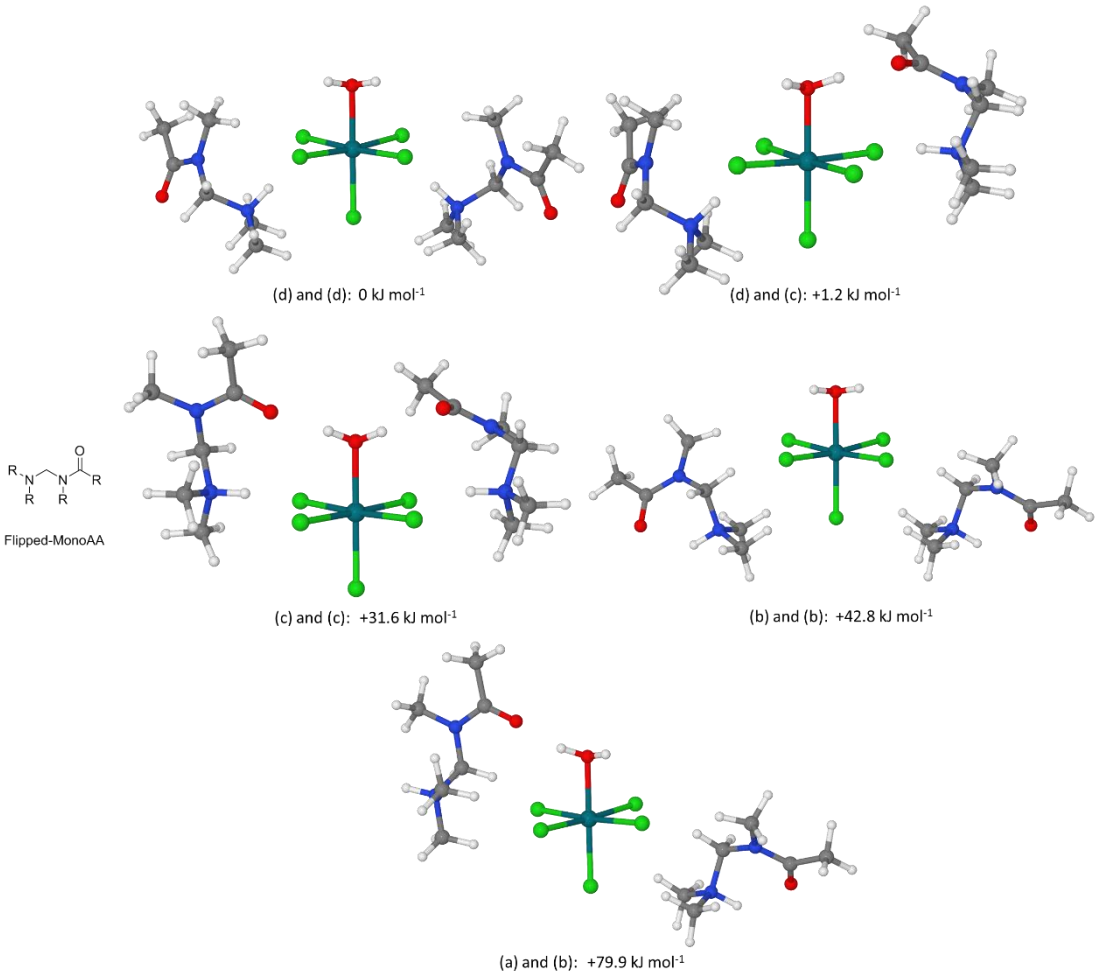

Figure 4.39. Binding modes for Flipped-MonoAAH^{+} with $[RhCl_5(H_2O)]^{2-}$.

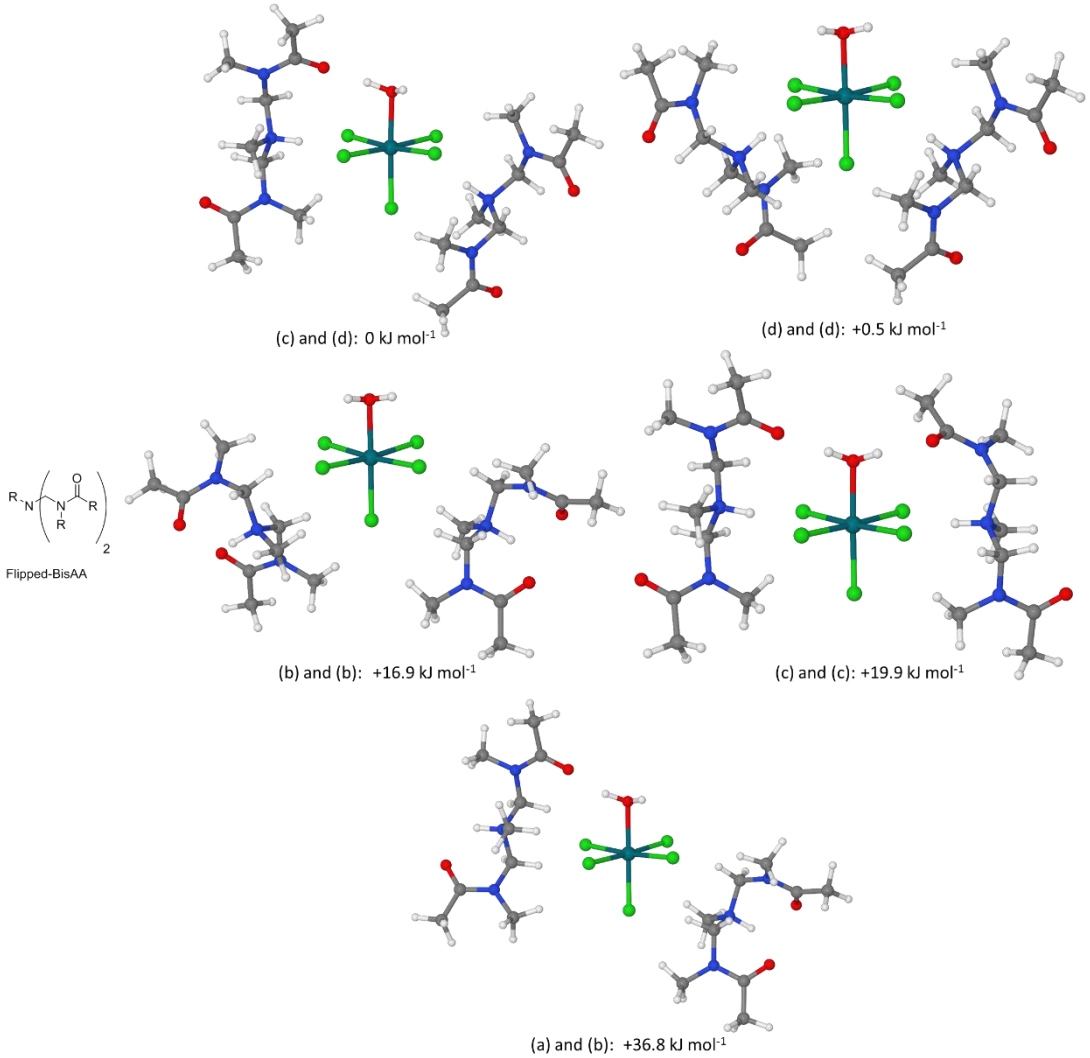

Figure 4.40. Binding modes for Flipped-BisAAH^{+} with $[RhCl_5(H_2O)]^{2-}$.

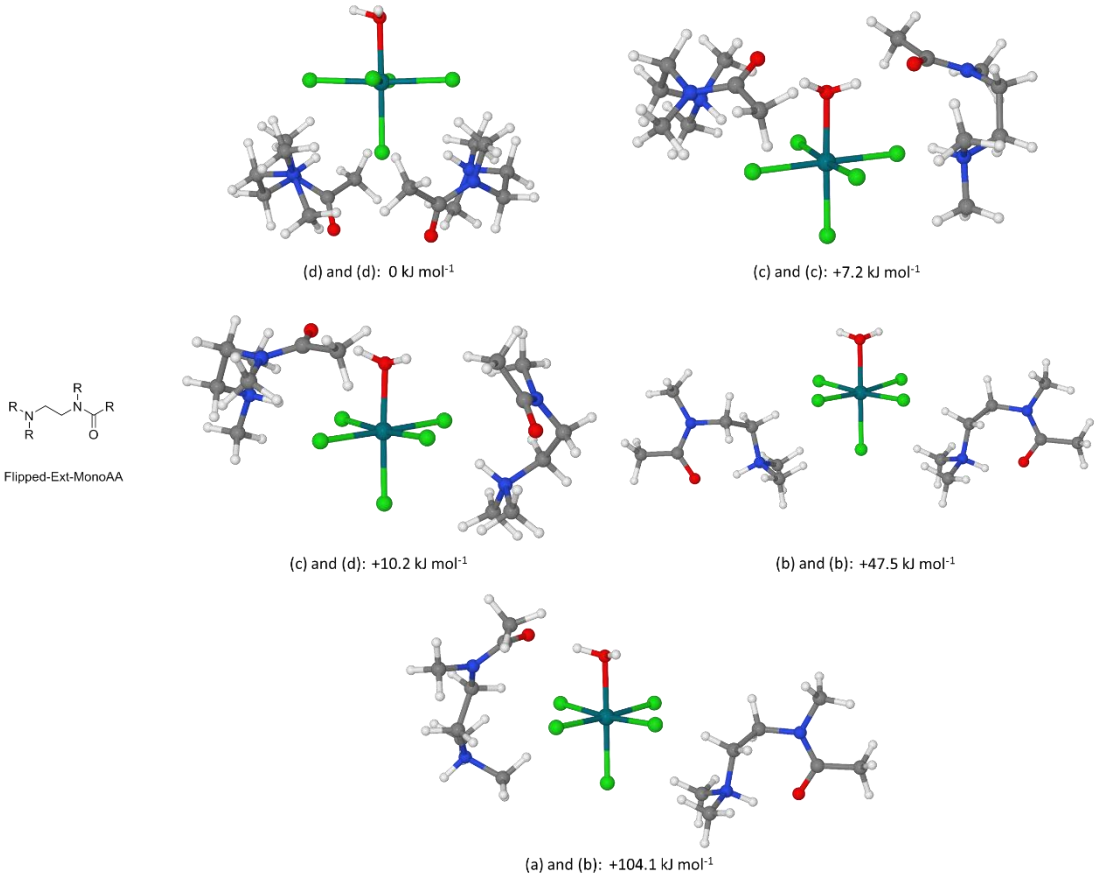

Figure 4.41. Binding modes for Flipped-Ext-MonoAAH^{+} with $[RhCl_5(H_2O)]^{2-}$.

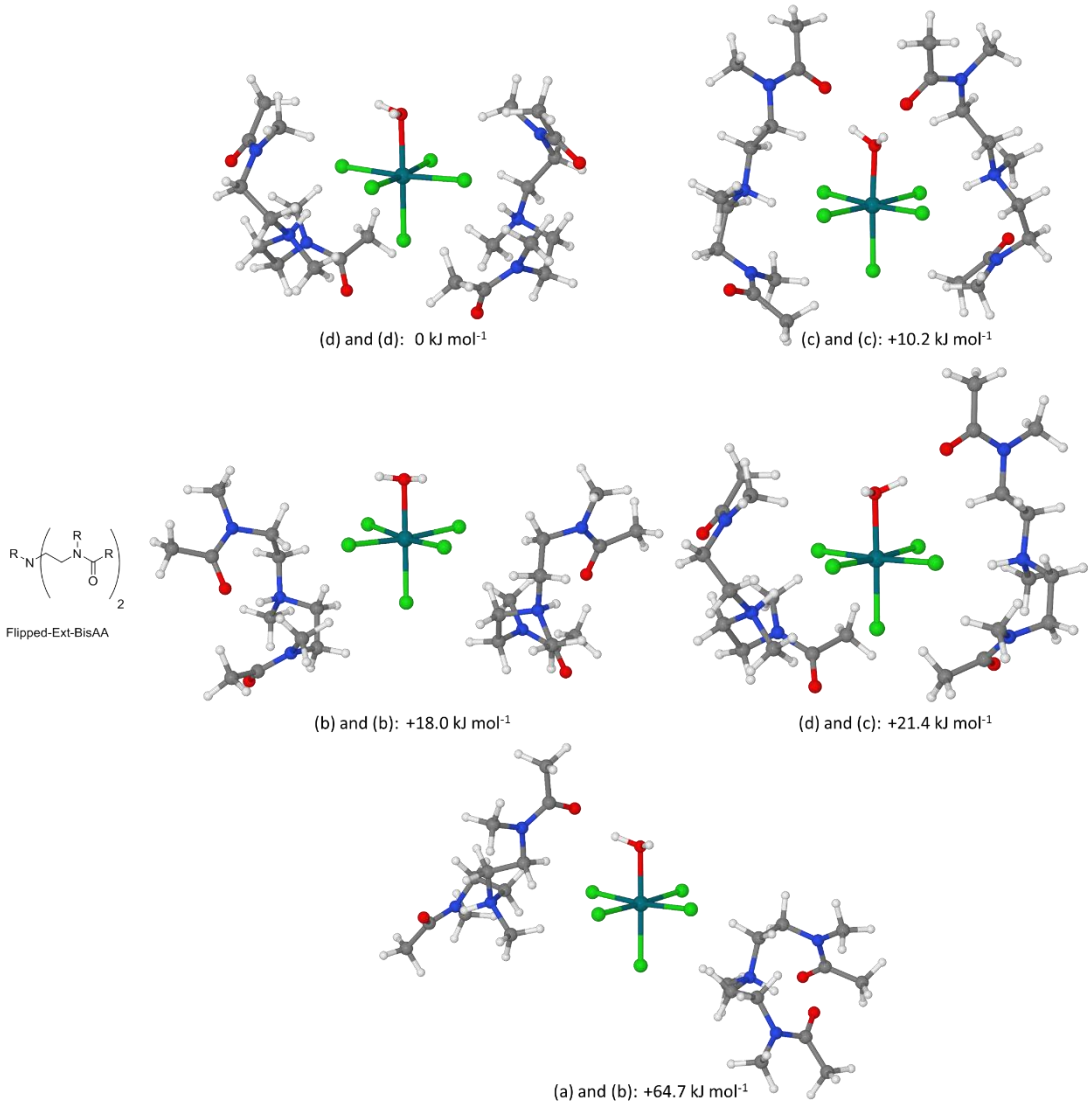

Figure 4.42. Binding modes for Flipped-Ext-BisAAH$^+$ with $[RhCl_5(H_2O)]^{2-}$.

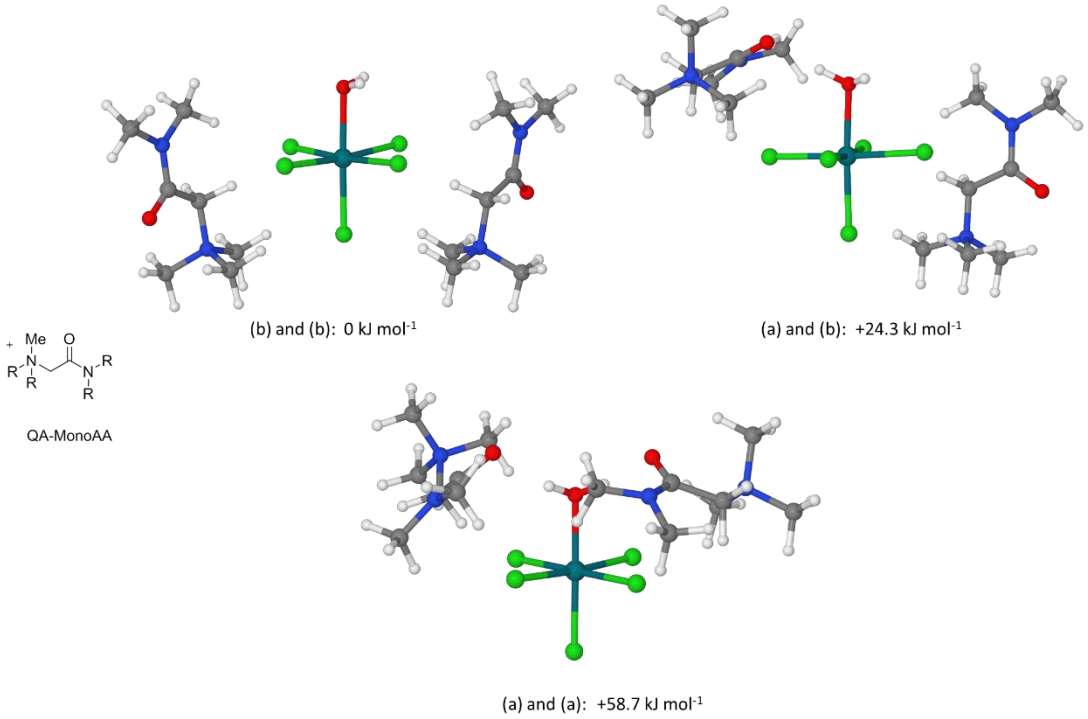

Figure 4.43. Binding modes for QA-MonoAA^{+} with $[RhCl_5(H_2O)]^{2-}$.

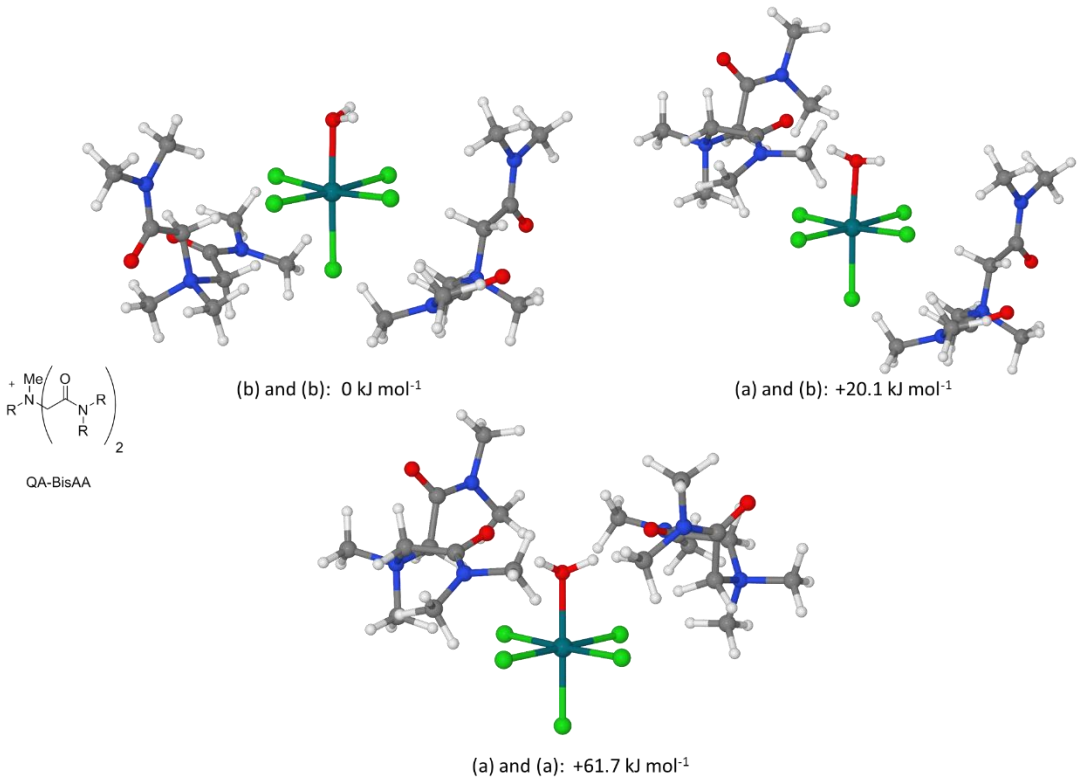

Figure 4.44. Binding modes for QA-BisAA^{+} with $[RhCl_5(H_2O)]^{2-}$.

As observed with Cl^-, with the exception of $BisAAH^+$ (Figure 4.32) (and the QA-extractants where an N-H binding mode does not exist, Figure 4.44) the lower energy binding modes are all N-H…Cl type. With Cl^-, these modes were found to have the protonated extractant in a less favourable conformation, as the strain on the protonated extractant is higher than for the C-H binding modes. With Rh, this could potentially be outweighed by the formation of a hydrogen bond with the *aquo* ligand, however, this does not occur in all cases; only $MonoAAH^+$, Sec-amide-$MonoAAH^+$, Sec-amide-$BisAAH^+$, Sec-amine-$BisAAH^+$ and Flipped-$BisAAH^+$ have one extractant molecule with a hydrogen bond with the *aquo* ligand (however, in several cases the energy difference between the mode with and without the hydrogen bond is very small – indeed when considering the SCF energies, as opposed to the Gibbs free energies, it can be found that the favourability of having a hydrogen bond with the *aquo* ligand vs not having one is switched).

In almost all cases, it is less favourable for both N-H binding extractant molecules to have a hydrogen bond with the *aquo* ligand than only one. The only exceptions to this are the two Flipped-Ext-type extractants (Figures 4.41 and 4.42). In both of these cases it is still more favourable for no hydrogen bond to be present at all, but having two is more favourable than having one. This is a curious result, with no immediately obvious reason behind it. It is possible the increased favourability is in part a result of the increased size and flexibility of the extractant imparted by having the extra $–CH_2–$ group and the reverse orientation of the amide group, meaning the extractant is more able to adopt a favourable position that satisfies both the N-H…anion interaction and the hydrogen bond with the *aquo* ligand. The unfavourability of the single hydrogen bond form may be due to it placing more of a strain on the $[RhCl_5(H_2O)]^{2–}$, which has to contort to accommodate the hydrogen bond (or at least the strain on the $[RhCl_5(H_2O)]^{2–}$ being less balanced by only the single hydrogen bond vs the double hydrogen bond interaction).

By considering the energy difference between the lowest energy N-H binding mode and the lowest energy C-H binding mode (given in Table 4.1), some trends can be found. For most extractant types, the C-H binding mode is less unfavourable for the BisAA-versions than for the MonoAA-versions. This is likely due to the breaking of two potential intramolecular hydrogen bonds with BisAA versions, compared to only one with MonoAA-versions, meaning that the structure the extractant has to adopt to undertake N-H based binding is less favourable for the former compared to the latter.

However, this trend is not observed for the Sec-amide-type extractants (Figures 4.33 and 4.34). This is likely due to the fact the C-H based binding mode also has amide N-H interactions with the anion, while maintaining their amine N-H to amide O intramolecular hydrogen bonds. It could be expected that Sec-amide-BisAAH$^+$ would still have a less unfavourable C-H binding mode, but for a different reason: due to its ability to form two amide N-H to anion interactions, compared with Sec-amide-MonoAAH$^+$'s one. This is not the case, most likely due to the constraints on the extractant in the C-H binding mode (to maintain the intramolecular hydrogen bonds) meaning that the interaction of the extractant with $[RhCl_5(H_2O)]^{2-}$ is a compromise between the two amide N-H interactions, resulting in interactions which are not as strong or direct as the single amide N-H interaction with Sec-amide-MonoAA. This is similar to the result observed with Cl^- as the anion, but there only one of the two amide N-H groups interacted with the smaller anion.

For the Sec-amine-type extractants, a comparison between the binding modes cannot be made as Sec-amine-MonoAAH$^+$ can maintain its single intramolecular hydrogen bond and have an N-H interaction with the Rh(III) metalate, and therefore an exclusively C-H based binding mode is very unlikely.

Table 4.1. Relative energies of the lowest energy N-H and C-H based binding modes.

Extractant	Relative Gibbs Free energy of binding modes / kJ mol^{-1}	
	N-H	C-H
MonoAAH$^+$	0	24.6
BisAAH$^+$	38.9	0
Sec-amide-MonoAAH$^+$	0	9.2
Sec-amide-BisAAH$^+$	0	12.6
Sec-amine-MonoAAH$^+$	0	NA *
Sec-amine-BisAAH$^+$	0	37.8
Ext-MonoAAH$^+$	0	37.7
Ext-BisAAH$^+$	0	16.8
Flip-MonoAAH$^+$	0	42.8
Flip-BisAAH$^+$	0	16.9
Flip-Ext-MonoAAH$^+$	0	47.5
Flip-Ext-BisAAH$^+$	0	18.0
QA-MonoAA$^+$	NA †	0
QA-BisAA$^+$	NA †	0

*Sec-amine-MonoAAH$^+$ can maintain the single intramolecular H-bond and have an N-H interaction with the Rh, and therefore an exclusively C-H based binding mode is very unlikely. †QA-MonoAA$^+$ and QA-BisAA$^+$ cannot form N-H interactions with Rh.

For the QA-extractants only C-H…Cl binding modes are possible, but it is interesting that neither QA-MonoAA$^+$ nor QA-BisAA$^+$ have a hydrogen bond with the *aquo* ligand in the lower energy binding mode. It was hypothesised that if an N-H group was not present and acting as a competitive hydrogen bond donor, this would make it more favourable and likely for a hydrogen bond with the *aquo* ligand of $[RhCl_5(H_2O)]^{2-}$ to form. At least theoretically, it appears this is incorrect, with a structure with one extractant molecule exhibiting a hydrogen bond with the *aquo* ligand being 24.3 and 20.1 kJ mol^{-1} higher in energy for QA-MonoAA$^+$ and QA-BisAA$^+$, respectively.

4.2.5 Formation and exchange energies

The formation energies for the protonated extractants, the chloride complexes and the Rh complexes (determined according to Equations 4.1, 4.2 and 4.3 respectively) along with the exchange energies (determined according to Equation 4.4) are presented in Table 4.2.

$$L_{(org)} + H_3O^+_{(aq)} \rightleftharpoons LH^+_{(org)} + H_2O_{(aq)} \quad \textbf{4.1.}$$

$$LH^+_{(org)} + Cl^-_{(aq)} \rightleftharpoons Cl{\cdot}LH_{(org)} \quad \textbf{4.2.}$$

$$2LH^+_{(org)} + [RhCl_5(H_2O)]^{2-}_{(aq)} \rightleftharpoons [RhCl_5(H_2O)]{\cdot}(LH)_{2\,(org)} \quad \textbf{4.3.}$$

$$2Cl{\cdot}LH_{(org)} + [RhCl_5(H_2O)]^{2-}_{(aq)} \rightleftharpoons [RhCl_5(H_2O)]{\cdot}(LH)_{2\,(org)} + 2Cl^-_{(aq)} \quad \textbf{4.4.}$$

There is variation in the protonation energy between the types of extractant (largest difference of 53.0 kJ mol^{-1} between Sec-amide-BisAA and Ext-BisAA), but, in general, the protonation energies are similar between the MonoAA and BisAA forms within a type (largest difference of 14.9 kJ mol^{-1} between Flipped-Ext-MonoAA and Flipped-Ext-BisAA). Though there can be a large difference in protonation energy between some types of extractant, it is likely that all these amidoamines will be strong bases and would readily accept a proton, therefore, it is unlikely that, at the HCl concentrations typically used in PM extraction, protonation would be difficult or limit extraction ability.

Table 4.2. Formation energies from Equations 4.1-4.4, calculated for the lowest Gibbs free energy optimised structures. Energies used in the calculation of these formation energies are given in the SI. Note, in order to keep the formation energy from Equation 4.4 consistent with those of Equations 4.2 and 4.3, BSSE corrected energies have been used for Cl·LH and $(RhCl_5(H_2O))\cdot(LH)_2$ in the exchange energy calculation. Green means "good" association with the anion or favourable exchange, yellow "neutral", and red "poor". Rankings are only to aid data interpretation and are roughly assigned based on comparison of all the energies. *Energy of a structure which is a 1st order transition state using to calculate these energies.

Extractant	Protonation and formation energies / kJ mol^{-1}			
	Protonation	Association with Cl	Association with Rh	Exchange
MonoAA	-116.4	-22.5	-18.2	26.8
BisAA	-117.5	-10.6	-31.4	-10.2
Sec-amide-MonoAA	-101.5	-37.3*	-37.8	36.8*
Sec-amide-BisAA	-95.7	-40.3*	-34.8	45.8*
Sec-amine-MonoAA	-112.5	-39.6	-47.8	31.3
Sec-amine-BisAA	-118.5	-26.6	-23.9	29.4
Ext-MonoAA	-139.9	-18.8	-15.9	21.7
Ext-BisAA	-151.2	-18.6	5.3	42.5
Flip-MonoAA	-110.1	-35.8	-38.2	33.4
Flip-BisAA	-105.8	-35.5	-16.3	54.7
Flip-Ext-MonoAA	-131.5	-23.2	-10.1	36.4
Flip-Ext-BisAA	-146.4	-16.7	23.7	57.1
QA-MonoAA	NA	-6.1	0.4	12.6
QA-BisAA	NA	-21.5	-14.9	28.1

Based on the favourability differences of the binding modes for chloride, it would be expected that MonoAA and BisAA would have less favourable chloride association energies than their counterparts of the other extractant types, because it is not as favourable for them to adopt a N-H…Cl binding mode (which would be expected to be the most favourable for a small, charge dense anion such as chloride). There are some exceptions, but for the most part MonoAA and BisAA are indeed found to have less favourable chloride association energies than the theoretical extractants.

BisAA has the lowest chloride association energy out of the BisAA-type reagents and the only MonoAA-type extractants with lower association energies than MonoAA are QA-MonoAA

(which cannot adopt a N-H…Cl binding mode) and Ext-MonoAA. This suggests that most of the theoretical extractants would be better chloride extractants than MonoAA and BisAA. Potentially, this means that they could be weaker Rh extractants, because there would be stronger competition from chloride. However, they could also have higher association energies with the Rh(III) complex in addition to with chloride, thereby balancing out the effect. Therefore, the Rh(III) metalate association energies and the exchange energies of chloride for the Rh(III) metalate must be determined to give a definitive answer.

The QA-extractants are interesting because they have less favourable, energies of association with chloride. This could be because they lack the N-H group of a protonated amine and so can only present C-Hs for the binding of an anion. As discussed, a C-H binding mode may be less favourable for a chloride anion but more favourable for the larger Rh(III) complex. On the other hand, the QA-extractants may simply be less strong binders for anions in general, so again knowing the association energies with the Rh(III) complex and the exchange energies is crucial to provide a full picture of the likely theoretical extraction behaviour.

As can be seen from the results reported in the above table, there is a wide spread of formation energies (-47.8 kJ mol^{-1} to 23.7 kJ mol^{-1}) for the association of the protonated extractants with $[RhCl_5(H_2O)]^{2-}$, with MonoAA sitting approximately in the centre of the spread and BisAA being towards the more negative, more favourable side. This shows that while BisAA has a relatively poor association energy with chloride, it has a relatively good association energy with the Rh(III) metalate, lending support to the idea that the proposed extractants may be poorer Rh extractants than BisAA.

This is seen to be true when the exchange energies are examined. BisAA has the most favourable energy of exchanging chloride for $[RhCl_5(H_2O)]^{2-}$, in fact, BisAA has the only negative exchange energy reported in the table. For all other extractants, the exchange energy is positive and so less favourable. MonoAA has the fourth lowest exchange energy, despite the energy being positive, making it one of the least unfavourable of the extractants. Based on the experimental extraction behaviour of MonoAA,[2] QA-MonoAA and Ext-MonoAA, which have the second and third lowest (though still positive) exchange energies, respectively, could make reasonable Rh extractants at low HCl concentrations. So potentially could QA-BisAA, Sec-amine-BisAA, Sec-amine-MonoAA, Flip-MonoAA and Flip-Ext-MonoAA, which all have exchange energies within 10 kJ mol^{-1} of MonoAA. However, the other

theoretical extractants all have very unfavourable exchange energies, suggesting that they would be poor Rh extractants.

Table 4.2 is coloured to show the general ranking of a protonated extractant as “good”, “neutral” or “poor” for the association with Cl^- and $[RhCl_5(H_2O)]^{2-}$ and for the exchange of the two. This highlights that poor exchange can be the result of low favourability of association with $[RhCl_5(H_2O)]^{2-}$ (e.g. as found for Ext-BisAA), of competitive high favourability of association with chloride (e.g. as found for Sec-amide-BisAA), or a mix of the two (e.g. as found for Flipped-BisAA). Only BisAA, which is “poor” at association with chloride and “good” at association with $[RhCl_5(H_2O)]^{2-}$ (the only extractant possessing this set of results) provides “good” exchange of chloride for $[RhCl_5(H_2O)]^{2-}$.

These results suggest that BisAA is the superior Rh extractant. This is likely due to its unique binding mode, where intramolecular hydrogen bonds are made in the protonated extractant and it presents an array of C-H sites for the $[RhCl_5(H_2O)]^{2-}$ anion to interact with. As discussed, this array of C-H interactions makes for a large, charge-diffuse cation: favourable for a large, charge-diffuse anion to interact with. This results in its strong interaction with $[RhCl_5(H_2O)]^{2-}$ and, crucially, in its weak interaction with chloride, a small, change-dense anion, thus making it a strong, selective extractant for Rh from chloride media. All the other extractants (with the exception of the QA extractants) bind via N-H to anion interactions, which tend to be more favourable for chloride and less so for $[RhCl_5(H_2O)]^{2-}$. The QA extractants have low association energies with both chloride and $[RhCl_5(H_2O)]^{2-}$, which results in reasonable exchange energies, but not comparable with BisAA.

It appears that none of the other amidoamines would perform better than BisAA as extractants, though a few might perform similarly to MonoAA. This implies that BisAA is an “optimised” extractant for $[RhCl_5(H_2O)]^{2-}$, in that it appears to possess an ideal binding mode for addressing the large, relatively charge-diffuse (when compared to chloride) anion and has a good balance of an unfavourable energy of association with chloride and a relatively favourable energy of association with $[RhCl_5(H_2O)]^{2-}$.

4.3 Conclusions and future work

The extraction ability of a number of amidoamines, based on MonoAA and BisAA but with small structural differences, was explored theoretically by using computational calculations to predict their theoretical binding modes and the relative formation energies.

The structures of all molecules were geometry optimised and their Gibbs free energies calculated, with a variety of potential binding modes considered for the interaction of the extractants with chloride and $[RhCl_5(H_2O)]^{2-}$. In all protonated forms, it is found that chelation of the proton is possible by the amide group(s), though in the case of Flipped-Ext-BisAAH$^+$ only one of the amide O atoms is able to form a hydrogen bond with the proton on the amine N atom.

ESP plots of the protonated extractants illustrates that both the amine N-H and an array of C-Hs can act as potential anion binding sites. In addition, where they are present, additional amine N-H and amide N-Hs can also act as anion binding sites. In the QA-extractants, only C-H interactions are present to bind an anion.

As a general rule, it is found that the N-H…Cl binding mode is favoured. This is true for all extractants except for BisAA (where the strain energy of adopting the conformation required for this binding mode does not appear to be outweighed by the favourability of forming the N-H…Cl interaction) and the QA-extractants (where such a binding mode does not exist). This is perhaps most surprising for the Sec-amide-extractants, particularly Sec-amide-BisAA, where it might have been assumed that chelation within the extractant and binding to the anion via amide N-H interaction(s) would be most favourable. In reality, it appears that losing chelation but gaining amine N-H…Cl and amide N-H…Cl interactions results in the lowest energy Cl·LH complexes.

Examination of the association energies of the extractants with chloride suggests that most of the theoretical extractants would be stronger chloride extractants than MonoAA and BisAA, at least if excluding the energy associated with protonation. This implied that they could be poorer Rh extractants as there would be more competition from chloride; this is subsequently generally supported by the results of the Rh(III) metalate calculations.

The results show that BisAA is likely to be the best Rh extractant, with most of the other potential extractants having far less favourable energies for the exchange of chloride for

$[RhCl_5(H_2O)]^{2-}$. This is in part due to the fact that BisAA displays a unique binding mode: intramolecular hydrogen bonding of the two amide O atoms with the N-H group means that an array of C-H groups are presented for interaction with the anion. This large, charge-diffuse binding site is likely to be a more favourable binding site for $[RhCl_5(H_2O)]^{2-}$, compared to chloride.

Though many of the other potential extractants are capable of forming this binding mode, a binding mode where an amine N-H interaction is made with the anion is more favourable for all other extractants (with the exception of the QA extractants where no N-H group is present). In some cases, other extractants have a stronger association with $[RhCl_5(H_2O)]^{2-}$ than BisAA does, however, this is outweighed by these extractants also having stronger interactions with chloride, likely due to the N-H binding site (small and charge-dense) being more favourable for chloride (a small, charge-dense anion) than for $[RhCl_5(H_2O)]^{2-}$.

These results suggest that all of the proposed extractants would make poorer Rh extractants than BisAA, with many also worse than MonoAA. This interesting result highlights how small changes in the structure of an extractant can theoretically have a large effect on the extraction ability, especially when the desired metal is in the presence of a competitively extracted anion.

The most obvious avenue for further work, had any of the extractants been proven to be theoretically better than BisAA, would have been to synthesise and test the theoretically best extractant(s). Although none of the extractants are likely to be better than BisAA based on these calculations, it would be hugely desirable to verify the theoretical predictions against experimental extraction performance anyway. Therefore, if future work is to be pursued it should involve the synthesis of, perhaps, three extractants in the series: one likely to be better than MonoAA (e.g. QA-MonoAA), one in the middle of the performance ranking (e.g. Flip-Ext-MonoAA), and one with very poor theoretical performance (e.g. Flip-Ext-BisAA). The extraction of Rh(III) from HCl solution could then be tested with the synthesised reagents and the extraction performance compared with the theoretical predictions.

4.4 Computational method and assumptions made

4.4.1 Computational details

All calculations were carried out as described in Chapter 2 Section 2.1.2.3.

The M06[15] exchange/correlation functional was used with the LANL2TZ[16] basis set/pseudopotential for Rh and the 6-311+G**[17, 18] basis set for all other atoms. Implicit solvent modelling was included in the optimisation (PCM[19] with the solvent model for chloroform or water, as appropriate).

Where geometry optimization did not result in minima (as evidenced by the presence of imaginary frequencies) this has been flagged in the results.

Starting structures for optimisation were built in a model builder. To test the different potential binding modes possible with the different anions (see Figure 4.30 for examples), different parts of the extractant molecule(s) were placed in close proximity with the anion.

Counterpoise calculations to obtain BSSE corrections were done for the formation of chloride and Rh(III) complexes, but not for the formation of protonated extractants. The fragments were defined in the calculations as given in Table 4.3 below.

Table 4.3. Fragments used for counterpoise corrections.

Structure	Fragment 1	Fragment 2	Fragment 3
LH·Cl	Cl^-	LH^+	—
$(LH)_2$·[$RhCl_5(H_2O)$]	$[RhCl_5(H_2O)]^{2-}$	LH^+	LH^+

All simulation outputs are included in the SI.

4.4.2 Assumptions made

A number of assumptions have been made to make this study achievable while still keeping the results realistic. These assumptions are:

i. Amidoamine molecules which are similar in structure to MonoAA and BisAA will extract in a similar manner; therefore, extraction will occur via an ion-pair (or ion-associate) mechanism.
ii. The binding modes which are likely to occur are limited to: C-H…anion or N-H…anion binding, with or without hydrogen bond(s) with the *aquo* ligand in the case of Rh(III) metalate extraction.
iii. Monomeric extraction of chloride (which is more straightforward to model) is representative of dimeric extraction of chloride (which has been shown to occur for BisAA).[20]
iv. The more favourable the theoretical energy of exchanging chloride for $[RhCl_5(H_2O)]^{2-}$ the more effective an extractant the amidoamine is likely to be.

The latter two assumptions are supported by the results reported in Chapter 3.

4.5 References

1. Narita, H.; Morisaku, K.; Tanaka, M., *Chem. Commun.* **2008,** *45*, 5921-5923.
2. Narita, H.; Morisaku, K.; Tanaka, M., *Solvent Extr. Ion Exch.* **2015,** *33*, 407-417.
3. Afzaletdinova, N. G.; Khisamutdinov, R. A.; Bondareva, S. O.; Murinov, Y. I., *Russ. J. Inorg. Chem.* **2015,** *60*, 1583-1587.
4. Afzaletdinova, N. G.; Khisamutdinov, R. A.; Bondareva, S. O.; Murinov, Y. I., *Russ. J. Gen. Chem.* **2015,** *85*, 1934-1938.
5. Afzaletdinova, N. G.; Murinov, Y. I.; Khazhiev, S. Y.; Bondareva, S. O.; Muslukhov, R. R., *Russ. J. Inorg. Chem.* **2010,** *55*, 460-467.
6. Bondareva, S. O.; Afsaletdinova, N. G.; Murinov, Y. I., *Russ. J. Appl. Chem.* **2011,** *84*, 1897-1902.
7. Carson, I.; MacRuary, K. J.; Doidge, E. D.; Ellis, R. J.; Grant, R. A.; Gordon, R. J.; Love, J. B.; Morrison, C. A.; Nichol, G. S.; Tasker, P. A.; Wilson, A. M., *Inorg. Chem.* **2015,** *54*, 8685-8692.
8. Wilson, A. M. Ditopic Reagents for the Solvent Extraction of Platinum Group Metals. University of Edinburgh, 2014.
9. Wilson, A. M.; Bailey, P. J.; Tasker, P. A.; Turkington, J. R.; Grant, R. A.; Love, J. B., *Chem. Soc. Rev.* **2014,** *43*, 123-134.
10. Gaikwad, A. P.; Suryavanshi, V. J.; Anuse, M. A., *Cogent Chem.* **2017,** *3*.
11. Firmansyah, M. L.; Kubota, F.; Goto, M., *J. Chem. Technol. Biotechnol.* **2017,** *93*, 1714-1721.
12. Hunter, J.; Dolezalova, S.; Ngwenya, B.; Morrison, C.; Love, J., *Metals* **2018,** *8*.
13. Steiner, T., *Angew. Chem. Int. Ed.* **2002,** *41*, 48-76.
14. Jeffrey, G. A., *An Introduction to Hydrogen Bonding*. Oxford University Press: Oxford, 1997.
15. Zhao, Y.; Truhlar, D. G., *Theor. Chem. Acc.* **2007,** *120*, 215-241.
16. Roy, L. E.; Hay, P. J.; Martin, R. L., *J. Chem. Theory Comput.* **2008,** *4*, 1029-1031.
17. Krishnan, R.; Binkley, J. S.; Seeger, R.; Pople, J. A., *J. Chem. Phys.* **1980,** *72*, 650-654.
18. Raghavachari, K.; Trucks, G. W., *J. Chem. Phys.* **1989,** *91*, 1062-1065.
19. Cossi, M.; Barone, V.; Cammi, R.; Tomasi, J., *Chem. Phys. Lett.* **1996,** *255*, 327-335.
20. Narita, H.; Nicolson, R. M.; Motokawa, R.; Ito, F.; Morisaku, K.; Goto, M.; Tanaka, M.; Heller, W. T.; Shiwaku, H.; Yaita, T.; Gordon, R. J.; Love, J. B.; Tasker, P. A.; Schofield, E. R.; Antonio, M. R.; Morrison, C. A., *Inorg. Chem.* **2019,** *58*, 8720-8734.

Chapter 5

Modified precipitants as rhodium extractants

5 Modified precipitants as rhodium extractants

6.1 Introduction

6.1.1 Background

As there is currently no commercial Rh solvent extractant reagent, Rh is typically recovered industrially via precipitation methods,[1, 2] using reagents such as diethylenetriamine, ammonium chloride and ammonium nitrate or by raising the pH to precipitate $Rh(OH)_4$.[2]

Other reagents are also able to precipitate Rh, such as the amines explored by Geswindt,[3] who tested a variety of commercially available amine-based compounds for their ability to precipitate Rh(III) and Pt(IV) from chloride solution (Table 5.1).

Table 5.1. Polyamine compounds tested by Geswindt, their structure and their ability to precipitate Rh(III) from chloride solution.[3]

Compound	Structure	Rh(III) Precipitation?
Diethylenetriamine (Deta)	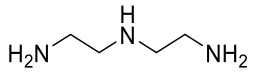	Yes
Triethylenetetramine (Teta)	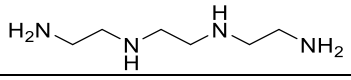	Yes
Tetraethylenepentamine (Tepa)	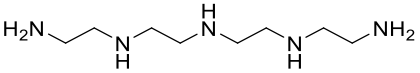	Yes
Ethylenimine oligomer mixture Avg. MW = 423 g mol^{-1}	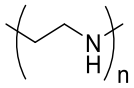	Yes, but slow and colloidal suspension formed
Lupamin® Avg. MW = <10000 g mol^{-1}	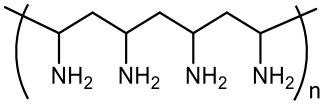	Yes, but colloidal suspension formed
Lupamin® Avg. MW = 340000 g mol^{-1}	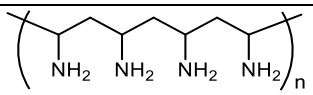	No
Tris(2-aminoethyl)amine (Tren)	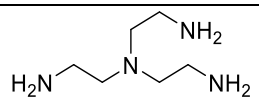	Yes
Tris[(2-isopropylamino)-ethyl]amine (Trien)	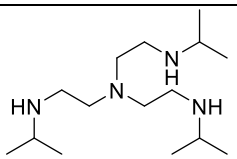	No
1,4,7-triazonane	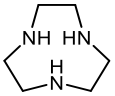	Yes

In their work they propose Rh(III) precipitation of either solely $[RhCl_6]^{3-}$ or both $[RhCl_6]^{3-}$ and $[RhCl_5(H_2O)]^{2-}$, based on reported crystal structures in their work and the literature.[3] Rh(III) is found to be more readily precipitated than Pt(IV), so it is possible to selectively precipitate Rh(III) over Pt(IV), though this is highly dependent on the precipitant concentration/the ratio of precipitant to metal.[3]

6.1.2 Potential for direct use of precipitants as extractants

In the work of Doidge it was found that a combination of an amine and an amide could be used to achieve synergistic extraction of Rh.[4] As illustrated in Figure 5.1, while the amine provides low extraction alone and the amide provides negligible extraction alone, together the reagents give good Rh(III) extraction of ~85% (from 4 M HCl).[4]

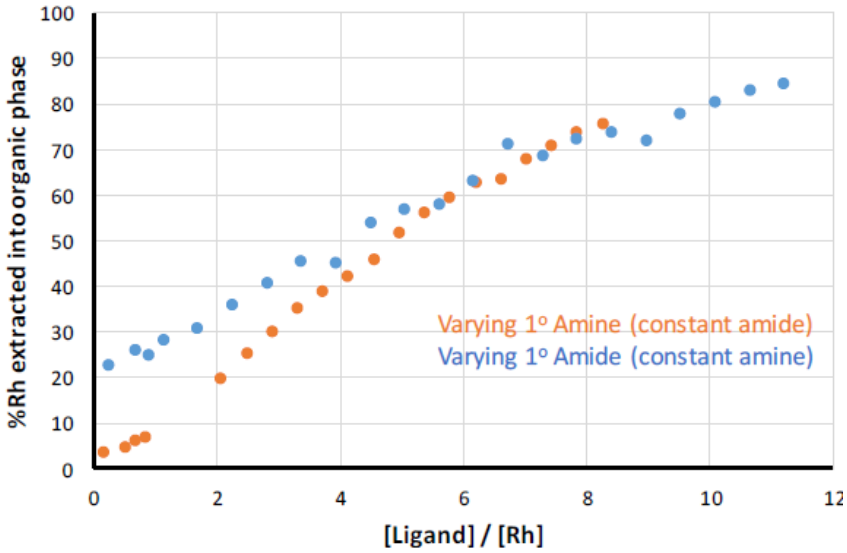

Figure 5.1. Percentage extraction of Rh(III) with ratio of amine or amide concentration to Rh(III) concentration (with concentration of other extractant held constant). Extraction from 0.01 M Rh(III) in 4 M HCl solution with 0.0-0.1 M extractant X and 0.1 M extractant Y in toluene. Reproduced from Doidge.[4]

Based on this finding, it may be possible that the precipitant amines could be used in conjunction with an organic-soluble amide, such as the one used in Doidge's work, to provide synergistic extraction of Rh(III), with the potential of achieving higher, and selective, extraction of Rh(III) over Pt(IV).

6.1.3 Potential for use of modified precipitants as extractants

Sánches-Loredo et al. synthesised organic-soluble tetra-amines and a tri-amine mono-quarternary ammonium, based on Tren, (see Figure 5.3) and tested the extraction of various anions.[5] They found that some of the reagents (B7T and B3T) were able to extract Pd(II) and Pt(II) chloridometalates, but unable to extract Rh(III) chloridometalates (BPT formed a precipitate). However, the extractions were carried out from aqueous solutions of very low chloride concentration (0.1 M NaCl or 0.1 M HCl). Therefore, it is possible that at higher chloride concentrations, where more Rh(III) would be present as $RhCl_6^{3-}$, extraction could occur.

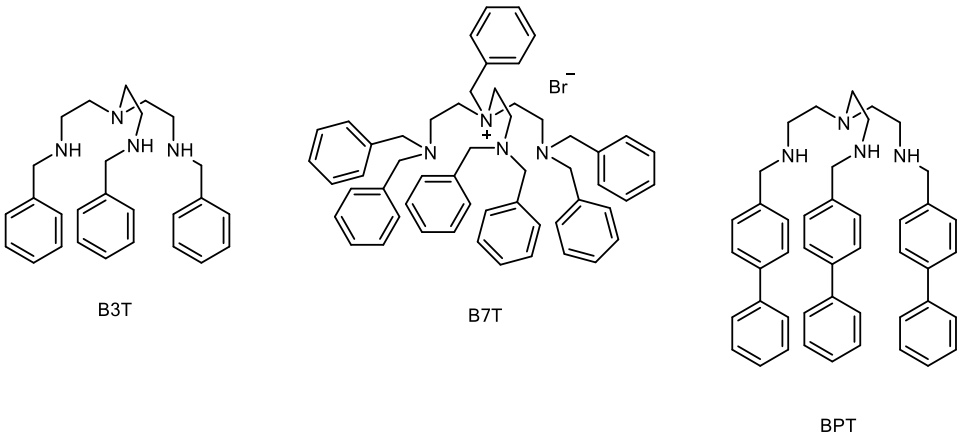

Figure 5.3. Reagents tested for the extraction of anions, including platinum-group metal chloridometalates, by Sánches-Loredo et al.[5]

6.1.4 Aims

The aims of this work are to:

i. Determine if known Rh(III) precipitants and related molecules can be used for Rh extraction in synergism with an organic-soluble amide
ii. Synthesise extended R-change variants of amine molecules known to act as Rh(III) precipitants and test the modified precipitants for their ability to extract Rh
iii. Characterise the Rh extraction behaviour of the most promising reagent
iv. Determine the conditions required for Rh stripping
v. Explore the potential for selective extraction of Rh over Pt

6.2 Results and discussion

6.2.1 Extraction tests of precipitating agents

A number of potential new extractants for Rh, some already known for their precipitant behaviour were initially tested, with the goal of identifying candidates that could either be modified or used in synergism with a second reagent to adapt the chemistry for SX. Reagents included in this study are summarised in Figure 5.4, and are specifically:

- diethylenetriamine (L1), a Rh precipitating tri-amine[3]
- bis(3-aminopropyl)amine (L2), a similar tri-amine to L1
- tris(2-aminoethyl)amine (L3), a Rh precipitating tetra-amine[3]
- tris[2-(isopropylamino)ethyl]amine (L4), a substituted tetra-amine, which does not act as a Rh precipitant[3]

Solutions of the reagents were tested alone and in the presence of a primary amide (PA, see Figure 5.4) for the extraction of Rh from 6 M HCl.

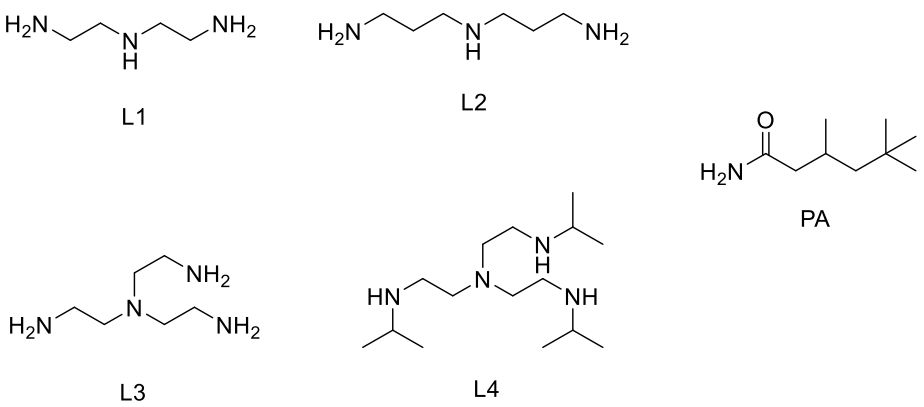

Figure 5.4. Structures of reagents used

Table 5.2 presents the concentration of Rh (as measured by ICP-OES) remaining in the aqueous phase following contact with the organic phase, as a percentage of the original Rh(III) content of the feed aqueous phase. In all cases, the concentration of Rh(III) in the organic phase was below the detection limit of the instrument (less than ~5% of the original Rh(III) content of the aqueous phase). It was found that both alone and in the presence of the primary amide, L1, L2 and L3 give no extraction of Rh(III), but precipitation occurred. The precipitant is likely to be of the form $[RhCl_6]^{3-}\cdot[LH_n]^{n+}\cdot(n\text{-}3)Cl^-$, based on the structures

reported in the literature for precipitated crystals formed with similar polyamines,[6-13] though it is possible that $[RhCl_5(H_2O)]^{2-}$ could be precipitated instead of or in addition to $[RhCl_6]^{3-}$, as suggested by Geswindt.[3] For reagent L4 (with and without PA), neither extraction nor precipitation occurred. L4 was also tested using chloroform as the solvent (both alone and with the primary amide) to see if this enabled any extraction to occur. However, it was once again found that neither extraction nor precipitation of Rh(III) occurred. Figure 5.5 shows the extraction mixtures after mixing, which show the precipitant formation with some reagents and the lack of extraction (indicated by absence of a red/pink colour in the organic phases, other than from the entrained Rh(III) precipitate).

Table 5.2. Rh(III) content of the aqueous phase, as percentage of the original Rh content, after attempted extraction using L1, L2, L3 and L4 alone and with PA. Extraction Label refers to the label in the photographs shown in Figure 5.5. 0.1 M amine or 0.1 M amine and 0.1 M PA in chloroform contacted with 0.01 M Rh in 6 M HCl solution (one hour contact time).

Extraction Label	Amine	PA?	Solvent	% Rh in aq.	Precipitation?
1A	L1	No	Toluene	0.5	Yes
1B		Yes		7.7	Yes
2A	L2	No		2.7	Yes
2B		Yes		1.3	Yes
3A	L3	No		29.2 *	Yes
3B		Yes		4.1	Yes
4A	L4	No		96.6	No
4B		Yes		95.8	No
8A		No	Chloroform	96.2	No
8B		Yes		92.6	No

* Given the colour of the aqueous phase after precipitation (see Figure 5.5), it seems likely that this value is incorrect (due to accidental transfer of precipitate with the aqueous phase when sampling for ICP-OES analysis)

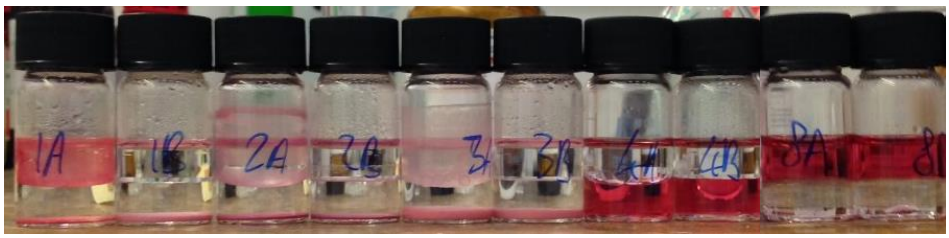

Figure 5.5. Images of the phases after mixing showing precipitant formation. Left to right: 1A, 1B, 2A, 2B, 3A, 3B, 4A, 4B, 8A and 8B. Note that in the last two vials the phases are reversed as chloroform is the organic solvent.

6.2.2 Synthesis of precipitant variants

Since the precipitating agents did not provide extraction of Rh, only precipitation, variants were synthesised with "greasy" R-groups to try and improve the reagents' solubility in the organic phase. Three reagents (L5, L6 and L7 – structures given in Figure 5.6) have been successfully synthesised as described in Section 5.4.

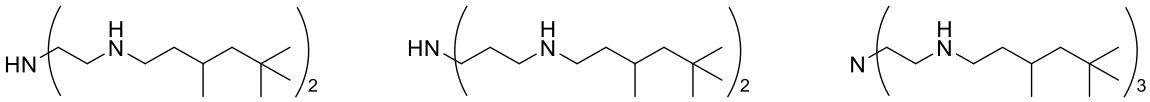

Figure 5.6. Structures of reagents synthesised

6.2.3 Extraction tests of precipitant variants

The three synthesised precipitant variants were tested as extractants for Rh from 6 M HCl both alone and in the presence of the primary amide. Both toluene, chloroform and 1-decanol were tested as solvents, as differences in performance were found depending on the solvent used. Figure 5.7 shows the phases after mixing, showing how in some samples emulsions or third phases form. Table 5.3 gives the content of Rh(III) in the aqueous and organic phases after mixing as a percentage of the Rh(III) content originally in the aqueous phase. In some cases, analysis of one or both phases was not carried out because phase separation was difficult or precipitation occurred on preparation of the sample for ICP-OES analysis.

L7 provides very good extraction (>95%) using chloroform as the solvent. L7 and L5 also appear to provide reasonable extraction using 1-decanol as the solvent (note that the sum of the aqueous and organic content is not 100%, but this may be due to volume change effects which have not been accounted for here).

L5 in toluene gives good removal of Rh from the aqueous phase, but a third phase forms which (by eye, based on colour) appears to contain the majority of the Rh. In chloroform more third phase forms, but similar levels of Rh are removed from the aqueous phase.

In toluene L7 appears to remove all Rh from the aqueous phase, but a large quantity of third phase/emulsion forms.

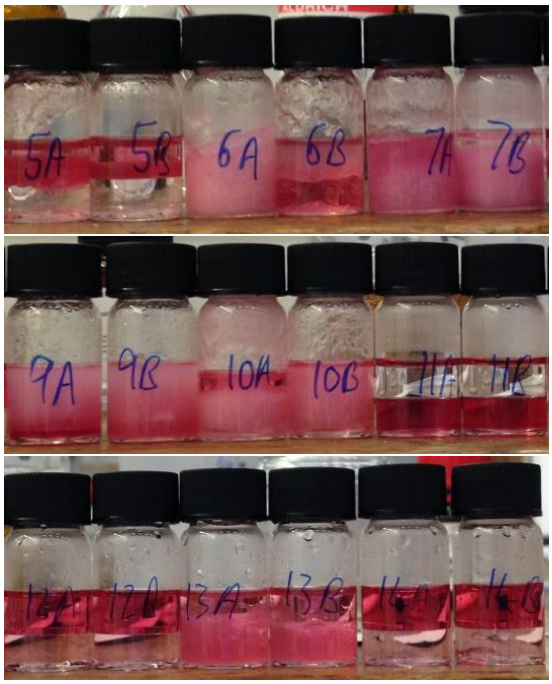

Figure 5.7. Images of the phases after mixing. Top to bottom the solvent is: toluene, chloroform, 1-decanol. 5, 9 and 12 are L5; 6, 10 and 13 are L6; 7, 11 and 14 are L7. A is the polyamimes alone, B is with addition of PA. (See Section 5.4 for full extraction test details).

L6 never provides full extraction, though its performance is better in 1-decanol than in toluene, where the two phases form a complete emulsion (see Figure 5.7), and in chloroform, where emulsion/third phase also forms.

Overall, there appears to be very little difference in the extraction behaviour on addition of the primary amide. However, in some cases, the presence of the primary amide appears to improve phase separation. For example, with L6 in toluene a complete emulsion of the two phases formed, but with the PA included phase disengagement did occur, though some emulsion remained. Therefore, the PA appears to be acting as a phase modifier. It is unclear if it offers any effect as a synergist as the extraction of Rh is high with the amine alone.

For some reagent and solvent combinations, the phase disengagement was slow and, for some, clean phase disengagement was not achieved. Though not performed as part of this study, further work could be done to determine if better solvents for these reagents or modifiers could improve the performance.

Table 5.3. Rh content of the aqueous and organic phases, as percentage of the original Rh content in the aqueous phase, after attempted extraction using L5, L6, and L7 alone and with PA. Extraction Label refers to the label in the photographs shown in Figure 5.7. 0.1 M extractant or 0.1 M extractant and 0.1 M PA in chloroform contacted with 0.01 M Rh in 6 M HCl solution (one hour contact time). An error of ±5% (absolute) is assumed on the values.

Extraction Label	Amine	PA?	Solvent	% Rh in aq.	% Rh in org.
5A	L5	No	Toluene	4	*
5B		Yes		4	*
6A	L6	No		#	#
6B		Yes		69	#
7A	L7	No		0	#
7B		Yes		#	#
9A	L5	No	Chloroform	4	#
9B		Yes		2	#
10A	L6	No		71	#
10B		Yes		60	#
11A	L7	No		0.1	98
11B		Yes		0.3	100
12A	L5	No	1-decanol	23	59
12B		Yes		22	58
13A	L6	No		#	*
13B		Yes		67	*
14A	L7	No		16	68
14B		Yes		16	67

Emulsion or third phase present which made sampling of liquid phase for ICP-OES analysis difficult/impossible

* Precipitation occurred on preparation of sample for ICP-OES analysis

6.2.4 Extraction of Rh with L7 with varying HCl concentration

When using chloroform as the solvent and L7 (or reagent L7 and the primary amide) as the extractant, Rh extraction was high, phase disengagement was relatively quick, and the phases were distinct, with no third-phase formation. Therefore, this combination was pursued for varying HCl concentration tests (see Figure 5.8 for the extraction plots).

There is some discrepancy between the amount of Rh extracted from the aqueous phase and the amount present in the organic phase. Some of this is simply due to experimental/analytical error. However, in some samples a precipitate/third phase formed

(see Figure 5.9 for images of the extraction mixtures) and, based on colour, it is likely that some Rh is present in this material.

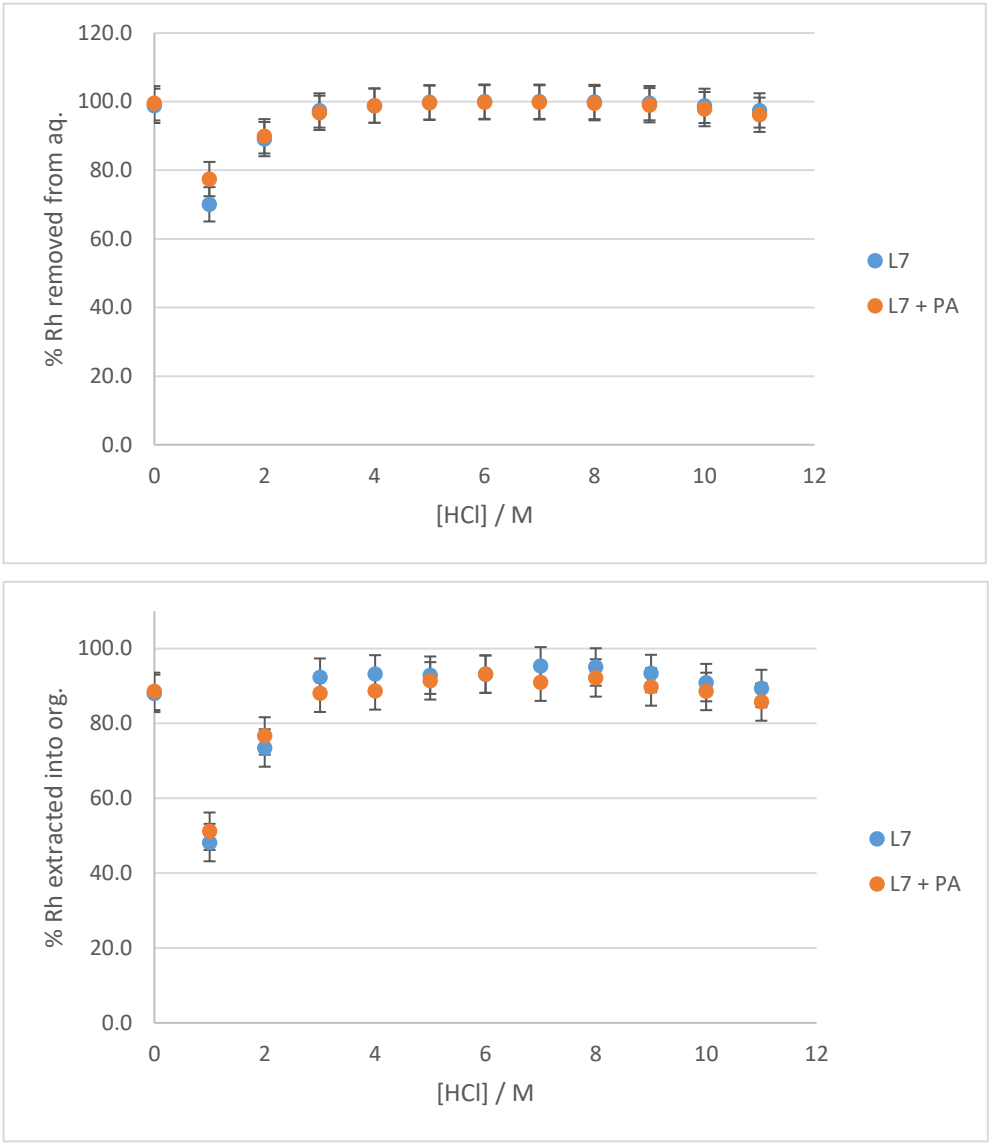

Figure 5.8. Top: percentage Rh removed from the aqueous phase with varying [HCl]; and bottom: percentage Rh extracted into the organic phase with varying HCl. 0.1 M L7 in chloroform contacted with 0.01 M Rh in 0-11 M HCl solutions (one hour contact time). Absolute error of ±5% in the percentage Rh displayed on plots.

Despite the difference between the percentage removed from the aqueous phase and the percentage in the organic phase, the plots conform to the same general shape. With the exception of the point for 0 M HCl, the extraction of Rh increases with increasing [HCl] up to

around 6-8 M HCl, after which the extraction decreases a little. In general, this plot follows what would typically be expected of a varying HCl plot, with high extraction at high HCl concentrations, where metalate formation is favoured, but decreasing at very high HCl concentrations, where competition for extraction of chloride over the metalate is greater. However, for Rh, this trend is a little unusual in that it is typically found that Rh extraction significantly decreases at higher HCl concentrations,[14] as strong extraction of Rh(III) metalate over chloride is difficult and the metalate speciation moves from $[RhCl_5(H_2O)]^{2-}$ to $[RhCl_6]^{3-}$,[3, 14] the latter of which is more difficult to extract due to its higher charge. This potentially implies that L7 can extract the $[RhCl_6]^{3-}$ metalate. More work would be required to confirm this, but this is in line with the ability of polyamines to precipitate this metalate.[6-13]

Figure 5.9. Photos of the extraction mixtures after stirring, with increasing HCl concentration (0-12 M, left to right). Top is L7 alone, bottom is L7 + PA. Note that the photographs were taken after the aq. phase in the 0 M HCl extraction using L7 alone had been removed.

It was observed that at 0 M HCl, where around 95% of Rh is extracted, the organic phase was yellow rather than the red/pink of the organic phases contacted with HCl solutions (see Figure 5.9). It seems likely here that the Rh has been extracted as an inner-sphere complex with L7, and further analysis (presented in Section 5.2.12) looks to confirm this.

Third phase/precipitant was only observed to form in the extractions from 1 to 4 M HCl (see Figure 5.9). This occurred with both L7 alone and L7 with the primary amide; however, the presence of the primary amide appeared to lessen the quantity of immiscible material which formed. At all other HCl concentrations good phase disengagement occurred, both with and without the primary amide.

Again, there is no obvious evidence of the PA providing a synergistic extraction effect. It is possibly acting as a modifier (decreasing third phase formation), but the extraction with L7 alone is very high for most HCl concentrations, so distinguishing a synergist improvement of extraction is difficult. This could be explored further by decreasing the concentration of the amine used, so as to provide a wider range of data points at which complete Rh extraction is not achieved with L7 alone. However, going forward, work focused on L7 alone since there is no obvious improvement to extraction percentage with the use of PA.

6.2.5 Extraction of Rh with L7 with varying time

As mentioned in Chapter 3, Afzaletdinova et al.[15, 16] have shown that monitoring metal extraction as a function of contact time provides insight into establishing the optimal time period to maximise extraction and to establish whether the extraction mechanism changes with time. To this end, an extraction over time experiment was carried out with L7, with results presented in Figure 5.10.

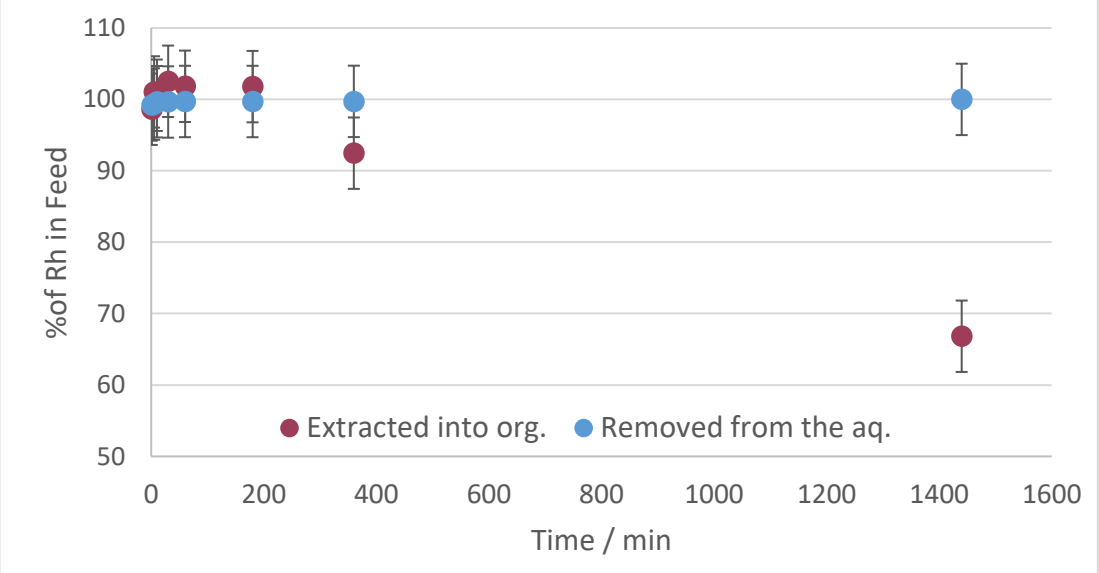

Figure 5.10. Plot of the percentage of Rh removed from the aqueous phase and extracted into the organic phase over time. 0.01 M Rh in 6 M HCl used as the aqueous phase and 0.1 M L7 in chloroform used as the organic phase. Absolute error of ±5% in the percentage Rh displayed on plots.

It appears that maximum extraction is reached after around 30 minutes, and this is constant until around three hours of contact time. However, it is clear from the data presented on the percentage of Rh in the organic phase that at contact times of 400 and 1500 minutes (six or 24 hours) precipitate or third phase containing Rh forms. Figure 5.11 gives a photograph of the extraction vials, where this material can be seen. It is interesting to note that this precipitate does not form in any of the shorter contacted loaded organics after separation and standing for 24 hours. Therefore, it is apparent that contact with the aqueous phase for a prolonged period of time is required for the formation of this precipitate.

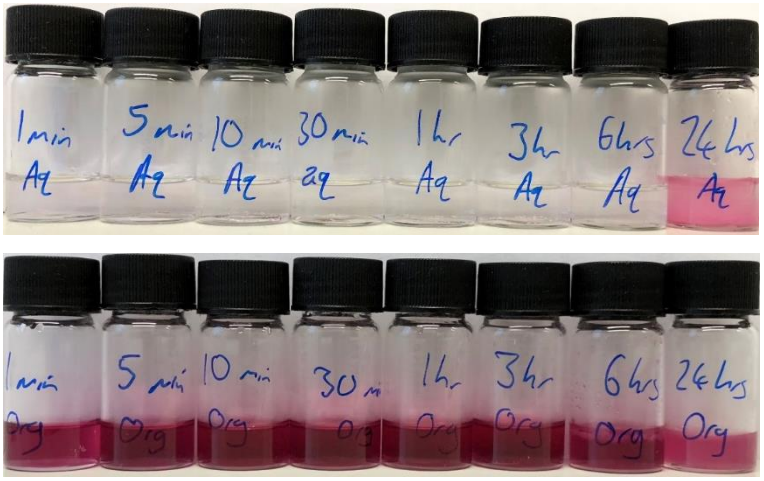

Figure 5.11. Photos of the extraction mixtures after separation. Top is the aqueous phase, bottom is the organic phase. Note that the photographs of all the vials were taken at the same time (after the 24 hour extraction was separated); therefore, the time from starting extraction to taking the photograph is approximately the same in all cases.

This experiment has highlighted that a different assembly must be forming on longer contact times: one that is not soluble in either the organic or aqueous phases. This behaviour can be very problematic for extraction systems. It is possible it could be combatted by the addition of a modifier, the use of a different solvent or by using different R-groups on L7. However, it is also possible that this issue could be avoided simply by keeping contact times short since most of the Rh is extracted within 30 minutes.

6.2.6 Extraction of varying Rh concentrations with L7

Extractions were carried out from aqueous solutions of varying Rh concentration, as shown in Figure 5.12. Once a ratio of extractant to metal of around 50 is reached, almost 100% of Rh is extracted. Some precipitation occurred in the extractions from higher (0.05 M and greater) Rh solutions (see Figure 5.13) (though note that for the "ca. 0.5 M" extraction some solid was present from the start as the solution was saturated with Rh salt). This may suggest that a different mode of extraction occurs when the ratio of extractant to metal is low.

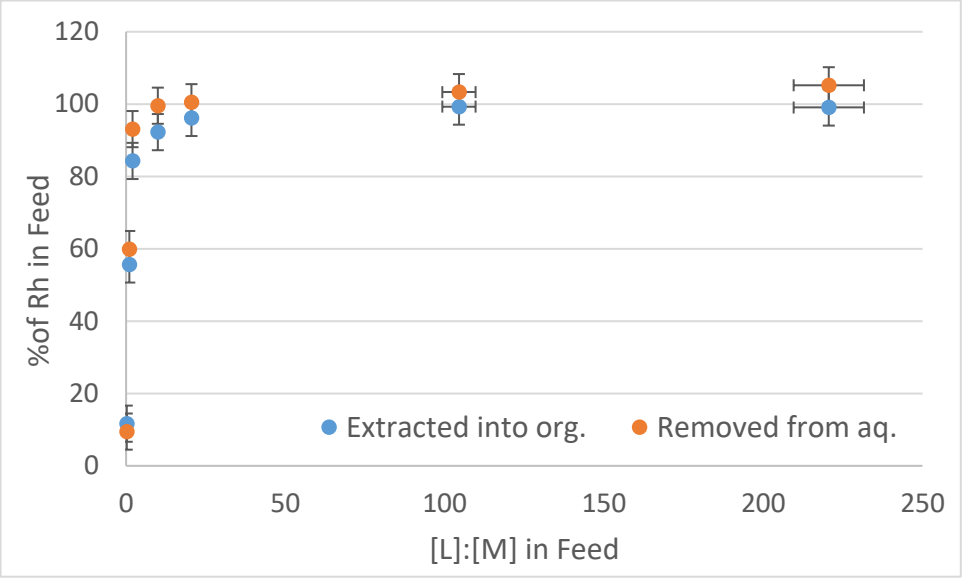

Figure 5.12. Percentage Rh extracted into the organic phase top with changing ratio of extractant in the organic phase to metal in the initial aqueous phase. 0.1 M L7 in chloroform contacted with 0.005-0.5 M Rh in 6 M HCl solutions (one hour contact time). Absolute error of ±5% in the percentage Rh and relative error of ±5% in the ratio of extractant to metal concentration displayed on plots.

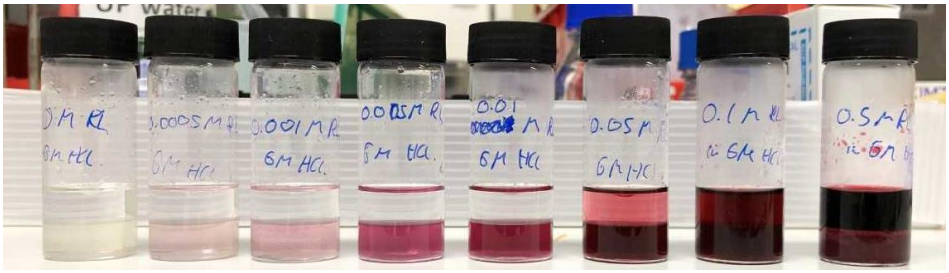

Figure 5.13. Photos of the extraction mixtures after stirring but before separation. Top is the aqueous phase, bottom is the organic phase. Note: in the case of the 0.5 M Rh extraction, not all of the Rh(III) salt used in the preparation of the aqueous feed solution was soluble in the aqueous phase, so there was some solid present from the start.

6.2.7 Extraction of water with L7

KF titrations of the loaded organic phases from the varying Rh concentration extractions produced an unusual trend (as shown in Figure 5.14). Initially, as is seen with Rh extraction with BisAA (see Chapter 3 Section 3.2.5),[17] the water concentration in the organic phase decreases as the Rh concentration increases, suggesting that water is extracted with chloride but less (or no) water is extracted with Rh. However, at much higher concentrations of Rh in the loaded organics the water concentration is found to increase. This may indicate that at higher concentrations of Rh, extraction is occurring via a different mechanism, however, further work (including an exploration of more Rh concentrations) would need to be conducted to determine this. Alternatively, the high concentration of Rh present could be causing an error in the results because the Rh(III) may be reduced in the titration cell.[18]

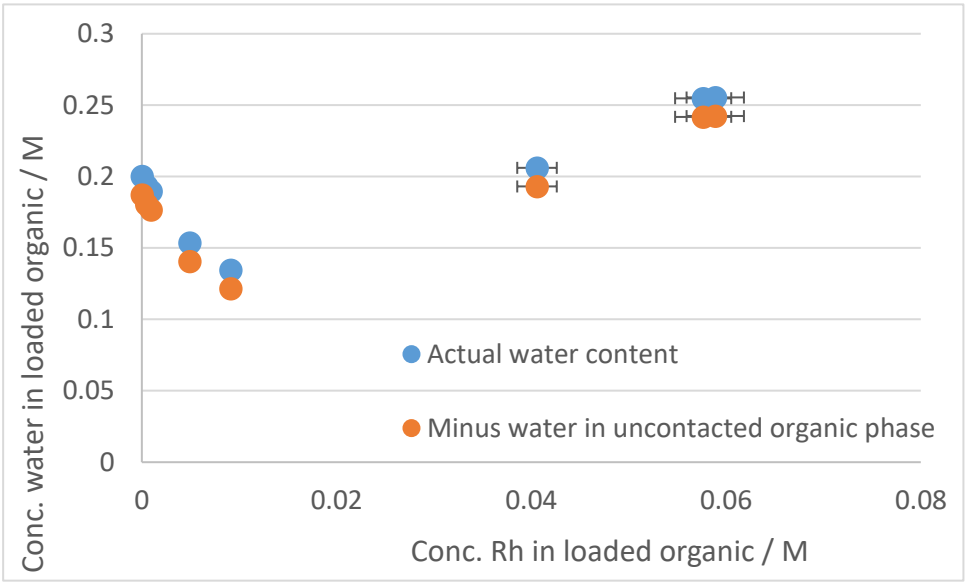

Figure 5.14. Concentration of water in the loaded organic versus the concentration of Rh in the loaded organic. From extractions of 0.1 M L7 in chloroform contacted with 0.0-0.5 M Rh in 6 M HCl solutions (one hour contact time). Relative error of ±5% in the Rh concentration displayed on the plots. Standard deviation in the water concentration values is included but all are below ±2% so the error bars are not visible.

6.2.8 Stripping Rh after extraction with L7

The ability to strip (or back extract) the Rh from the loaded organic phase was tested with a variety of aqueous solutions, based on those tested by Narita et al. for stripping in their

synergistic Rh extraction system.[19] Results shown in Figure 5.15 and 5.16 indicate that half had phase issues during mixing. For water and 0.5 M thiourea, the "aqueous" phase appeared to form an emulsion (which will contain entrained organic material); for HNO_3 a liquid third phase (likely containing most of the Rh, based on its colour) formed; and for 0.5 M NaOH a precipitate (also likely containing Rh, based on its colour) formed. With 10 M HCl the stripping was very poor, with less than 5% of the Rh back-extracted into the aqueous phase. This is to be expected, though, given that extraction of Rh is still high at 10 M HCl. However, 5 M NaOH gives reasonable stripping, of ~70%, and 0.5 M and 28% ammonium hydroxide solutions give very effective stripping, with greater than 95% of the Rh back-extracted in to the aqueous phase.

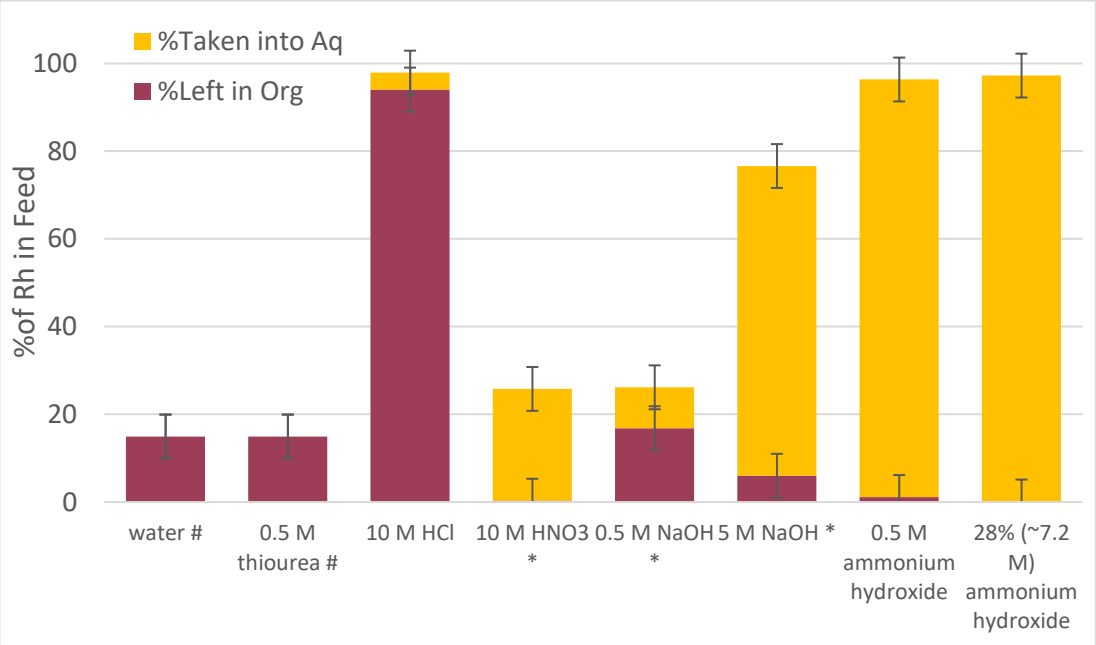

Figure 5.15. Test stripping of Rh with different aqueous phase compositions for one hour of contact time. Organic phase from an extraction of 0.01 M Rh in 6 M HCl solution with 0.1 M L7 in chloroform solution (one hour contact time). Absolute error of ±5% in the percentage Rh displayed on plots. #"Aqueous" phase formed an emulsion and so was not analysed for its metal content *Third phase/precipitate formed – "missing" Rh is likely in this material

Stripping was tested with varying ammonium hydroxide concentration (see Figure 5.17). It is observed that greater than 97% stripping of Rh from the organic phase is possible across all concentrations tested. Using 0.5 M ammonium hydroxide solution the aqueous phase is slightly cloudy (see Figure 5.16) and the amount of metal taken into the aqueous phase is

ca. 92%, suggesting a small amount of precipitate is present. Over time, precipitate tends to form in the aqueous phases, even in the higher concentration ammonium hydroxide solutions. However, as can be seen from Figure 5.16, initially the phase behaviour of the higher ammonium hydroxide concentration strips is good.

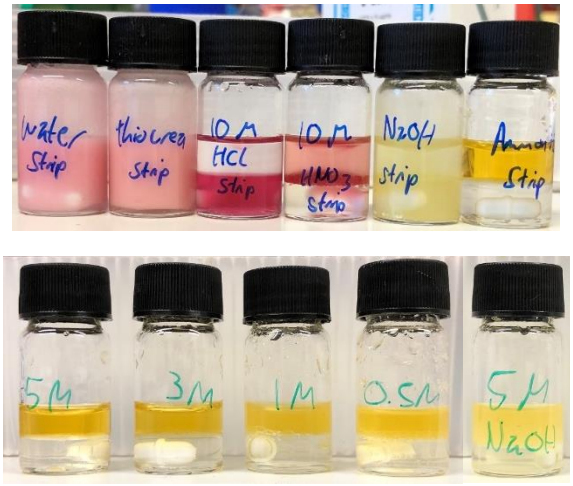

Figure 5.16. Stripping mixtures after stirring for one hour, from left to right, top to bottom: water, 0.5 M thiourea, 10 M HCl, 0.5 M NaOH, 28% (~7.2 M) ammonium hydroxide, 5 M ammonium hydroxide, 3 M ammonium hydroxide, 1 M ammonium hydroxide, 0.5 M ammonium hydroxide, 5 M NaOH.

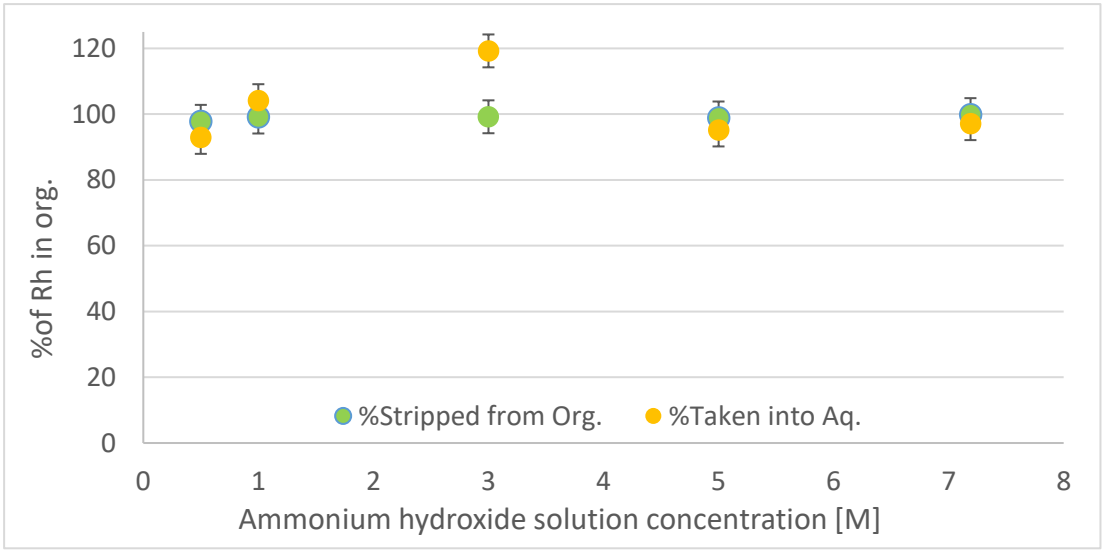

Figure 5.17. Stripping Rh with varying ammonium hydroxide solution (one hour contact time). Organic phase from an extraction of 0.01 M Rh in 6 M HCl solution with 0.1 M L7 in chloroform solution (one hour contact time). Absolute error of ±5% in the percentage Rh displayed on plots. Note: the percentage Rh(III) taken into the aqueous phase at 3 M ammonium hydroxide exceeds 100% – this is an anomalous result which may be due to sample preparation or instrumentation error, resulting in an error larger than ±5%.

Although ammonium hydroxide solution of moderate concentration is able to back extract Rh, the requirement to use base is not ideal. From both a recyclability of the reagents point of view and for incorporation into existing flowsheets, it is preferable to strip with water or with a lower or higher concentration of the media that extraction is carried out from. In this particular instance, if acid needs to be added to regenerate the Rh chloridometalate species, any ammonium hydroxide solution added in the strip step cannot be recycled and additional reagent is therefore required. If there are other metals present which are incompatible with basic solution it will thus be difficult and/or expensive to introduce this extraction process to existing flowsheets. However, if Rh can be selectively extracted over the residual metals remaining in solution at the end of the PM extraction flowsheet and it can be reduced out from basic solution while recycling the ammonium hydroxide then this system could be sustainable.

6.2.9 Recyclability of L7

Stripping Rh from the organic phase is possible with ammonium hydroxide solution. However, for a SX system to be efficient the extractant in the organic phase must be recyclable. To test this for L7 multiple load (extraction) and strip cycles were carried out (as described in Section 5.4.2.6). Figure 5.18 gives a plot of the percentage of Rh extracted into the organic phase and stripped from the organic phase with each cycle. The differences between each cycle are within error, suggesting that the extractant is fully recyclable over five cycles using 3 M ammonium hydroxide solution as the stripping agent. It was noted during the subsequent extractions after stripping, however, that the phases fumed on contact. This was likely due to the presence of entrained residual ammonium hydroxide in the organic phase reacting with the HCl in the aqueous phase. Though this does not appear to have affected the extraction performance, it could be combatted by washing the organic phase with water prior to reusing for Rh extraction.

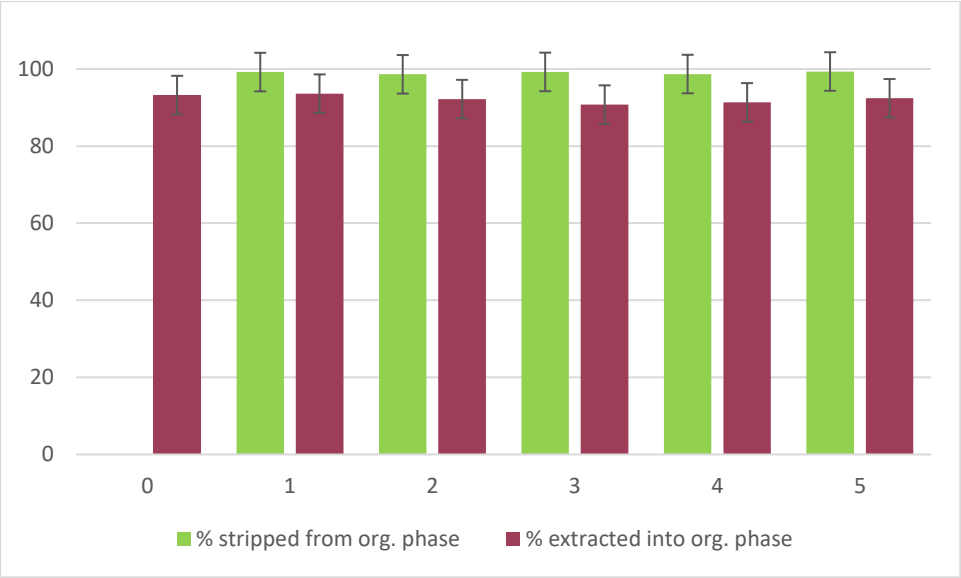

Figure 5.18. Rh extraction and stripping across five cycles. Initial extraction ("cycle 0") used fresh 0.1 M L7 in chloroform, all subsequent cycles used this solution recycled after stripping. All extractions were a contact of the organic phase with a 0.01 M Rh in 6 M HCl solution for 1 hour; all strips were a contact of the loaded organic with a 3 M ammonium hydroxide solution for 1 hour. Absolute error of ±5% in the percentage Rh displayed on plots.

6.2.10 Extraction of Pt and potential for the separation of Pt and Rh with L7

Since Tren (L3) has been shown to selectively precipitate Rh(III) over Pt (IV),[3] L7 was tested for its ability to selectively extract Rh(III) over Pt(IV). In Geswindt's work,[3] it was shown that selectivity occurred when ratios of reagent to metal were low (approximately 5:1 or less). Unfortunately, precipitate was found to form when low ratios of L7 to metal were employed (see Figure 5.19), and the lowest ratio for which metal extraction was able to be quantified accurately was 10:1 L7 to metal.

At the ratios of L7 to metal explored, there does not appear to be any notable selectivity for Rh(III) over Pt(IV), as shown in Figure 5.20. The extraction of both metals is relatively comparable. There is some fluctuation in the amount extracted into the organic phase, though this may be as a result of small amounts of precipitate forming, which are not visible in solution. However, within error, there is no difference found in the percentage of Rh or Pt removed from the aqueous phase.

Figure 5.19. Photos of the extraction mixtures after stirring but before separation. 0.1 M L7 in chloroform contacts with 0.0005-0.1 M Rh in 6 M HCl, 0.0005-0.05 M Rh and 0.0005-0.05 M Pt in 6 M HCl, and 0.0005-0.1 M Pt in 6 M HCl, for 1 hour. Note: in the case of the 0.1 M Rh, 0.1 M Pt, 0.05 M Pt, and 0.05 M Rh/Pt extractions precipitate was found to form, and in the 0.05 M Rh extraction the two phases formed an emulsion.

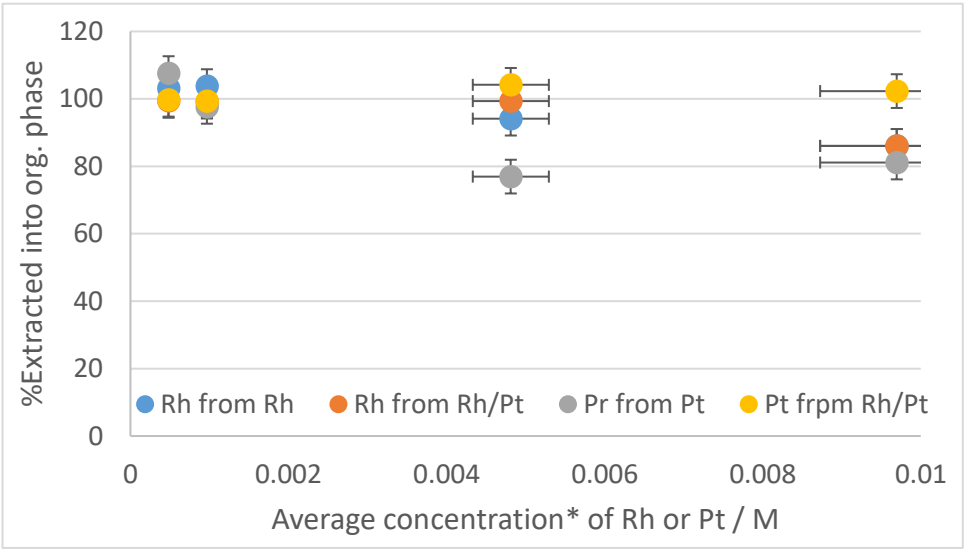

Figure 5.20. Extraction of Rh(III) and Pt(IV) from single metal and mixed-metal solution. Percentage metal extracted into the organic phase. 0.1 M L7 in chloroform contacts with 0.0005-0.01 M Rh in 6 M HCl, 0.0005-0.01 M Rh and 0.0005-0.01 M Pt in 6 M HCl, and 0.0005-0.01 M Pt in 6 M HCl, for 1 hour. Absolute error of ±5% in the percentage metal and relative error of ±10% in the metal concentration displayed on the plots (higher error than normal used for latter due to average concentration being used). *Average concentration used as concentrations are slightly different between metals and between solutions.

6.2.11 Extraction of Ir

The extraction of Ir(III) by L7 was also tested, as it was expected that if Rh(III) is being extracted as $[RhCl_6]^{3-}$ then Ir(III) should also be extractable as it would be present in a chloride solution as $[IrCl_6]^{3-}$. As Ir and Rh are usually the last metals to be recovered in the PM flowsheet (as discussed in Chapter 1), it is important to know if Ir will need to be recovered first to avoid co-extraction with Rh(III). It was found that a 0.1 M solution of L7 in chloroform was able to extract essentially all (101(5)% extracted into organic phase) the Ir from a 0.001 M solution in 6 M HCl and most (82(5)% extracted into organic phase) of the Ir from a 0.01 M solution in 6 M HCl. Figure 5.21 shows the phases after extraction.

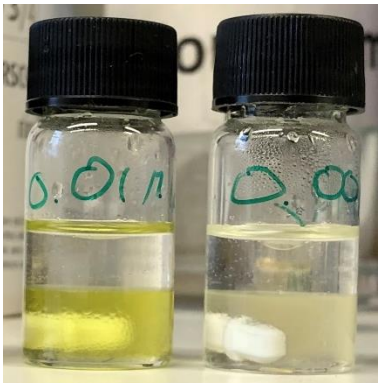

Figure 5.21. Ir extractions after stirring for one hour. Aqueous solution of 0.01 M Ir (left) or 0.001 M Ir (right) in 6 M HCl contacted with 0.1 M L7 solution in chloroform. 0.01 M Ir solution: 82±5% extracted into organic phase, 98±5% removed from aqueous phase; 0.001 M Ir solution: 101±5% extracted into organic phase, 99±5% removed from aqueous phase.

6.2.12 ESI-MS of the Rh and Pt L7 LOs

Following on from the information gained by ESI-MS for the amidoamine extractant in Chapter 3, it was hoped that ESI-MS would provide key insight into the nature of the extracted species with this new extractant. ESI-MS analysis was carried out on the loaded organic phases of some extractions, but, as can be observed in Figure 5.22, only the spectra for 0 M HCl extraction displays a peak that can be identified as a Rh-containing species. Negative mode was checked (see Figure 5.23) for the loaded organic from the 6 M HCl extraction but again, no Rh-containing species were identified, possibly due to the Rh(III) concentration in the loaded organic being too low to generate Rh-containing ions in the MS with this system.

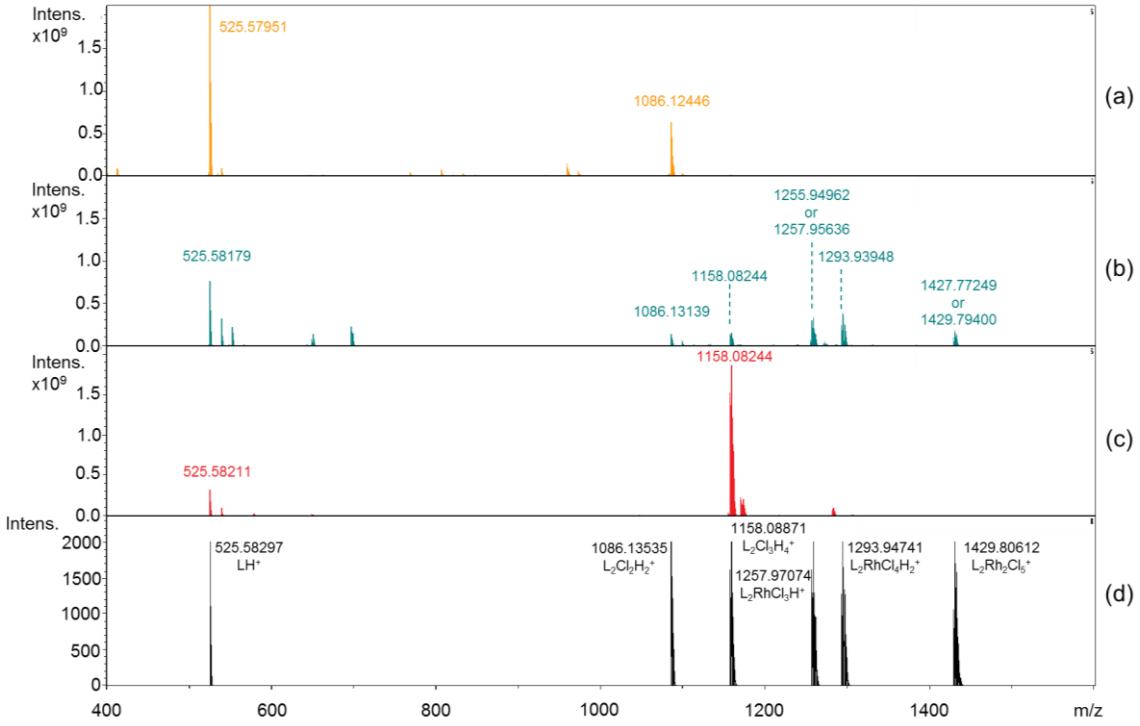

Figure 5.22. Positive ion ESI-MS spectra of L7 and loaded organics from varying HCl Rh extractions: **(a)** L7 in chloroform, **(b)** 0.1 M L7 in chloroform contacted with 0.01 M Rh(III) in water, and **(c)** 0.1 M L7 in chloroform contacted with 0.01 M Rh(III) in 6 M HCl. **(d)** gives the predicted spectra. All samples were diluted in acetonitrile prior to analysis.

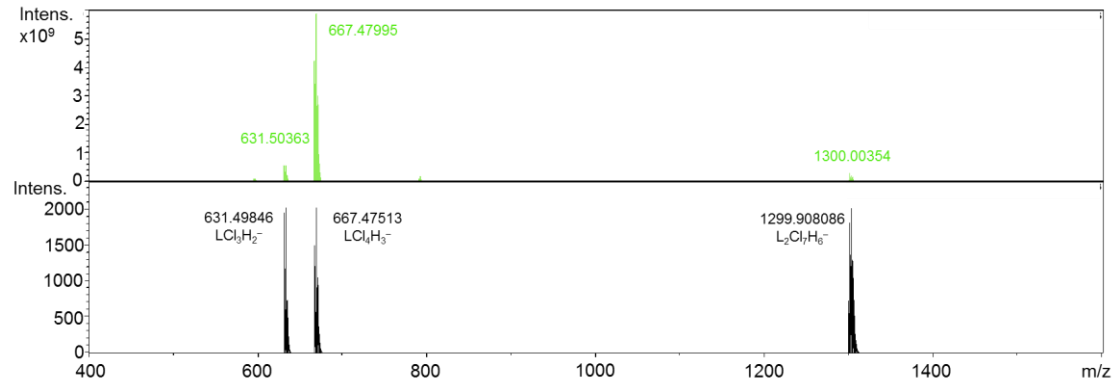

Figure 5.23. Negative ion ESI-MS spectra of the LO from 0.1 M L7 in chloroform contacted with 0.01 M Rh(III) in 6 M HCl. The lower spectrum is predicted. Sample diluted in acetonitrile prior to analysis.

Although this analysis has not aided identification of the extracted species from high concentration HCl solution, it has confirmed what was suspected about the nature of the species on extraction from water. As suggested by the yellow colour of the loaded organic

after contact with 0.01 M Rh in water, a complex(es) where L7 is binding directly to the Rh(III) centre appear(s) to form on extraction.

A $[L_2H_2Cl_4Rh]^+$ Rh(III) containing ion is identified from the mass spectrum and potentially $[L_2HCl_3Rh]^+$ and $[L_2Cl_5Rh_2]^+$ ions are also observed, though this cannot be confirmed due to possible peak overlap. A $[L_2HCl_3Rh]^+$ ion could consist of a $[RhCl_3(\underline{\kappa}^3\text{-L})]$ complex flying with LH^+ to make the whole assembly positive and the $[L_2H_2Cl_4Rh]^+$ ion could be the same but with an additional HCl bound. A $[L_2Cl_5Rh_2]^+$ ion is particularly interesting as it could indicate a dinucluear Rh complex is present (potentially of the suggested structures given in Figure 5.24), or one mono-nuclear complex and one partial one (one $[RhCl_3(\underline{\kappa}^3\text{-L})]$ and one $[RhCl_2(\underline{\kappa}^3\text{-L})]^+$ fragment, where a chloride ion has been lost to impart a positive charge on the assembly) flying together.

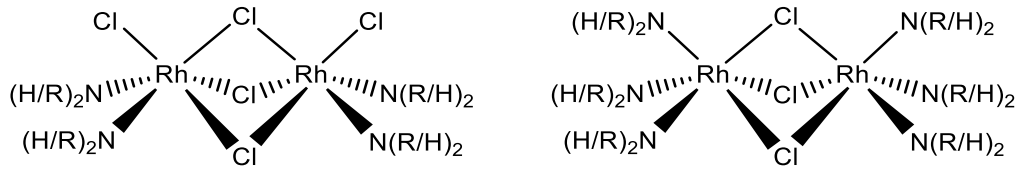

Figure 5.24. Potential structures of a dinuclear Rh complex suggested by the presence of the $[L_2HCl_5Rh_2]^+$ ion in the mass spectrum. $N(H/R)_2$ indicates one of the amine (either secondary or tertiary) present on the L7 molecule. $[Rh_2Cl_5L_2]^+$ (left) is an exact match to the ion in the spectrum and considers each L7 bound in a bidentate manner to Rh while $[Rh_2Cl_3L_2]^{3+}$ (right) would be accompanied by two additional chloride ions in the mass spectrometer and considers L7 bound in a tridentate manner to Rh.

6.3 Conclusions and future work

The work in this chapter has found that polyamine Rh(III) precipitants are not effective as solvent extractants, either alone or in the presence of a primary amide, with only precipitation (likely of $[RhCl_6]^{3-}$ with protonated polyamine) occurring. However, on the modification of the molecule structure to incorporate branched-chain R-groups, it is possible to modify the precipitants to behave as extractants. On consideration of both Rh extraction ability and phase performance, L7 (a modified Tren reagent) in chloroform was chosen as the extractant and solvent combination to be further explored.

L7 is able to extract Rh from high HCl concentration aqueous solutions (>90% extraction from 5 M HCl and upwards). Precipitation is found to occur if lower HCl concentrations are used, except in the case of the Rh(III) salt dissolved in water (where the HCl concentration would be expected to be a maximum of 0.03 M, based on the maximum number of chloride ligands displaced by water molecules to be three per rhodium),[20] where a yellow loaded organic is observed and the extractant is found to be binding to Rh(III) in the inner-sphere.

Extraction at 6 M HCl is fast (99% extraction occurring in 1 minute), but precipitation can occur if the organic and aqueous phases are contacted for longer than 3 hours. Precipitation also occurs when low ratios of extractant to metal are employed (<10:1). However, greater than 90% extraction is possible with 10:1 and extraction is maximised by 100:1.

It is possible to recover Rh from the loaded organic phase by stripping with ammonium hydroxide solution, and the organic phase is able to be recycled (no decrease in performance found over five cycles when stripping with 3 M ammonium hydroxide solution).

Although the polyamine precipitants have demonstrated the ability to selectively precipitate Rh(III) over Pt(IV), there is no evidence that L7 is able to selectively extract Rh(III) over Pt(IV). Rh(III) and Pt(IV) extraction are comparable in extraction from 6 M HCl aqueous solutions of up to 0.01 M metal (above which precipitate was found to form). Ir(III) is also extracted by L7 in chloroform.

L7 is a promising reagent for the SX of Rh, for which there exist no commercial reagents. That Rh can be extracted from high HCl concentration solutions (similar in concentration to those used in industry in the PM SX flowsheets) and L7 can be recycled is excellent. The requirement to use ammonium hydroxide solution for stripping is not ideal. However, as L7

does not show any selectivity for Rh(III) over Pt(IV) and can also extract Ir(III), it is likely that if L7 were to be employed it would be used to extract Rh from residual metals at the end of the PM recovery flow-sheet. Therefore, the use of ammonium hydroxide would not interfere with any other metals in the process.

As ammonia-based precipitants are often used in the recovery of Rh industrially and the ammonium hydroxide strip solutions precipitate over time it would need to be weighed if there is a benefit to using L7 to SX Rh, if the ultimate product is going to be an ammonia-based precipitate containing Rh in either case. However, if the Rh and ammonia-based precipitant is purer after extraction and striping than in the case of direct precipitation or if Rh can be electrowinned from the ammonium hydroxide strip solution before precipitation occurs, then the use of extraction with L7 could be an improvement over the existing industrial process.

For L7 to be usable industrially, an alternative R-group, a different solvent or a modifier would need to be employed to achieve good phase behaviour in a purely hydrocarbon or alcohol-based solvent, as chloroform cannot be used industrially for extraction for practical (high volatility) and safety (it is too toxic) reasons.

Johnson Matthey, the industrial sponsors of this work, will assess whether L7 (or a modified version) could be industrially viable. If it is deemed so, further work would need to be conducted to find an alternative R-group or solvent system and extraction testing in the presence of the residual metals remaining in solution with Rh after the recovery of all other PMs in the flowsheet would need to be done, ideally using real solutions from a PM refinery.

If the extractant is not deemed to be of industrial interest, it is still important to pursue an understanding of how L7 operates. It is shown here that it binds in the inner-sphere of Rh(III) on extraction from solutions of very low chloride concentration, however, very little has been elucidated on the mode of extraction from high chloride concentration solutions. Based on the known precipitation behaviour of Tren (L3) and the high extraction at high HCl concentration, it is likely that $[RhCl_6]^{3-}$ is being extracted in an anion extraction mode, but nothing is known about how L7 is protonated and interacting with the metalate. In addition, it is possible that some $[RhCl_5(H_2O)]^{2-}$ is being extracted. Therefore, slope analysis should be used to determine the ratio of L7 to metalate present in the extracted complex(es) and acid/base and chloride titrations to measure the number of protonated sites on L7 and the

amount of chloride present in the loaded organic. Structural characterisation techniques such as EXAFS and NMR may be useful in characterising the binding mode of L7 to the metalate and chloride. ESI-MS could be pursued further to see if higher concentrations of Rh in the loaded organic would allow for Rh-containing ions to be seen the spectra. Computational modelling would also be a valuable avenue, with classical MD simulations potentially able to show the assemblies present in the organic phase and the interactions occurring and subsequent QM calculations able to quantify interaction strength.

6.4 Experimental

6.4.1 Extractant synthesis

The three extractants (L5, L6 and L7) were all initially synthesised by the same general procedure given below (Figure 5.25 gives the general synthesis scheme). L7 was then synthesised on larger scales (see below for details).

General procedure: 3,5,5-trimethylhexanal (2 or 3 eq.) was dissolved in ethanol and added slowly to amine (1 eq.) dissolved in ethanol and the mixture was heated to reflux. After heating had stopped, $NaBH_4$ (2.5 or 3.5 eq.) was added slowly and, once effervescence stopped, the mixture was heated to reflux. The majority of the solvent was removed on a rotary evaporator and NaOH was added. The product was then extracted 3x into DCM. The majority of the solvent was removed, the remaining solution washed with water and dried over magnesium sulfate, before the solvent was removed. For later larger scale syntheses of L7, column chromatography was required for purification, as detailed below.

Details for L5: 3,5,5-trimethylhexanal (8.0640 g, 0.0567 mol) and diethylenetriamine (2.9040 g, 0.0281 mol) in 300 mL ethanol. Approximately 2.5 g of $NaBH_4$ and 350 mL of 2.5 M NaOH used. Reflux times of 1 hour each. ^{1}H NMR (500 MHz, $CDCl_3$, ppm): δ 0.83 (s, 18H), 0.86 (d, 6H), 0.97-1.03 and 1.13-1.19 (m, 4H), 1.23-1.32 and 1.37 to 1.45 (m, 4H), 1.43-1.51 (m, 2H), 2.50-2.58 (m, 4H), 2.64-2.70 (m, 8H). ^{13}C NMR (126 MHz, $CDCl_3$, ppm): δ 22.76, 27.43, 29.99, 31.04, 39.90, 48.08, 49.54, 49.72, 51.35.

Details for L6: 3,5,5-trimethylhexanal (3.7195 g, 0.0261 mol) and bis(3-aminopropyl)amine (1.7075 g, 0.0130 mol) in 250 mL ethanol. Approximately 2.4 g of $NaBH_4$ and 220 mL of 2.5 M NaOH used. Reflux times of 1 hour each. ^{1}H NMR (500 MHz, $CDCl_3$, ppm): δ 0.86 (s, 18H), 0.89 (d, 6H), 1.00-1.06 and 1.16-1.22 (m, 4H), 1.25-1.34 and 1.39-1.47 (m, 4H), 1.45-1.52 (m, 2H), 1.59-1.68 (m, 4H), 2.52-2.59 (m, 4H), 2.63 (t, 8H). ^{13}C NMR (126 MHz, $CDCl_3$, ppm): δ 22.77, 27.47, 30.00, 30.55, 31.07, 39.90, 48.23, 48.63, 48.69, 51.38.

Details for L7 (example smaller scale preparation): 3,5,5-trimethylhexanal (8.2074 g, 0.0577 mol) and tris(2-aminoethyl)amine (2.7882 g, 0.0191 mol) in 300 mL ethanol. Approximately 2.5 g of $NaBH_4$ and 370 mL of 3.6 M NaOH used. Reflux times of 1 hour each. ^{1}H NMR (500 MHz, $CDCl_3$, ppm): δ 0.85 (s, 27H), 0.89 (d, 9H), 0.99-1.05 and 1.16-1.22 (m, 6H), 1.25-1.34

and 1.39-1.48 (m, 6H), 1.42-1.52 (m, 3H), 2.50-2.59 (m, 12H), 2.58-2.66 (m, 6H). ^{13}C NMR (126 MHz, $CDCl_3$, ppm): δ 22.82, 27.60, 30.00, 31.06, 40.02, 47.95, 48.28, 51.40, 54.55.

Details for L7 (example larger scale preparations): 3,5,5-trimethylhexanal (16.3789 g, 0.1151 mol) and tris(2-aminoethyl)amine (5.5729 g, 0.0381 mol) in 300 mL ethanol. Approximately 5 g of $NaBH_4$ and 535 mL of 3.6 M NaOH used. Reflux times of 1 hour each. The crude product was purified by column chromatography (silica gel; 9:1 methanol:aqueous ammonium hydroxide solution (35 wt% ammonium hydroxide stock) in DCM gradient: 2 v/v% methanol solution to start then ramping up to 7-10%), dissolved in DCM, dried over magnesium sulfate and the solvent removed *in vacuo* to yield a yellow oil.

3,5,5-trimethylhexanal (88.1070 g, 0.6194 mol) and tris(2-aminoethyl)amine (27.8350 g, 0.1903 mol) in 1000 mL ethanol. Approximately 60 g of $NaBH_4$ and 1000 mL of 3.6 M NaOH used. Overnight refluxes. Additional wash with 10% NaOH before water washes. The crude product was purified by column chromatography (silica gel; 9:1 methanol:aqueous ammonium hydroxide solution (35 wt% ammonium hydroxide stock) in DCM gradient: 2 v/v% methanol solution to start then ramping up to 7-10%), dissolved in DCM, dried over magnesium sulfate and the solvent removed *in vacuo* to yield a yellow oil. This was deemed to still be impure by NMR and was columned again (same conditions as first column) to yield a pale yellow oil.

The purified products from these larger scale preparations were then combined into one batch. ^{1}H NMR (500 MHz, $CDCl_3$, ppm): δ 0.86 (s, 27H), 0.90 (d, 9H), 1.01-1.06 and 1.17-1.23 (m, 6H), 1.27-1.36 and 1.41-1.49 (m, 6H), 1.43-1.53 (m, 3H), 2.52-2.61 (m, 12H), 2.61-2.67 (m, 6H). ^{13}C NMR (126 MHz, $CDCl_3$, ppm): δ 22.81, 27.61, 30.01, 31.07, 39.92, 47.89, 48.22, 51.39, 54.47. ESI-MS (m/z): $[(C_{33}H_{72}N_4)+H]^+$ calculated: 525.58297; found: 525.58211. Elemental Analysis: calculated for $C_{33}H_{72}N_4$: C, 75.50; H, 13.82; N: 10.67; found. C, 75.36; H, 13.73; N, 10.57.

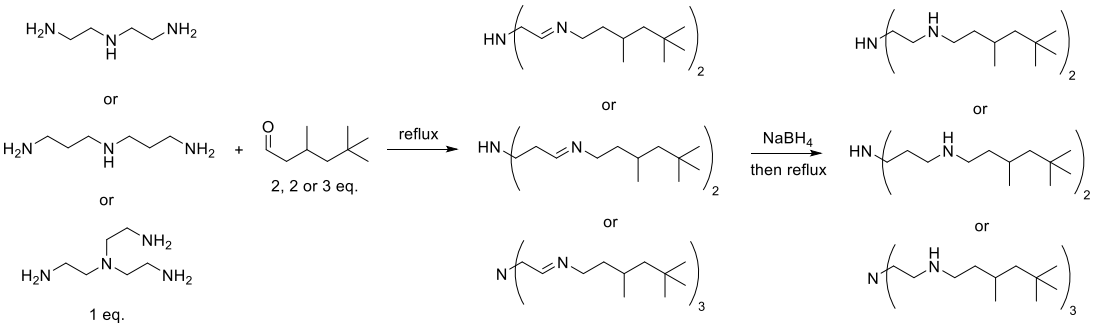

Figure 5.25. Synthesis scheme for L5, L6 and L7

6.4.2 Extractions and analysis

Metal solution preparation: The appropriate mass of Na_3RhCl_6, Na_2PtCl_6 and/or Na_3IrCl_6 was dissolved in the desired concentration of HCl or water. This solution was then either used as is or diluted to achieve the desired metal and acid concentration. All Rh-containing aqueous solutions used in the SX experiments were prepared 24 hours in advance, and used within 48 hours of preparation.

Organic solution preparation: The appropriate mass of extractant was dissolved in organic solvent.

Solvent extraction procedure: Chapter 2 Section 2.2.1 describes the general solvent extraction procedure. For specific details of each extraction see corresponding section below.

ICP-OES analysis: The metal content of the aqueous and organic phases was determined via organic ICP-OES analysis. See Chapter 2 Section 2.2.2 for details.

6.4.2.1 Test extraction conditions

0.1 M amine or 0.1 M amine and 0.1 M PA in toluene or chloroform was contacted (for 60 minutes) with 0.01 M Na_3RhCl_6 in 6 M HCl solution.

6.4.2.2 Extraction of Rh with varying HCl concentration

0.1 M L7 or 0.1 M L7 and 0.1 M PA in chloroform was contacted (for 60 minutes) with 0.01 M Na_3RhCl_6 in 0-11 M HCl solutions.

6.4.2.3 Extraction of Rh with L7 with varying time

0.1 M L7 in chloroform was contacted with 0.01 M Na_3RhCl_6 in 6 M HCl solution for varying amounts of time (1 minute to 24 hours).

6.4.2.4 Extraction of varying Rh concentration with L7 and water content measurements

0.1 M L7 in chloroform was contacted (for 60 minutes) with 0.0005-0.5 M Na_3RhCl_6 in 6 M HCl solutions.

The organic phases were analysed in duplicate for their water content by KF titration (see Chapter 2 Section 2.2.3 for details).

6.4.2.5 Stripping of Rh after extraction with L7

The loaded organic phase was prepared by contacting (for 60 minutes) 0.1 M L7 in chloroform with 0.01 M Na_3RhCl_6 in 6 M HCl solution. Stripping was then done by contacting (for 60 minutes) the loaded organic with water, 0.5 M thiourea, 10 M HCl, 10 M HNO3, 0.5 M NaOH and 28% ammonium hydroxide solutions.

This was then repeated, with the loaded organic prepared in the same way as before, and the stripping done with 5 M NaOH and 0.5, 1, 3 and 5 M ammonium hydroxide solutions.

6.4.2.6 Recyclability of L7

The loaded organic phase was prepared by contacting (for 60 minutes) 0.1 M L7 in chloroform with 0.01 M Na_3RhCl_6 in 6 M HCl solution. Stripping was then done by contacting (for 60 minutes) the loaded organic with 3 M ammonium hydroxide solution. The stripped organic was then used again for extraction by contacting it with 0.01 M Na_3RhCl_6 in 6 M HCl solution. The stripping and re-extraction process was done five times in total.

6.4.2.7 Extraction of Pt and potential for the separation of Pt and Rh with L7

0.1 M L7 in chloroform was contacted (for 60 minutes) with 0.0005-0.1 M Na_3RhCl_6 in 6 M HCl solutions, 0.0005-0.1 M Na_2PtCl_6 in 6 M HCl solutions, and 0.0005-0.05 M Na_3RhCl_6 and 0.0005-0.05 M Na_2PtCl_6 in 6 M HCl solutions.

6.4.2.8 Extraction of Ir with L7

0.1 M L7 in chloroform was contacted (for 60 minutes) with 0.001 and 0.01 M Na_3IrCl_6 in 6 M HCl solutions.

6.4.2.9 ESI-MS of the Rh L7 LOs

0.1 M L7 in chloroform was contacted (for 60 minutes) with 0.01 M Na_3RhCl_6 in 0 M HCl and 6 M HCl solutions.

The loaded organic phases were analysed by ESI-MS within 48 hours of the extraction being carried out (see Chapter 2 Section 2.2.5 for details).

6.5 References

1. Cox, M., Solvent Extraction in Hydrometallurgy. In *Solvent Extraction Principles and Practice*, 1st ed.; Rydberg, J.; Claude, M.; Choppin, G. R., Eds. Taylor & Francis: New York, USA, 1992; pp 357-412.
2. Crundwell, F. K.; Moats, M. S.; Ramachandran, V.; Robinson, T. G.; Davenport, W. G., Chapter 37 - Refining of the Platinum-Group Metals. In *Extractive Metallurgy of Nickel, Cobalt and Platinum Group Metals*, Crundwell, F. K.; Moats, M. S.; Ramachandran, V.; Robinson, T. G.; Davenport, W. G., Eds. Elsevier: Oxford, 2011; pp 489-534.
3. Geswindt, T. E. Chemical speciation of RhIII complexes in acidic, halide-rich media by means of ^{103}Rh NMR spectroscopy : the importance of speciation in the selective separation and recovery of rhodium. Stellenbosch University, 2013.
4. Doidge, E. D. Designing reagents for the solvent extraction of critical metal resources. University of Edinburgh, 2018.
5. Sánches-Loredo, M. G.; Wenzel, M.; Gloe, K.; Gloe, K.; Grote, M.; Holdt, H.-J.; Kelling, A. In *Polyamines as oxoanion and chlorocomplex receptors*, International Solvent Extraction Conference, 2008; pp 1049-1055.
6. Zipp, S. G.; Madan, S. K., *Inorg. Chim. Acta* **1975,** *14*, 83-6.
7. Frank, W.; Reiss, G. J., *Inorg. Chem.* **1997,** *36*, 4593-4595.
8. Frank, W.; Reiß, G. J., *Chem. Ber.* **1996,** *129*, 1355-1359.
9. Frank, W.; Reiss, G. J.; Kleinwaechter, I., *Z. Anorg. Allg. Chem.* **1996,** *622*, 729-33.
10. Bujak, M.; Frank, W., *Z. Kristallogr. NCS* **2014,** *229*, 147-148.
11. Bujak, M.; Frank, W., *Z. Kristallogr. NCS* **2014,** *229*, 297-298.
12. Hahn, T.; Frank, W., *Acta Crystallogr. E* **2008,** *64*, m257.
13. Gillard, R. D.; Hibbs, D. E.; Holland, C.; Hursthouse, M. B.; Abdul Malik, K. M.; Sykara, G., *Polyhedron* **1996,** *15*, 225-232.
14. Benguerel, E.; Demopoulos, G. P.; Harris, G. B., *Hydrometallurgy* **1996,** *40*, 135-52.
15. Afzaletdinova, N. G.; Khisamutdinov, R. A.; Bondareva, S. O.; Murinov, Y. I., *Russ. J. Inorg. Chem.* **2015,** *60*, 1583-1587.
16. Afzaletdinova, N. G.; Murinov, Y. I.; Khazhiev, S. Y.; Bondareva, S. O.; Muslukhov, R. R., *Russ. J. Inorg. Chem.* **2010,** *55*, 460-467.
17. Narita, H.; Nicolson, R. M.; Motokawa, R.; Ito, F.; Morisaku, K.; Goto, M.; Tanaka, M.; Heller, W. T.; Shiwaku, H.; Yaita, T.; Gordon, R. J.; Love, J. B.; Tasker, P. A.; Schofield, E. R.; Antonio, M. R.; Morrison, C. A., *Inorg. Chem.* **2019,** *58*, 8720-8734.
18. Tocher, M. I.; Whitney, D. C.; Diamond, R. M., *J. Phys. Chem.* **1964,** *68*, 368-374.
19. Narita, H.; Morisaku, K.; Tanaka, M., *Solvent Extr. Ion Exch.* **2015,** *33*, 462-471.
20. Palmer, D. A.; Harris, G. M., *Inorg. Chem.* **1975,** *14*, 1316-21.

Chapter 6

Mode of action in gold chloridometalate extraction

6 Mode of action in gold chloridometalate extraction

8.1 Introduction

8.1.1 Background

Chloride leaching is an alternative to the more toxic cyanide leaching that is used to recover an estimated 90% of gold from primary sources.[1] It is important, for both human health and the environment, to move away from the use of toxic chemicals in metal recovery. As discussed in Chapter 1, methyl isobutyl ketone (MIBK) (Figure 6.1) is an industrial reagent, used by Matthey Rustenberg Refiners, for the SX of gold from chloride solutions.[2] Despite being used on an industrial scale, little is actually known about how MIBK achieves gold extraction at the atomistic level, as is also the case with other industrially employed "solvating"[2] reagents, e.g. dibutyl carbitol. This information is key to the improvement of extraction processes for the recovery of Au from chloride solution. It has been stated that reagents such as MIBK operate via the mechanism given in Equations 6.1 and 6.2 (where waters of hydration – said to be one to four – are omitted).[3]

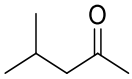

MIBK

Figure 6.1. Structure of methyl iso-butyl ketone (MIBK).

$$R_2O_{(org)} + HCl_{(aq)} \rightleftharpoons [R_2O(H_3O)^+Cl^-]_{(org)} \quad \textbf{6.1}$$

$$[AuCl_4]^-_{(aq)} + [R_2O(H_3O)^+Cl^-]_{(org)} \rightleftharpoons [R_2O(H_3O)^+AuCl_4^-]_{(org)} + Cl^-_{(aq)} \quad \textbf{6.2.}$$

This suggests that the extractant molecules themselves are not protonated, presumably due to their weakly basic nature, and that water is required to be extracted to transport the anion to the organic phase. However, work done with amides, which are also relatively weak bases, has suggested that such molecules can protonate in the extraction of $[AuCl_4]^-$.[4, 5] Therefore, there are a variety of possible structures for the positively charged entity which may be present in the organic phase following extraction (see Figure 6.2), ranging from the ketone or a water molecule being the H^+ charge carrier, and the absence, or presence, of a small

number of water molecules. Similar structures have been proposed for other extractants (notably DBC[3] and TBP[6]) by others.

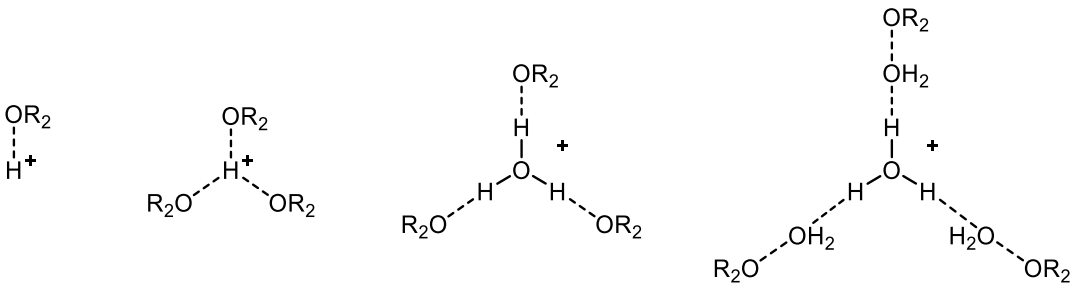

Figure 6.2. Possible models for the positively charged counter ion in the extraction of $[AuCl_4]^-$ by MIBK.

The presence of water in the organic phase following extraction could mean that a reverse micelle-type mechanism is occurring. It is possible that the $[AuCl_4]^-$ anion and/or the hydronium cation (if it is present) is surrounded by a "pool" of associated water molecules. Figure 6.3 gives an illustration of possible assemblies forming in the organic phase, depending on the location of the proton (on an extractant molecule or a water molecule) and whether or not the ions are hydrated. It is also likely that some chloride will be extracted into/HCl will be solubilised in the organic phase, due to the high concentrations of HCl in the aqueous phase. It is of interest to determine the structure of assemblies containing chloride, which could also be of one of the forms shown in Figure 6.3.

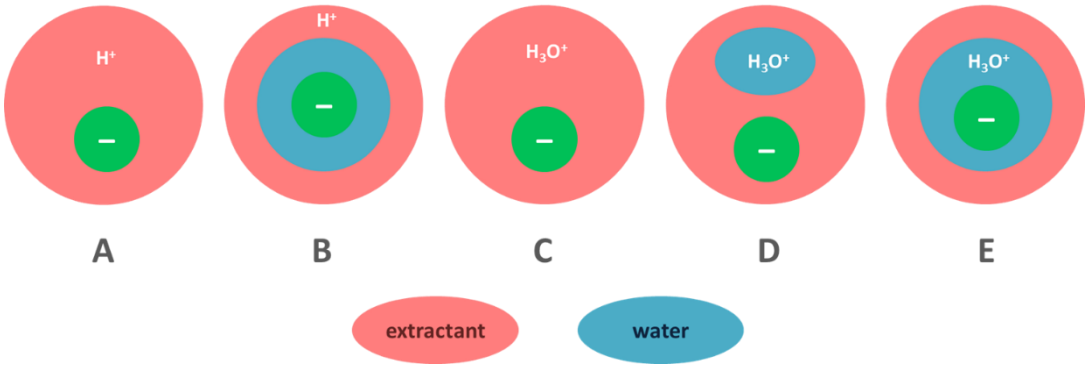

Figure 6.3. Models for the possible modes of extraction occurring in the extraction of an anion by MIBK. A: protonated extractant associating with anion; B: protonated extractant associating with hydrated/water-solvated anion; C: hydronium cation associating with anion; D: hydrated/water-solvated hydronium cation associating with anion; and E: hydrated/water-solvated hydronium cation associating with hydrated/water-solvated anion, all with surrounding neutral extractant molecules. Note that the ions many be closely associated with one another or have neutral MIBK molecules or water molecules in between.

8.1.2 Scope of this work

This work aims to elucidate the mode(s) of extraction of $[AuCl_4]^-$ by MIBK using classical molecular dynamics (MD) simulations. In this way, the formation of organic assemblies can be simulated and the effect of changing the positive charge carrier and the concentration of water present can be explored.

The results of experimental work, in the form of extraction experiments and analysis of the water content of the organic phase, and existing experimental data provide information which guide realistic model construction for the simulations. However, simulation also offers the opportunity to explore non-realistic models and, in this way, the role water plays, if any, in the extraction of gold with this commercial reagent can be explored in ways that would be impossible experimentally.

8.1.3 Aims

The aims of this work are to:

i. Experimentally determine the water content of the organic phase post extraction
ii. Classically model the extraction of $[AuCl_4]^-$ with MIBK at varying levels of water and with protonated extractant or hydronium cation
iii. For comparison, classically model the extraction of chloride with MIBK
iv. Compare the modes of action demonstrated

8.2 Results and discussion

8.2.1 Contributions to this work

The work presented in this chapter was partly carried out by two final year undergraduate project students, under the supervision of the author of this thesis. Their project reports are included in the SI. In addition, many of the data analysis tools employed here were developed by other PhD students at the University of Edinburgh. The contributions to the work are detailed below.

Work carried out by the author of this thesis:

- MD modelling.
- Script modification and some script development.
- Data analysis.

Work carried out by other contributors:

- KF titrations, protonation site calculations, and MIBK parameter selection and test MD modelling by Álvaro Gallego Jurado (University of Edinburgh MChem project student).
- Script development by Kirstian MacRuary and Innis Carson (previous University of Edinburgh PhD students), Álvaro Gallego Jurado (University of Edinburgh MChem project student) and Michael Kennealy (University of Edinburgh BSc project student).

8.2.2 Experimental phase composition

Although a variety of water concentrations will be modelled to better assess the role of water in extraction, it is important to know the actual concentration of water in the organic phase. Therefore, a series of extractions were carried out and KF titrations of the organic phase were conducted, with results shown in Table 6.1.

The water content of MIBK as received is less than 0.02 M and after contact with an aqueous phase the water content of the organic phase has increased. The highest water content is

observed in the organic that has been contacted with water. The organic phases contacted with 6 M HCl and 0.01 M Au in 6 M HCl are lower, likely as it is unfavourable to concentrate the 6 M HCl solutions by removing water. A slightly higher water content is observed after contact with the Au containing HCl solution compared to HCl alone, suggesting additional water is taken over into the organic phase upon Au extraction. This may indicate that water is required to be taken into the organic phase for $[AuCl_4]^-$ extraction to occur, either as part of a reverse micelle-type assembly or as the positively charged species (i.e. water is present as a hydronium ion). However, it should be noted that there may be an error in the water concentration obtained when Au(III) is present, as it may be reduced in the titration cell and affect the value obtained.[6]

Table 6.1. Water content of MIBK organic phases contacted with different aqueous phases, and translation into the number of water molecules required in a cubic box length 55 Å to achieve the desired ratio of water molecules to Au(III).

Aqueous phase composition	**Organic phase water content**		**No. water molecules in simulation box** (to nearest whole number)
	/ %wt	**/ M**	
No aqueous phase contact	0.040(2)	0.0178(9)	2
H_2O	1.868(18)	0.830(8)	83
6 M HCl solution	1.008(5)	0.448(2)	45
0.01 M Au in 6 M HCl solution	1.124(4)	0.499(2)	50

The concentration of Au in the organic phase is likely to be approximately 0.01 M, as Doidge showed that neat MIBK is able to extract approximately 100% of Au from a 0.01 M Au in 6 M HCl solution.[5] (Note: the Au concentration could not be determined at the time the work presented in this chapter was performed due to ICP-OES instrument failure).

For the purposes of the MD simulations an Au(III) concentration of 0.01 M is assumed which translates into one $[AuCl_4]^-$ metalate anion in a cubic box of length 55 Å, filled with 800 explicit MIBK molecules to match the experimental solvent density.

The water contents of the organic phases can be also converted to the number of water molecules in a particular volume. Table 6.1 also gives the water contents as the number of water molecules per cubic box length 55 Å. For the purposes of the MD simulations, 50 water molecules is assumed to be the “experimental” water content and is used in the simulations. Additional water contents of zero, 24 (arbitrary, lower than experimental content), and 100

(double the experimental content) water molecules per cubic box length 55 Å are also simulated.

8.2.3 Protonation site calculations

While there is no direct evidence in the literature that the charge-balancing species in $[AuCl_4]^-$ extraction by extractants such as MIBK is the hydronium cation, it is suggested often.[3, 7, 8] As discussed in Chapter 1, where the extractant is an "oxygenated organic"[3] type molecule, i.e. with an oxygen-based functional group, water is commonly found to be extracted/taken up by the organic phase and it is possible that the proton which balances the charge of the Au metalate will be solvated by this water.

In order to explore theoretically the most favourable position of the proton, QM geometry optimisation calculations were carried out. The input models consisted of an MIBK molecule, a water molecule and an additional proton, either located on the MIBK molecule, the water molecule, or placed between the two molecules. Following geometry optimisation, it is found, for all inputs, that the proton is located on the MIBK molecule but there is a clear hydrogen bond to the water molecule (see Figure 6.4 for an example).

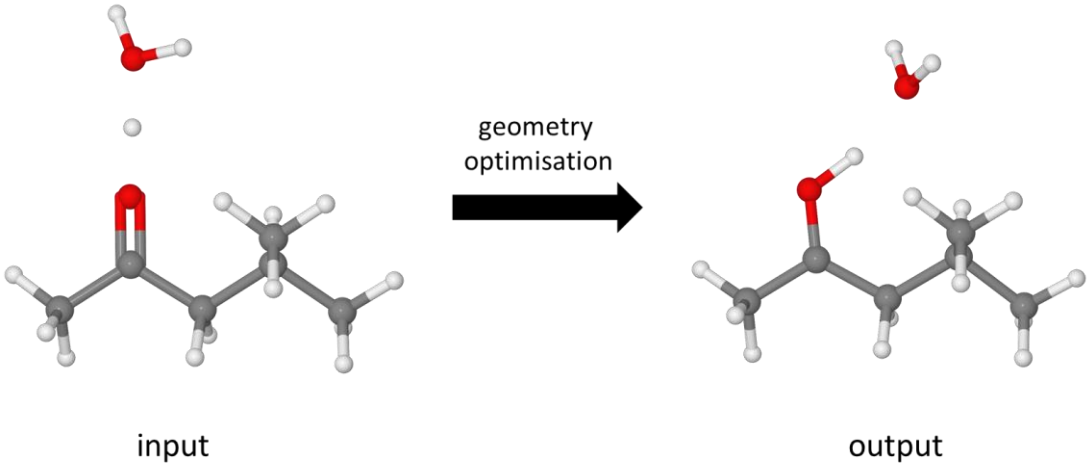

Figure 6.4. Example geometry optimisation input and output where the proton resides on the extractant and the water molecule is not protonated. All structures are given in the SI.

The calculations just described are of course limited in scope, as stabilisation effects from other MIBK molecules or water molecules have not been included. This, along with the literature which assumes that water acts as the proton carrier, necessitates the need to consider both options. As classical MD simulations do not allow for bond breaking and forming to be modelled the position of the proton must be explicitly defined and will not change over the course of the simulation. To this end it is therefore necessary that the simulations be carried out in two sets, where an extractant or a water molecule acts as the proton carrier, respectively.

8.2.4 MD simulations

MD simulations were carried out for a variety of systems, to include both protonated MIBK or hydronium as the cation, various water levels, and chloride as an alternative anion. Table 6.2 gives a list of the simulation runs conducted and Section 6.4.3.2 provides the method details.

8.2.4.1 Experimental water content

Simulations matching the experimental water content (50 water molecules in the box) represent the baseline model in the MD simulations performed. Due to the uncertainty in the identity of the cation, simulations with both a protonated MIBK or a hydronium ion were carried out. Figures 6.5 through 6.8 display data analysis in relation to the coordination shell around $[AuCl_4]^-$, and H_3O^+ / the $MIBKH^+$ cation. This model was run in duplicate to ensure convergence of results; analysis for the second data set (which was concurrent with the first) is available in the SI. The “coordination” shell cut-offs shown are determined from the analysis done (see Section 6.4.4. for details) and allow the production of example coordination shell images from representative frames from the simulation (note: the more fluctional the behaviour of the system, the less representative this coordination shell example will be; in all cases a best attempt at capturing the average behaviour has been made).

Table 6.2. Details of the simulations carried out. All run as periodic boundary conditions on a cubic box of starting length 55 Å.

Simulation code	Run	Box contents / number of molecules					
		$[AuCl_4]^-$	Cl^-	H_3O^+	$MIBKH^+$	MIBK	Water
A	1	1	0	1	0	799	0
	2	1	0	1	0	799	0
B	1	1	0	1	0	799	23
	2	1	0	1	0	799	23
C	1	1	0	1	0	799	49
	2	1	0	1	0	799	49
D	1	1	0	1	0	799	99
	2	1	0	1	0	799	99
E	1	1	0	0	1	800	0
	2	1	0	0	1	800	0
F	1	1	0	0	1	800	1
	2	1	0	0	1	800	1
G	1	1	0	0	1	800	24
	2	1	0	0	1	800	24
H	1	1	0	0	1	800	50
	2	1	0	0	1	800	50
I	1	1	0	0	1	800	100
	2	1	0	0	1	800	100
J	1	0	1	1	0	799	0
	2	0	1	1	0	799	0
K	1	0	1	1	0	799	23
	2	0	1	1	0	799	23
L	1	0	1	1	0	799	49
	2	0	1	1	0	799	49
M	1	0	1	1	0	799	99
	2	0	1	1	0	799	99
N	1	0	1	0	1	800	0
	2	0	1	0	1	800	0
O	1	0	1	0	1	800	1
	2	0	1	0	1	800	1
P	1	0	1	0	1	800	24
	2	0	1	0	1	800	24
Q	1	0	1	0	1	800	50
	2	0	1	0	1	800	50
R	1	0	1	0	1	800	100
	2	0	1	0	1	800	100

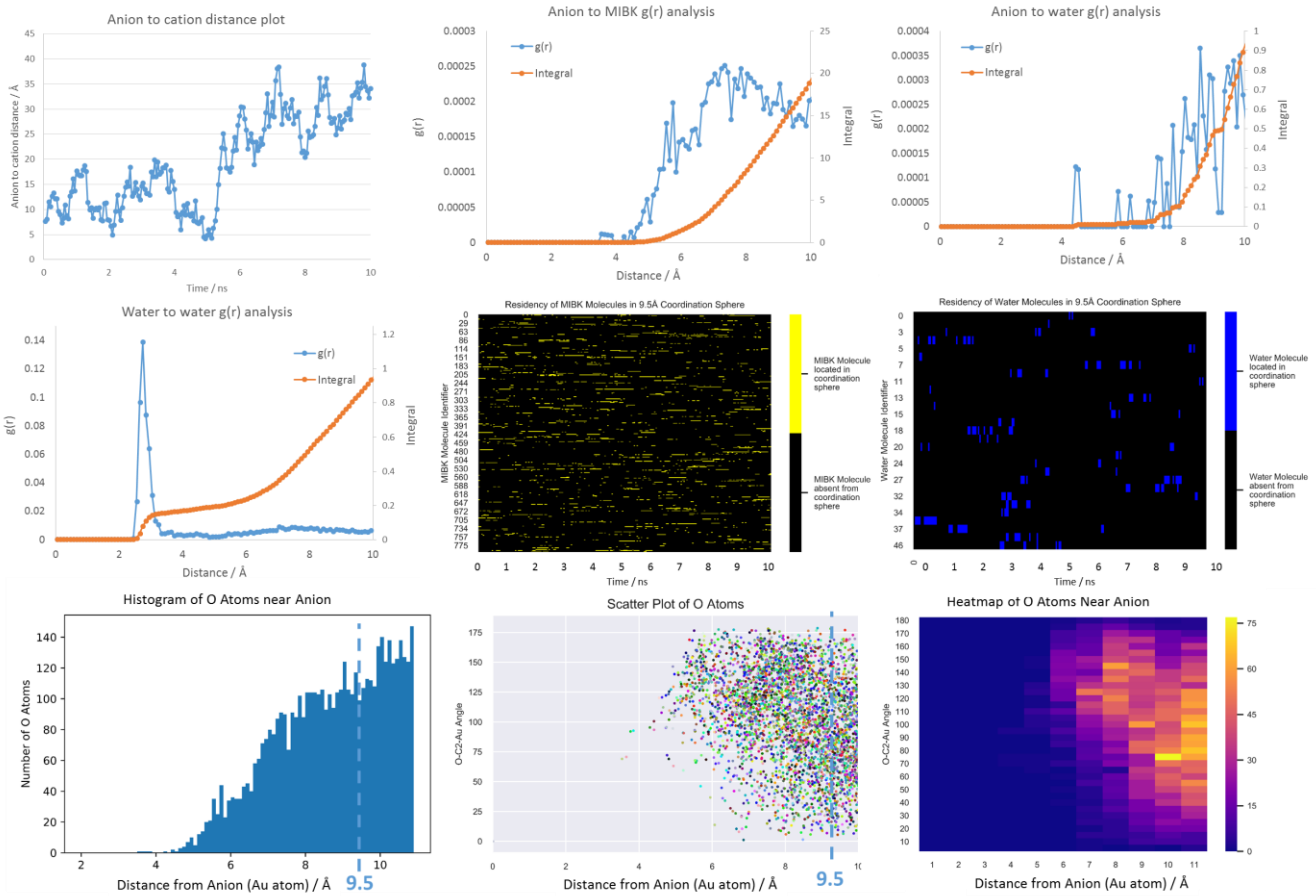

Figure 6.5. Coordination environment of $[AuCl_4]^-$ (simulation C run 1). Left to right, top to bottom: anion (Au atom) to cation (hydronium O atom) distance plot; anion (Au atom) to MIBK (O atom) g(r) analysis plots; anion (Au atom) to water (O atom) g(r) plots; water (O atom) to water (O atom) g(r) plots; MIBK residency around anion plot; water residency around anion plot; histogram of MIBK O atom distance to anion (Au atom); scatter plot of size of angle MIBK carbonyl groups makes to Au atom with distance from the anion; and heat map of the former. All for the $[AuCl_4]^-$ and H_3O^+ system with 49 additional water molecules and 800 MIBK molecules.

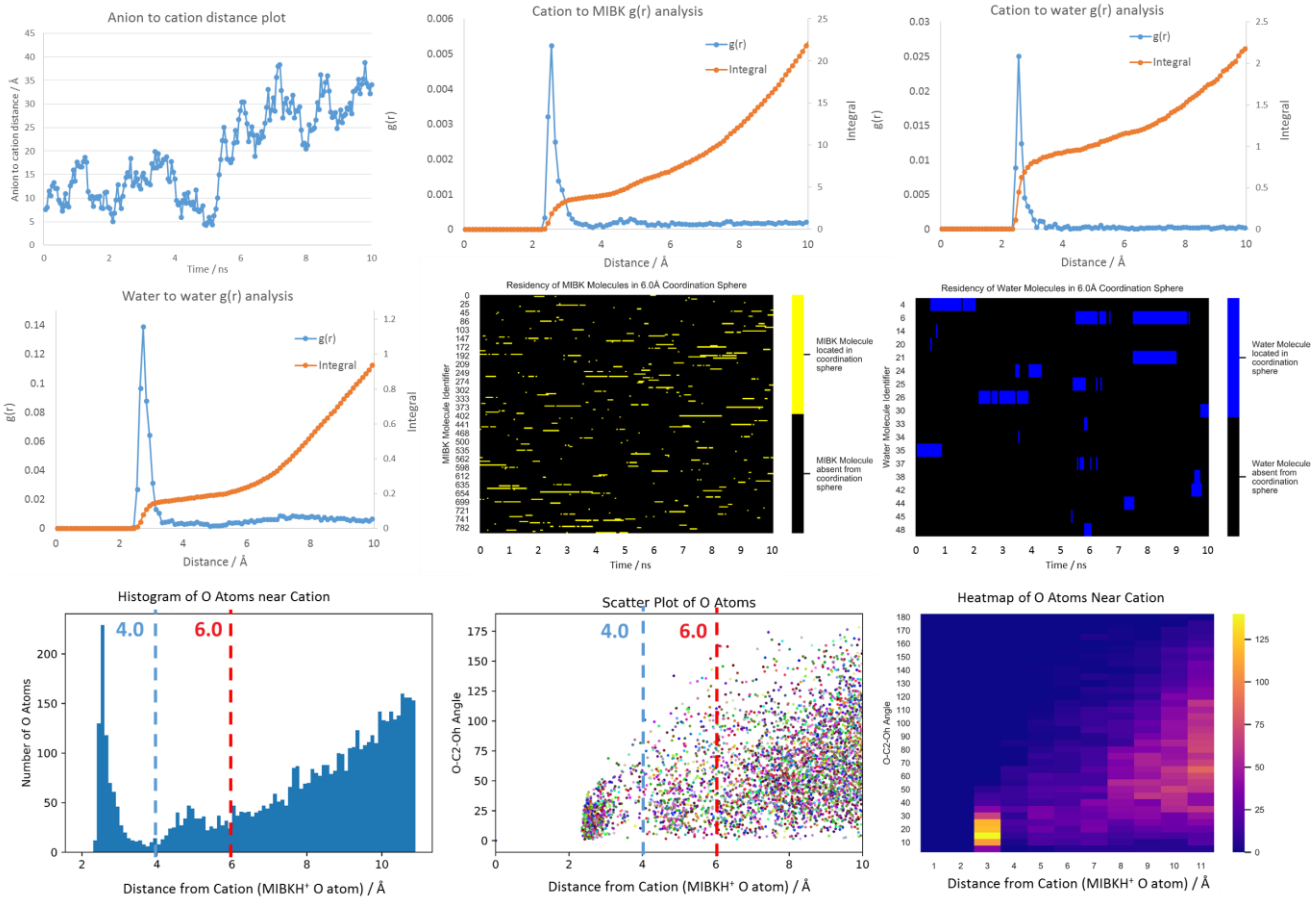

Figure 6.6. Coordination environment of H_3O^+ (simulation C run 1). Left to right, top to bottom: anion (Au atom) to cation (hydronium O atom) distance plot; cation (H_3O^+ O atom) to MIBK (O atom) g(r) analysis plots; cation (H_3O^+ O atom) to water (O atom) g(r) plots; water (O atom) to water (O atom) g(r) plots; MIBK residency around cation plot; water residency around cation plot; histogram of MIBK O atom distance to cation (H_3O^+ O atom); scatter plot of size of angle MIBK carbonyl groups makes to H_3O^+ O atom with distance from the cation; and heat map of the former. All for the $[AuCl_4]^-$ and H_3O^+ system with 49 additional water molecules and 800 MIBK molecules.

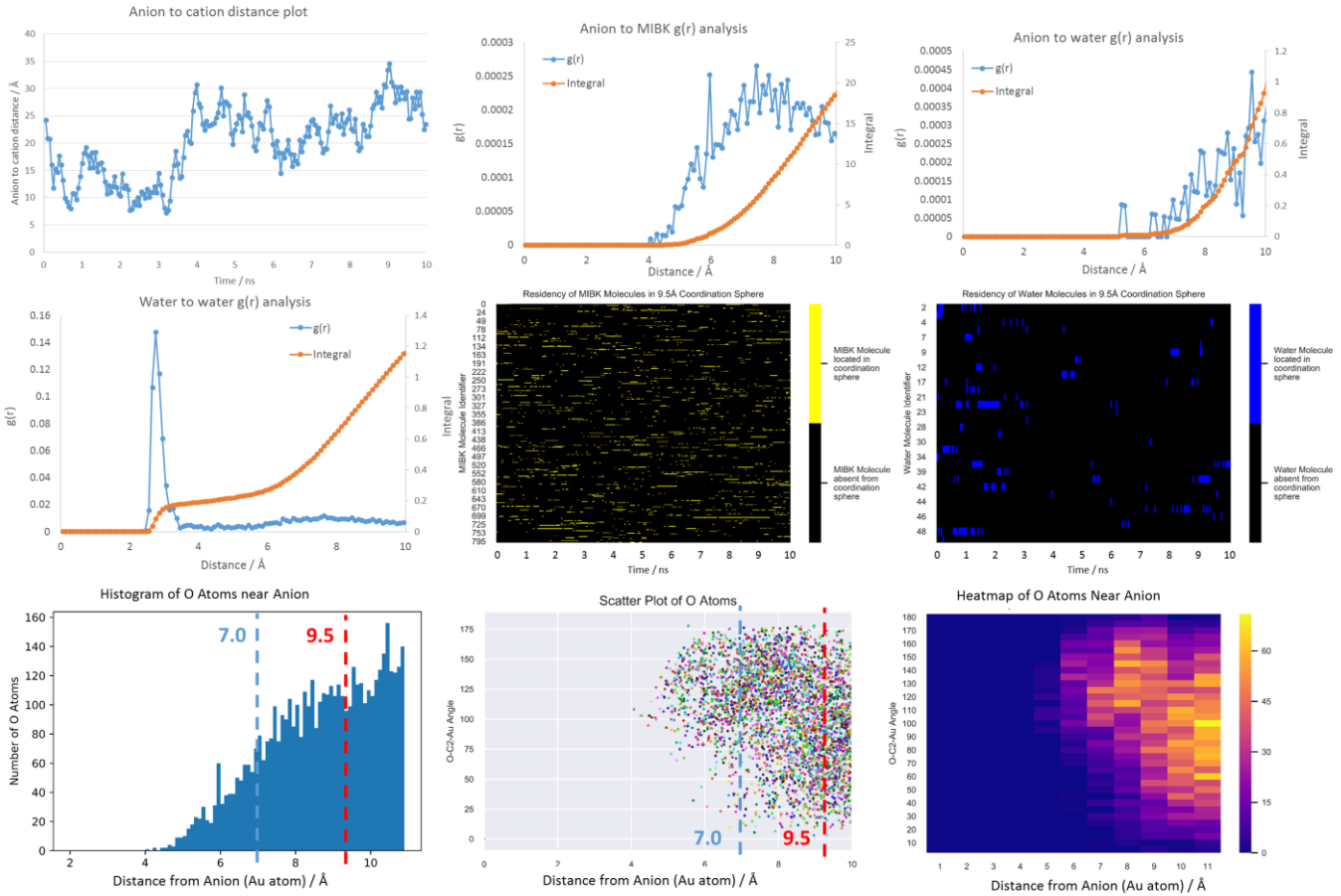

Figure 6.7. Coordination environment of $[AuCl_4]^-$ (simulation H run 1). Left to right, top to bottom: anion (Au atom) to cation ($MIBKH^+$ O atom) distance plot; anion (Au atom) to MIBK (O atom) g(r) analysis plots; anion (Au atom) to water (O atom) g(r) plots; water (O atom) to water (O atom) g(r) plots; MIBK residency around anion plot; water residency around anion plot; histogram of MIBK O atom distance to anion (Au atom); scatter plot of size of angle MIBK carbonyl groups makes to Au atom with distance from the anion; and heat map of the former. All for the $[AuCl_4]^-$ and $MIBKH^+$ system with 50 water molecules and 799 neutral MIBK molecules.

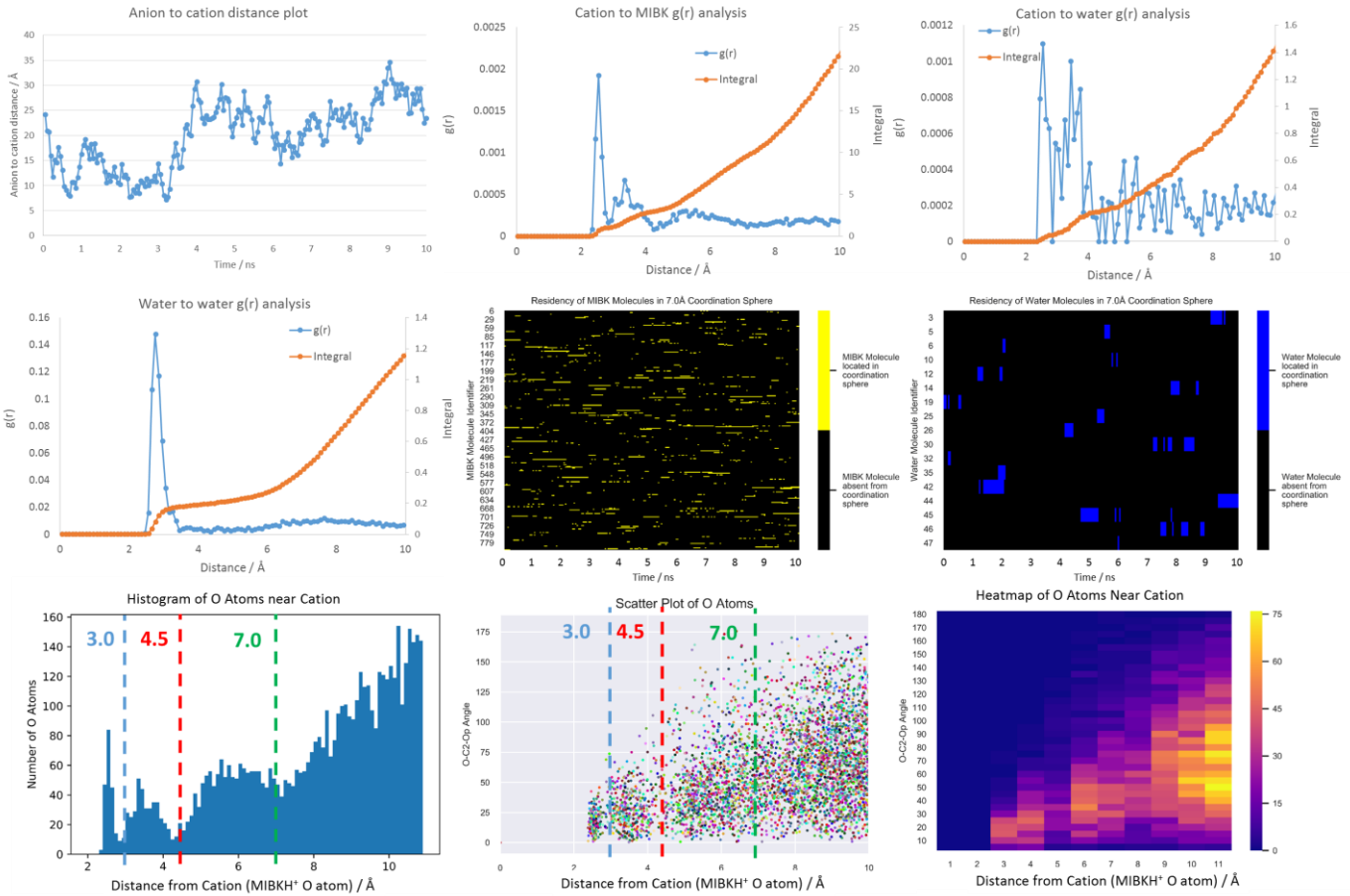

Figure 6.8. Coordination environment of $MIBKH^+$ (simulation H run 1). Left to right, top to bottom: anion (Au atom) to cation ($MIBKH^+$ O atom) distance plot; cation ($MIBKH^+$ O atom) to MIBK (O atom) g(r) analysis plots; cation ($MIBKH^+$ O atom) to water (O atom) g(r) plots; water (O atom) to water (O atom) g(r) plots; MIBK residency around cation plot; water residency around cation plot; histogram of MIBK O atom distance to cation ($MIBKH^+$ O atom); scatter plot of size of angle MIBK carbonyl groups makes to $MIBKH^+$ O atom with distance from the cation; and heat map of the former. All for the $[AuCl_4]^-$ and $MIBKH^+$ system with 50 water molecules and 799 neutral MIBK molecules.

Example coordination shells are given in Figures 6.9 and 6.10 for the anions and cations of the two systems, showing the structure around the ions. It is found that, in general, the anion ($[AuCl_4]^-$) and the cation (either H_3O^+ or $MIBKH^+$) do not associate closely with one another during the simulations runs, as illustrated by the absence of the anion and cation from one another's coordination shells. As can be seen from the plots of anion to cation distance (top left panel in Figures 6.7 and 6.9), although the ions do come close to one another at some points, they do not aggregate as a tightly bound ion-pair. Instead, the "ion-pair" is much more dynamic. This is unusual as in most extraction simulations the ions are found to aggregate, such as in the MD simulations presented in the work of MacRuary et al.[9] and Doidge et al.[4] for precious metal chloridometalate extraction. However, these simulations differ from previous systems investigated in that the extractant molecules are also the solvent. Typical (commonly aliphatic or aromatic hydrocarbon) solvent molecules would be less likely to interact with the ions or polar extractant molecules, thus favouring a more tightly associated ion-pair aggregate. Therefore, in this system, the presence of a fluctional ion-pair may arise because MIBK molecules compete to interact with an ion.

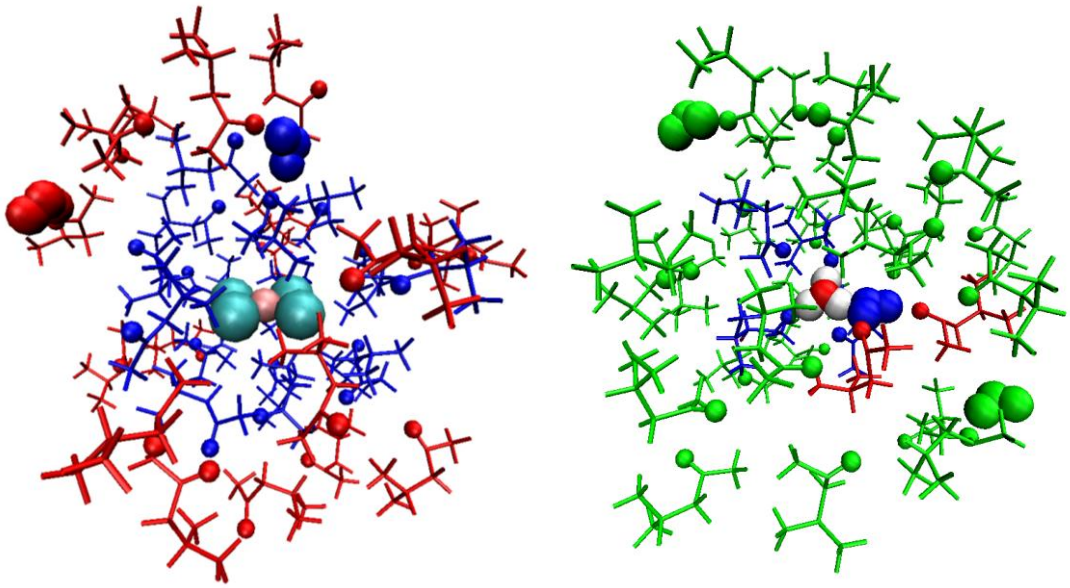

Figure 6.9. Anion (left) and cation (right) coordination shells for the $[AuCl_4]^-$ and H_3O^+ system with 49 additional water molecules and 800 MIBK molecules. Anion coordination shell cut-offs are 9.5 (blue) and 12.0 Å (red); cation cut-offs are 4.0 (blue), 6.0 (red) and 11.0 Å (green). $[AuCl_4]^-$, H_3O^+, H_2O and MIBK O atoms are displayed as spheres (with the latter of a smaller radius) for clarity.

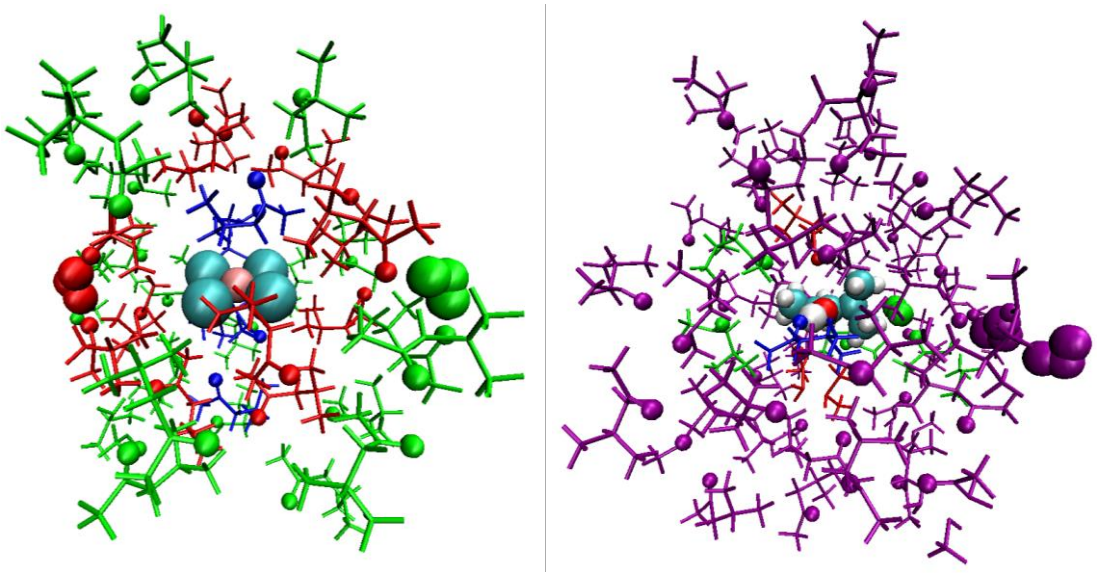

Figure 6.10. Anion (left) and cation (right) coordination shells for the $[AuCl_4]^-$ and $MIBKH^+$ system with 50 water molecules and 799 neutral MIBK molecules. Anion coordination shell cut-offs are 7.0 (blue), 9.5 (red) and 12.5 (green) Å; cation cut-offs are 3.0 (blue), 4.5 (red), 7.0 (green) and 12.5 Å (purple). $[AuCl_4]^-$, $MIBKH^+$, H_2O and neutral MIBK O atoms displayed as spheres (with those of $MIBKH^+$ and MIBK O of smaller radii) for clarity.

MIBK molecules appear to interact with the anion via C-H…anion interactions, or dispersion interactions, as seen in the coordination shell images shown in Figures 6.9 and 6.10, where the carbonyl groups generally face away from the $[AuCl_4]^-$ metalate. This is also illustrated by the large angles seen in the scatter plots and heatmaps in Figures 6.5 and 6.7 (bottom middle and right panels, respectively), which show the carbonyl group is pointing away from the anion.

MIBK molecules are likely to associate more strongly with the cation, with which it can form hydrogen bonds, than the $[AuCl_4]^-$ metalate anion. Certainly, it appears very common for the cation to form hydrogen bonds with the MIBK molecules, as seem from the g(r) plots presented in Figure 6.6 and 6.8 (top middle panel). This is also indicated in the scatter plots and heatmaps in Figures 6.6 and 6.8 (bottom middle and right panels, respectively), where a clear cluster of MIBKs with their carbonyl groups making a small angle (indicating that the O atom is pointing towards the cation) can be seen. The H_3O^+ cation has, on average, two to three MIBK O atoms closely interacting, i.e. one hydrogen bonded to each of the three H atoms (as shown in Figure 6.11), or two bonding if a water molecule is hydrogen bonded to one of the H atoms, as pictured in the example coordination shell (see right image in Figure

6.9). Protonated MIBK has, on average, one MIBK O atom closely interacting, as pictured in the example coordination shell (see right image in Figure 6.10).

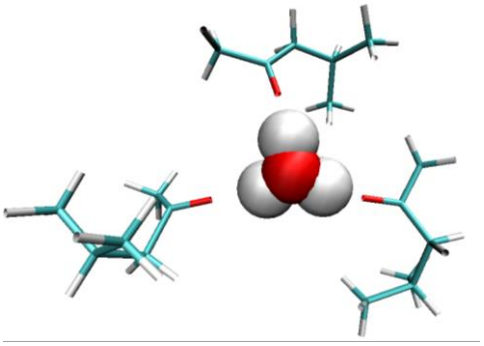

Figure 6.11. Molecule selection from simulation frame showing H_3O^+ hydrogen bonded to three MIBK molecules. Frame selected from simulation C run 1.

It is not just the anion to cation interaction which appears to be variable; the MIBK system as a whole is dynamic. This is portrayed in the residency plots in Figures 6.5 and 6.7 (central panel), where the identity of the MIBK molecules closest to the ions is constantly changing. In these plots, colour (yellow or blue) indicates that a molecule is considered "associated" with the ion (within the defined coordination shell cut-off, see Section 6.4.4 for details), while black indicates that that molecule is not present in the coordination shell. The absence of long streaks of colour shows that few MIBK molecules are associated for a significant period of time. This is, perhaps, unsurprising as MIBK is a relatively small molecule (high diffusion rate) which only possess a hydrogen bond donor group, and thus cannot hydrogen bond to itself. Therefore, MIBK molecules will not strongly associate with one another and all the MIBK molecules will compete for the stronger interactions with the cation and water molecules, the latter which can act as a hydrogen bonding bridge between MIBK molecules. Although water is present at significant levels according to experiment, the number of water molecules is still very much lower than the number of MIBK molecules in the system (50 vs 800). Most of the molecule-to-molecule interactions will be MIBK-to-MIBK, and the small molecule size will likely enable more freedom of movement.

Although the water content in the system is relatively high, reverse micelles do not appear to form. The water concentration in the organic phase is comparable to that reported by MacRuary et al. for the extraction of chloride and $[PtCl_6]^{2-}$ by TBP in toluene where reverse

micelles were observed in modelling simulations.[9] While water molecules are found within the coordination shells around $[AuCl_4]^-$ immersed in MIBK (Figure 6.9 and 6.10), water does not from a mediating layer between the extractant molecules and the anion, as would be expected in a reverse micelle. Instead, a few water molecules are found in the inner-coordination shell and a few more in the outer-coordination shell (as defined by the cut-offs chosen, see Section 6.4.4. for more details).

Water is found to interact more significantly with the cation than the anion, particularly in the case of H_3O^+, where the average number of water molecules in the inner coordination shell is approximately 0.7 (average of the two simulation runs, see top right panel in Figure 6.6 for C run 1 and representative snapshot in Figure 6.9). With $MIBKH^+$ as the cation, the average number of water molecules close to the cation is closer to zero (as can be seen from a comparison of the cation to water g(r) plots in Figures 6.6 and 6.8), but still slightly greater than found for the anion.

Interestingly the water molecules do not appear to aggregate significantly at all, as seen from the g(r) plots in the centre left panels in Figures 6.6 and 6.8. Some water molecules exist as small aggregates of two or three water molecules hydrogen bonded to one another (see Figure 6.12), but many are simply hydrogen bonded to the MIBK molecules. This is the likely reason why water is so soluble in MIBK and is likely to also account for why much of the water molecules do not form a hydration pool around the ions: there are other, favourable states it can adopt in the mixture.

There is little difference in behaviour observed between the simulations with a hydronium ion or protonated MIBK acting as the cation. In both cases the cation is most commonly found bound to MIBK (see the g(r) plots top middle panel in Figures 6.6 and 6.8), though hydrogen bonds to water molecules are also often observed, more so when H_3O^+ is the cation (contrast the g(r) plots top right panel in Figures 6.6 and 6.8). That water pooling around the cation is not significantly observed is surprising, given the suggestions in the literature that the cation is likely to be hydrated in systems with extractants of this type (namely, a solvating extractant with an oxygen-base functional group).[3] However, the hydration could be as simple as the proton residing on a single water molecule,[6] such that any further water molecules are simply soluble (i.e. dispersed) in the organic phase. This would then suggest that the primary purpose of water as part of an extraction mechanism is to act as the positive charge carrier,

or to stabilise protonation on an MIBK molecule, not to allow for the formation of wet reverse micelles or to act as a mediating layer between the anion and the extractant molecules.

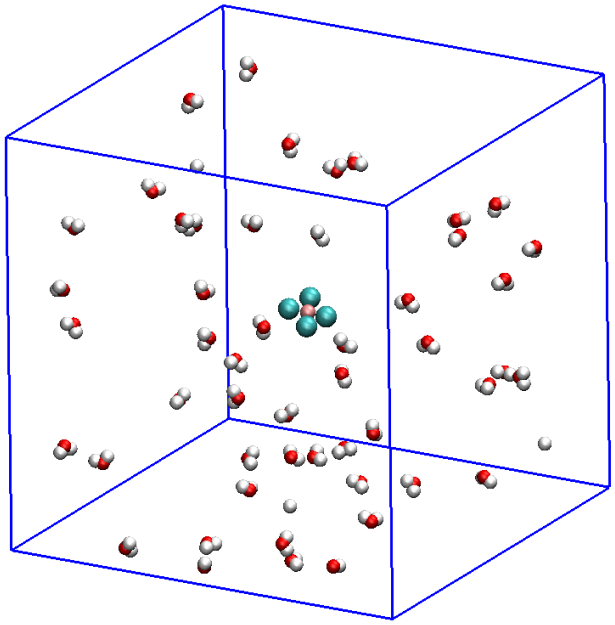

Figure 6.12. Example simulation frame showing water positioning within the simulation box. Frame selected from simulation C run 1. MIBK molecules not shown for clarity.

Loosely associated MIBK molecules appear to be able to encapsulate the anion or cation reasonably well, depending on the coordination shell considered. Porosity values (a measure of how exposed the ion is: a higher number means a higher porosity of the shell, i.e. more exposure of the ion – see Section 6.4.4 for a description of how this analysis is done) can be calculated for the coordination shells (see Table 6.3 and 6.4 for the results). Values of around 18% (considering the average porosity around the anion over the four simulations at the coordination shell of 9/9.5 Å cut-off) are found for the inner-coordination shells around the $[AuCl_4]^-$ anion. Including the outer-coordination shells (up to the 12/12.5 Å cut-offs) gives significantly lower porosity values of around 5%. The inner coordination shells for the cations give poorer encapsulation (around 34% porosity on average) but this is due to the smaller size of the shell. If the outer coordination shell (11.5-12.5 Å cut-off) is considered better porosity values of 2% on average are obtained. This contrasts with the TBP in toluene system explored by MacRuary et al. for which porosity values of over 50% were found.[9] Direct comparison is perhaps not possible, however. In the TBP system reverse micelles were found to form and the water molecules were considered part of the system requiring shielding,

rather than part which could provide shielding. In addition, the number of extractant molecules involved in the coordination shell was much more distinct (as the solvent is not the same as the extractant). However, there is still a large difference in porosity value, with the MIBK systems having significantly lower porosity, suggesting that MIBK well encapsulates the ions.

Table 6.3. Porosity values of the coordination shells (of cut-offs specified – see Section 6.4.4 for cut-off selection criteria) around $[AuCl_4]^-$ and H_3O^+. Porosity values included here are the average of the 20 simulations frames analysed and are accompanied by standard deviation error values.

Simulation	%Porosity of anion coordination shell		%Porosity of cation coordination shell		
	Cut-off 9.5 Å	Cut-off 12.0 Å	Cut-off 4.0 Å	Cut-off 6.0 Å	Cut-off 11.0 Å
C run 1	19(2)	6.0(2)	33(2)	23(2)	3.3(4)
C run 2	15(2)	4.4(4)	31(2)	18(1)	2.4(2)

Table 6.4. Porosity values of the coordination shells (of cut-offs specified – see Section 6.4.4 for cut-off selection criteria) around $[AuCl_4]^-$ and $MIBKH^+$. Porosity values included here are the average of the 20 simulations frames analysed and are accompanied by standard deviation error values. Note the difference in the cut-off used between the two simulations runs.

Simulation	%Porosity of anion coordination shell			%Porosity of cation coordination shell			
	Cut-off 6.5/7.0 Å	Cut-off 9.0/9.5 Å	Cut-off 12.0/12.5 Å	Cut-off 3.0 Å	Cut-off 4.0 Å	Cut-off 7.0 Å	Cut-off 11.5/12.5 Å
H run 1	64(1)	17(1)	4.3(3)	35(2)	20(2)	9(1)	0.7(1)
H run 2	78(2)	22.9(8)	5.0(5)	38(1)	24(3)	10(2)	1.6(4)

8.2.4.2 Alternative water concentrations

The comparison simulations at differing levels of water allow for a clearer understanding of the role water plays in the extraction, considering it appears reverse micelles do not form. From the data presented in Figure 6.13 it would seem that for the simulations with no water, very little is different, aside from the obvious absence of water molecules in the coordination shells. The ions still do not form a constant, fixed ion-pair and the MIBK molecules still exchange rapidly. Full sets of figures from the analysis are given in the SI.

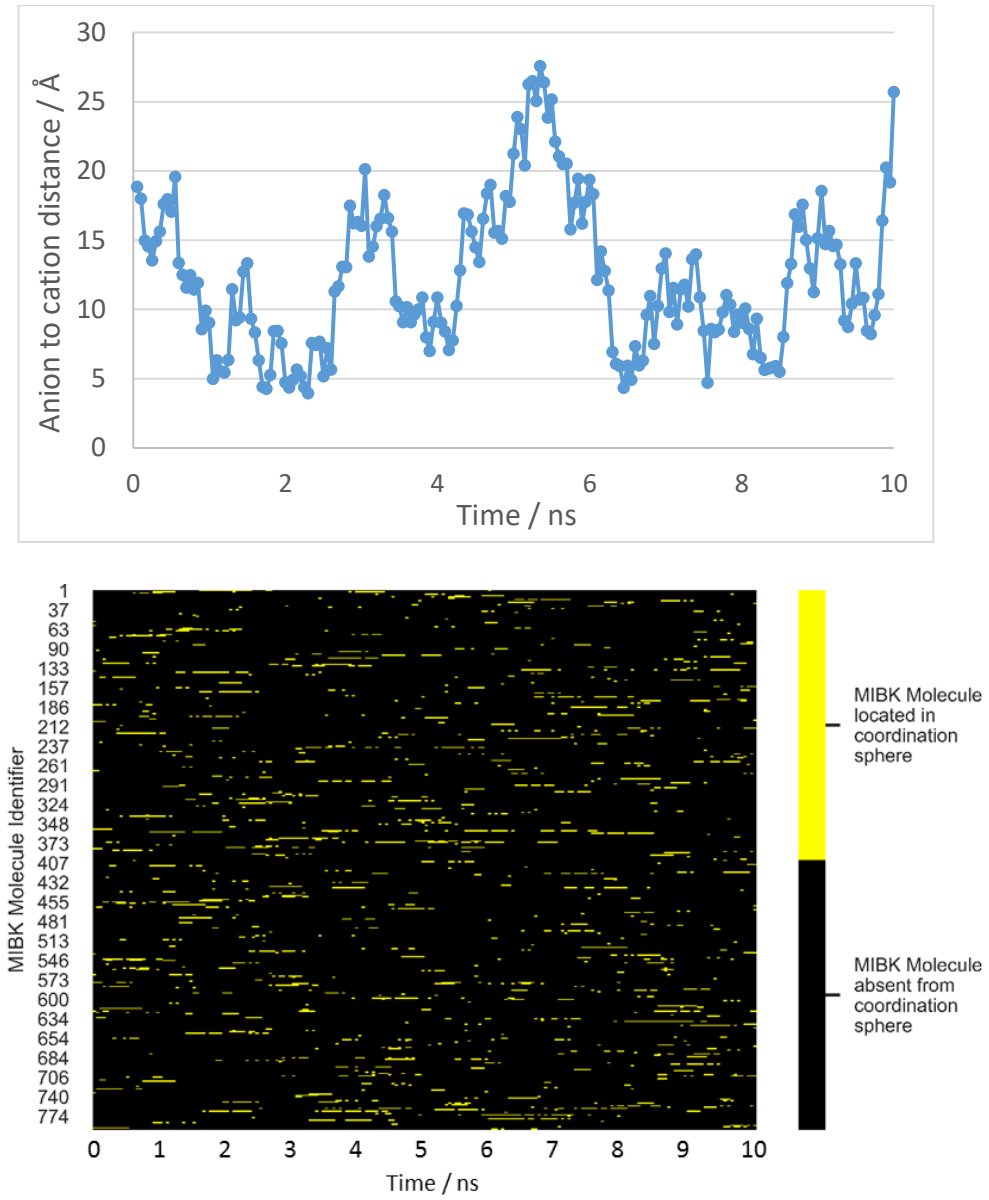

Figure 6.13. Top: Anion ($[AuCl_4]^-$) to cation ($MIBKH^+$) distance plot over time, and bottom: MIBK residency plot for 9 Å coordination shell. Both for E run 1 (1 $AuCl_4^-$, 1 $MIBKH^+$, and 800 MIBK).

For lower water content than experimental levels (i.e. 24 water molecules per simulation box), again very little difference is observed. For some frames of the simulations, water molecules do enter the $[AuCl_4]^-$ coordination shells, though to a lesser extent. There is an average 0.18 water molecules present in the coordination shell, compared to 0.71 for the experimental water concentration simulations (averages of the replicate simulations, see Table 6.5 for per-simulation data) when H_3O^+ is the cation; and 0.30, compared to 0.69, when $MIBKH^+$ is the cation (using the coordination shells from cut-offs 8.5-9.5 Å). This is likely a

simple reflection of the lower number of water molecules present in the system. Figure 6.14 provides example coordination shell images.

Table 6.5. Average number of water molecules in the coordination shells (of cut-offs specified – see Section 6.4.4 for cut-off selection criteria) around $[AuCl_4]^-$ and H_3O^+ or $MIBKH^+$. Values are obtained from the g(r) analysis.

Simulation	Anion coordination shell		Cation coordination shell	
	Cut-off / Å	Average number of water molecules	Cut-off / Å	Average number of water molecules
B run 1	8.5	0.15	4.0	0.02
B run 2	9.0	0.20	4.0	0.30
C run 1	9.5	0.64	4.0	0.94
C run 2	9.5	0.78	4.0	0.54
D run 1	9.5	1.78	3.5	1.24
D run 2	9.5	1.65	4.0	0.94
F run 1	9.0	0.00	4.5	0.00
F run 2	9.0	0.00	4.5	0.00
G run 1	9.0	0.33	4.5	0.23
G run 2	9.0	0.27	4.5	0.19
H run 1	9.5	0.68	4.5	0.23
H run 2	9.0	0.69	4.5	0.38
I run 1	9.0	0.85	4.5	0.76
I run 2	9.0	0.82	4.5	0.99

Increasing the level of hydration beyond experimental values results in more water molecules entering the anion coordination shells (average of 1.71 when H_3O^+ is the cation and 0.84 when $MIBKH^+$ is the cation, see Figure 6.15), but still no reverse micelle behaviour or water pooling is observed. This is demonstrated in the g(r) shown in Figure 6.16 for water-to-water distances; water molecules are not associated with many other water molecules on average.

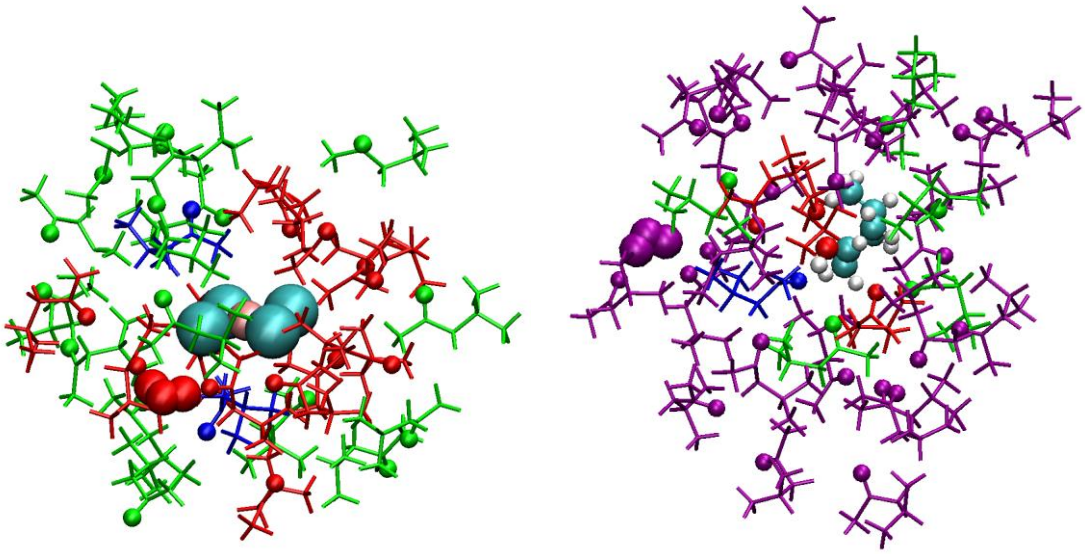

Figure 6.14. Anion (left) and cation (right) coordination shells for the $[AuCl_4]^-$ and $MIBKH^+$ system with 24 water molecules and 799 neutral MIBK molecules (G run 2). Anion coordination shell cut-offs are 7.0 (blue), 9.0 (red) and 11.5 (green) Å; cation cut-offs are 3.0 (blue), 4.5 (red), 7.0 (green) and 11.5 (purple) Å. $[AuCl_4]^-$, H_3O^+, H_2O and MIBK O atoms displayed as spheres (with those of $MIBKH^+$ and MIBK O of smaller radii) for clarity.

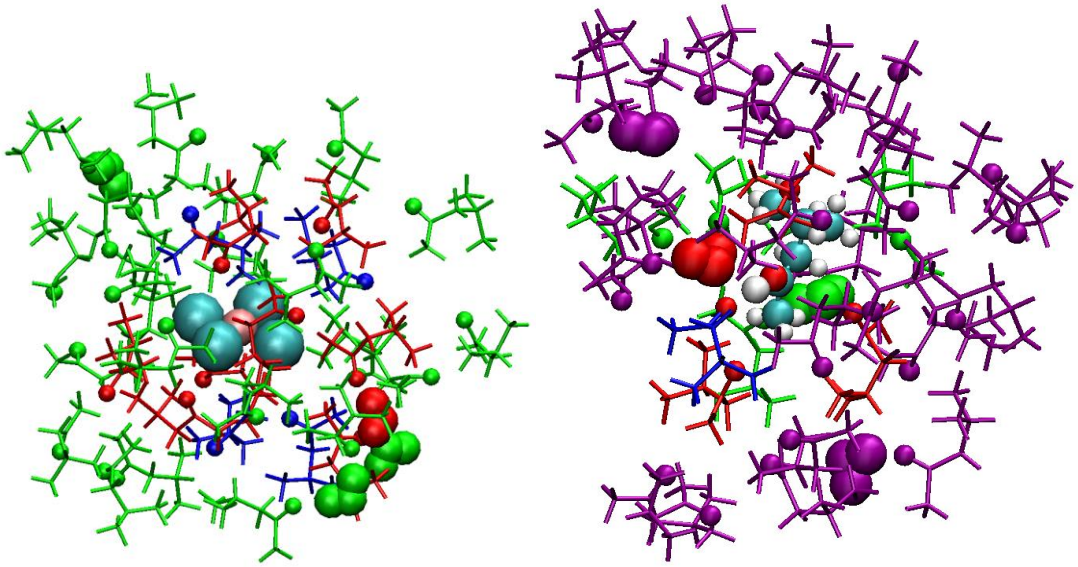

Figure 6.15. Anion (left) and cation (right) coordination shells for the $[AuCl_4]^-$ and $MIBKH^+$ system with 100 water molecules and 799 neutral MIBK molecules (I run 2). Anion coordination shell cut-offs are 7.0 (blue), 9.0 (red) and 12.0 (green) Å; cation cut-offs are 3.0 (blue), 4.5 (red), 7.0 (green) and 12.0 (purple) Å. $[AuCl_4]^-$, $MIBKH^+$, H_2O and neutral MIBK O atoms displayed as spheres (with those of $MIBKH^+$ and MIBK O of smaller radii) for clarity.

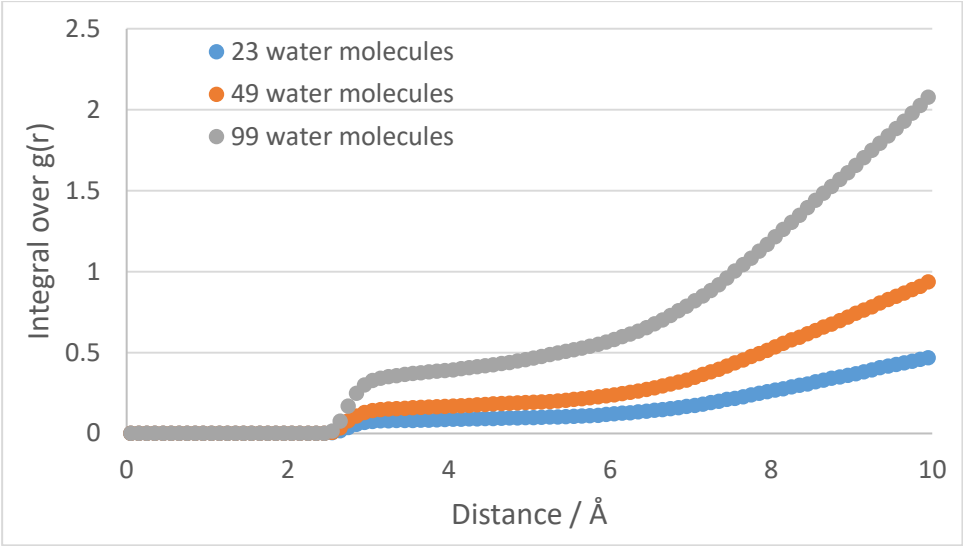

Figure 6.16. Integral over water (O atom) to water (O atom) g(r) plots for 23 (B run 1), 49 (C run 1) and 99 (D run 1) water molecule simulations with $[AuCl_4]^-$ and hydronium (with additional water molecule present in each as H_3O^+ but not counted as part of the g(r) analysis).

At the higher levels of hydration (experimental and double experimental) the cation (particularly the hydronium ion) appears to adopt greater structure definition. This is clear from the plots given in Figure 6.17, where a second peak in the histogram and cluster in the scatter plot for the 99 water molecule system indicates an additional coordination shell or a different structure in the outer coordination shell. These differences in the coordination shells are due to the presence of more water molecules (see Table 6.5 for average number of water molecules present in the coordination shells (of the 4 Å cut-off)).

The effect is much less evident when $MIBKH^+$ is the cation (see Figure 6.18, where there is very little difference between the scatter plots for the system with no water and the system with 100 water molecules present), though more water molecules are found in the coordination shell (see Table 6.5 for average number of water molecules present in the coordination shells (of the 4.5 Å cut-offs). A similar effect may be occurring with the anion, though to a lesser extent. It is possible that the increased number of hydrogen bonds contribute to the stabilisation of the ions in the organic phase, by linking extractant molecules together and producing a more network-like array of interactions than could be present in the absence of water. Thus, while water does not act as a mediating layer between the extractant molecules and the anion or cation, it may contribute to the stability of the assembly.

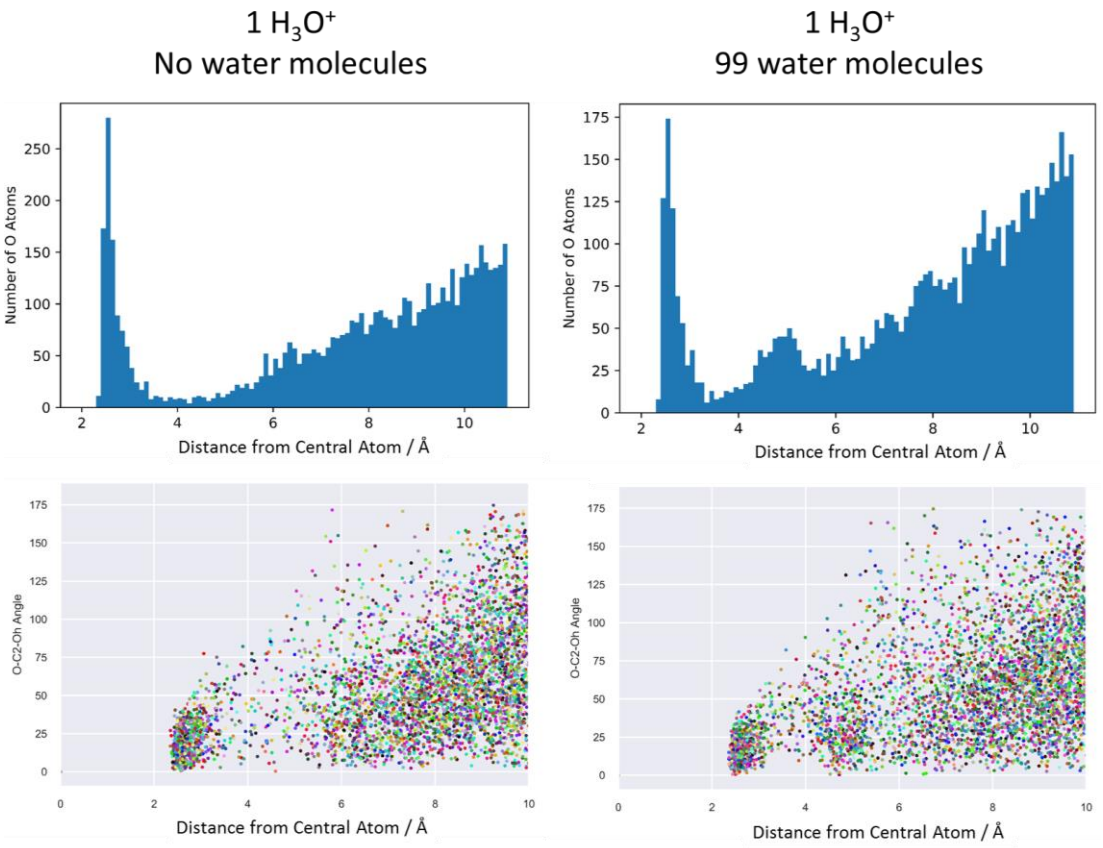

Figure 6.17. Comparison of top: histogram of hydronium O to MIBK O distances and bottom: scatter plots of size angle MIBK carbonyl groups makes to the hydronium O atom with distance from the cation for A run 1 (left) versus D run 1 (right).

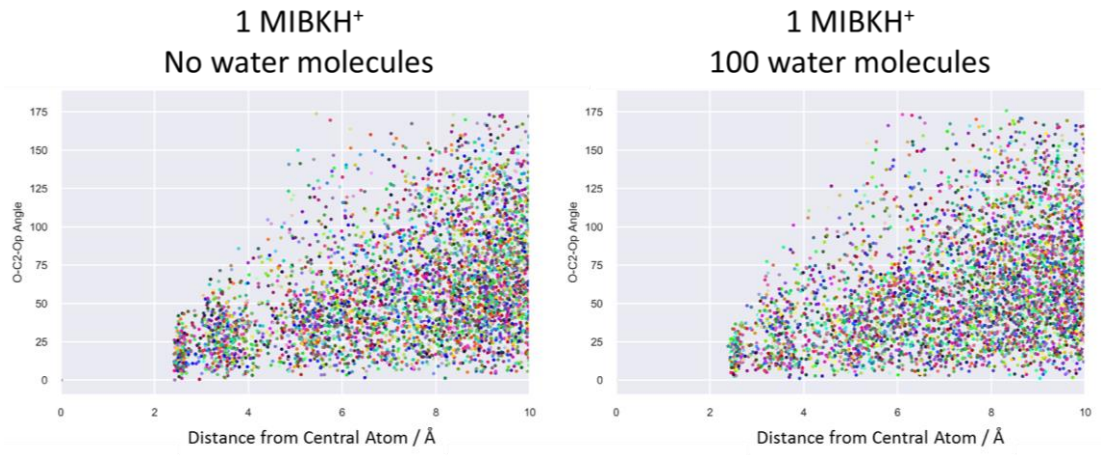

Figure 6.18. Comparison of scatter plots of size angle MIBK carbonyl groups makes to the $MIBKH^+$ O atom with distance from the cation for E run 2 (left) versus I run 2 (right).

8.2.4.3 Chloride as the anion

Simulations were also carried out with chloride as the anion. For these simulations $[AuCl_4]^-$ was simply swapped for chloride and while all other components were kept the same. Note this does not guarantee that models remain true to the experimental composition (e.g. although on contacting MIBK with 6 M HCl the organic was found to take up a similar amount of water to a contact with 0.01 M $[AuCl_4]^-$ in 6 M HCl (see Table 6.1), it is likely that the concentration of chloride in the organic phase is not exactly the same as $[AuCl_4]^-$, i.e. not 0.01 M). Therefore, these simulations are only for comparison purposes, to see how interactions with a smaller, more charge dense anion may differ.

The main difference observed with chloride as the anion is that now, in all cases, the anion and cation (either H_3O^+ or protonated MIBK) closely associate, at least by the end of the simulation run. This can be seen in the example anion to cation distance plots given in Figure 6.19 and pictures of the example assemblies are given in Figure 6.20. In some cases this close association can be seen to form at the beginning of the simulation run time analysed, suggesting that, although the total energy of the system had equilibrated (criteria for the run time to be analysed – see Section 6.4.4 for discussion), the equilibrium assembly had not formed by the start of the time analysed. In all cases once the anion and cation have come together, they do not separate and are found within a distance of approximately 5 Å for the rest of the simulation. This implies that the two ions are very strongly associated, in a more traditional ion-pair. This is consistent with the small, charge dense nature of both the anion and the cation/cation functional group.

For the hydrated models, more water molecules are found close to the chloride than found in the corresponding comparative simulations with the Au metalate. For example, in the shells shown in Figure 6.20, water molecules can be seen directly interacting with the chloride anion. This is in contrast with those for $[AuCl_4]^-$ in Figures 6.9 and 6.10, where, on average, no such interaction was found. This may be as a result of the anion and the cation being close together, so the water molecules that would otherwise associate with each are now together close to both ions. In the case of the example metalate simulation, there is often a water molecule close to the cation (particularly so for H_3O^+), but the cation is not found close to the anion, on average. Alternatively, this may be due to chloride being a

smaller, more charge dense anion, with which it is more favourable for the polar water molecules to interact with than $[AuCl_4]^-$.

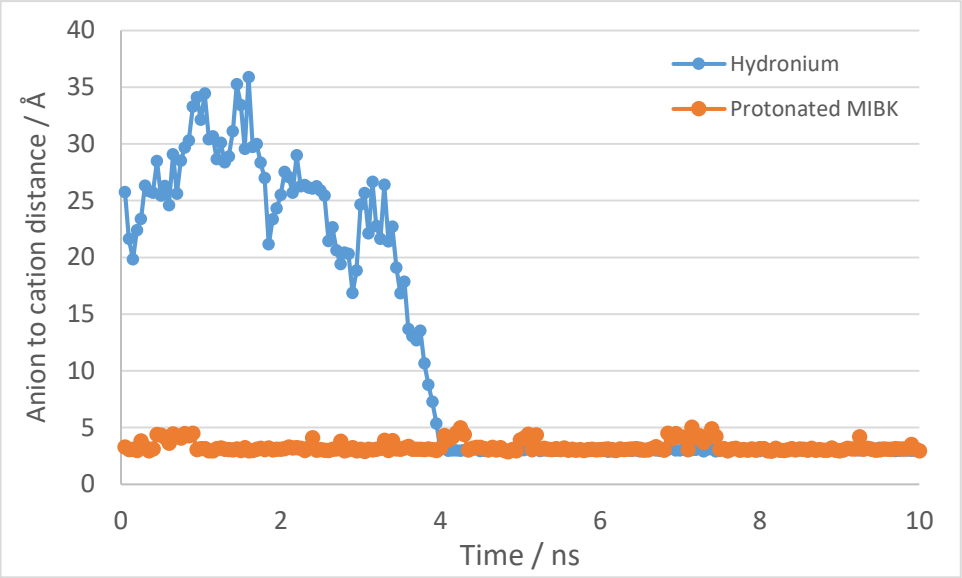

Figure 6.19. Anion (Cl^-) to cation (H_3O^+ or $MIBKH^+$) distance plot over time, for systems with no additional water molecules.

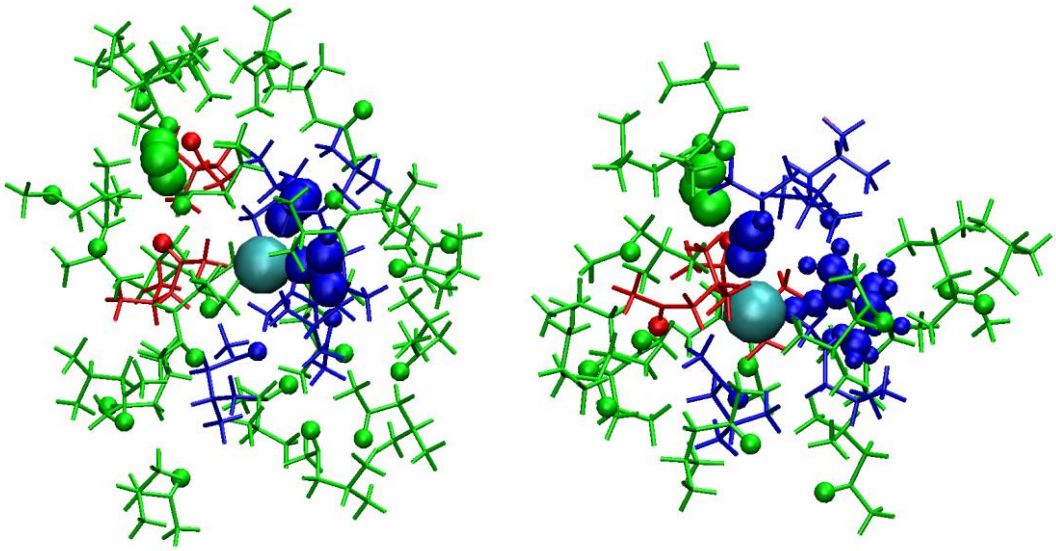

Figure 6.20. Coordination shells for the Cl^- with H_3O^+ (L run 1, left) and $MIBKH^+$ (Q run 1, right). Coordination shell cut-offs for H_3O^+ system are 5.0 (blue), 7.0 (red) and 11.0 (green) Å and for $MIBKH^+$ systems are 5.5 (blue), 7.0 (red) and 10.0 (green) Å. Cl^-, H_3O^+, $MIBKH^+$, H_2O and neutral MIBK O atoms displayed as spheres for clarity.

The increased presence of water molecules close to the ion-pair in the Cl^- models does not appear to act as a mediating layer between the anion and the cation. Instead, the chloride anion and the cation interact directly (via an O-H…Cl interaction) and the water molecules are found more in association with the chloride anion. However, the water molecules do tend to mediate the interactions of the neutral MIBK molecules with the chloride ion (as illustrated in the example shown in Figure 6.20). Essentially, it appears that the chloride ion remains partially hydrated and the neutral MIBK molecules hydrogen bond to the water molecules, which in turn hydrogen bond (via O-H…Cl interactions) to the anion. This is particularly evident when H_3O^+ is the cation, likely because H_3O^+ is also able to mediate the interaction, and can be seen from the scatter plots of the angle the MIBK carbonyl groups make with the anion (see Figure 6.21). Low angles are present, showing that the carbonyl is pointing more towards the anion. This would be unfavourable if there is not another molecule(s) in between the anion and the electronegative carbonyl O atom.

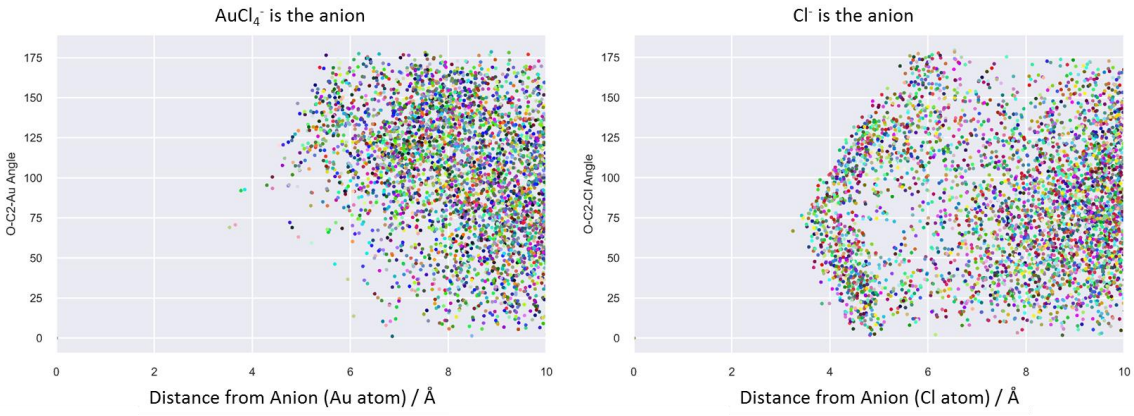

Figure 6.21. Comparison of scatter plots of size angle MIBK carbonyl groups makes to the anion (Au or Cl atom) with distance from the anion for the $[AuCl_4]^-$ (C run 1, left) and chloride system (L run 1, right) with H_3O^+ and 49 additional water molecules.

8.2.5 Likely mode of extraction

From the results discussed above it is possible to now determine the likely mode of action in the extraction of $[AuCl_4]^-$ by MIBK. Although experimentally it is observed that a significant amount of water is taken up into the organic phase on contact with an Au(III) metalate containing HCl solution, it does not appear that water acts to form a reverse micelle, where the role of water would be to act as a mediating layer between the anion and the cation or

neutral MIBK molecules. Instead, only a few water molecules are found within the inner- and outer-coordination shells of the neutral MIBK surrounding the anion, hydrogen bonded to the MIBK molecules to impart increased structure to the coordination shells. Water is found to more often associate with the cation, particularly H_3O^+, than the metalate anion. This suggests that the main function of water in the extractions is to solvate the proton.

Therefore, the most likely mode of extraction is similar to mode D, illustrated in Figure 6.3, where the $[AuCl_4]^-$ anion is not hydrated and is instead simply surrounded by neutral MIBK molecules and the cation proton is hydrated (or at least partially hydrated if $MIBKH^+$ is able to be a stable cation in the system). The picture in Figure 6.22 presents this, showing less hydration of the cation than implied in Figure 6.3.

For chloride, the simulations suggest a different mechanism: one where the ions are closely associated with one another and are partially hydrated (particularly so for the chloride ion). This suggests that mode E, or a version of it where there is less water present and it is less of a pool surrounding the ions, occurs for chloride. This is illustrated in Figure 6.22

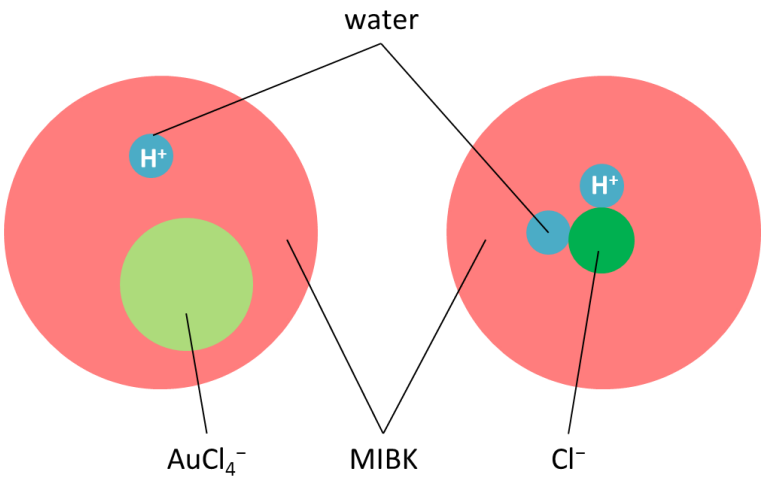

Figure 6.22. Extraction assemblies likely to form with $[AuCl_4]^-$ and Cl^- based on the results of the MD simulations.

8.3 Conclusions and future work

Despite the uptake of considerable amounts of water into the organic phase, no reverse micelle behaviour is observed in the MD simulations of $[AuCl_4]^-$ extraction with MIBK. While some water molecules are found associated with MIBK molecules surrounding the Au(III) metalate, few associate directly with the anion. Instead, water molecules are more likely to be associated closely with the cation, particularly with H_3O^+, but not to the degree that could be ascribed to water pooling. Overall, most of the water molecules are in a non-aggregated state and are most likely to be found hydrogen bonded to the carbonyl groups of MIBK.

An interesting aspect of the Au(III) metalate simulations is the fact that, regardless of the cation being present as a hydronium ion or a protonated MIBK molecule, the cation and the anion do not form a closely associated ion-pair complex. Instead the system is much more dynamic, with the ions sometimes relatively close to one another, though rarely interacting directly, and sometimes quite distant. This is likely due to the fact that the $[AuCl_4]^-$ is a larger, more diffusely charged ion in comparison to the hydronium or the functional group of the protonated MIBK, such that the $[AuCl_4]^-$ can better interact with the C-H groups of neutral MIBK molecules via dispersion interactions and the cation with the carbonyl groups of neutral MIBK molecules via a hydrogen bond.

Simulations of chloride for comparison show that this smaller and more charge dense anion does form a closely associated ion-pair with the cation. This is expected, as a charge dense to charge dense interaction will be occurring. Chloride is also found to be more hydrated, again likely due to it being more charge dense, and so it associates more strongly with polar water than the larger less polar MIBK.

This work suggests that the role of water in $[AuCl_4]^-$ extraction by MIBK is likely to be to hydrate the proton, most likely as hydronium. It is possible that some water, which may appear to be transported to the organic phase in association with Au extraction, may actually be associated with chloride, if chloride is co-extracted alongside $[AuCl_4]^-$. Further experimental work would be required to verify this. However, the bulk of the water appears to simply be soluble (and dispersed in) the MIBK. In addition, further experimental work, would also be useful to allow simulations to be run for organic phases of compositions representative of extraction from different HCl concentrations.

If time had permitted, simulations using different charge parameters would have been conducted to verify that the charges used do not affect the results such that they introduce error. In addition, the simulations would have been run for a longer time. This should perhaps be considered for future work.

It would be of interest to carry out simulations of more than one $[AuCl_4]^-$ anion in the simulation box or of a mixture of $[AuCl_4]^-$ and chloride (with the appropriate number of cations) to determine if the ions form large clusters containing more than one ion-pair.

It would also be of interest to carry out simulations for other gold extractants, such as DBC and alcohols. Some work on DBC and 2-ethylhexanol was done by final year undergraduate students under the supervision of the author, and the results of this work is given in the SI. However, full studies on these extractants are desirable.

8.4 Method details

8.4.1 Experimental analysis

0.01 M $[AuCl_4]^-$ in 6 M HCl was prepared by dissolving the appropriate mass of $HAuCl_4$ in 6 M HCl. Test extractions were carried out by contacting 5 mL of an aqueous phase (water, 6 M HCl, or 0.01 M $[AuCl_4]^-$ solution) with 5 mL of MIBK for 1 hour, before the phases were separated. KF analysis of the organic phases (and of uncontacted MIBK) was then carried out. See Chapter 2 Section 2.2.3 for details.

8.4.2 QM calculations

Geometry optimisation and frequency calculations were carried out following the general procedure given in Chapter 2 Section 2.1.2.3.

Minimised energy structures were obtained for all the components required for the simulation boxes: MIBK, protonated MIBK, water, hydronium, and $[AuCl_4]^-$. The M06[10] functional was used for all calculations, with the LANL2DZ[11] pseudopotential/basis set for Au and the 6-31+G**[12, 13] basis set for all other atoms.

The calculations conducted with the MIBK, water molecules, and an additional proton, to try to identify the preferred protonation site used the same functional/basis sets as listed above. Calculations were performed both *in vacuo* and using PCM[14] implicit water model, to mitigate against any bias in results due to stabilisation effects induced by a solvent field.

8.4.3 MD simulations

8.4.3.1 Parameters

Most parameters were obtained from the available literature parameters. The OPLS parameter set is used for the non-bonded (pair), bond, angle and dihedral parameters for MIBK and protonated MIBK. The TIP3P parameters[15] are used for the non-bonded (pair), bond and angle parameters for water molecules in this work and were adapted for use with hydronium. The OPLS non-bonded parameters are used for chloride but there are no

parameter sets for PM metalates, so the non-bonded (pair), bond, angle and dihedral parameters for $[AuCl_4]^-$ were taken from the work of Carson et al.[16]

The charge parameters for water, H_3O^+, MIBK and $MIBKH^+$ were not taken from literature, owing to the absence of charges for the protonated structures and the desire to keep the charge type the same between the neutral and protonated forms. Therefore, different partial charge systems were tested for MIBK and the theoretical densities obtained in classical MD simulations were computed and compared with the literature values (Table 6.6). The atomic polar tensor (APT) charge system was chosen as it gave the density closest to the literature value (excepting the OPLS parameter set) and to that obtained when the OPLS charge parameters were employed.

Table 6.6. Densities obtained from classical MD simulations, using a variety of charge systems, compared to the literature density (at 20 °C)[17, 18] of MIBK. ESP is electrostatic potential.

	Reagent
Density / g mL^{-1}	**MIBK**
Literature density	0.80
OPLS density[6]	0.815
% difference	+1.9
Mulliken density[9]	0.823
% difference	+2.9
APT density[10]	0.818
% difference	+2.3
ESP density[11]	0.243
% difference	-69.6

APT charges were also calculated for water and H_3O^+ and used (with averaging over the same atom types) as the charge parameters in the simulations with water and/or H_3O^+. The partial

charges for the atoms of $[AuCl_4]^-$ were again taken from the work of Carson et al.,[16] while the charge on the chloride anion is simply −1.

All the parameters used for the different molecules are included in the SI.

8.4.3.2 MD simulation details

All simulations were carried out according to the procedure given in Chapter 2 Section 2.1.4.2.

The simulations of MIBK alone for the purposes of determining the charge parameters to use were carried out on cubic boxes of length 40 Å, but all other simulations used cubic boxes of length 55 Å.

The simulations were found to reach energy equilibrium in the NVT run or within approximately the first 1 ns of the NPT run (see Figure 6.23 for example plot of the total energy over the course of the simulation runs). Data analysis was performed over the final 10 ns of each simulation.

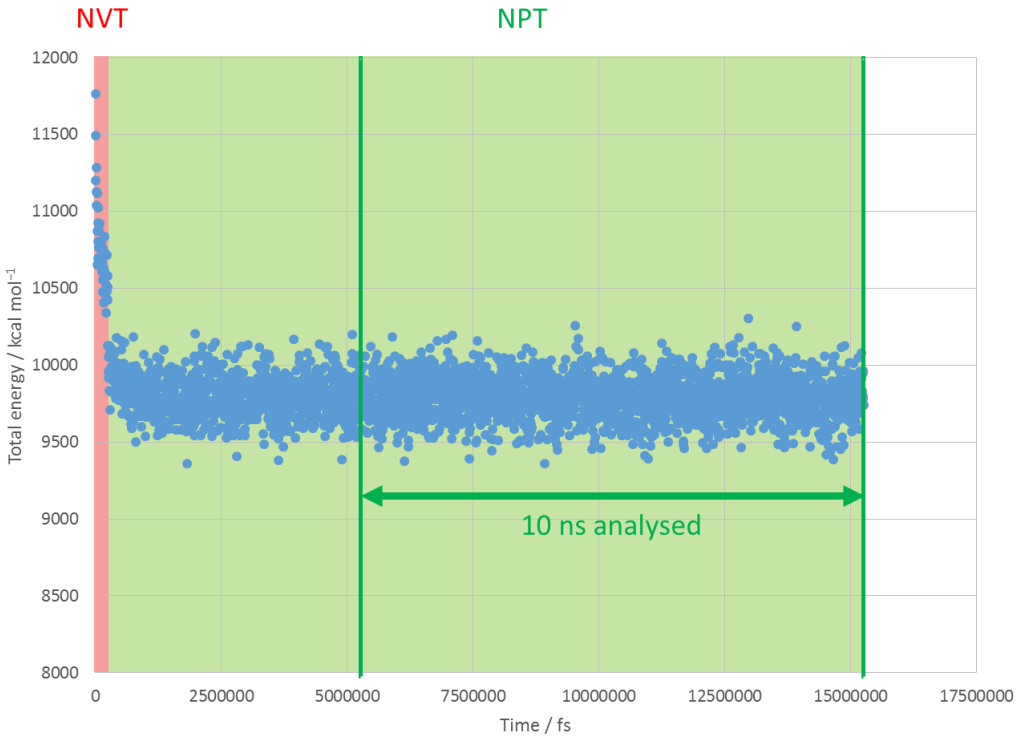

Figure 6.23. Example total energy plot H run 1. NVT and NPT regions are marked. The energy plateaus at around 1 ns of run time. As with all simulation runs (all around 12 to 15 ns of NPT run time) only the final 10 ns of NPT run time is analysed.

8.4.4 Data processing and analysis

8.4.4.1 Scripts

A variety of scripts for the data processing and analysis of the MD simulation outputs were developed, either based on existing scripts or written from scratch. A brief summary of each is given below and examples of the scripts can be found in the SI.

Scale Coordinates script: This Fortran 95 script positions the ion at the centre of the simulation box and moves all other atoms accordingly. It takes into account the changing box size that occurs during each frame of the NPT simulation. This script was developed by Dr K. MacRuary for her PhD work and was modified by M. Kennealy for this work.

Angles scripts: These Python scripts read in the centred coordinates file and calculate the distance between the O atom in each MIBK molecule to the central ion as well as the angle (X-C2-O, see Figure 6.24) the carbonyl group of each uniquely identified MIBK molecule makes to the central ion, where the central ion can be the Au atom of $[AuCl_4]^-$, the Cl^- anion, the O atom of H_3O^+ or the O atom of $MIBKH^+$. The output of this script is a histogram showing the number of O atoms at various distances from the central ion. These scripts were developed by M. Kennealy for this work and were modified by the author.

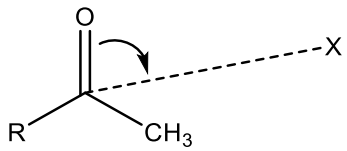

Figure 6.24. Angle considered by the angle scripts. Carbonyl O atom to carbonyl C atom to ion atom (the Au atom of $[AuCl_4]^-$, the Cl^- anion, the O atom of H_3O^+ or the O atom of $MIBKH^+$).

Scatter plots and heat maps scripts: These Python scripts create a scatter plot and heat map showing the density of O atoms at various distances from the central ion and show how the X-C2-O angle varies as a function of distance from the central ion. In addition to the histogram produced above, these allow for the coordination sphere cut-off radii to be determined. These scripts were developed by M. Kennealy for this work and were modified by the author.

Residency scripts: These Python scripts read the centred coordinates file, calculate which MIBK and water molecules are resident (i.e. have an oxygen atom of the molecule within the

cut-off distance in the case of MIBK or possess one or more atom within the cut-off distance in the case of water) in the coordination sphere around either the anion or the cation, and produce a graph showing how the residency of those molecules varies with each frame of the trajectory. The script also produces a percentage residency for each molecule, allowing quantification of how dynamic the system is, and to what extent "coordinated" MIBK or water molecules remain in the coordination sphere for the duration of the simulation. These scripts were developed by M. Kennealy for this work and were modified by the author.

Coordination shell calculator scripts: These Fortran 95 scripts return the positions of all the MIBK molecules that have their O atom within the cut-off radius and all water molecules that contain one or more atoms within the cut-off radius from the central atom. In addition, the anion scripts also return the position of the cation if it has an O atom or protonating H atom within the cut-off, in the case of protonated MIBK, or any of its atoms, in the case of hydronium, while the cation scripts also return the position of the anion if any of its atoms are within the cut-off. This identified the molecules present in the coordination sphere and excluded all others, allowing only the coordination sphere to be visualised. These scripts were developed by Á. Gallego Jurado for this work and were modified M. Kennealy and the author.

Number of molecules script: This Fortran 95 script counted the number of each type of molecule within the coordination shell coordinate sets and provided a count for each molecule type per frame. This allowed for the selection of relatively representative frames to be chosen for display. This script was developed by the author.

Porosity script: This Fortran 95 script fires a probe point from 5,000 random positions placed on the surface of a sphere of radius X+10 Å (with X Å being the cut-off defined for the coordination shell being assessed for its porosity) towards the centre point. The number of probe spheres which hit an atom in the central ion (which are represented as spheres of appropriate van der Waal radii), as a proportion of the total number of probe spheres (which otherwise hit an atom in a MIBK molecule, a water molecule or the counter-ion), is measured as a percentage. This quantifies how encapsulated the central ion is, determining the extent to which the extractant molecules shield the ion. The central ion is either $[AuCl_4]^-$, Cl^-, H_3O^+ or the OH^+ part of the protonated MIBK (with the rest of this molecule not considered to be part of the central ion). This script was developed by Dr I. Carson for his PhD work and was modified for this work by Á. Gallego Jurado, M. Kennealy and the author.

Figure 6.25 provides an illustration of the features of the assemblies probed using the scripts.

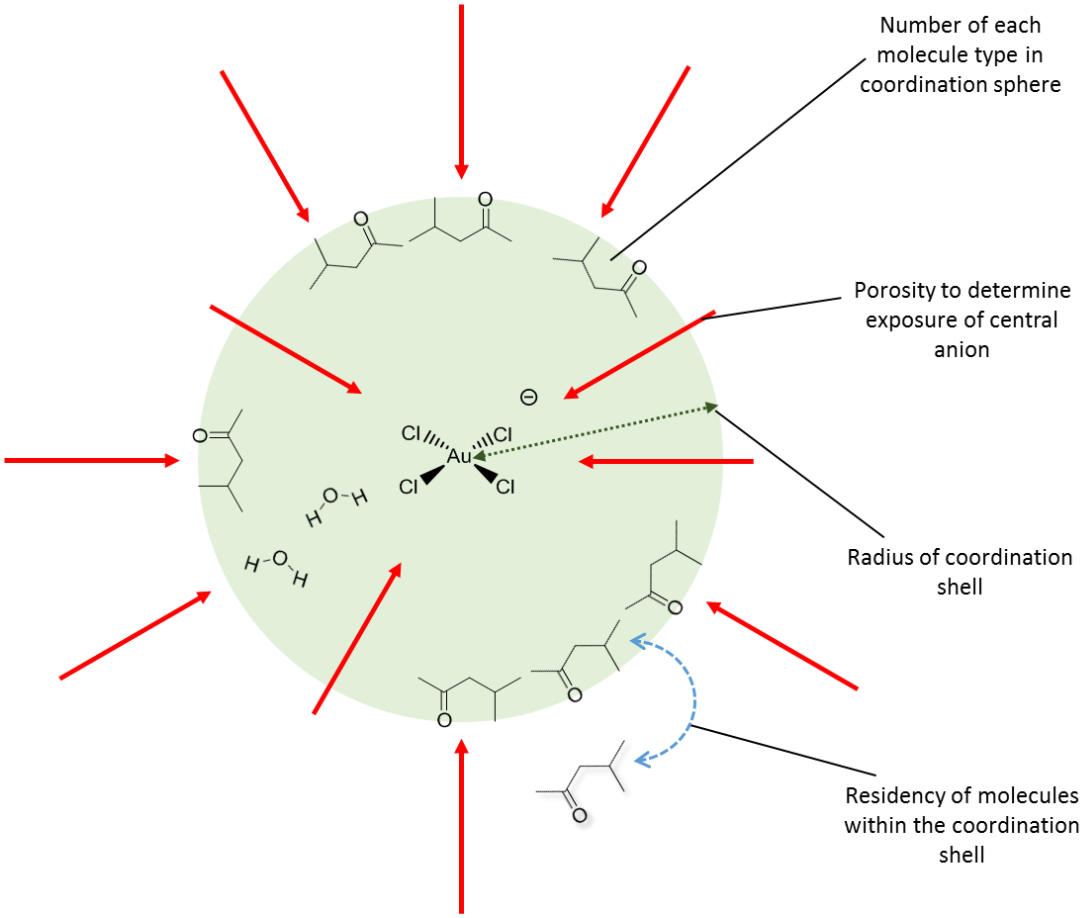

Figure 6.25. Features of the assemblies analysed using the scripts developed.

8.4.4.2 Additional analysis

VMD[19] was used to perform additional analysis on the simulation outputs. This consisted of anion to cation distance analysis and g(r) analyses, allowing production of plots such as those shown in Figures 6.5 through 6.9.

The histogram of MIBK distances to the ion and the scatter plot and heatmap plots of the angle the MIBK carbonyl group makes to the ion with distance from the ion (see bottom three panels in Figures 6.5 to 6.8 for examples) were used to manually decide on cut-off distances for the coordination shells. For example, in Figure 6.26 a cut-off of 9.5 Å was chosen for the inner coordination shell around the $[AuCl_4]^-$ because from the scatter plot and heat map this was the point at which the full range of angles was covered and there was a more even

distribution across the angles sizes (suggesting that random solvent behaviour was occurring). From the histogram there was little definition seen, except for a slight plateauing around that point. A later cut-off of 12.0 Å was chosen for the outer-coordination shell as the scatter plot (see Figure 6.26 below for the scatter plot over a larger distance range) appeared to show a near completely random distribution of angles from that point.

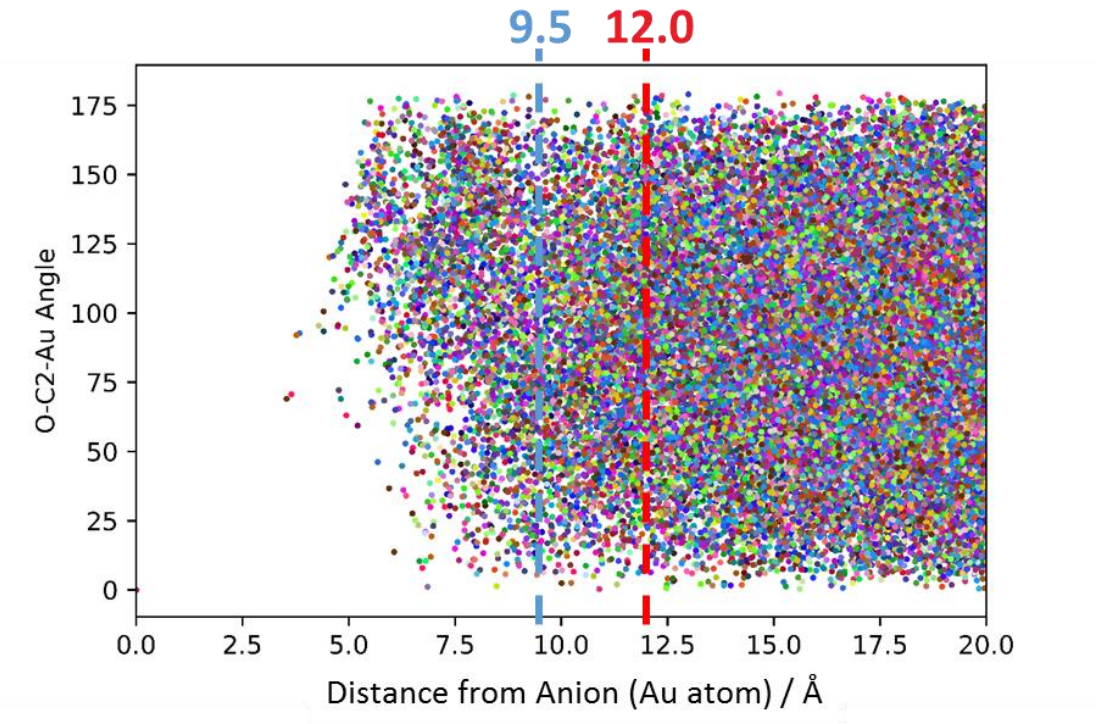

Figure 6.26. Scatter plot of size of angle MIBK carbonyl groups makes to Au atom with distance from the anion for C run 1, showing inner- and outer-coordination shell cut-offs chosen.

For the coordination shells around the H_3O^+ cation, the histogram (shown in Figure 6.6 bottom left panel) clearly displays two peaks at distances close to the cation, and the troughs in between them are chosen as two inner-coordination shell cut-off. These two peaks can be seen as clusters at low angles on the scatter plot and heat map. Later cut-offs were chosen in a similar manner to for the anion: when the angle distribution appeared to be more or mostly random.

These chosen cut-offs, particularly the later ones, are still subjective, despite best effort to make an informed choice based on the analysis plots obtained. However, they are mainly used to give a general sense of the structure surrounding the ions, in a qualitative manner.

Although they are utilised to provide average numbers of molecules in the different coordination shells and porosity values, these are only meant to provide a picture of the extraction assembly and a rough idea of how well the ions are encapsulated.

8.4.4.3 Data processing and analysis scheme

The general scheme of data processing and analysis was as follows:

1. Trim the full 12 to 15 ns data sets to only the final 10 ns (to give 2000 frames with 5 ps between each).
2. Select every 10th frame to give a 200 frame data set (with 50 ps between each frame) and select every 100th frame to give 20 frame data set (with 500 ps between each frame).
3. Scale the coordinates to centre either the anion or the cation in the middle of the box.
4. Perform angles, scatter/heatmap and residency analysis on the 200 frame data set.
5. Use distance and angle vs distance plots (histogram, scatter and heatmap plots) to manually choose cut-off distances for the coordination shells.
6. Do coordination shell cutting (using chosen cut-off distances) on the 20 frame data set.
7. Run porosity analysis on the coordination shells.

The outputs of these analyses are given for the full set of simulations in the SI. Figures 6.5 to 6.8 give examples of the plots produced for the $[AuCl_4]^-$ with H_3O^+ or $MIBKH^+$ at experimental levels of water simulations.

8.5 References

1. Yarar, B., Long term persistence of cyanide speciesin mine waste environments. In *Tailings and Mine Waste 2002: Proceedings of the 9th International Conference*, Colorado School of Mines, Swets & Zeitlinger: Colorado, 2002; p 197.
2. Cox, M., Solvent Extraction in Hydrometallurgy. In *Solvent Extraction Principles and Practice*, 1st ed.; Rydberg, J.; Claude, M.; Choppin, G. R., Eds. Taylor & Francis: New York, USA, 1992; pp 357-412.
3. Kyriakakis, G., Extraction of gold from platinum group metal (PGM) ores. In *Developments in Mineral Processing*, Adams, M. D.; Wills, B. A., Eds. Elsevier: 2005; Vol. 15, pp 897-917.
4. Doidge, E. D.; Carson, I.; Tasker, P. A.; Ellis, R. J.; Morrison, C. A.; Love, J. B., *Angew. Chem. Int. Ed.* **2016,** *55*, 12436-12439.
5. Doidge, E. D. Designing reagents for the solvent extraction of critical metal resources. University of Edinburgh, 2018.
6. Tocher, M. I.; Whitney, D. C.; Diamond, R. M., *J. Phys. Chem.* **1964,** *68*, 368-374.
7. Petrova, A. M.; Nikolaev, A. E.; Kasikov, A. G., *Russ. J. Appl. Chem.* **2014,** *87*, 234-240.
8. Jordanov, N.; Havesov, I., *Fresenius Z. Anal. Chem.* **1969,** *244*, 176-181.
9. MacRuary, K. J.; Gordon, R. J.; Grant, R. A.; Woollam, S.; Ellis, R. J.; Tasker, P. A.; Love, J. B.; Morrison, C. A., *Solvent Extr. Ion Exch.* **2017,** *35*, 531-548.
10. Zhao, Y.; Truhlar, D. G., *Theor. Chem. Acc.* **2007,** *120*, 215-241.
11. Hay, P. J.; Wadt, W. R., *J. Chem. Phys.* **1985,** *82*, 299-310.
12. Hehre, W. J.; Ditchfield, R.; Pople, J. A., *J. Chem. Phys.* **1972,** *56*, 2257-2261.
13. Francl, M. M.; Pietro, W. J.; Hehre, W. J.; Binkley, J. S.; Gordon, M. S.; DeFrees, D. J.; Pople, J. A., *J. Chem. Phys.* **1982,** *77*, 3654-65.
14. Cossi, M.; Barone, V.; Cammi, R.; Tomasi, J., *Chem. Phys. Lett.* **1996,** *255*, 327-335.
15. Jorgensen, W. L., *J. Am. Chem. Soc.* **1981,** *103*, 335-340.
16. Carson, I.; MacRuary, K. J.; Doidge, E. D.; Ellis, R. J.; Grant, R. A.; Gordon, R. J.; Love, J. B.; Morrison, C. A.; Nichol, G. S.; Tasker, P. A.; Wilson, A. M., *Inorg. Chem.* **2015,** *54*, 8685-8692.
17. Lewis, R. J., *Hawley's Condensed Chemical Dictionary*. John Wiley & Sons Inc: New York, 2001.
18. *Some Chemicals Present in Industrial and Consumer Products, Food and Drinking-water*. International Agency for Research on Cancer (IARC): France, 2013; Vol. 101.
19. Humphrey, W.; Dalke, A.; Schulten, K., *J. Mol. Graph.* **1996,** *14*, 33-38.

Chapter 7

Conclusions

7 Conclusions

The primary aims of this work were to explore the recovery of rhodium and gold via hydrometallurgical solvent extraction, with particular focus on understanding the mechanisms of extraction. Rh and Au are two valuable and important (technologically and chemically) precious metals. Continued research into their recovery is key to maintaining their supply for the future. An understanding of how solvent extraction occurs at the molecular level is important for the development of improved processes or new regents. This work considered the modes of action occurring with promising Rh extractants and a commercial Au extractant, to elucidate their mechanisms and identify the key components which provide strong extraction. In addition, potential new extractants were explored for Rh, which is not currently recovered via solvent extraction industrially due to the lack of a suitable reagent. In this work a variety of experimental techniques and computational modelling were employed.

Chapter 3 determined the mode of action for a series of amidoamine extractants in the recovery of Rh(III) from chloride solution. It was determined that $[RhCl_5(H_2O)]^{2-}$ is extracted via an ion-pair mode of action by two protonated amidoamine extractant molecules, with EXAFS, FT-IR and ^{1}H-^{15}N and ^{1}H-^{13}C NMR analysis all supporting the conclusion that $[RhCl_5(H_2O)]^{2-}$ is the Rh(III) species extracted. Computational modelling suggests the reason for the success of these extractants, particularly the bis- and tris-amidoamine derivatives, over simple amine extractants, is their good selectivity for the Rh(III) metalate over the chloride ion. EXAFS and ESI-MS analysis found a species corresponding to a dinuclear Rh complex, most likely based on $[Rh_2Cl_9]^{3-}$, in extractions from aqueous solutions of high Rh concentration. Analysis suggests that this could either be extracted from the aqueous phase or formed upon extraction, and computational modelling also suggests either is possible. ESI-MS, FT-IR and X-ray crystallography show that over time an inner-sphere complex can form, but this does not appear to occur to any appreciable level on the extraction timescale. This work has confirmed the ion-pair/ion-associate mode of extraction of the $[RhCl_5(H_2O)]^{2-}$ but has also highlighted the complex nature of Rh(III) speciation in the organic phase in addition to the aqueous phase.

The potential to improve extraction of Rh by using different amidoamine extractants was explored theoretically in Chapter 4. A variety of structurally modified amidoamines and amido-quaternary ammoniums based on the mono- and bis- amidoamines investigated in Chapter 3 were selected for study. It was found that the parent bis-amidoamine extractant is unique in terms of setting up a farourable C-H…anion binding mode, through proton chelation, and that this binding arrangement is the most energetically favoured for $[RhCl_5(H_2O)]^{2-}$ extraction over Cl^-. For the other amidoamines, which favoured direct N-H…anion interactions, association with the chloride ion was more favourable than association with the Rh(III) metalate. This work has therefore highlighted the importance of a favourable charge-diffuse C-H…anion binding mode in providing selective extraction of Rh(III) over chloride and has shown how small structural changes can potentially have a very large effect on extraction behaviour. For future study a selection of these theoretical extractants could be synthesised and their experimental extractant performance tested to verify the computational findings.

Polyamines are known Rh(III) precipitants and have been shown to selectively precipitate Rh(III) over Pt(IV). Chapter 5 explored the possibility of modifying these compounds for suitability in a solvent extraction environment through the addition of 'greasy' R-groups, to favour organic phase solubility of the Rh-containing complexes. The modified extractants were found to extract Rh(III) well (> 90%) from 5 M HCl (and above) solutions and back-extraction can be achieved by contact with an aqueous solution of ammonium hydroxide. Extractant recyclability was tested over five cycles with no drop in performance found. Unfortunately, no selectivity for Rh(III) over Pt(IV) or Ir(III) was found, meaning that while the modified polyamine extractants offer promise to change current practise for Rh(III) recovery away from precipitation methods, should they be introduced into an industrial flowsheet they would have to be utilised at the end of the hydrometallurgy circuit, when the other precious metals have already been removed. Overall, however, the modified polyamine precipitant shows promise as a Rh extractant; the industrial sponsor of this work, Johnson Matthey, will assess whether this new extractant has industrial potential. Regardless, it would be of interest to determine the mechanism of extraction exhibited by this polyamine in more depth. A study involving experimental analysis and computational modelling, such as that employed in Chapter 3 for mode of action determination, would be the most effective means to probe this.

Chapter 6 investigated the mechanism of extraction of $[AuCl_4]^-$ with the industrial reagent methyl isobutyl ketone by employing classical molecular dynamics simulations. It is found that, although water is present in the organic phase at significant levels, no reverse micelles with incorporation of a water pool are observed. Instead the water disperses throughout the solvent, and the charge-diffuse $[AuCl_4]^-$ anion is surrounded by neutral extractant molecules in a very dynamic assembly. It is also found that the $[AuCl_4]^-$ metalate and the charge-balancing cation do not form a traditional, closely bound ion-pair. Rather, the system is very fluctional, with the ions moving towards and away from one another over the course of the simulations. This work has allowed the likely assemblies in the organic phase to be visualised and rationalised. It would be of interest to carry out simulations with more than one anion and cation, to see if clusters can form, and to extend this work to consider other industrial extractants, such as dibutyl carbitol.

Overal this thesis has shown the merit of using a variety of experimental analytical and computational modelling techniques in tandem to elucidate the mode of action for metal recovery in solvent extraction processes. The complexities of Rh(III) metallate extraction have been highlighted, a potential new Rh(III) chloridometalate extractant with industrial relevance has been developed, and the likely mode of action of a commercial reagent for $[AuCl_4]^-$ extraction, which is used industrially with little fundamental understanding, has been demonstrated.